RF signal sensing and source localisation systems using Software Defined Radios

Junming (Jamie) Wei

A thesis submitted for the degree of
Doctor of Philosophy
The Australian National University

November 2016

Declaration

I hereby certify that this thesis is an original work. None of the work has been previously submitted by me for the purpose of obtaining a degree or diploma in any university or other tertiary education institution. To the best of my knowledge, this thesis does not contain material previously published by another person, except where due reference is made in the text. Most of the results in this thesis have been submitted to or published at refereed journals and international conferences, and they are listed:

1. J. Wei, C. Yu. Joint TDOA and FDOA based passive source localization using two sensors. IEEE Communications Letters, 20(9), pp. 1880 - 1883, 2016.

2. J.Wei, C. Yu. Accuracy enhancement of low-cost spatially distributed passive localisation system. IET Electronics Letters, 51(12), pp. 945-947, 2015.

3. J. Yi, C. Yu, J. Wei and B. Anderson. Localization bias reduction in wireless sensor networks. IEEE Transactions on Industrial Electronics, vol. 62(5), pp. 3004 - 3016, 2015.

4. J.Wei, C. Yu. Improvement of Software Defined Radio based TDOA source localization. The 40th Annual Conference of IEEE Industrial Electronics Society (IECON 2014), 5307 - 5313, 2014, Dallas, TX, USA.

5. J. Wei, J. Yi, C. Yu. Improvement of Software Defined Radio based RSSI localization with bias reduction. The 19th World Congress of the International Federation of Automatic Control (IFAC2014), pp. 7164 - 7169, 2014, Cape Town, South Africa.

6. J. Wei, J. Yi, C. Yu. Experimental verification of bias reduction in TDOA based localization. The 11th IEEE International Conference on Control and Automation (ICCA2014), pp. 7 - 12, 2014, Taichung, Taiwan.

7. J. Wei, C. Yu. Performance analysis of TDOA based localization using SDRs. The 3th Australian Control Conference (AUCC2013). pp. 91-92, 2013, Perth, Australia.

8. J.Wei, Technical Report: The feasibility studies of TDOA based geo-localization using Software Defined Radios (SDRs). Accepted as the final version by Defence Science Technology Group (DSTG), Adelaide. 2012.

Junming (Jamie) Wei
10 November 2016

To my parents,

Laihua Wei and Xiuling Li

and my wife,

Xiang (Shaylee) Li

Acknowledgments

Abstract

Radio frequency (RF) source localisation is a critical technology in numerous location-based military and civilian applications. In this thesis, the problem of RF source localisation has been studied from the perspective of the system implementation for real-world applications. Commercial off-the-shelf Software Defined Radio (SDR) devices, Universal Software Radio Peripheral (USRP) N210s, are used to demonstrate the practical RF source localisation systems. Compared to the conventional localisation systems, which rely on dedicated hardware, the new SDR-based platform is developed using general-purpose hardware and most of the specific signal processing functions for particular applications are software-defined, which can offer great flexibility and cost efficiency in system design and implementation.

In this thesis, the theoretical results of source localisation are evaluated and put into practice. To be specific, the practical localisation systems using different measurement techniques, including received-signal-strength-indication (RSSI) measurements, time-difference-of-arrival (TDOA) measurements and joint TDOA and frequency-difference-of-arrival (FDOA) measurements, are demonstrated to localise the stationary RF signal sources using the SDRs. The RSSI-based localisation system is demonstrated in small indoor and outdoor areas with a range of several metres using the SDR-based transceivers. Furthermore, interests from the defence area motivated us to implement the time-based localisation systems. The TDOA-based source localisation system is implemented using multiple spatially distributed SDRs in a large outdoor area with the sensor-target range of several kilometres. Moreover, they are implemented in a fully passive way without prior knowledge of the signal emitter, so the solutions can be applied in the localisation of non-cooperative signal sources provided that emitters are distant. To further reduce the system cost, and more importantly, to deal with the situation when the deployment of multiple SDRs, due to geographical restrictions, is not feasible, a joint TDOA and FDOA-based localisation system is also demonstrated using only one stationary SDR and one mobile SDR.

To improve the localisation accuracy, the methods that can reduce measurement error and obtain accurate location estimates are studied. Firstly, to obtain a better understanding of the measurement error, the error sources that affect the measurement accuracy are systematically analysed from three aspects: the hardware precision, the accuracy of signal processing methods, and the environmental impact. Furthermore, the approaches to reduce the measurement error are proposed and verified in the experiments. Secondly, during the process of the location estimation, the theoretical results on the pre-existing localisation algorithms which can achieve a good trade-off between the accuracy of location estimation and the computational cost are evaluated, including the weight least-squares (WLS)-based solution and the Extended

Kalman Filter (EKF)-based solution. In order to use the pre-existing algorithms in the practical source localisation, the proper adjustments are implemented.

Overall, the SDR-based platforms are able to achieve low-cost and universal localisation solutions in the real-world environment. The RSSI-based localisation system shows tens of centimetres of accuracy in a range of several metres, which provides a useful tool for the verification of the range-based localisation algorithms. The localisation accuracy of the TDOA-based localisation system and the joint TDOA and FDOA-based localisation system is several tens of metres in a range of several kilometres, which offers potential in the low-cost localisation solutions in the defence area.

Contents

7 Conclusion and Future Work   **145**

List of Figures

List of Tables

Introduction

Source localisation aims to find the position of a signal source of interest by utilising its emitted signal, which is measured at multiple spatially-separated receiving locations known as priori. In fact, source localisation has been one of the central problems in many fields such as radar, sonar Carter [1993], telecommunications Huang and Benesty [2007], mobile communications Caffery Jr [2006]; Jagoe [2003], wireless sensor networks Stojmenovic [2005], as well as human-computer interaction Rolshofen et al. [2005]. For example, in 1996, the Federal Communications Commission (FCC) introduced regulations requiring wireless service providers to be able to locate mobile callers in emergency situations with specified accuracy: 100-metre accuracy 67 percent of the time. Such emergency service is called E-911 in the US and E-112 in many other countries Commission et al. [1996]. Apart from emergency assistance, location information is also the key enabler for a large number of innovative applications such as personal localisation and monitoring, fleet management, asset tracking, travel services, location-based advertising, and billing. More recently, technological advances in wireless communications and micro system integration have enabled the development of small, inexpensive, low-power sensor nodes, which has great potential in numerous remote monitoring and control applications So [2011].

Source localisation can be achieved using different measurement techniques, such as time measurements, received signal strength measurements, angle measurements and frequency measurements, etc. As shown in Figure 1.1, the localisation systems can be classified into two categories: global localisation systems and local localisation systems. The Global Positioning System (GPS) is the most important technology to provide location-awareness globally with a constellation of at least 24 satellites Spilker [1978]. A local localisation system is a relative localisation system and can be classified into self-localisation and remote localisation. Self-localisation systems allow each person or object to find its own position within some environment at any given time and location, such as the inertial navigation system (INS). Remote localisation systems can find the relative position of a target located in its coverage area by using either static or mobile sensor, and they can be further categorised into active remote localisation systems and passive remote localisation systems. In the first case, the target is active and cooperative in the process of positioning, such as radio frequency identification (RFID) and wireless local positioning systems (WLPSs), while in the second case, the target is passive and noncooperative, such as tracking radars
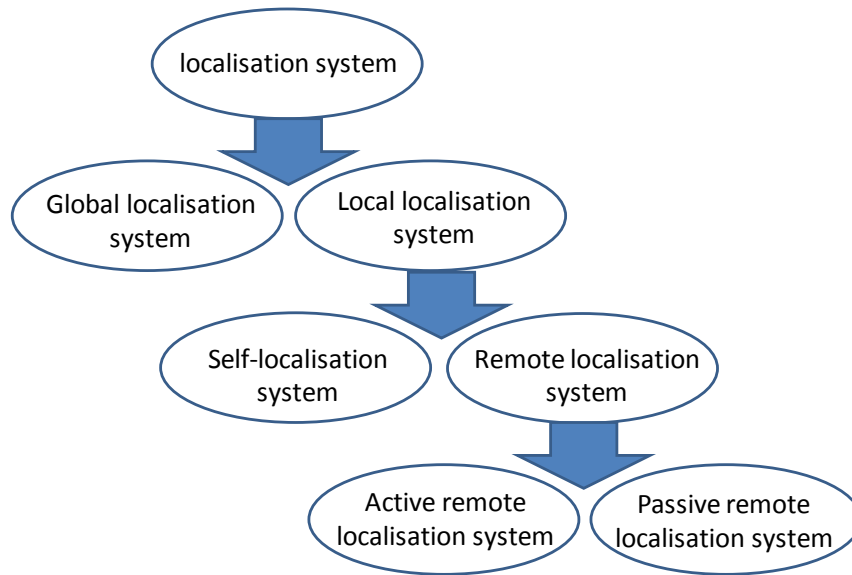
Figure 1.1: Classification of localisation systems

and vision systems Zheng and Jamalipour [2009].

Recent years have seen rapidly increasing demand for services and systems that depend on accurate positioning of people and objects. This has led to the development and evolution of numerous localisation algorithms. However, the practical development of source localisation systems cannot be taken for granted because it involves much complicated design and implementation. During the process of system design, people always expect high localisation accuracy. Generally speaking, expensive localisation solutions offer good localisation performance. However, there is a trend that people also want to achieve accurate localisation using low-cost solutions. Moreover, if the practical low-cost localisation solution can provide some additional features, such as flexibility in system upgrade and adaptability of different localisation techniques, other bonuses can be obtained. When localisation systems are implemented, additional factors also need to be considered, including the computing cost of determining the source position, the influence of the real-world signal propagation channels and even the security of the localisation systems.

1.1   Motivation

Conventional localisation systems usually rely on customised hardware or devices that are designed for particular localisation techniques. The disadvantage of these localisation systems is expensive because the replacement of these systems due to design error is costly. Moreover, localisation systems developed using conventional devices lack flexibility in the system design and development. Software Defined Radios (SDRs) is a relatively new technology. Based on general-purpose communica-

tion devices, all customized signal processing functions are software-defined, which offers great flexibility in the system design and implementation. With the availability of these low-cost signal processing and communication devices, low-cost localisation solutions become possible.

SDR-based cost-efficient implementation of localisation systems attracts the attention from the defence area. The Defence Science and Technology Group (DSTG) in Australia has a particular interest in SDRs from a situational awareness perspective, specifically the detection and geolocation of emitters using low-cost spatially separated receivers that are built upon the SDR technology. Apart from considering the cost of localisation systems, they are also concerned about the accuracy that the SDR devices can achieve; therefore, a feasibility study was jointly proposed between DSTG and NICTA (now Data61 in the Commonwealth Scientific and Industrial Research Organisation [CSIRO]) to develop and demonstrate geolocation systems based on such receivers in a ground-based configuration, utilising commercially available SDRs and open-source software.

1.2   Thesis research topics

This section narrows down our research domain to form the focus of the thesis. In this thesis, we have completed a comprehensive study of the radio frequency (RF) source localisation problems using multiple spatially distributed Software Defined Radios (SDRs). This content falls in the domain of "remote localisation system". The SDR devices are developed into a universal localisation system. To be specific, the SDRs are able to demonstrate practical source localisation systems dealing with different types of signal sources, such as FM signal, TV signal, etc., and different measurement techniques, including received-signal-strength-indication (RSSI) measurements, time-difference-of-arrival (TDOA) measurements and joint TDOA and frequency-difference-of-arrival (FDOA) measurements.

Both active and passive RF source localisation are investigated in this thesis. Firstly, a received-signal-strength-indication (RSSI)-based localisation system is developed using multiple SDRs, and it is a valuable platform for us to verify range-based localisation algorithms in small indoor and outdoor areas. However, the RSSI-based localisation system only offers limited localisation accuracy, and its implementation requires the cooperation of the signal emitter. Then, we started to explore the possibility of demonstrating a TDOA-based passive source localisation system using multiple spatially distributed SDRs, which is much more challenging. Firstly, the accurate source localisation needs to be achieved in a fully passive way. Secondly, the experiments need to be conducted in a large outdoor area with several-kilometre sensor-target ranges because the achievable time measurement accuracy requires large baseline between sensors. A crucial issue to overcome in the TDOA-based localisation with spatially distributed SDRs is the establishment of a common time reference between the different SDRs, so the methods to achieve accurate synchronisation of the local clocks of different SDRs are studied. Furthermore, to deal

with the situation when the reception of the signal from the source using multiple SDRs is not feasible, a passive source localisation solution only using two SDRs is proposed and demonstrated by taking joint TDOA and FDOA measurements, which is an important and timely report on the practical joint TDOA and FDOA-based localisation using SDRs.

In the implementation of source localisation, the SDR devices are developed into both stationary sensors and mobile sensors to implement signal sensing, measurement, and location estimation. The signal sources used in the demonstration are stationary, but the localisation systems are also able to distinguish whether the signal source is mobile or stationary by taking FDOA measurements between pairs of SDRs. While the localisation results are obtained in an "after the event" manner, the localisation systems are capable of acquiring signals to achieve automatic signal transmission via the network connection to a central server for real-time processing and source location estimation.

To improve the performance of the localisation systems, the efforts are made from two aspects. Firstly, we focus on improving the accuracy of measurements. After the factors that influence the measurement accuracy are systematically analysed, they are divided into three categories: the hardware precision, the accuracy of signal processing methods and the environmental impact. Then, the effective measurement error reduction approaches are designed for different types of error sources, and their effectiveness is verified in experiments. Secondly, since the measurement error is inevitably in the real-world environment due to signal interference, multipath effect, and none-line-of-sight (NLOS) error, etc., the localisation algorithms with good performance in terms of dealing with measurement noise need to be developed. Moreover, for the practical localisation systems, the computing cost also needs to be considered. Therefore, the accurate and computationally efficient localisation algorithms are evaluated and implemented for the localisation systems, such as the least-squares-based closed-form solutions and the Extended Kalman Filter-based solutions. In addition, the influence of two generic factors, the sensor-target geometry, and the location estimation bias, on the localisation accuracy are also investigated using the experimental data to improve the accuracy of the source location estimates.

1.3   Thesis outline

In the first Chapter, we present the background information relevant to this thesis, covering a broad view of the source localisation research, the motivation of this study, the domain of the research problems addressed in this thesis and the contribution of this thesis.

In Chapter 2, the related works on the measurement techniques and improvement, the source location estimation and optimisation algorithms, and Software Defined Radio (SDR) and its applications are reviewed. The remaining chapters provide a comprehensive description and analysis of our methods and findings.

Chapter 3 introduces a specific SDR device, USRP N210, which is used to de-

velop the source localisation systems in this thesis. To start with, an RSSI-based localisation system is demonstrated using multiple SDR-based transceivers. The detailed system design, experimental implementation and localisation results in both indoor and outdoor environment are presented. Then, the design and development of a practical TDOA-based localisation system using multiple spatially distributed SDRs and a joint TDOA and FDOA-based localisation system using two spatially distributed SDRs are provided.

Chapter 4 evaluates the accuracy of the TDOA measurements and the joint TDOA and FDOA measurements. The sources of the measurement error are systematically analysed from three aspects: the hardware precision, the accuracy of signal processing methods, and the environmental impact. In addition, the solutions to the measurement error reduction are proposed and verified in the experiments.

Chapter 5 presents the algorithms to obtain the source location estimates in the presence of noisy measurements. Two types of computationally efficient algorithms are studied. The least-square-based closed-form solutions are applied to obtain the source location estimates in the TDOA-based localisation with multiple stationary SDRs and the joint TDOA and FDOA-based localisation with one mobile SDR and one stationary SDR. The Extended Kalman Filter (EKF) is another way to update the location estimates when new measurements are available. To further improve the localisation accuracy, the influence of the sensor-target geometry and the location estimation bias are investigated.

Chapter 6, firstly, shows the improved localisation results of the RSSI-based localisation system obtained using the bias reduction algorithms. Then, the experimental setups, the measurement results and the localisation results of the TDOA-based localisation system and the joint TDOA and FDOA-based localisation system are shown. The introduction of the system setups includes the emitters we are using, the environment where the experiments are implemented and the geographic deployment of the SDRs. The measurement and localisation results are assessed against the ground truth, and they are obtained in the real-world environment using the proposed measurement error reduction approaches and the location optimisation algorithms.

The last chapter draws the conclusion, restates the main contribution, and explores other possible research topics that can be developed based on the work of this thesis as the future work.

1.4   Contribution

This work seeks to fill the gap between theoretical study and practical implementation of source localisation systems and deliver reference for researchers who are interested in low-cost source localisation solutions in the real-world environment. To achieve this goal, an RSSI-based localisation system, a TDOA-based passive source localisation system, and a joint TDOA and FDOA-based passive source localisation system are demonstrated using commercial-off-the-shelf low-cost SDR devices. One key feature of this thesis is the study of the source localisation problems from the

perspective of practical localisation systems. The thesis consists of a large number of experimental investigations and analysis and provides a comprehensive study and effective solutions to the practical source localisation problems. The main contributions of this thesis can be summarised as follows:

1. To implement localisation systems, dedicated hardware or circuits are usually designed and manufactured. These conventional localisation systems are expensive, lack flexibility in the system upgrade, and are limited in terms of the achievable functions. For example, they are usually designed for a particular type of signal source or measurement technique. In this thesis, we explored the possibility of developing localisation systems using the new SDR technology, which can bring about the advantages of low cost and great flexibility in system design. To the best of the author's knowledge, this thesis is the first comprehensive study of a universal RF source localisation platform in practice using multiple spatially distributed SDRs, at least when the research was started in Australia in early 2012.

2. When it comes to time-based localisation, accurate time synchronisation among multiple sensors is an important premise. For the TDOA-based localisation using multiple spatially distributed SDRs, based on the investigations of different synchronisation methods, a global time-based synchronisation scheme is proposed, which relies on the GPS signal. The cost of this synchronisation solution is low because GPS receivers are cheap. Moreover, the solution has a wide range of applications because the GPS signal is easy to access. In addition, with the GPS-based synchronisation solution, the distribution of sensors can be large, which enlarges the coverage of the localisation system. Besides the TDOA-based localisation, the synchronisation issue of the practical joint TDOA and FDOA-based localisation is also resolved using this global time-based solution.

3. The implementation of accurate source localisation in the real-world complex signal propagation environment is very challenging. In this thesis, our findings suggest ways to deal with the measurement error and improve the localisation accuracy in the practical source localisation. To deal with the measurement error, the sources of the error are systematically analysed and divided into three categories, and their influences are evaluated. Following that, the methods to deal with each type of error sources are proposed. While the measurement error can be reduced to some extent, their existence is inevitable. When the effect of measurement error reduction methods on the localisation accuracy reaches a limit, the localisation optimization algorithms need to be implemented to further enhance the localisation accuracy. To use the pre-existing localisation algorithms in the practical source localisation, the adjustments need to be made. The results of extensive experiments have verified the effectiveness of our methods in enhancing localisation accuracy in the real-world environment.

Background and Related Work

This Chapter provides a detailed review of the existing works and results that are relevant to the thesis. In the first part, the theoretical results of the source localisation study are reviewed. In Section 2.1, two types of localisation procedure are compared. Section 2.2 introduces the measurement techniques that are widely used in the source localisation, and to improve the measurement accuracy, the methods to resolve outliers are discussed. In Section 2.3, the localisation algorithms that are used to obtain the source location estimates are reviewed. Especially, the approaches to deal with the sensor-target geometry and the location estimation bias are discussed. In the second part, related works on the source localisation implementation are reviewed. Section 2.4 focuses on the related works on the practical implementation of the localisation systems using commercial off-the-shelf SDR devices. A specific series of SDR devices, USRPs, are introduced, and the USRP-based system implementations are reviewed.

2.1 Active localisation and passive localisation

According to whether the signal source participates in the localisation process, the source localisation can be classified into active localisation and passive localisation So [2011]. In active localisation, the signal source or emitter is actively involved in the localisation process. One form of the involvement is that the signal source communicates and transmits useful parameters, such as the signal transmission time, the transmission power and the height of the signal emitter, etc., to the localisation system in a cooperative way to assist it to accurately calculate the source location. For example, in the formation maintenance of a group of UAVs (Unmanned Aerial Vehicle), one way to keep some particular shapes is that each UAV sends the signal with some useful parameters to other UAVs to make sure that they can accurately determine the location of each other Van der Walle et al. [2008]. Another application of active localisation can be found in tracking animals over time and over very wide ranges to answer questions about animal behavior Juang et al. [2002]. VHF transmitter collars can be attached to animals, and to improve the localisation accuracy, the customised signal with easily identified parameters can be transmitted to the localisation system. Similarly, consider deploying a sensor network in an office building,

a shopping mall or a hospital. By carrying a transmitter, the person's location in the building can be determined to avoid getting lost or implementing monitoring. The transmitter can be a user-designed device or a general-purpose device, such as a mobile phone, but the device needs to provide useful information to the localisation system to be accurately localised.

On the other hand, in passive localisation, the signal source does not participate in the localisation process or cooperates with the localisation system. The signal source may not know the existence of the devices that are trying to localise it, or it may even make some effort to avoid being detected and localised by the localisation system. Therefore, the localisation systems need to estimate the value of useful parameters by overhearing the signal transmitted by the source to determine the source location themselves, rather than obtaining assistance from the signal source. The system to receive the signal can be spatially distributed sensors, or a closely placed sensor array, or a combination of them. There are many examples of passive localisation Huang and Barkat [1991]; Chen et al. [2002]; Engelbrecht [1983]. In civilian applications of law enforcement, an illegal radio transmitter or station that violates the local RF regulation needs to be detected and localised. In search and rescue applications, the source of an emergency signal or a rescue signal has to be quickly localised to implement rescue to the people who need help. On the battlefield, it is beneficial to find the enemy signal sources that are used for the communication between enemies or producing interference to the communication signal in order to either cause interference or destroy them. Another type of passive localisation is called device-free passive localisation Youssef et al. [2007]; Xu et al. [2011]. The object can be localised from the change of signal propagation patterns caused by the object.

2.2 Signal sensing and measure

2.2.1 Measurement techniques

Different types of measurements can be used in source localisation, and they are broadly classified into four categories: angle measurements, time measurements, signal strength measurements and frequency measurements. In general, all of the measurement techniques can be used in both active localisation and passive localisation. As for the accuracy, time measurements-based localisation are the most accurate among these types of measurement techniques, followed by angle measurements, frequency measurements, and the localisation using signal strength measurements has the lowest accuracy. For localisation in a large area, signal strength measurements are not suitable to implement source localisation because the signal strength is very susceptible to the change of propagation environment. In contrast, the other three types of measurement techniques can be used in large-scale localisation implementation. In the aspect of measurement complexity, it is simple to obtain signal strength measurements, and signal strength-based localisation has very low cost. However, obtaining time measurements and frequency measurements requires the accurate clock to achieve accurate time and frequency synchronisation, which may cause high

cost. In addition, the acquisition of angle measurements requires multiple antennas, which increases the complexity of the system implementation.

2.2.1.1 Angle of arrival measurements

Angle of arrival (AOA) measurements can be used to localise the signal source by finding the intersection point determined by the AOA measurements, which is obtained by spatially distributed sensors or sensor arrays in the absence of noise. In the presence of noise, the bearing lines pointing from the sensors to the source formed by the AOA measurements will give a region where the source is located, not a single point. AOA measurements can be obtained in two different ways by making use of the receiver antenna's amplitude or RSS response and the antenna's phase response Mao et al. [2007b].

For an anisotropy array or a directional antenna, the beam pattern of the receiver antenna can be rotated electronically or mechanically, and the direction of the maximum signal strength is taken as the direction of the transmitter. The measurement accuracy is relevant to the sensitivity of the receiver and the beam width. Sometimes, two (or more) directional antennas located on the sensors are used. Two directional antennas point in different directions, such that the overlap of their main beams, can be used to estimate AOA from the ratio of their individual RSS value. There is a technical problem by obtaining AOA using RSS or amplitude. When the signal source has varying signal strength, the receiver antenna cannot differentiate the signal strength variation due to the varying amplitude of the signal source and the signal strength variation caused by the anisotropy in the reception pattern. In this case, a non-rotating omnidirectional antenna can be used. By normalising the signal strength received by the rotating directional antenna with respect to the signal strength received by the non-rotating omnidirectional antenna, the influence of the variance of signal strength can be largely reduced Patwari et al. [2005].

The other widely used method to obtain AOA measurements is to measure the phase difference in the arrival of a wave front, known as phase interferometry Rappaport et al. [1996a]. The method typically requires an antenna array. The antenna elements in the antenna array can be organised in different patterns and the pattern of five antenna elements are shown in Figure 2.1. Different antenna array patterns in different environments give different AOA measurement resolution, which is the minimum discernable angle difference between two neighboring AOAs, and the accuracy of measuring angles. The most simple and commonly used antenna array is linear array. Denoting the distance from an RF source signal to the first antenna by η, the phase of the signal arriving at the receiver φ_1 will be

$$\varphi_1 = \frac{2\pi\eta}{\lambda} + \varphi \tag{2.1}$$

where $\lambda = \frac{c}{f_c}$ is the wave length of the signal and c is the propagation speed of the signal. The change of the distance η will change the phase of the received signal. Now a second antenna can be added adjacently to the first antenna and the antenna
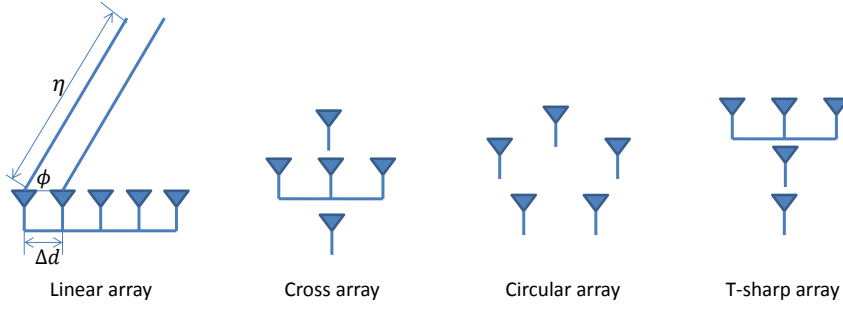
Figure 2.1: Four patterns of antenna array

spacing is Δd. Assuming the AOA of the signal with respect to the two-antenna array is $\phi \in (\frac{-\pi}{2}, \frac{\pi}{2}]$ and, without loss of generality, $\eta \gg \Delta d$. Since the distance from the signal source to the second antenna can be denoted by $\eta + \Delta d \sin \phi$, so a constant phase difference between the two antenna elements can be denoted by $\Delta \varphi = \frac{2\pi \Delta d \sin \phi}{\lambda}$. If the antenna spacing is half of the wavelength, e.g. $\Delta d = \frac{\lambda}{2}$, then $\Delta \varphi = \pi \sin \theta$. As a result, by obtaining $\Delta \varphi$, the AOA measurement can be found as $\phi = \arcsin(\frac{\Delta \varphi}{\pi})$.

The accuracy of AOA measurements is influenced by the multipath and shadowing because AOA measurements rely on a direct line-of-sight (LOS) path from the signal source to the receiver. However, when the multipath effect occurs, the direction of multipath components may be detected as the AOA measurement, which may give large AOA measurement error. The maximum likelihood (ML) algorithms can be used to address multipath problems in AOA measurements Rappaport et al. [1996a]. ML methods estimate the AOA of each separate path in a multipath environment. The implementation of the ML methods is computationally intensive and requires complex multidimensional search. The dimension of the search is equal to the number of paths taken by all the received signals. Another class of methods to calculate AOA is subspace-based algorithms. The most well-known methods in this category is MUSIC (multiple signal classification) Schmidt [1986] and ESPRIT (estimation of signal parameters by rotational invariance techniques) Roy and Kailath [1989]. A vector space formulation is utilised in this eigen analysis-based direction finding algorithms, which takes advantage of the underlying parametric data model for the sensor array problem. Multi-array antenna needs to be used in order to form a correlation matrix using signals received by the array. Utilising an eigen-decomposition of the correlation matrix, the vector space is separated into signal and noise subspaces. Then the MUSIC algorithm searches for nulls in the magnitude squared of the projection of the direction vector onto the noise subspace. The nulls are a function of angle-of-arrival, from which angle-of-arrival can be estimated. ESPRIT is based on the estimation of signal parameters via rotational invariance techniques. It uses two displaced sub-arrays of matched sensor doublets to exploit an underlying rotational invariance among signal subspaces for such an array.

2.2.1.2 Time measurements

Time-based measurement techniques transform the signal propagation time into distance measurements to implement source localisation. Time measurements can be further divided into two categories: Time-of-Arrival (TOA) and Time-Different-of-Arrival (TDOA).

TOA measurements can be further divided into two subclasses: one-way TOA and two-way (or round trip) TOA. One-way TOA measures the time at which a signal first arrives at a receiver. The measured TOA is the time of signal transmission plus a propagation-induced time delay. This time delay between the signal source and the reception sensor is equal to the transmitter-receiver separation distance divided by the signal propagation speed. TOA measurements require accurate synchronisation of the local time between the transmitter and the receiver. This synchronisation requirement may increase the system cost by demanding highly accurate clock and/or system complexity by demanding sophisticated synchronisation mechanism. The "Cricket" system Priyantha et al. [2000] solves the synchronisation problem of one-way TOA measurements by using additional hardware. Both the RF signal and the ultrasonic pulse are used, and they are transmitted at the same time at the transmission side. When the RF signal is received, the ultrasonic signal receiver is turned to listen for the ultrasonic pulse. Since the speed of an RF signal is much higher than the speed of an ultrasonic signal, the time difference between the reception of the RF signal and the reception of the ultrasonic signal is used as the estimates of one-way TOA measurements.

In recent years, ultra-wide band (UWB) signals have been increasingly popular for TOA-based localisation. A signal is considered as UWB if either its fractional bandwidth (the ratio of its bandwidth to its centre frequency) is larger than 0.2 or if it is a multiband signal with total bandwidth greater than 500 MHz. A valuable aspect of the UWB technology is the ability for a UWB radio system to determine the TOA of the transmission at various frequencies. This helps overcome multipath propagation, as at least some of the frequencies have a line-of-sight trajectory. With a cooperative symmetric two-way metering technique, distances can be measured with high resolution and accuracy by compensating for local clock drift and stochastic inaccuracy Aftanas et al. [2008]. The very high bandwidth of a UWB signal leads to very high temporal resolution, making it ideal for high-precision radio location applications Steggles and Gschwind [2005]; Sathyan et al. [2011]; Jones and Hum [2013]; Zhou et al. [2011]; Alsindi et al. [2009]. However, the cost of UWB receivers is higher than the cost of narrowband signal receivers.

One error source of TOA measurements is the additive noise. The estimation of time delay in additive noise is typically obtained by maximising the cross-correlation between the received signal and the known transmitted signal. The generalised cross-correlation (GCC) proposed in Knapp and Carter [1976] extends the signal cross-correlation by pre-filtering the received signal in order to amplify the spectral components of the signal that have little noise and attenuate components with large noise. Another error source of TOA measurements is the multipath effect which

causes even more TOA measurement error than the additive noise. The multipath components from the reflected paths can arrive at a time very close to the LOS signal or severely attenuate or interfere the line-of-sight (LOS) signal, which causes wrong TOA measurements. For a given bandwidth and signal-to-noise ratio (SNR), the TOA measurements can only achieve a certain accuracy. The CRB provides a lower bound on the variance of the TOA measurements in the absence of multipath signals. For a signal with bandwidth B in (Herz), when B is much lower than the centre frequency, f_c (Hz), and the powers of signal and noise are constant over the signal bandwidth, the variance of TOA measurements are lower bounded by Robinson and Quazi [1985]

$$var(TOA) \geq \frac{1}{8\pi^2 B T_s f_c^2 SNR} \tag{2.2}$$

where T_s is the signal duration in seconds. (2.2) presents that the accuracy of TOA measurements is related to the signal duration, the bandwidth and the SNR.

Another type of TOA measurements that does not require the synchronisation between the transmitter and the receiver is the two-way TOA. Two-way TOA measurements measure the difference between the time when a signal is sent by a sensor and the time when the signal returned by a second sensor is received at the original sensor. There is no synchronisation requirement because the same clock is used. The major error source of two-way TOA measurements is the signal processing delay of the second sensor. The use of two-way TOA measurements in localisation is reported in Werb and Lanzl [1998]; Liu et al. [2010]. Liu et al. [2010] presents a synchronisation-free localisation in underwater sensor networks using round-trip TOA measurements.

While two-way TOA measurements do not have the synchronisation problem, it generally requires a high-power transmitter for a long-range implementation and/or the cooperation of the second sensor to send the signal back. Another category of time measurements is TDOA measurements. It measures the difference between the arrival times of the same signal at two sensors. A TDOA measurement does not depend on the clock bias of the transmitting sensor, so it has been used in source localisation for locating asynchronous transmitters for decades. The widely-used TDOA measurement method is the generalised cross correlation. The cross correlation can also be obtained from an inverse Fourier transform of the cross-spectral density function in frequency domain. The accuracy and temporal resolution capabilities of TDOA measurements can be improved by increasing the separation between receivers because this increases the differences between time of arrival measurements. Closely spaced multiple receivers may give rise to multiple received signals that cannot be separated. For example, TDOA measurements of multiple signals that are not separated in time that is more than the width of their cross correlation peaks usually cannot be resolved by conventional TDOA measurement techniques Gardner and Chen [1992]. The accuracy of TDOA measurements is also affected by the multipath effect. Multipath signals can cause overlapping cross-correlation peaks. Even the distinct peaks can be resolved, the correct peak needs to be selected, such as choosing the largest or the first peak Rappaport et al. [1996a]. TDOA-based localisation can be

found in Moeglein and Krasner [1998]; Barnes et al. [2003].

2.2.1.3 Received signal strength measurements

Received signal strength (RSS) is defined as the voltage measured by a receiver's received signal strength indication (RSSI) circuit. RSS is equivalently reported as measured power, i.e., the squared magnitude of the signal strength. Localisation using RSS measurements is relatively inexpensive and simple to implement. However, RSS measurements are notoriously unpredictable, so the localisation error is relatively large. RSS measurements can be used in two ways in source localisation: RSS measurement-based distance estimation and RSS fingerprinting Patwari et al. [2005].

The RSS measurements-based distance estimation is to estimate the distance of a signal source using the attenuation of the emitted signal strength. The method attempts to calculate the signal path loss due to propagation. Different theoretical and empirical models can be used to translate the difference between the transmitted signal strength and the received signal strength into a distance estimate. There are a wide variety of measurement results and empirical evidence Hashemi [1993]; Cox et al. [1984]; Coulson et al. [1998] that support that it is reasonable to model RSS measurements at a certain distance as a random and the log-normally distributed random variable with a distance-dependent mean value. The mean of the received signal strength under log-normal path loss model can be expressed as

$$\hat{P}_i = P_0 - 10\gamma \log \frac{r_i}{r_0} + X_{\sigma_p} \tag{2.3}$$

where P_0 is the received power (dBm) at a short reference distance d_0. γ denotes the path loss exponent in the specific signal propagation environment and its value is typically between 2 to 4. X_{σ_p} is a zero mean Gaussian distributed random variable with standard deviation σ_p and it accounts for the random effect of shadowing Rappaport et al. [1996b]. The shadowing is an environment-dependent error in RSS measurements and it causes the attenuation of the signal due to obstructions (e.g. walls, furniture, buildings and tree, etc.) that a signal must pass through or diffract around on its propagation path. Another factor that causes inaccurate RSS measurements is the multipath. In the presence of multipath, multiple signals with different amplitudes and phases that arrive at the receiver can add constructively or destructively as a function of the frequency, causing frequency-selective fading. The effect of this type of fading can be reduced by using a spread-spectrum method Durgin [2003].

The path loss exponent (PLE) is a key parameter in the log-normal model. It is an oversimplification to assume a free space environment, therefore, the PLE is usually obtained through extensive channel measurements and modeling by measuring both RSS and distances in the same environment prior to system deployment. A constant PLE can be used to estimate the distances among different transmitter-receiver links, or different PLEs for the links can be used to improve the distance estimation accuracy Shirahama and Ohtsuki [2008]. However, the estimation accuracy of the

PLE may decrease because the channel characteristics may change considerably over a long period of time due to seasonal changes and weather changes. To solve this problem, several techniques have been proposed for online calibration of the path loss exponent in Mao et al. [2007a]. Instead of relying on distance measurements, the PLE can be estimated using only the received signal strength and the geometric constraints associated with planarity in a sensor network. After the PLE is obtained, if the transmission power of the signal source is known, distance measurements can be obtained from RSS measurements. If the transmission power is unknown such as implementing emitter localisation in hostile or inaccessible environments, the transmitter's power can be considered as an unknown parameter to be estimated Bishop [2011]; Gorji and Anderson [2013]. An alternative method is to consider only the difference between the RSS value measured by pairs of receivers, which is analogous to time difference of arrival (TDOA) measurements. The RSS difference (RSSD) between two sensors indicates information about their relative distance from the emitter and removes the dependence on the actual transmitter power Lohrasbipeydeh et al. [2014a,b].

RSS fingerprinting is the second alternative method to use RSS measurements to determine emitter location Bshara et al. [2010]. The method is generally implemented in two phases. In an offline phase, the RSS fingerprints associated with each location across a whole given area are obtained to create a database. Location estimates are then obtained in the online phase by matching observations of RSS to the database using pattern recognition techniques. The advantage of the fingerprint is a large gain in the SNR and less sensitivity to multipath effect and NLOS conditions. RSS fingerprinting-based localisation is proved to provide better performance than the localisation using RSS measurement-based distance estimates Bshara et al. [2010]. Not only does the accuracy of RSS fingerprinting-based localisation depend on the accuracy and the resolution of obtained RSS fingerprints, it is also affected by the matching/recognition algorithms. Many RSS fingerprinting-based localisation algorithms have been proposed Alsindi et al. [2014], such as k-nearest neighbor (kNN), probabilistic, neural networks and support vector machines. The performance of RSS fingerprinting-based indoor localisation and outdoor localisation has been analysed in Wen et al. [2015] and Arya et al. [2009].

2.2.1.4   Doppler shift measurements

When there is a relative movement between the target and the sensors, one can obviously gain important additional information about the source location by measuring the Doppler shift. If adequate number of receivers is available, Doppler shift measurements are sufficient to determine the source location or trajectory when other measurement techniques are not reliable. The idea of using the Doppler effect for localisation can be found in applications like radar, sonar, passive location systems (both for radio signals and acoustic signals), satellite positioning and navigation Xiao et al. [2010]; Shames et al. [2013]; Ristic and Farina [2013]; Amar and Weiss [2008]; Nguyen and Dogangay [2015]. The Doppler shift-based localisation mainly focuses

on examining the observability of a Doppler-shift sensor system Xiao et al. [2010]; Shames et al. [2013], developing target localisation and tracking algorithms for different applications Ristic and Farina [2013]; Amar and Weiss [2008] and evaluating the performance of the localisation under different sensor-target geometries Nguyen and Dogangay [2015].

An alternative use of Doppler effect in source localisation is differential Doppler (DD), also known as frequency difference of arrival (FDOA). FDOA consists of measuring frequency differences between receivers since it eliminates the need to know the exact transmit frequency. The FDOA can be obtained by estimating the frequency at each receiver and then computing the difference Chestnut [1982] or by directly measuring the frequency difference using the cross correlation of signals Stein [1993]. A more common use of FDOA information in source localisation is to combine TDOA and FDOA measurements, known as joint TDOA and FDOA-based localisation Amar et al. [2012]; Yeredor and Angel [2011]; Ho and Chan [1997]. The combination of Doppler shift or FDOA measurements with other measurement techniques can be found in Papakonstantinou and Slock [2009]; Luo et al. [2013]; Sprang [2015].

2.2.2   Measurement outlier detection and removal

Outliers can be defined informally as an observation that appears to deviate markedly from other members of the sample in which it occurs Hodge and Austin [2004]. The causes of outliers are generally divided into three aspects Yang et al. [2013a]. Firstly, the measurements will be meaningless if hardware malfunction or failure happens. Moreover, incorrect hardware calibration and configuration also deteriorate measurement accuracy. For example, AOA measurements are wrong if the phases of antenna elements in the antenna array are not aligned. The inaccuracy of clock synchronisation results in distance measurement error. RSS measurements suffer from the variability of transmitter, receiver and antenna. Secondly, environmental factors can influence measurement accuracy. For example, RSS is sensitive to channel noise and interference, all of which influence RSS measurements significantly, especially in complex indoor environments. Multipath and shadowing effects have large impact on the accuracy of AOA measurements and TOA/TDOA measurements. Moreover, for the propagation time-based ranging measurements, the signal propagation speed often exhibits variability as a function of temperature and humidity, so the propagation speed across a large field cannot be assumed to be constant. Thirdly, the localisation infrastructure is becoming the target of adversary attacks because location-based services are increasingly prevalent. By reporting fake location or ranging results, an attacker node can completely distort the coordinate system and cause measurement outliers.

The sample mean $\hat{\mu}$ and the sample standard deviation $\hat{\sigma}$ are usually used as metrics to qualify the variance of measurements. Their mathematical representations

are given by the following equations:

$$\hat{\mu} = \frac{1}{n} \sum_{i=1}^{n} a_i \tag{2.4}$$

$$\hat{\sigma} = \sqrt{\frac{1}{n-1} \sum_{i=1}^{n} (a_i - \hat{\mu})^2} \tag{2.5}$$

where n is the number of measurements and a_i is the ith measurement. The Maximum-Likelihood Estimator (MLE) maximises the likelihood (or minimises the negative log-likelihood) of signals with a given distribution function $f(x)$ Kay [1993]. It estimates the signal parameters, μ_{MLE} and σ_{MLE}, proportional to the probability of a signal measurement inside the measurement set by

$$\hat{\mu}_{MLE} = arg \min_{\hat{\mu}} \sum_{i=1}^{n} -\log(f(a_i - \hat{\mu})) \tag{2.6}$$

$$\hat{\sigma}_{MLE} = arg \min_{\hat{\sigma}} \sum_{i=1}^{n} \log(\hat{\sigma}) - \log(f(\frac{a_i - \hat{\mu}_{MLE}}{\hat{\mu}_{MLE}})) \tag{2.7}$$

(2.6) returns the value of $\hat{\mu}$ which minimises the function $\sum_{i=1}^{n} -\log(f(a_i - \hat{\mu}))$ and (2.7) returns the value of $\hat{\sigma}$ which minimises the function $\sum_{i=1}^{n} \log(\hat{\sigma}) - \log(f(\frac{a_i - \hat{\mu}_{MLE}}{\hat{\mu}_{MLE}}))$. arg min defines a function that returns the parameter value that minimises the value of the function. If the distribution functions of measurement model cannot be specified, M-estimators Huber [2011] which use a loss function rather than a measurement distribution function can be used.

The outliers will affect the localisation results because they appear to violate the conditions or boundaries of the experimental design, so effective methods to identify and detect the outliers in a set of measurements need to be implemented. For distance-based localisation, a straight-forward solution to detect outliers is to judge graph embeddability based on triangle inequality. A graph-violating triangle inequality is, by no means, embeddable. However, the use of triangle inequality may fail to detect outliers, and for a triangle violating the inequality, one can detect at least one distance measurement is incorrect but cannot identify them. To solve the problem, a graph rigidity theory-based outlier detection method is proposed for wireless sensor network localisation in Yang et al. [2013b]. The concept of verifiable edges is proposed and the condition for an edge to be verifiable is derived as the basis to detect outliers. The method explicitly eliminates the distance measurements with large errors before location computation, thus increasing location accuracy.

The RANdom SAmple Consensus (RANSAC) algorithm is a general parameter estimation approach designed to cope with a large proportion of outliers in the input data Fischler and Bolles [1981]. Unlike conventional sampling techniques that use as much of the data as possible to obtain an initial solution and then proceed to prune outliers, RANSAC uses the smallest set possible and proceeds to enlarge this set with consistent data. The basic algorithm is summarised as follows Derpanis [2010]:

- Step 1: Randomly select the minimum number of measurements required to determine the model parameters.

- Step 2: Solve for the parameters of the model.

- Step 3: Determine how many points from the set of all points fit with a predefined tolerance ϵ.

- Step 4: If the fraction of the number of inliers over the total number points in the set exceeds a predefined threshold, re-estimate the model parameters using all the identified inliers and terminate.

- Step 5: Otherwise, repeat steps 1 through 4.

In addition, Picard and Weiss [2010] derives the bound on the number of identifiable outliers for AOA, RSS, TOA and TDOA-based localisation. It is shown that the measurement set corrupted by unknown outliers can be solved correctly, provided that the number of outliers does not exceed a bound. The proposed solution formulate nonlinear localisation problem using linear equations, then define an optimisation problem in terms of ℓ_1 norm minimisation and solve the optimisation problem using efficient linear programming methods.

After outliers are identified, one can remove or give it a lower weighting in the localisation procedure. As a result, the error in location estimates can be reduced.

2.3 Source location estimation and localisation optimisation

Source localisation uses a number of spatially separated sensors that measure the emitted signal from the source. Then the source location is determined using the measured signal parameters, such as AOA, RSS, TOA, TDOA and FDOA. Solving localisation problem is challenging because of the highly nonlinear relationship between the measurements and source location. In order to obtain more accurate localisation results, it is also necessary to make the effort to reduce the influence of some factors to obtain optimised estimation results. In this section, widely used source localisation algorithms will be reviewed. Moreover, the algorithms that are used to deal with two generic factors that influence the accuracy of most of the location estimation will also be investigated.

2.3.1 Source location estimation

There is a rich literature of source localisation techniques. As summarised in Huang et al. [2001], the difference between them includes likelihood-based versus least-squares and linear approximation versus direct numerical optimisation (maximisation or minimisation), as well as iterative versus closed-form algorithms.

The ML estimator (MLE) has been proven to be asymptotically consistent and efficient, so several localisation algorithms have been proposed based on the maximum likelihood (ML) principle. To find the solution to the MLE, a linear approximation

and iterative numerical techniques have to be used because of the nonlinearity of the equations. For example, the Newton-Raphson iterative method Nash and Walker-Smith [1987], the Gauss-Newton method Foy [1976], and the least mean squares (LMS) algorithm can be used. However, for these iterative approaches, a carefully chosen initial guess that is near the actual solution is required. In addition, one could end up with a local minimum solution and convergence to the optimal solution cannot be guaranteed. Therefore, the ML-based estimator may not be a suitable choice for practical source localisation systems, especially passive localisation in which no prior knowledge on the source location is available.

To obtain location estimates, another alternative is to use a closed-form solution Cheung et al. [2006]. Closed-form solutions are not iterative and avoid the local convergence problem, so they are desired and appropriate for practical localisation systems. Triangulation-based estimation is the most straightforward closed-form solution Wang and Chu [1997], but it cannot take advantage of extra sensors and the measurement redundancy. Currently, most closed-form algorithms use a least-squares principle, which makes no additional assumption about the distribution of measurement errors. A closed-form solution which employs a spherical LS criterion is proposed in Schau and Robinson [1987] and it is termed as spherical intersection (SX). While it is mathematically simple, the SX procedure requires a priori knowledge for the source range, which may not exist or may not be unique in the presence of measurement errors. On the basis of the same criterion, Abel and Smitht [1987] proposes the spherical interpolation (SI) method which also uses a least-square method, but the solution is not optimal. Chan and Ho [1994] improves the SI estimation by developing a well-known closed-form solution through nonlinear parameter transformation, which can be used as an approximation of the maximum likelihood (ML) estimator. It has been shown in both theory and simulation that the solution reaches the Cramer-Rao lower bound (CRLB) accuracy under Gaussian noise at moderate to high SNR, especially when the source is distant.

Recently, convex optimisation techniques have been applied in source localisation. The maximum likelihood estimation for source localisation problem is a non-convex optimisation problem. If the original problem can be transformed into a convex optimisation problem by relaxing measurement constraints, cheap and scalable algorithms can be applied. The optimisation techniques can be grouped into two categories: seconder order cone programming (SOCP) and semidefinite programming (SDP). Both categories apply various types of relaxation methods to the original problem to arrive at convex SOCP Biswas et al. [2006] and SDP Yang et al. [2009]; Tseng [2007] problems.

Apart from using a deterministic model to describe the localisation problem, a probabilistic model can also be applied and so the problem can be solved using Bayesian approaches. A recursive optimal Bayesian estimator for a linear state-space model with Gaussian noises (process and measurement) is given by the Kalman filter. Unfortunately, this solution is not applicable to the localisation problem due to the nonlinear relationship between the state (position) and the measurements Levy et al. [2011]. A detailed survey of Bayesian techniques for location estimation is provided

in Fox et al. [2003]. Among them, due to its robustness, Extended Kalman filter (EKF) is by far the most widely used algorithm for problems in localisation and navigation Leonard and Durrant-Whyte [1991].

2.3.2   Localisation optimization with optimal sensor-target geometry and localisation estimation bias reduction

In this thesis, special attention has been paid on two generic factors that influence the accuracy of almost all localisation systems. They are sensor-target geometry and location estimation bias.

2.3.2.1   Localisation with optimal sensor-target geometry

It is well known that relative sensor-target geometry can significantly influence the potential performance of any particular localisation algorithm Gustafsson and Gunnarsson [2005]. The Cramer-Rao bound (CRB) is a function of the relative sensor-target geometry along with the specific measurement technology employed by the sensors. A number of authors have attempted to identify the geometric configurations that minimise some measure of the variance lower bound. Popular measures of the optimal design criterion are T-optimality, which maximises the trace of the Fisher Information Matrix; E-optimality, which maximises the minimum eigenvalue of the Fisher Information Matrix and D-optimality which explores to maximize the determinant of the Fisher Information Matrix Ucinski [2004]. The FIM quantifies the amount of information that the observable random measurements carry about the unobservable parameters to be estimated. The CRB matrix is related to the FIM by taking the inverse matrix operation.

Different localisation scenarios have been considered in the design of optimal sensor-target geometry. Most of studies consider static localisation problems with a single stationary target and multiple stationary sensors located in two-dimensional space. Bishop et al. [2010] analyses, in depth, the geometry of the optimal sensor-target angular geometries for range-only and TOA-based localisation. It is shown that the optimal sensor-target angular geometries for range-only and TOA-based localisation are not unique. An infinite number of optimal sensor-target geometric configurations can be found if the number of sensors exceeds a certain small number. In addition, the optimal sensor-target angular geometries for bearing-only localisation is also explored for an arbitrary number of sensors and for fixed, but arbitrary, sensor-target ranges. Unlike range-only and TOA-based localisation which is independent on the sensor-target range, the optimal sensor-target geometry for bearing-only-based localisation is explicitly dependent on the sensor-target ranges and the change of even a single sensor-target range can change the optimal geometry significantly. Again, the optimal sensor-target angular geometries for bearing-only localisation is not unique and an infinite number of optimal configurations can be identified when the number of sensors exceeds a small number. In addition, the optimal sensor-target angular geometries for TDOA-based localisation, is studied in

Meng et al. [2011, 2012]. They study two types of sensor pairing, the centralised sensor pairing and the decentralised sensor pairing. It is shown that the optimal sensor pair geometry does not depend on the ranges between the source and sensors. It only depends on sensor-target angular geometries. Furthermore, in the optimal sensor-source geometry setting, any sensor can be chosen as the reference, which results in the same lower bound of the localisation performance. For decentralised sensor pairing, under the condition without sensor sharing in a group of sensors, to achieve the optimal sensor pair geometry, two factors need to be met: 1) large angle between a pair of sensors that subtend to the target and 2) large intersection angle among different sensor pairs. Moreover, the optimal sensor-target geometry for hybrid localisation are also studied, such as AOA/scan-based localisation Dogançay [2007].

As an extension of the static localisation problem, the optimal sensor-target geometry of mobile localisation with either mobile sensors or mobile targets is also studied. This is known as optimal trajectory. The optimal trajectory is usually obtained from the optimal sensor-target geometry at each time instant. Similar to the static case, the measure in the mobile case is generally the same, but instead of taking measurements once in the static case, the measure needs to be implemented at every time instant during the movement of either the sensors or the targets in the mobile localisation problem. The study of optimal trajectory is usually followed by the motion coordination of the sensors to meet the condition of optimal trajectory to reduce the localisation error. If the target is mobile, the extended Kalman filter (EKF) is used to track the target Oshman and Davidson [1999]; MartíNez and Bullo [2006]; Bishop and Pathirana [2008]; Meng et al. [2012]; Kaune and Charlish [2013].

2.3.2.2   Localisation geometric constraints

When conditions of optimal sensor-target geometry or optimal trajectory are met, the localisation accuracy can be improved. Another way to use the geometric information to improve the localisation accuracy is to implement the constrained optimisation during the process of location estimation using the underlying sensor-target geometry, so the localisation problem can be formulated as a constrained optimisation problem. Bishop et al. [2008] derives a constraint for range-difference-of-arrival based localisation of a stationary emitter, which accounts for the relationship among the underlying geometry, the measurements and the nature of the true measurement errors. With the constraints, the measurement error which is consistent with the geometrical requirements can be estimated to correct the noisy measurements. Another constrained optimisation algorithm is derived following the similar principle for bearing-only localisation Bishop et al. [2009]. In addition, when more than one emitters need to be localised, the emitter-emitter distance can also be used as a geometric constraint in the constrained optimisation process for emitter localisation Ekanayake et al. [2012].

2.3.3   Location estimation bias reduction

A localisation process normally involves a nonlinear transformation of the measurements. Once the measurements are noisy, it is then virtually guaranteed that, from the nonlinear processing of noisy measurements to achieve localisation, biased location estimates will be obtained. Therefore, enhancement techniques have been proposed to reduce the bias, hence improving the localisation accuracy.

Ho [2012] proposes two different methods to reduce the localisation bias, called BiasSub and BiasRed. In the first method, BiasSub, the theoretical bias is obtained and the expected bias is subtracted from the estimated positions to improve the localisation accuracy. The second method, BiasRed, expands the parameter space and imposes a quadratic constraint to reduce the bias. Though different techniques are applied in these two methods, both of them can reduce the localisation bias considerably, as they are demonstrated by the simulation results. Nevertheless, the proposed two bias reduction methods are restricted to localisation algorithms with TOA and TDOA measurements. Moreover, in Gavish and Weiss [1992], the performance of two well-known bearing-only location algorithms is examined, viz. the maximum likelihood and the Stansfield estimators Wang et al. [2013]. Analytical expressions are derived for the bias, which permit performance comparison for any case of the two algorithms. In order to obtain the analytical expressions for bias, the first derivative of the maximum likelihood cost function is expanded by a Taylor series. Three expansions of different orders are obtained separately. The final expression for the bias involves the variance of the measurement noise and various derivatives of the cost function. To take a further step, a generic approach that is independent of the type of measurements is proposed in Ji et al. [2013] to correct the bias in two-dimensional and three-dimensional localisation algorithms with an arbitrary number of independent usable measurements. The analytical expressions of bias are obtained by expanding the localisation mapping, which maps from the measurements to produce location estimates, by a Taylor series to second order in the measurement noise and then obtains the expected values of the second-order term. The effectiveness of this localisation bias reduction algorithm is illustrated in simulation in localisation problems with distance, bearing-only and TDOA measurements.

2.3.4   Robust geolocation in mixed LOS and NLOS environment

In the practical localisation, the LOS signal propagation path does not always exist. When the signal propagation path between the sensor and the source is blocked in an environment with complex buildings or in dense urban areas, the NLOS error will be produced in the measurement. Actually, the NLOS error is a generic problem for most of localisation systems and it will significantly degrade the localisation performance. Various methods have been proposed to mitigate the effect of NLOS error and they can be classified into four types of methods according to Guvenc and Chong [2009], namely, the maximum likelihood (ML)-based method, the least squares (LS) method, the constrained localisation method, and the identify-and-discard method.

ML approaches for NLOS mitigation require prior knowledge regarding the distribution of NLOS bias. Riba and Urruela [2004] considers several hypothesis for different sets of sensors, and then, using the ML principle, the best set which is composed of sensors with LOS propagation path is selected for location estimation. The LS techniques can be used to suppress the effects of NLOS error, through some appropriate weighting. A simple realisation is to put less weight on NLOS term in the LS solution. In Caffery and Stuber [1998], by assuming the variances of the distance measurements are larger for the sensors affected by NLOS error, the inverses of these variances are used as a reliability metric for the calculation of the weights. An alternative weighting technique is to use certain statistics of the multipath components of the received signals, such as kurtosis, mean excess delay, and root mean square (RMS) delay, to evaluate the likelihood value of the received signal to be LOS. The likelihood values are then used to evaluate the weights Güvenç et al. [2007]. Constrained localisation methods can be achieved using four techniques: quadratic programming Wang et al. [2003], linear programming Venkatesh and Buehrer [2007], geometry-constrained location estimation Chen and Feng [2005] and interior point optimisation Kim et al. [2006]. The simplest way of NLOS mitigation is achieved by identifying and discarding the NLOS sensors, and estimating the source location by using one of the LOS techniques. However, this method could also cause the problem of false-alarms, which identifies an LOS sensor as an NLOS sensor, and missed detections, which identifies an NLOS sensor as an LOS sensor. Both of the cases will degrade the localisation accuracy.

To use the methods discussed above to resolve NLOS error in source location estimation, two conditions need to be met: 1) knowing partial statistic information of the NLOS errors, and 2) knowing the NLOS status or its probability for all paths. However, in practical localisation, it is hard to promise them. Firstly, the statistics of the NLOS errors are not easy to obtain due to the environmental variances. Secondly, detection errors during detection of the path status always exist. To release these requirements, Wang et al. [2014] proposed several localisation methods using second-order cone relaxation (SOCR) and semi-definite relaxation (SDR) techniques, including a robust SDR method [8]. These methods do not require any statistics of the NLOS errors to be known. They only requires the upper bound of the NLOS errors to be known. More importantly, the robust SDR method is not sensitive to detection errors, and, thus, it can be widely used in practice. Moreover, Wang et al. [2016] took a further step from TOA-based localisation to propose robust TDOA-based localisation algorithms under NLOS conditions using convex approximation. The motivation is that the error caused by the NLOS condition in a TDOA measurement can be negative and/or small in magnitude due to potential cancellations of the NLOS errors at different sensors. In contrast, the NLOS error in a TOA measurement is always non-negative. In addition, in TDOA based localisation, the error caused by the NLOS condition is the difference of the NLOS errors incurred at two different sensors, which will complicate the implementation of maximum-likelihood estimators.

Company	Model	Frequencies	Software	Description
Ettus Research	USRP200 Series	50 MHz~4.4 GHz	GNU Radio	Tx&Rx
FlexRadio Systems	FLEX-3000, FLEX-5000	10 kHz~65 MHz	FlexRadio PowerSDR	Tx&Rx
Microtelecom	PERSEUS	VLF-LF-MF-HF	SDRDK	Rx
Simple Software Radio Peripheral	SSRP	0~15MHz	GNU Radio	Tx&Rx
Saelig	RTG003	up to 60 MHz	N/A	Rx
SRL QuickSilver	QS1R	15 kHz ~ 55 MHz	SDRMAX	Rx

Table 2.1: Comparison of available SDR Products

2.4 Software defined radio-based system implementation

2.4.1 Commercial off-the-shelf SDR products (hardware and software)

Software defined radio (SDR) is a relatively new technology which allows for great improvements in the capability and flexibility of conventional radio systems, and which should, theoretically, be applicable to a wide field of communications and sensor systems. The concept behind SDR is to minimise the amount of specialised hardware required and to implement the majority of components (and, hence, the desired functionality) in software. In recent years, SDR technology has been developed rapidly; many commercial SDR products and techniques are available. At the time when this research was started (early 2012), we have evaluated the capability of several SDRs available in the market. As can be seen from Table 2.1, there are many products available which offer different frequency coverage and features for various applications.

After comparing the characteristics between different products, the USRP devices developed by Ettus Research Ettus [2008] are chosen to implement our research because they provide good trade-off between the cost and the system performance. Moreover, there are some other good features that helped us choose them. The USRPs are compilable with many different daughter boards to provide different frequency coverage and a different number of receiving and transmission channels. They use configurable FPGA and expansion interfaces, such as GPSDO (GPS disciplined oscillator) and MIMO (Multi-input Multi-output). The development software of the USRPs is GNU Radio which is an open source framework for the development of software defined radios, and the "gnuradio-discussion" forum is a useful resource for problem solving and technique learning. All the features of the devices not only meet our demand at that time but also enable us to implement cost-efficient expendable development and applications in the near future without the replacement of devices.

With the rapid development of SDR technology, Ettus Research has continuously launched new USRP products to meet different demands for research and commercial purposes. The USRP products are mainly classified into four categories: USRP X Series, USRP Networked Series, USRP Bus Series and USRP Embedded Series. The USRP X Series are high-end products, which include USRP X310 and USRP X300. They can be used to design and deploy next generation wireless communications systems. Its hardware architecture combines two extended-bandwidth daughterboard slots covering DC $\sim$ 6 GHz with up to 120 MHz of baseband bandwidth, multiple high-speed interface options (PCIe, dual 10 GigE, dual 1 GigE), and a large user-programmable Kintex-7 FPGA in a convenient desktop or rack-mountable half-wide 1U form factor.

With around one-third of the price of the USRP X Series, USRP Networked Series are very popular for SDR-based development and applications. They are intended for demanding communications applications requiring this type of rapid development. It can also cover DC $\sim$ 6 GHz, but only achieve 40 MHz of baseband bandwidth. The data stream interface between the USRP and the host processor is through Gigabit Ethernet connection. The product is particularly suitable for multi-SDR development and applications as it has an expansion port that allows multiple USRP N210 series devices to be synchronised and used in a MIMO configuration. An optional GPDSO module can also be used to discipline the USRP N210 reference clock to within 0.01 ppm (parts per million) of the worldwide GPS standard. Apart from USRP N210, this series also include USRP N200, which uses a different FPGA and has a slightly low price than USRP N210.

Another category of URSP is the USRP Bus Series, which includes USRP1, USRP B200/B210 and USRP B200mini/B210mini. The USRP1 is the first generation of USRP and provides entry-level RF processing capability. The size of USRP1 is similar to USRP N210. USRP B200/B210 provides a fully integrated, single board solution and it is designed for low-cost experimentation. Different from the previous products, which require additional power supply, they are USB powered. The products offer continuous frequency coverage from 70 MHz $\sim$ 6 GHz and combine a fully integrated direct conversion transceiver providing up to 56MHz of real-time bandwidth. Instead of using Gigabit Ethernet connection, USRP B200/B210 has a high-speed USB 3.0 connection for streaming data to the host computer. The newly released USRP B200mini and USRP B210mini are in the amazing size of a business card. The USRP B200mini also includes connectors for GPIO, JTAG, and synchronisation with a PPS trigger or 10 MHz reference input signal. The USRP Bus Series is half the price of the USRP Networked Series.

The USRP E310 belongs to the USRP Embedded Series and it is a pocket sized, stand-alone software defined radio. It provides 2x2 MIMO support covering 70 MHz $\sim$ 6 GHz and up to 56 MHz of instantaneous bandwidth. At roughly the footprint of a mobile phone, with a typical power consumption of 2$\sim$6 watts, the USRP E310 is ideal for mobile and embedded applications with limited size, weight, and power requirements. The price of the USRP E310 is a little lower than the USRP X Series, but higher than other USRP series.

Software is an important part for the system development using USRPs. The software should provide cross-platform code portability and flexible design, which enables system developers to maximise their productivity and minimise development effort. The SDR supported software is UHD (USRP Hardware Driver), GNU Radio, RFNoC, LabVIEW and MATLAB Simulink as they are listed on the official Ettus Research website EttusResearch [2014]. Among them, the UHD and GNU Radio are supported by all USRP SDRs.

USRP Hardware Driver   The UHD is the official driver for all Ettus Research products, as shown in Figure 3.1 (b). It supports Linux, Mac OSX, and Windows. The UHD implements a full network stack so that it is routable and does not need root access or custom drivers. The functionality provided by the UHD can also be accessed directly with the UHD API, which provides native support for C++. Any other language that can import C++ functions can also use UHD. This is accomplished in Python through SWIG. Two important classes are *uhd::usrp::multi usrp* and *uhd::device*. The former class provides a high level interface to one or multiple USRPs and it is the class that is used to manipulate the RF parameters of the USRP. For example, it is used to control centre frequency, bandwidth, gain, channel selection and the antenna. It is also used to start transmit or receive streams. The latter class is the low level interface to the USRP. This API is used for discovering USRP devices, reading and writing device parameters, and controlling "low level" data streams, i.e. transmit/receive samples with meta-data Kelly [October, 2012].

GNU Radio   GNU Radio is a free and open-source software development toolkit that provides signal processing blocks to implement software defined radios. It can be used with readily-available low-cost external RF hardware to create software-defined radios, or without hardware in a simulation-like environment. It is widely used in hobbyist, academic and commercial environments to support both wireless communications research and real-world radio systems. GNU Radio applications are primarily written using the Python programming language, while the supplied, performance-critical signal processing path is implemented in C++ using processor floating point extensions where available. Thus, the developer is able to implement real-time, high-throughput radio systems in a simple-to-use, rapid-application-development environment GNURadio [2012]. GNU Radio provides blocks one can use to access the UHD and it also provides a tool called GNU Radio Companion (GRC) which is a graphical tool for creating signal flow graphs and generating flow-graph source code.

A WBFM (Wide Band FM) receiver built using a USRP N210 which can receive signal from a FM radio station is shown in Figure 2.2. After received by the *UHD USRP source* block, the signal is demodulated by block *WBFM Receive* and re-sampled by the block *Rational Resampler* to fit the frequency of speaker on PC connected by *Audio Sink*.

GMSK transceivers developed using USRP N210s are shown in Figure 2.3 respectively. At the transmit side, an audio signal is stored in a *wav* file as the file source
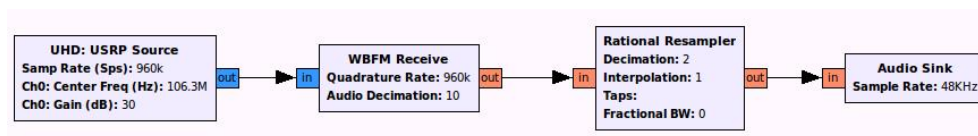
Figure 2.2: A WBFM receiver developed using the GRC
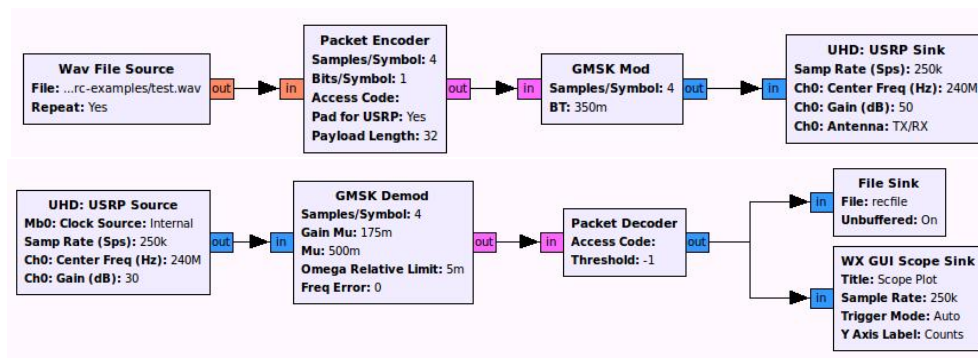
Figure 2.3: GSMK transceivers developed using the GRC

and sent to the USRP for transmission at a frequency of 240Mz, having first been packetised and modulated using GMSK. At the receive side, the signal is received by the USRP source, where it is demodulated, decoded and stored in a binary data file. The waveform of the received signal can also been displayed on the host computer.

2.4.2 Related work on SDR-based system design and implementation

In recent years, SDRs have become a favorite platform for researchers to evaluate theoretical work in practice. Paired with specific daughter-boards, the USRP products are capable of processing signals from DC to 6GHz. In Di et al. [2012], USRP N210 and two daughter-boards, RFX1200 and RFX1800, are used to develop a GNSS and interference signal generator and playback system. The generation of GPS L1, L2C and L5 signal using code division multiple access (CDMA) technology and the GLONASS signal using frequency division multiple access (FDMA) modulation technology is demonstrated. The SDR platform is also used to evaluate the effectiveness of Wireless Network Coding (WNC) in lab-scale experiments by modifying the MAC and PHY layers of the 802.11 protocol stack in Firooz et al. [2013]. It demonstrates that the design of MAC layer network coding improves system throughput by 20% ∼ 30%, and the design and implementation of OFDM-based PHY layer network coding increases throughput by 30% comparing to the traditional 4-step TDMA exchange. In addition, a cooperative testbed is developed using USRP and GNU Radio to evaluate the performance of various cooperative communication schemes in Zhang et al. [2010]. Both single-relay cooperation and multi-relay cooperation can be supported in the testbed. Some key techniques to do maximum ratio combine and synchronised transmission among multiple nodes in this testbed are provided. The benefits

of cooperative communication in enhancing the transmission reliability by exploiting spatial and user diversity are demonstrated through extensive experiments rather than simulation. Distributed beamforming is a cooperative transmission technique that can achieve orders of magnitude increases in range or energy efficiency of wireless communication systems. Quitin et al. [2013] demonstrates that the theoretical beamforming gains can be attained with commodity SDR hardware with moderate overhead. The precise synchronisation of multiple transmitters is achieved through periodically transmitted feedback packets from the receiver. The implementation is in a fully wireless way and it can be used in wireless networks without requiring hardware innovations. In De Donno et al. [2013], the RFID reader and listener are developed using SDRs. Different timing recovery schemes for the reception of the RFID tag signal in the uplink are tested. In addition, the impact of spectral nulls induced by the multipath in the uplink RFID channel is evaluated for different indoor scenarios and the maximum "uplink range" of a conventional RFID system is measured.

While SDRs have been used as popular devices for many different applications, the use of multiple SDRs in localisation is few at the time when our research topic was proposed in early 2012. To the best of our knowledge, our work is the first laboratory-based demonstration of practical passive source localisation using multiple spatially distributed SDRs in the world or at least the first in Australia. With the SDR devices becoming increasingly popular, SDR-based localisation began to attract researchers' attentions. The SDRs have been used to demonstrate many localisation systems using different measurement techniques, including RSSI, AOA, tow-way TOA and TDOA.

In Alyafawi et al. [2014], an indoor passive localisation system is demonstrated using software defined radios. A GSM capturing tool is developed using the USRP and the SBX daughter-board, and the RSSI measurements of the GSM signal are obtained using multiple SDRs to implement source localisation. The location of the GSM source is estimated using two proximity-based algorithms: Combined Differential RSS (CDRSS) and Weighted Circumcentre (WCC). The experiments are implemented on a floor of a multi-story office building with the size of 17m by 23m. The average localisation error is 3.21m for CDRSS algorithm and 2.43m for WCC algorithm, which are lower than the average localisation error obtained using the traditional linear weighted centroid. This work was published in August 2014. In our research group, a generic location estimation bias reduction algorithm for source localisation Ji et al. [2013] has been proposed. The advantage of the algorithm is that it can be applied in different measurement techniques. While the algorithms are verified in simulation, the performance of the algorithm in practical localisation is unknown. Therefore, in late 2013, we came up an idea to implement an RSSI-based localisation system using multiple SDRs to verify the bias reduction algorithm in practical range-based localisation because RSSI-based localisation is simple and the experiment can be implemented in a small area. Both the transmitter (target) and the receivers (anchors) are developed using USRP N210s. The experiments are implemented in a 8m by 10m office Wei et al. [2014] and a 12m by 15m outdoor area Ji et al. [2015]. The area of the implementation is restricted to a small area due to

the limited transmission power of the SDR transmitter. The localisation results show that the localisation error is reduced by 50% to 80% for both indoor and outdoor localisation after the bias reduction algorithm is implemented.

SDRs can also be used to measure the angle of arrival of the signal source and implement AOA-based localisation. One way to measurement AOA is to use one SDR together with an antenna array, but a more interesting and challenging way to obtain AOA measurements is to develop an antenna array using multiple SDRs because the frequency and the phase of multiple SDRs have to be accurately synchronised. In Chen et al. [2012], an antenna array is developed using three USRP N210s with omnidirectional antennas and a 10MHz synchronisation signal is used to provide frequency synchronisation through *cable connection*. Among them, two SDRs are used to collect the signal and measure AOA and the other SDR is used to transmit a reference signal for phase synchronisation. The localisation experiments are implemented in a 20m by 20m open outdoor area and the localisation error is 3m in average. Another SDR-based localisation system using AOA measurements, iLocScan, is proposed in Zhang et al. [2014]. The antenna array consists of six US-RPs. A common reference with 10 MHz frequency output and 1 PPS output is used to achieve clock synchronisation of multiple SDRs through *cable connection* and an additional USRP is used to send a calibration signal for phase synchronisation. The localisation is implemented in a 20m by 40m indoor lab with a known floor plan and the system explores the AOA of the direct path and the reflective path of the signal source to implement source localisation. The average localisation error is $3 \sim 5$m.

While RSSI measurements and AOA measurements can be used to implement localisation, they have some drawbacks. The RSSI-based localisation is more suitable for small areas because of the limitation of the transmission power and the fact that RSSI measurements are not accurate in a long-distance propagation due to the interference and multipath effect. AOA-based localisation is suitable to localise distant targets, but the localisation accuracy is limited. Compared to RSSI measurements and AOA measurements, time measurements are more accurate and suitable to localise both distant and nearby signal sources. Therefore, it is also attractive to explore time based localisation using multiple SDRs. Time-based measurement techniques include TOA, TDOA and round-trip TOA. TOA measures the flight time of the signal from the transmitter to the receiver, so both the signal transmission time and the receiving time needs to be known. However, in many situations, the localisation system consists of signal receivers only and does not have access to the signal source, so it is impossible to know the signal transmission time and, thus, it is unable to obtain TOA measurements. TDOA measures the time difference of the signal received by two receivers, so TDOA-based localisation does not need to know the signal transmission time, but the accurate time synchronisation of multiple receivers is necessary to obtain accurate TDOA measurements. Another type of time measurement is round-trip TOA which does not require the synchronisation between the receivers. However, to obtain round-trip TOA measurements, a signal transmitter needs to be developed and the localisation range is limited by the transmission power. Moreover, the round-trip TOA measurement requires some kinds of cooperation between the

transmitter and the receivers to bounce the signal back immediately after the signal arrives at the receivers. After reviewing these three time measurement techniques, TDOA measurements are more scalable for practical source localisation, even when the signal source is non-cooperative to the localisation system.

We started the TDOA-based passive source localisation using multiple SDRs in early 2012. The preliminary results have been obtained in the middle of 2012, and since then, we have been focusing on improving the localisation accuracy of the system. We have systematically analysed the error sources that influence the localisation accuracy from three aspects: the hardware precision, the performance of signal processing algorithms and the environmental impact. Then, we have implemented improvement strategies to the localisation system from two aspects: measurement error reduction and localisation estimation optimisation. Our localisation system is implemented using multiple fully distributed USRP N210s and has a large coverage with several-kilometre sensor-target range. The details of the implementation will be presented later in this thesis. Other implementation of TDOA-based localisation using multiple SDRs can be found later on. One of the differences between our work and others' work is that the implementation range. The minimum sensor-target range in our implementation is 2.1km, while the sensor-target range in other implementation is less than 1 km. For example, the sensor-target range of the works Bhatti et al. [2012], El Gemayel et al. [2013], Li et al. [2014] are 700m ~ 900m, 80m ~ 230m, up to 30m respectively in an outdoor area. The recent work Li et al. [2015] implements TDOA-based localisation in a 16m by 18m indoor area. The other difference is that the signal source we are trying to localise is an established signal tower which cannot be accessed by the system, so our demonstration is *fully passive*. In contrast, others' works use self-developed signal source to do the demonstration. The access to the signal sources will help to obtain more accurate localisation results.

The source localisation can also be achieved by using another measurement technique: Doppler shift or FDOA. The Doppler shift measurements and the FDOA measurements are well known in Radar system and there are many theoretical results on multiple sensors-based localisation using FDOA measurements (see subsection 2.2.1.4), however, to the best of our knowledge, there is no published work on the practical SDR-based implementation of passive localisation systems using FDOA measurements until writing of this thesis. In this thesis, the joint TDOA and FDOA-based localisation is demonstrated using two spatially distributed SDRs.

2.5   Summary

In this Chapter, the background and the related work on the source localisation are reviewed. Two types of source localisation procedures are introduced. Different from the active localisation, in the passive localisation, the signal source does not cooperate with the localisation system. Different measurement techniques can be used in the source localisation, and we divided the measurement techniques into four categories: angle measurement, received signal strength measurement, time

measurement and frequency measurement. For each category of the measurement techniques, different methods can be used to obtain measurements. For example, the time measurements can be obtained from one-way propagation time (TOA), two-way TOA and TDOA. In addition to the measurement techniques, the factors that influence the measurement accuracy are briefly reviewed. Moreover, to improve the localisation accuracy, the related works on the outlier detection are discussed because the outliers can dramatically degrade the accuracy of the localisation systems. At the stage of the source location estimation, various location estimation algorithms can be used to determine the source location. However, for the passive localisation, the closed-form solutions are desired and appropriate because the initial guess of the source location is usually unknown in practice. In addition, special attention has been paid to the related works which address two generic problems in the source localisation. One is the sensor-target geometry and the other one is the location estimation bias.

To implement the practical localisation systems, commercial off-the-shelf Software Defined Radio (SDR) products are investigated. After evaluating the hardware parameters and the operation software of different SDR devices, we focus on the USRP products developed by Ettus Research. In our implementation, the USRP N210 is chosen which is a high-performance SDR device and has been widely used in many research topics in the domain of signal processing and communication. Compared to other SDR-based localisation systems, our implementation of the RSSI-based localisation system focuses on the verification of a generic bias reduction algorithm, not only in the indoor environment, but also in the outdoor environment. Moreover, our implementations of the TDOA-based localisation system and the joint TDOA and FDOA-based localisation system are in a fully passive way without the need to access to the signal source, and they cover a large area with a sensor-target range of several kilometres.

In the next Chapter, the design and implementation of the localisation systems using multiple SDRs will be presented.

Design and Implementation based on software defined radios

In this Chapter, the design and implementation of the RSSI-based, the TDOA-based and the joint TDOA and FDOA-based localisation systems using multiple SDRs are studied respectively. In the first Section, the devices that are used to implement the source localisation systems are introduced, including the core equipment (USRP N210), the RF front end (WBX daughterboard), different types of antennas and a GPSDO unit. To start with, in Section 3.2, a relatively simple localisation system is developed by taking RSSI measurements using multiple SDR-based transmitters and receivers. The system design, the system implementation in the small indoor and the small outdoor environment, and the results of the RSSI-based localisation system are given. In Section 3.3, a passive source localisation system which is more challenging to implement in practice is designed using multiple spatially distributed SDRs by taking the TDOA measurements. Furthermore, a joint TDOA and FDOA-based passive source localisation system is designed using only two SDRs in Section 3.4.

3.1 Devices for source localisation

3.1.1 USRP N210

Among different categories of the USRP products, we are particularly interested in the USRP network series, such as USRP N210, because it has a good trade-off between the performance and the cost. Actually, at the time when our research was started in early 2012, only the USRP1, USRP2 and USRP 200 series were available. A block diagram of the receiving and transmission chains of the USRP N210 and the WBX daughterboard is shown in Figure 3.1 (a) Alyafawi et al. [2014].

In the receiving link, the signal is received by the antenna on the motherboard, and the antenna switch is used to determine which channel the received signal should go, either the receiving channel or the transmitting channel. Then the daughterboard is responsible for amplifying and converting the RF signal into a baseband signal. Then it is filtered by a low pass filter with dynamic bandwidth up to 20 MHz.
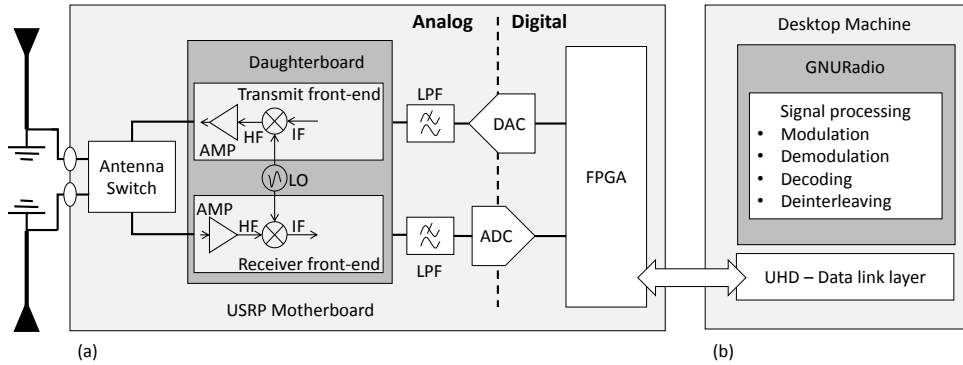
Figure 3.1: A block diagram of the receiving and transmission chains of the USRP N210 and the WBX daughterboard

The filtered signal is then digitalized by a ADC inside the FPGA with sampling rate of 100 MS/s (million sample per second). The ADC resolution is 14 bits and the sampled signal is expressed in In-phase and Quadratic (I/Q) form. The FPGA can produce 8-bit sample (8-bit I and 8-bit Q) or 16-bit sample (16-bit I and 16-bit Q). The digitalized samples are then transferred to the host computer over Gigabit Ethernet. Limited by the data transmission interface, the FPGA needs to decimate the samples by an integer. The USRP N210 supports 50 MS/s sampling rate for 8-bit samples and 25 MS/s sampling rate for 16-bit samples. The transmission link works similarly but in a reversed way. The samples produced by the host computer is interpolated inside the FPGA and processed by the DAC which supports the sampling rate of 400 MS/s with 16-bit resolution.

On the host computer side, GNU Radio is used to implement signal processing functions on the received samples, such as signal modulation, demodulation, decoding and de-interleaving, etc, as shown in Figure 3.1 (b). The UHD is the interface between the USRP and the host computer for data exchange.

3.1.2 Daughterboards

The daughterboards work as the RF front end to implement functions of up-conversion, down-conversion, amplification and filtering, etc. Various types of RF daughterboards are available and the selection of them can be made according to the application requirements on the frequency coverage, the signal bandwidth and the number of channels Ettusresearch [2015]. In this study, the WBX daughterboard (see Figure 3.2) is used.

The WBX is a wide bandwidth transceiver that provides up to 100 mw (milliwatts) of output power and a noise figure of 5 dB. It provides 2 quadrature front ends (1 transmit, 1 receive) and it can be used in direct conversion mode and low IF (intermediate frequency) mode. The local oscillators (LOs) for the receiving and transmission chains operate independently and can be synchronized for MIMO operation. The WBX supports full-duplex operation on different transmission and re-
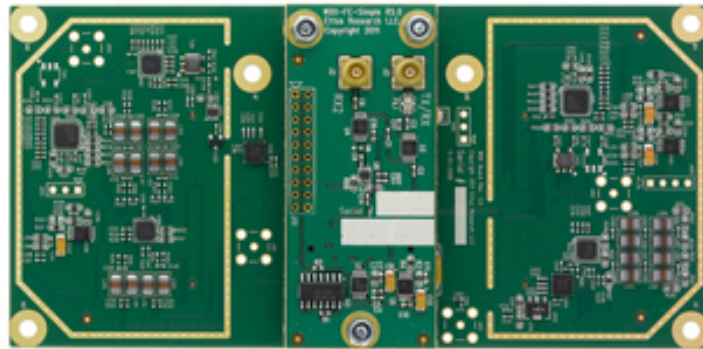
Figure 3.2: The WBX daughterboard

LP0410   **VERT400**   **Telescopic antenna**
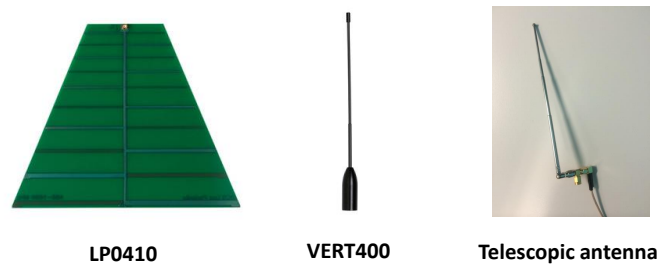
Figure 3.3: Antennas

ceiving frequencies. It provides 40 MHz of bandwidth capability and covers 50 MHz to 2.2 GHz frequency range. Example application areas include land-mobile communications, maritime and aviation band radios, cell phone base stations, PCS and GSM multi-band radios, coherent multi-static radars, wireless sensor networks, transceiver covering 6 amateur bands, broadcast TV, white spaces, public safety and ISM.

3.1.3   Antenna

Both antenna developed by Ettus Research and third-party companies can be used with the USRPs with suitable connection adaptors. Three types of antennas are used according to different frequency coverage and applications in this research as shown in Figure 3.3. The LP0410 is a Log Periodic PCB directional antenna with 5-6 dBi gain and has frequency coverage from 400 MHz to 1 GHz. The VERT400 is a 144 MHz, 400 MHz, and 1200 MHz Tri-band omnidirectional vertical antenna with extended receive range: 118-160MHz, 250-290MHz, 360-390MHz, 420-470MHz, 820-960MHz and 1260-1300MHz. The telescopic antenna is an omnidirectional antenna which covers FM radio and digital TV band.

3.1.4   GPSDO (GPS disciplined oscillator)

When talking about "a GPS", we usually mean a GPS (Global Positioning Service) receiver. The Global Positioning System (GPS) is actually a constellation of 27 Earth-orbiting satellites (24 in operation and three extras in case one fails). A GPS receiver's job is to locate four or more of these satellites, figure out the distance to each by timing how long it took the signal to arrive, and use this information to deduce its own location. This operation is based on a simple mathematical principle called "Trilateration".

To measure the travelling time of signal from GPS satellite, the receiver and satellite both need clocks that can be synchronized down to nanosecond. To make a satellite positioning system using only synchronized clocks, atomic clocks are needed not only on all the satellites, but also on the receiver itself. But atomic clocks cost somewhere between $50,000 and $100,000, which makes them a just a bit too expensive for everyday consumer use. The Global Positioning System has a clever and effective solution to this problem. Every satellite contains an expensive atomic clock, but the receiver itself uses an ordinary quartz clock, which is constantly reset. In a nutshell, the receiver looks at incoming signals from four or more satellites and gauges its own inaccuracy. The receiver can easily calculate and reset its clock to be in synchronization with the satellite's atomic clock. The receiver does this constantly whenever it's on, which means it is nearly as accurate as the expensive atomic clocks in the satellites.

The GPS signal structure has a 1500-bit message sent at a rate of 50 bits/second taking 30 seconds. Most receivers require the copying of a complete, unbroken 1500 bit message block to use the signals. If the decoding is started right at the beginning, it takes 30 seconds. If the decoding is started one bit later, the first complete message block that can be decoded starts 30 seconds later, so one does not get the message until 60 seconds after the initial acquisition, and the average latency is 45 seconds. However, the discussion above is based on one satellite, if the receiver can receive signals from many satellites, the time of calculation and calibration will be reduced.

In our application, the GPSDO unit uses the GPS to "discipline" the 10MHz oscillator to continuously calibrate it. GPSDOs are usually used in many time-based applications. As just discussed, the GPS receiver can obtain the time as accurate as the expensive atomic clock. However, the time output of GPS receivers also depends on the accuracy of the internal oscillator. During the time when no complete message from GPS satellite is available, the oscillator is used to time and continuously steer the phase of the clock to maintain 1PPS (pulse per second) as close as it can to the GPS time. The 1PPS accuracy of GPSDO kit we are using is +/-50 ns, which means the time output deviation of the GPS receiver is less than 50 ns comparing to accurate GPS time. The size of the GPSDO is only 2.5 cm by 6.25 cm, as shown in Figure 3.4, which can be installed on the USRP N210's montherboard.

Another parameter is the holdover stability (<+/-11μs over 3 hour period at +25°C) of the GPSDO, which means the accuracy of GPSDO time output when GPS satellite signals are not available. In this case, the GPSDO will only relay on the oscil-
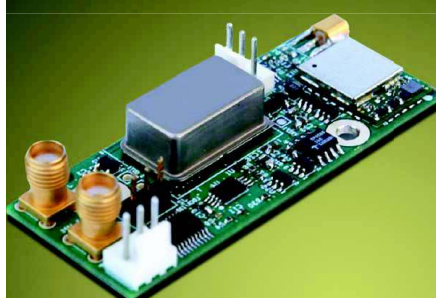
Figure 3.4: GOSDO (GPS disciplined oscillator)

lator to keep the 1 PPS without being calibrated by the message from GPS satellites. Therefore, the accuracy will be lower, which is consistent with our test results when the GPSDO is not locked. In other words, GPSDOs make use of the GPS signal to continuously calibrate and output accurate 1PPS and time.

During the process of source location estimation, the position of the SDR is required, which can also be obtained from GPSDOs. The NMEA sentences of GGA and RMC outputted from GPSDOs can not only provide position of the SDRs, but also provide the ground speed and the number of satellites in view, etc. Since the sensor position accuracy also influences the source location estimation result, to investigate the position accuracy of GPSDO modules, a large number of position outputs are collected and analysed statistically. The distance standard deviations caused by sensor position error of GPSDOs are 4.66m in latitude and 5.08m in longitude, which is not large in large-area localisation, e.g. several kilometers.

3.2   RSSI-based localisation using multiple SDRs

3.2.1   RSSI-based localisation

RSSI-based localisation can be divided into two categories: the distance estimation-based technology and the RSS profiling-based technology Mao et al. [2007a]. In this thesis, our focus is the distance estimation one. RSSI-based localisation is intended to measure the power decay of the signal transmitted by the electromagnetic source, and to transform the measured signal power loss into the distance the signal travels in space. The distance estimate is then used to localise the signal source. One distance measurement determines a circle where the location of the emitter locates in 2-dimensional space with the sensor position at the center and the distance measurement as the radius. In 2-dimensional space, at least 3 sensors are required to uniquely determine the emitter location by finding the intersection of the circles formed by 3 distance measurements. In the absence of noise, the three circles will intersect exactly on one point which is the location of the target. However, in the presence of noise, the three circles will give more than one intersection, so it is hard to determine which intersection should be the localisation solution. As illustrated in Figure 3.5, in the case of noisy measurements, the true source location may fall in the region
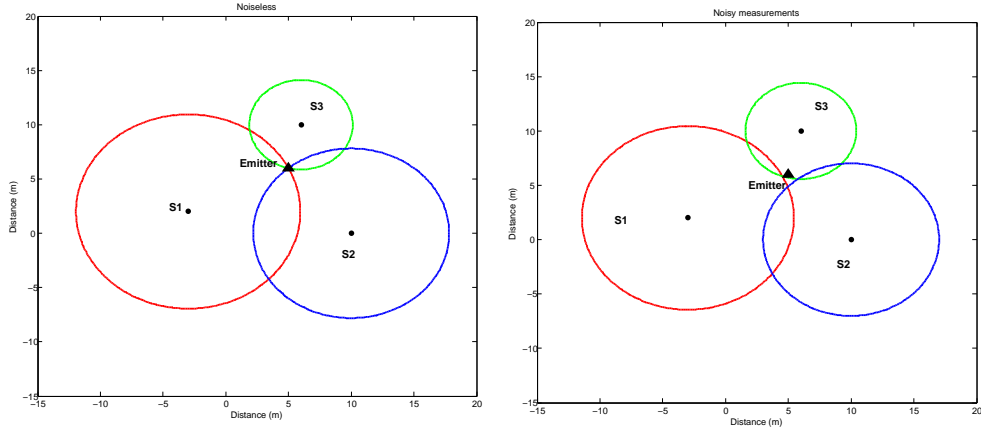
Figure 3.5: Distance estimation-based RSSI localisation in noiseless and noisy case

formed by the three intersection points. To solve this situation, we need to convert the localisation problem into an estimation problem to find the optimal point inside or around the intersection region to determine the localisation solution.

Consider a simple scenario with one stationary emitter as the target and N stationary sensors that measure the power level of the signal transmitted by the emitter at different locations in 2-dimensional space. Define $\mathbf{s}_i = [x_i \ y_i]^T, i \in 1, ..., N$ as the known position of the sensor at ith location. Also, let $\mathbf{p} = [x \ y]^T$ be the unknown position of the emitter.

The received signal power at the ith location can be expressed by a log-normal model as Pahlavan and Levesque [2005]

$$P_i = \bar{P}_i + \epsilon_i \tag{3.1}$$

where $\bar{P}_i$ denotes the mean received power, and ϵ_i represents the log-normal shadow fading effect in a multi-path environment. Here the received signal power data is measured in dB milliwatts (dBm). It is assumed that ϵ_i is Gaussian distributed with zero mean and the correlation defined as follows:

$$\mathbf{E}(\epsilon_i \ \epsilon_j) = \begin{cases} 0 & i \neq j \\ \sigma_p^2 & otherwise \end{cases} \tag{3.2}$$

where σ_p^2 is the known variance and it is measured in dB milliwatts squared. The received average power is a function of the distance between the emitter and the sensor, and the Path Loss Exponent (PLE). It has been shown in Pahlavan and Levesque [2005] that the received average power can be written in the following form:

$$\hat{P}_i = P_0 - 10 * \gamma * log_{10}(\frac{r_i}{r_0}) \tag{3.3}$$

with r_i being the Euclidean distance between the emitter and the sensor at the *i*th location, viz

$$r_i = \sqrt{(x - x_i)^2 + (y - y_i)^2} \tag{3.4}$$

In (3.3), r_0 refers to the known reference distance at which P_0 is measured. The value of P_0 can be measured at the reference distance through experiments. The PLE γ measures the rate at which the received signal strength decreases with distance. The value of γ depends on the specific propagation environment, so it can only be determined empirically. A generic method based on the quantile-quantile (q-q) plot Hyndman and Fan [1996] is used to estimate the unknown constant γ. To be specific, in practical experiments, to estimate the value γ, a number of received signal power P_i at the corresponding distance r_i can be measured first. Then, a 1-degree polynomial function can be found to fit the data set formed by p_i and r_i, which can be denoted by $p(x) = ax + b$. The coefficient of the polynomial is equal to the estimated value of γ.

Once the unknown parameters P_0 and γ are determined, the distance r_i between the sensor at the *i*th location and the emitter can be estimated by measuring the received signal strength at that location according to equation (3.3). With adequate distance measurements between the emitter and the receivers, the location of a target can be obtained by solving the following formulation in the noiseless case:

$$\mathbf{r} = \mathbf{f}(\mathbf{p}) \tag{3.5}$$

where the function $\mathbf{f}$ can be obtained analytically according to the geometry of the emitter and the sensors at the known positions. For example, with three distance measurements in 2-dimensional space, the mapping $\mathbf{f}$ can be easily formulated as follows:

$$r_1 = f_1(x, y) = \sqrt{(x - x_1)^2 + (y - y_1)^2}$$
$$r_2 = f_2(x, y) = \sqrt{(x - x_2)^2 + (y - y_2)^2}$$
$$r_3 = f_3(x, y) = \sqrt{(x - x_3)^2 + (y - y_3)^2}$$

In the real-world situations, the errors in distance measurements are inevitable due to the radiating influence from other signal sources in the environment and reflection, etc. Though when the usable number of measurements $N = n$ (*n* denotes the dimension of the space, *n*=2 or 3), one can still obtain an emitter location estimate in effect by solving $\hat{\mathbf{r}} = \mathbf{f}(\hat{\mathbf{p}})$. However, generally when $N \geq n + 1$, this equation will have no solution in the noisy case. The main idea of obtaining approximate estimate in this situation is to convert the localisation problem to an optimization problem as follows and solve it using methods such as maximum likelihood, least-square, etc. Foy [1976], Torrieri [1984].

$$\hat{\mathbf{p}} = \arg\min_{\mathbf{p}} C(\mathbf{p}, \hat{\mathbf{d}}) \tag{3.6}$$

where the cost function C is related to $\mathbf{f}$ and it can be possibly formulated as follows:
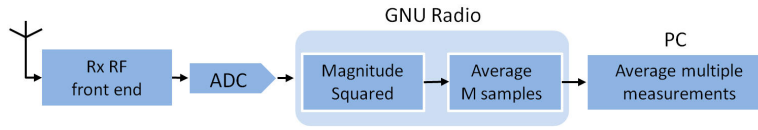
Figure 3.6: Block diagram of RSSI measurements

$$C = \sum_{i=1}^{N}[(f_i)^2 - (\tilde{r}_i)^2] \tag{3.7}$$

By solving the minimization problem, the estimated positions of the unlocated sensors can be obtained.

3.2.2   RSSI measurement acquisition and analysis

In the RSSI-based localisation, both the emitters and the receivers are developed using SDRs and they are equipped with omnidirectional antennas. The system design using SDRs is very flexible, and the SDR can be developed into a signal emitter or a signal receiver by just changing the software flow graph in GNU Radio. The principle to obtain RSSI using the SDR is described in Figure 3.6 (The arrow shows the order how the received signal is processed.) . The SDR receiver obtains RF signal through its RF front end and the signal is sampled by the 14-bit ADC. Then, the sampled signal is processed by GNU Radio and stored in the host PC. The RSSI is calculated by obtaining the magnitude of the I/Q components of each samples, denoted by $\sqrt{I^2 + Q^2}$, and averaging the magnitude of M samples in one measurement. To enhance the reliability of the measurements, the measurements are implemented many times at one position and the average RSSI is obtained.

RSSI measurements are simple to obtain, but they have drawbacks of poor consistency and low accuracy due to the hardware precision and environmental influence. One of the influences from the hardware is the change of the transmission power of the SDR-based emitter. A fluctuation of the transmission power in one power cycle is observed during the experiments in Figure 3.7, where the y-axis denotes the RSSI value measured by a SDR receiver at a certain distance and the x-axis denotes the number of measurements that are taken by the receiver with the time interval of 30s. One can see that when the USRP is just powered on the RSSI reading has its maximum value about -10 dBm. As the time goes, the RSSI reading starts to decrease gradually. A 2-dBm drop in the transmission power can be seen after the USRP runs for a few minutes. After that the RSSI readings keep almost constant. After running for half an hour, the RSSI reading starts to drop slowly again and the power fluctuation is increased. In different power cycles, sometimes even the initial RSSI readings when the USRP is just turned on is also different, which could produce in-consistent RSSI measurements. The main reasons of the power drop could be the electric current variance of the power supply and the cooling problem of the USRP N210.
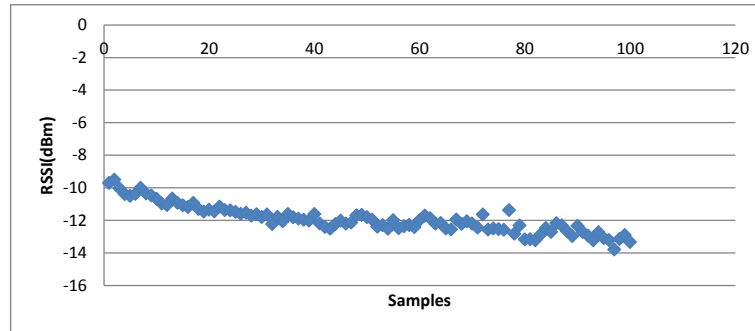
Figure 3.7: Power fluctuation of the SDR-based transmitter

Another hardware issue comes from the antenna. According to the definition of omni-directional antenna, in the same horizontal plane, the radio wave power should experience equal gain in all directions on the plane. However, the antenna we use in the measurement (omni-directional VERT400 antenna) is not perfect omnidirectional probably due to the manufacturing reasons. That is to say, even from the same distance, different orientation of the transmit antenna has different radio wave power gains. When the relative position or facing angle between a pair of emitter and receiver changes, the consistency of RSSI measurements will be disturbed. Although the difference is not obvious (often the difference is less than 2 dBm), it still affects the measurement accuracy to some extent.

Apart from the hardware influence, the accuracy of RSSI measurements are also affected by the environment. Due to the wireless channel characteristics, like shadowing, scattering and fast fading, even the transmitter and the receiver are stationary during all the testing period and the transmit power keeps unchanged, the received signal strength could change dramatically. Among different environmental impacts, the multipath effect is a common error source for RSSI measurements. Both the indoor and outdoor RSSI-based localisation are demonstrated using the SDR-based transceivers. For the outdoor RSSI-based localisation, the influence of multipath effect is not severe because the measurements are taken in an open-space environment and we can make sure the transmitter and the receiver are under LOS condition. Moreover, the power of the SDR transmitter is low, so the power of the signals from the reflected paths is weak. However, for indoor RSSI-based localisation, the reflection from the objects in the room, the surrounding walls, even the ceilings and the floors, is serve and hard to control so that the influence of multipath is more serve in the indoor environment than that in the outdoor environment. We have observed that the reflection of walls could let signal strength gain several dBm if the transceivers are too close to the wall, especially the room corners. In addition to the multipath effect, the inference signals can also cause RSSI measurement noise.

To improve the consistency and accuracy of RSSI measurements, the efforts have been made to reduce the influence of hardware precision and the environmental impact. Firstly, to avoid the large changes on the transmitter power in different

power cycles, the RSSI measurements in the experiments are obtained in one power cycle, and we take effective RSSI readings by waiting for a few minutes to make sure the power of the transmitter is almost stable. In addition, to obtain consistent RSSI measurements, the connection between the antennas and the SDRs needs to be firmly contacted. To deal with the antenna issue, the antennas are marked, and a low-cost laser device is used to align the marks on the antennas on SDRs to obtain the consistent antenna radiation patterns. The methods above can effectively ensure the RSSI measurements are obtained within a reasonable error range. Secondly, to reduce the influence of the interference signal, the emitter is programmed to transmit signal in a frequency band with little interference signals. With the WBX daughterboard, the USRP N210 is able to transmitter signal at frequency band between 50 MHz and 2.2 GHz. The flexible frequency band choice benefits from the software defined-feature of the USRP N210. To reduce the signal reflection and multipath effect in the indoor environment, the USRPs are placed on bar stools instead of being put on the ground, which can reduce the reflection from the ground. At least 1 meter away from the walls or the room corners is necessary to effectively reduce the influence of the wall reflection. In addition, while the effect of wall and room corner reflection could not be eliminated, we can reduce their influence by putting all the USRPs under the similar environment. For example, we decided to place all three SDR receivers at the corners of the room and they are all 1 meter away from the walls. With this deployment, all the three receivers experience similar RSSI gain enhancement from the wall reflection such that the influence of the wall reflection can be cancelled out to some extent.

3.2.3 The implementation of the RSSI-based localisation using multiple SDRs

The parameters of the emitter are listed in Table 3.1. For simplicity, a sine wave with a bandwidth of 1 MHz is generated and transmitted continuously as the signal source. 1.2 GHz central carrier frequency and 440 MHz central carrier frequency are used in the indoor experiments and the outdoor experiments respectively. A lower central frequency is used in outdoor environment than that in indoor environment because the low frequency can increase the transmission range of the RF signal. Since the Signal-to-Noise ratio (SNR) generally drops when the range between the emitter and the receiver increases, to obtain a high SNR, the gains of both the emitter and the receiver are set to a large value. The sampling rate of 1M sps is used. During the experiments, the receivers are tuned to the desired frequency to receive M (M=102400) complex samples of the signal source in order to calculate the RSSI value in each measurement cycle. We did not use the highest sampling rate and limited the length of received signal samples indoors to reduce the computing burden of the SDR and increase the updating rate of the system. In 2-dimensional space, at least 3 receivers are required to localise the emitter. For a basic setup, three SDR-based receivers are deployed around one SDR-based emitter to receive signal and implement source localisation, as shown in Figure 3.8.

Parameter	value
Central frequency	1.2 GHz (indoor) & 440 MHz (outdoor)
Waveform	Sine
Bandwidth	1MHz
Sampling rate	1M Sps
Antenna	omni-directional

Table 3.1: Parameters used in our evaluation.
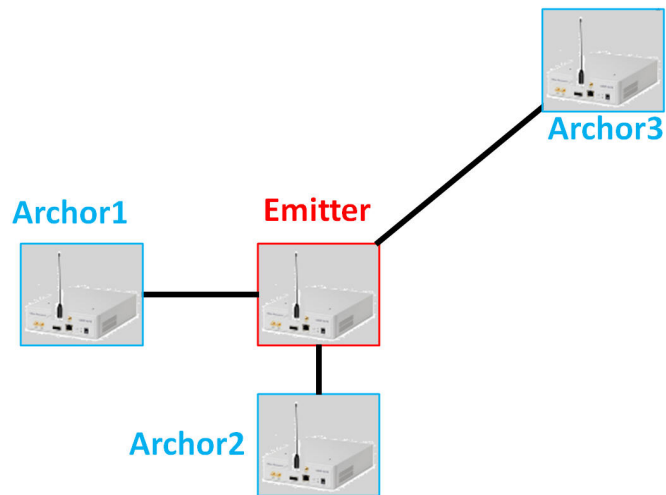
Figure 3.8: Three receivers and one emitter
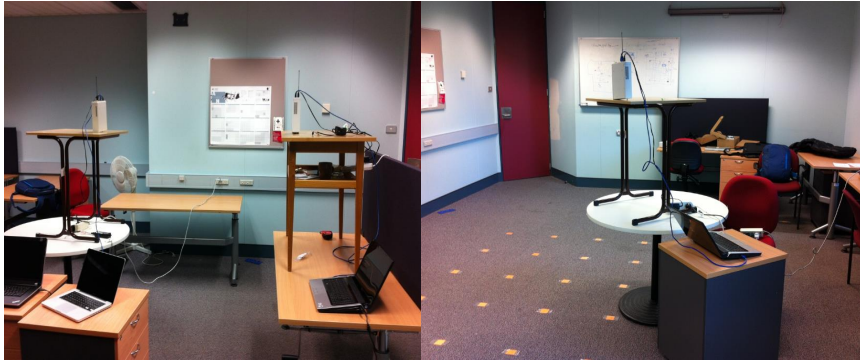
Figure 3.9: Indoor environment

Figure 3.10: Outdoor environment

To obtain the environmental specific PLE, two SDRs are used. One is used as a signal emitter and the other one is used as a receiver. The process of obtaining the PLE is described as follows: the emitter is fixed at one position, and then the receiver is moved away from the emitter in a straight line by steps of certain meters (0.5 m for indoor environment and 1 m for outdoor environment) and the RSSI measurements are obtained at each position. Smaller steps, such as 0.1 m or 0.2 m, are not chosen because no obvious change of the received signal strength can be observed. After the estimated value of the PLE is obtained, the localisation experiments under different emitter-receiver setups are implemented. The indoor environment is an office with the size of 8m by 10m, as shown in Figure 3.9. The SDRs are put on tables at the same height about 1.8m above the ground to reduce the influence of the floor reflection. The outdoor environment is an open area with the size of 12m by 15m as shown in Figure 3.10. The weather of the day when the experiments were implemented was stable, sunny, no wind and at about $20°C$.

The indoor environment is generally more stable than the outdoor environment

and the area of the indoor environment is usually enclosed, so for the RSSI-based indoor localisation, two approaches are used to obtain transmitter location estimates. One approach is based on RSSI measurement matching, which requires a training phase to obtain a RSSI measurement pattern lookup table or database of the whole indoor floor plan. This method is more suitable for the indoor localisation in a small and enclosed area. The other approach is based on the distance measurements. To be specific, it transfers the RSSI measurements into the distance measurements which are further used to infer the location of the transmitter. This distance based approach is widely used in both the indoor and the outdoor RSSI-based localisation.

3.2.3.1 RSSI matching based-indoor localisation

The RSSI matching based indoor localisation can be divided into three steps:

1. Estimate the PLE of the environment empirically.

2. In the training phase, obtain a RSSI pattern lookup table. The position of each training point in the area of interest will have a unique RSSI pattern which consists of the normalized RSSI values with the same numbers of receivers used in the localisation.

3. In the localisation phase, obtain RSSI measurements, do normalization and find the best matching RSSI pattern in the lookup table, so the corresponding location of the transmitter can be determined.

In Step 1), to estimate the PLE of the environment, the RSSI measurements at a few corresponding training points need to be obtained firstly. A RSSI-distance plot can be seen in Figure 3.11, in which the RSSI measurements at a distance up to 7m with 0.5m distance interval are obtained. Theoretically, the RSSI value should reduce gradually with the increasing distance between the emitter and the receiver. However, some fluctuations can be observed, especially at 2m to 3m and 6m to 7m. Even though many tests are implemented at these abnormal points, the results are almost the same. The fluctuation is caused by reflection characteristics of the indoor area. Rooms with different size or sharp will give different fluctuation patterns of the RSSI-distance plot. After a corresponding relationship between RSSI measurements and distance measurements is obtained, a fitting curve is generated to fit the data. The fitting curve is denoted by the pink curve in Figure 3.11. Therefore, the approximated PLE of this indoor area is 2.0838. This value is very close to the empirical value in the free space because the emitter and receiver are placed at the same height and in a line-of-sight condition.

In step 2), the indoor area can be divided into a number of grids. The size of the grid depends on the desired localisation accuracy. In theory, the smaller the grid is, the higher the localisation accuracy is as long as the RSSI measurements are accurate. However, more grids mean more points to be surveyed, which is time consuming. Then the receivers can be deployed to cover the area of interest. In our
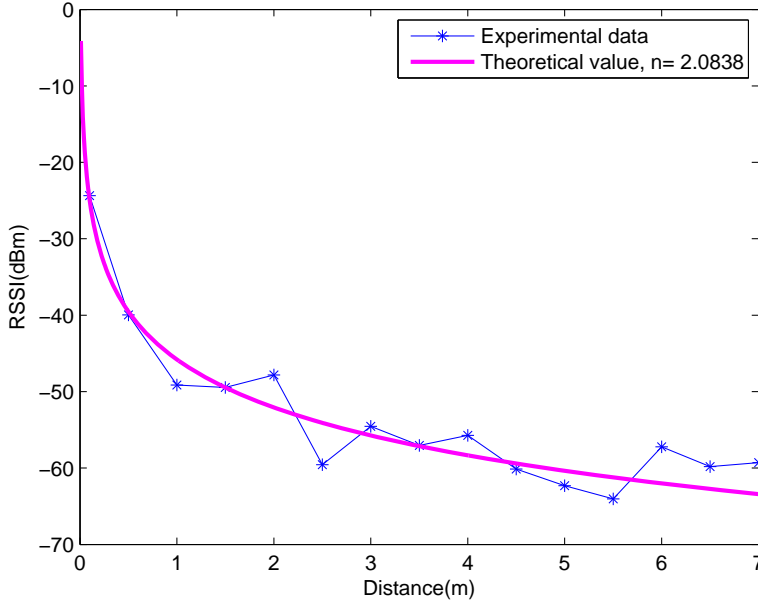
Figure 3.11: PLE estimate of the indoor area

implementation, 3 SDR-based receivers are used to localise the transmitter. After that, find the intersection points of the grid lines and assign a local coordinates on those points. Followed by marking the points by sticking a small piece of paper on it to make their position easy to identify, as shown in Figure 3.12, where the grid size is 0.5m by 0.5m. Next, measure the distances between each marked spots and the position of the SDR-based receivers and then calculate the RSSI of the three receivers by assuming there is a virtual signal transmitter with constant transmission power at each spot according to (3.3). Store the calculated RSSI measurements in a triple. Since the transmission power of the emitter P_0 is unknown, the calculated RSSI value is actually equal to $\hat{P}_i - P_0$. To remove the unknown transmission power, the RSSI triple can be normalized by substituting the minimum value among the three values. After normalizing, the minimum RSSI value among the three RSSI measurements will be zero while the other two will be positive values. We can demote the normalized RSSI by $< RSSI_{1test}, RSSI_{2test}, RSSI_{3test} >$. After the training process described above is completed, a RSSI pattern lookup table can be obtained.

In Step 3), when they are a real signal transmitter, the three SDR-based receivers are used to acquire the signal and calculate RSSI value. Then, the real RSSI measurements are normalized using the same way as in the training step, so a new RSSI triple $< RSSI_1, RSSI_2, RSSI_3 >$ can be obtained. After finding the same or most similar RSSI pattern in the lookup table, the location of the emitter can be determined.

Figure 3.13 shows the results of three localisation experiments using the proposed RSSI matching-based methods, where the triangles denotes true emitter location, the square mark denotes the estimated emitter location, different color is used to

Figure 3.12: Marks on the intersection of grid lines in indoor area

distinguish different experiments. Green color denotes the first experiment, blue color denotes the second experiment and the red color denotes the third experiment. In the first experiment, the true position of the signal emitter is at position $(4, 4)$ and the estimated emitter location is at $(5, 4)$, so there is a 0.5m localisation error. In the second experiment, the true position of the signal emitter is at position $(4, 3)$ and the estimated emitter location is at $(4, 3)$, so there is no localisation error. In the third experiment, the true position of the signal emitter is at position $(1, 5)$ and the estimated emitter location is at $(1, 5)$, so there is also no localisation error. From the localisation results, one can see that the RSSI matching-based method can be used to implement indoor localisation and the localisation error is around 1 grid side length. The advantage of this method is that it is influenced by the change of the transmitter power because the P_0 is removed through the normalization, but it takes some time to calculate RSSI pattern lookup table.

3.2.3.2   Distance estimation-based indoor RSSI localisation

The RSSI-based localisation using distance estimation directly is widely used in both the indoor and the outdoor environment. By transforming the RSSI measurements into the distance measurements, the emitter location can be determined using the distance based-localisation algorithms, e.g. trilateration. The distance estimation based-localisation using RSSI measurements consists of 2 steps:

1. Estimate the PLE of the environment empirically.

2. Obtain the RSSI measurements using the receivers and transfer the RSSI measurements into distance measurements using the known path loss model. Next, implement location estimation using distance measurements.
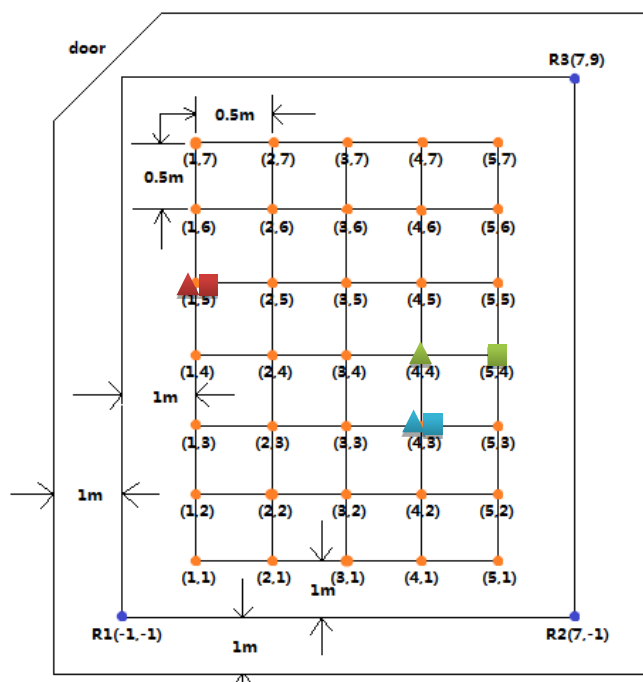
Figure 3.13: Results of RSSI matching-based indoor localisation

Comparing to the RSS matching-based methods, the distance estimation-based method does not require the calculation of the RSSI pattern lookup table, but the accuracy of distance measurements can be influenced by the change of the transmitter power. Three scenarios are considered to verify the performance of the distance estimation-based RSSI indoor localisation. In each scenario, the locations of the receivers are known. The locations of the transmitters are unknown and to be estimated. The PLE estimation can be found in Figure 3.11.

Scenario 1 Firstly, the simplest scenario with three receivers and one emitter is considered as shown in Figure 3.14. The dashed line denotes the distance measurements of a receiver-emitter pair. To improve the accuracy of distance measurements, the average value of multiple measurements is used as the final distance measurement. With three distance measurements obtained by the three non-linear receivers in 2-dimensional space, the emitter location can be determined.

In Table 3.2, the real distance between the emitter and the receiver, the mean and variance of distance measurements, and the error ratio of the distance measurements to the true value are presented. One can see that the variance of distance measurements is small and the measured distance is close to the true distance. The largest measurement error ratio is 6.78 % with regard to the true distance. With the measured distance, the location of the emitter is estimated using the trilateration algorithm. The localisation results show the RMSE of the location estimates comparing to the ground truth is 0.3521m.
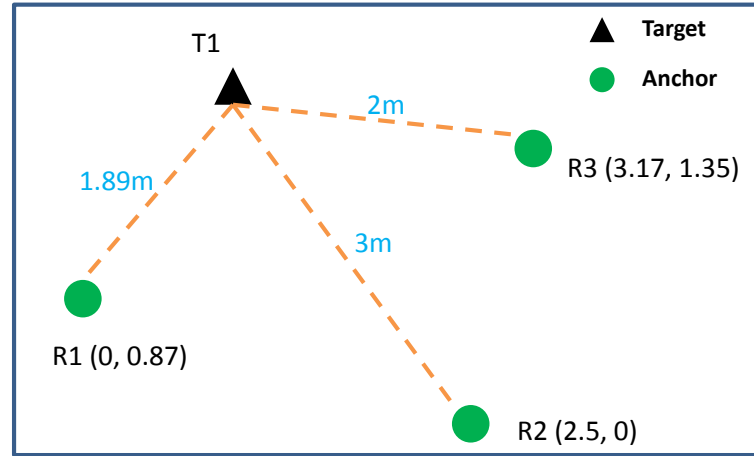
Figure 3.14: Localisation scenario 1

Real distance(m)	Average distance measurement(m)	Variance(m)	Error ratio
1.89	1.7619	0.0015	6.78%
2	1.9068	0.008	4.66%
3	2.7992	0.0195	6.69%

Table 3.2: Error statistics of distance measurements in scenario 1

Scenario 2 A complex case is considered in Figure 3.15, where the three receivers are used to localise one emitter T_1, then the localised emitter is used as one receiver to localise the other emitter T_2 with two original receivers R_1 and R_3. The error statistics of the measured distance are shown in Table 3.3. Similar to the results of scenario 1, the variance of distance measurements is small. The distance measurement between R_1 and T_1 shows the largest error ratio 19.29%, while other measurements give less than 10% error ratio. The large measurement error in the distance between R_1 and T_1 increases the localisation error of T_1. Then since T_1 is used as a receiver in the location estimation of T_2, the localisation error of T_1 will further influence the localisation accuracy of T_2. The localisation results show the RMSE of location estimates comparing to the ground truth is 0.4193m for $T1$ and 0.2011m for $T2$.

Real distance(m)	Average distance measurement(m)	Variance(m)	Error ratio
4.5	4.7509	0.0792	5.58%
2	2.3857	0.0036	19.29%
3.4	3.2346	0.0157	5.97%
1.5	1.492	0.00074	1.84%
2.24	2.1298	0.0086	4.92%
2.04	2.0566	0.0031	0.81%

Table 3.3: Error statistics of distance measurements in scenario 2
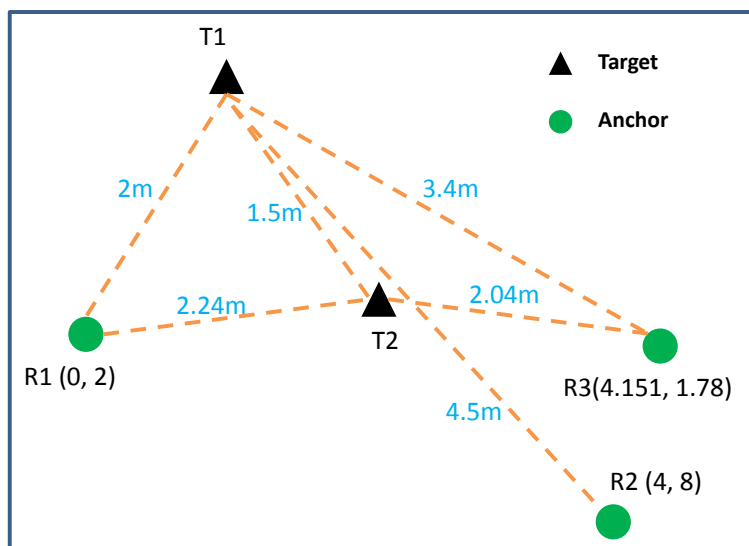
Figure 3.15: Localisation scenario 2

Scenario 3   A more complex scenario is considered in Figure 3.16, where the location of T_1 is estimated by three receivers, the location of T_2 is estimated using R_1, R_3 and T_1, the location of T_3 is estimated using R_2, T_1 and T_2, and the location of T_4 is estimated using T_1, T_2 and T_3. Apart from T_1, the location estimates of T_2, T_3 and T_4 are also influenced by the accumulated localisation error from pre-localised emitters. The error statistics of distance measurements are shown in Table 3.4. Similar to Scenario 2, while the variances of distance measurements are small, some distance shows large measurement error, such as 2.85m, 2.26m, 2.3m and 3.5m. The error is caused by the combined influence of the inaccurate PLE estimate and RSSI measurements at those distances due to the hardware noise and environmental noise. The localisation results show that the RMSE of location estimates comparing to the ground truth for $T1$, $T2$, $T3$ and $T4$ is 1.35m, 0.9434m, 2.2245m and 1.6055m.

3.2.3.3   Distance estimation-based outdoor RSSI localisation

For the distance estimation-based RSSI outdoor localisation, the localisation process is similar to the indoor one. Firstly, the PLE of the outdoor environment where the experiments are implemented needs to be determined. Similarly, an emitter is fixed at one position. Then, a receiver is moved away from the emitter in a straight line by steps of 1 m, and the RSSI measurements are obtained at each position. The outdoor RSSI-distance plot is shown in Figure 3.17, where the RSSI measurements show a downward trend when the receiver is moved farther away from the emitter. There are still some fluctuation on the RSSI measurements at some training points which is similar to the case in the indoor environment. A curve in pink shown in Figure 3.17 is generated to fit the RSSI-distance plot. The estimated PLE is 1.58389 which is in the reasonable range.
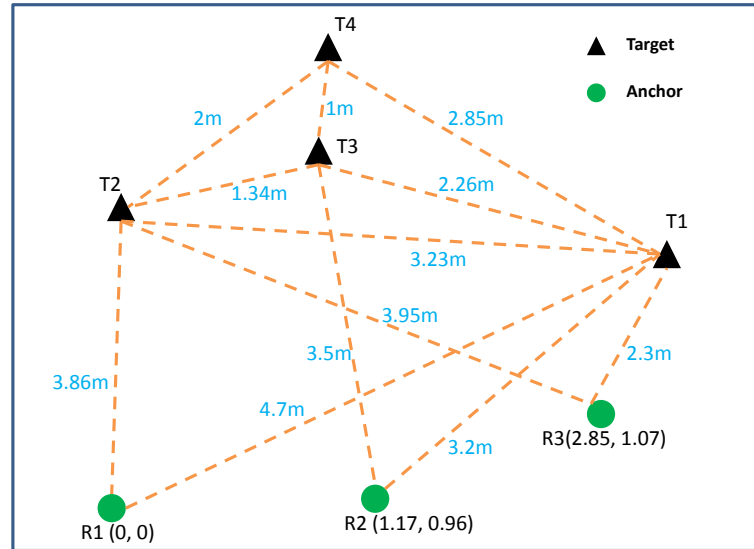
Figure 3.16: Localisation scenario 3

Real distance(m)	Average distance measurement(m)	Variance(m)	Error ratio
1	1.0002	0.00068	0.02%
2	1.7602	0.0073	11.99%
2.85	1.9362	0.0238	32.06%
1.34	1.226	0.0016	8.51%
2.26	1.5626	0.0206	30.86%
3.5	2.5968	0.0155	25.81%
3.23	3.3467	0.0206	3.61%
3.86	4.1787	0.1241	8.26%
3.95	3.816	0.0632	3.39%
3.2	2.8322	0.039	11.49%
2.3	1.8477	0.008	19.67%
4.7	4.1885	0.1833	10.88%

Table 3.4: Error statistics of distance estimates in scenario 3
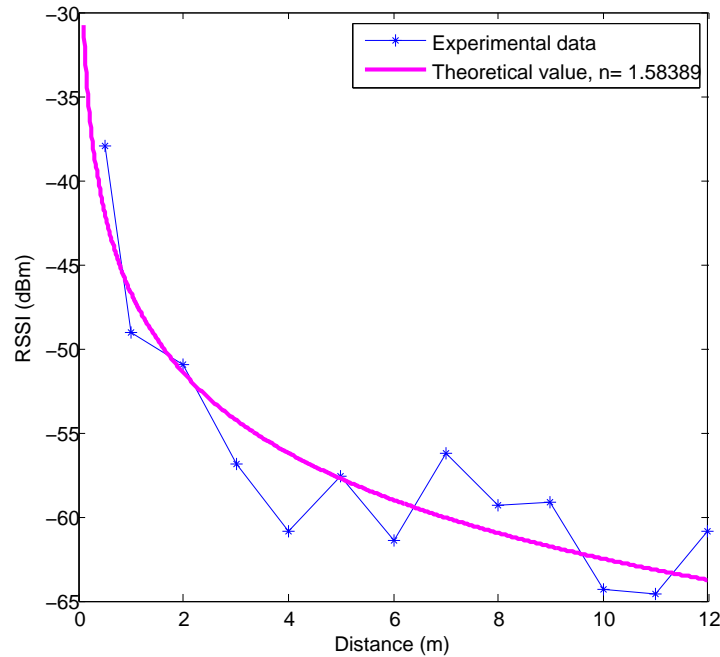
Figure 3.17: PLE estimate of the outdoor environment

True distance(m)	Average Estimated Distance Measurement(m)	Measurement noise(m) Standard Deviation (m)	Measurement Error Ratio
7.19	8.3251	1.9476	15.79%
9.17	8.8435	1.1282	3.56%
6.32	5.8211	0.5993	7.89%
4.25	4.0475	0.2978	4.76%
3.48	2.8116	0.4187	19.21%
8.54	8.1082	0.82	5.06%

Table 3.5: Error statistics of distance estimate in outdoor localisation

The outdoor experiment is implemented in a 12 m by 15 m open outdoor area. A localisation scenario with three receivers and two emitters is demonstrated using multiple SDRs. The three receivers are located at (0, 2), (4.75, 0), and (7.26, 4.97), whereas the two emitters are at (2.26, 8.83) and (6.45, 8.36) as shown in Figure 3.18. The statistics of distance measurements are shown in Table 3.5. Comparing to the results in the indoor environment, the variance of distance measurements is increased. The distance measurement error is similar to the error in the scenario 2 of indoor localisation. The RMSE of RSSI based-localisation error in the outdoor environment is 1.65m for the emitter $T1$ and 1.40m for the emitter $T2$.
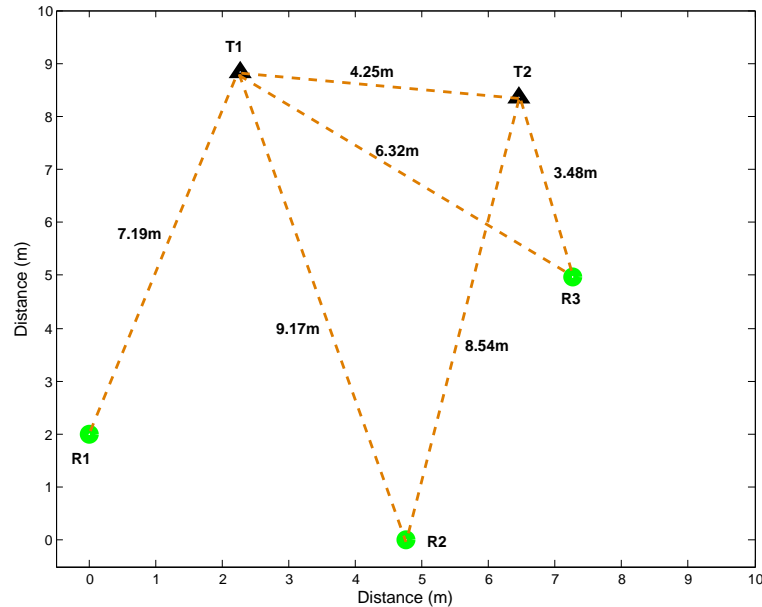
Figure 3.18: RSSI-based localisation in outdoor environment

3.2.4   Brief summary

The RSSI-based localisation system is demonstrated in both the indoor and the outdoor environment using multiple SDR-based transceivers. The localisation estimates can be obtained using the RSSI matching-based algorithm and the distance estimation-based algorithm. The localisation results show that the localisation error is around 0.5m $\sim$ 2m in a range of several meters. The disadvantage of the RSSI-based localisation system is that the PLE of the environment needs to be obtained empirically, which is time-consuming. Moreover, the noise in the RSSI measurements still influences the localisation accuracy significantly even though many efforts have been made to enhance the accuracy of the RSSI measurements. To further improve the localisation accuracy, localisation optimization algorithms need to be designed and implemented.

3.3   TDOA-based passive source localisation using multiple SDRs

While the RSSI-based localisation is simple to implement, the poor localisation accuracy remains to be a serious problem in many location-based applications and services. Moreover, the RSSI measurements become unreliable when the distance between the signal transmitter and the receiver is large because the target signals are more likely to suffer from the multipath effect and interference signals on a long propagation path. This drawback limits the applications of RSSI-based localisation in small region only. Among different measurement techniques, the time-based mea-

surements generally offer higher localisation accuracy and the sensor-target distance has little influence on the accuracy of time measurements. Therefore, a TDOA-based passive source localisation system is demonstrated using multiple spatially distributed SDRs. The TDOA measurements are used because the TDOA-based localisation can be implemented in a fully passive way without the cooperation of the signal source. Moreover, our implementation has a large sensor-target range which is several kilometers. The following parts will give a detailed design and implementation of the TDOA-based passive source localisation system developed using multiple spatially distributed SDRs.

3.3.1 TDOA-based source localisation

TDOA-based localisation systems, also known as hyperbolic localisation systems, are to determine the position of an emitter from measurements of the time differences of arrival of the emitter's signal at pairs of receivers whose location are known. In $\mathbb{R}^2$, suppose there is a stationary emitter or target whose location is given by $\mathbf{p} = [x \ y]^T$. Let $i \in 1, ..., N \geq 2$ indexes a number of sensors with the location of ith sensor given by $\mathbf{s}_i = [x_i \ y_i]^T$. Denote the range between the ith sensor $\mathbf{s}_i$ and the emitter $\mathbf{p}$ by $r_i = \|\mathbf{p} - \mathbf{s}_i\|$. Without loss of generality we take sensor 1 as the reference sensor, the noisy TDOA measurements between sensor 1 and sensor i, $(i \neq 1)$ are given by

$$\hat{t}_{i1} = \frac{d_{i1}}{v} + e_{i1}, \forall i \in 2, ..., N. \tag{3.8}$$

where v is the signal propagation speed, $d_{i1} = r_i - r_1$ and e_{i1} is the TDOA error. The error e_{i1} is assumed to be mutually independent and Gaussian distributed with zero mean and the same variance σ_t^2. A system of N sensors provides $N - 1$ independent TDOA measurements. Writing the time difference equations in vector form gives

$$\hat{\mathbf{t}} = \frac{\mathbf{d}}{v} + \mathbf{e} = [d_{21} \ d_{31} \ ... \ d_{N1}]^T + [e_{21} \ e_{31} \ ... \ e_{N1}]^T \tag{3.9}$$

The $N - 1$ TDOA measurements define $N - 1$ hyperbolas (or hyperboloid) in 2-dimensional (or 3-dimensional) space. $N = 4$ sensors are necessary and sufficient to uniquely localise an emitter in $\mathbb{R}^2$. In the absence of noise and interference, one can determine the position of the emitter by finding the intersection of hyperbolas. However, in the presence of noise the over-determined equations formed by the 3 independent TDOA measurements have no solution (see Figure 3.19). In order to obtain an approximate position estimate, various methods have been proposed Gholami et al. [2013]; Wang and Ho [2013]; Bishop et al. [2010]. The main idea of these approaches is similar: convert the localisation problem to an optimization problem.

3.3.2 Clock model and synchronization

TDOA-based localisation presents stringent requirements on the time synchronization accuracy between multiple sensors that are used to receive signal and calcu-
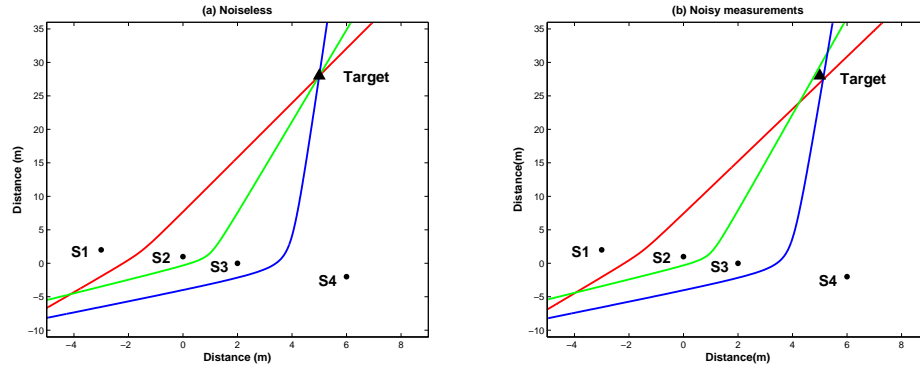
Figure 3.19: Hyperbolas of 3 independent TDOAs from four sensors in noiseless and noisy case

late TDOA measurements. Small time synchronization error can cause large distance error as the propagation speed of the electromagnetic signal is very high ($\approx 3 * 10^8$m/s). Assume the clock model of the local oscillators of ith SDR to be

$$C_i(t) = \alpha_i * t + \beta_i \tag{3.10}$$

where α_i and β_i denote clock skew and clock offset. For an ideal clock, we assume $\alpha_0 = 1$ and $\beta_0 = 0$, however, in practice, there are some clock skew and clock offset between the local clocks of different SDR units. Figure 3.20 shows an intuitive expression of how local clocks perform differently as a function of time. Here we assume the clock skew is constant. With different intrinsical time offsets and clock skews, the time stamps on the received samples will not be accurate such that time synchronization error is produced; therefore, accurate time synchronization solutions are required to correct the difference of the clock skews and clock offsets of different SDRs.

In general, time synchronization is mainly achieved through distributed methods using mutual communications between sensors or centralized methods using the reference broadcasting signal. Distributed methods usually require mutual communications between different sensors; however, in this source localisation implementation, different SDRs are far from each other (several kilometers), so the mutual communication between them is not available. Even if the communication between SDRs is possible, the SDRs which can actively send signals that carry time synchronization information must be developed, which will make the system more complex and consume more energy than current receiver-only-based implementation. Therefore, the centralized synchronization methods are chosen. Three methods are evaluated for the time synchronization of multiple SDRs, including NTP (Network Time Protocol), MIMO (Multi-input Multi-output) cable and the GPSDO.

NTP   NTP can be used to synchronize PCs running a Linux operating system to the time on a common network server. Using NTP, the hosts to which the USRP units are
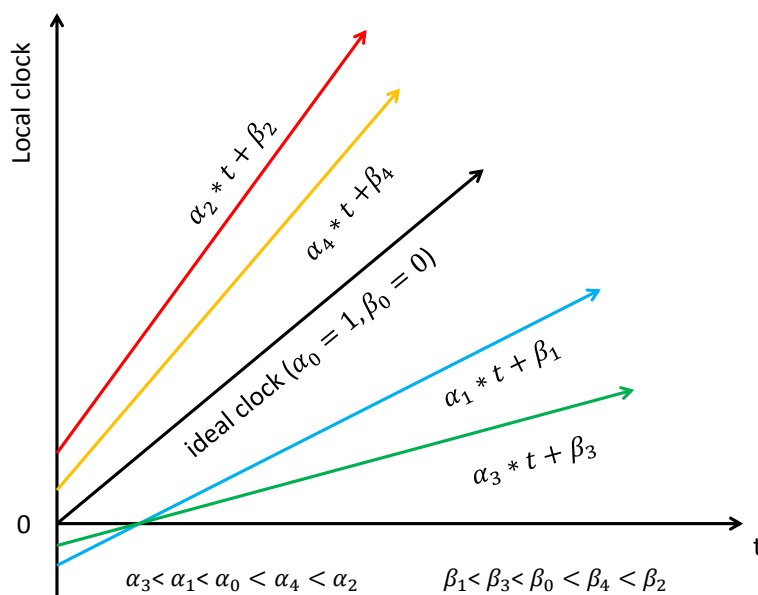
Figure 3.20: Different local clock running on different SDRs

attached can be connected to the Internet and all of them can be calibrated against public time servers. The process for using NTP involves installing NTP server in Ubuntu, configuring NTP server by running commend *editing /etc/ntp.conf* and then running *ntpdate* plus server name to synchronize the PC to the public server. In order to obtain a highly accurate result, it is recommended to use local country (national) servers, e.g. server 0.*au.pool.ntp.org* and listen to multiple servers.

Another method to use NTP was also attempted. Rather than calibrating time against a public server, a different approach is to set up a local area network consisting of multiple SDRs, where one SDR acts as the NTP server and others are clients. The same method as described above can then be used to synchronize the SDRs. The accuracy of this approach is similar to the previous one.

However, there are some limitations to the NTP-based synchronization method. Firstly, the time resolution of the NTP is 0.1 ms, which is not accurate enough for the TDOA-based localisation. This time resolution corresponds to 30 kilometers in distance. It means that, to use this synchronization method, the minimum distance (baseline) between two SDRs needs to be 30km, which is too far for experiments. Another major drawback of this method is that the NTP synchronizes the time of the host PCs, not the time reference of the USRP N210s directly. This introduces a second synchronization problem to be solved between the SDR and its host PC, which is not straight forward to tackle.

MIMO The MIMO expansion cable has a length of 0.5m and is used to link a pair of USRP N210 devices together. This method relies on physical connection to synchronize a pair of USRPs. The MIMO cable allows two connected USRPs to communicate clock and time reference information. To use it, one USRP must be configured as

the master and the other as the slave. The USRP reads the status of "mimo locked" sensor either "locked" or "unlocked" to indicate whether the two devices are synchronized through the MIMO cable. With correct setting, two devices are synchronized immediately after they are powered on. The synchronization accuracy is high as time deviation between the USRPs is 0. However, it can only be used to synchronize a pair of closely placed SDRs at a time, which is not suitable for multi-SDR-based applications.

GPSDO   To achieve high-accuracy synchronization among multiple spatially distributed SDRs in a large area, GPSDOs can be used. By installing one GPSDO unit on the motherboard of each USRP, the time and frequency reference of SDRs can be provided by GPSDOs. As opposed to physical cable connection, time synchronization using GPSDOs only requires the SDRs have access to the GPS satellites. Without working with the GPSDO, the local oscillator of the USRP is TCXO (Temperature Compensate crystal Oscillator) which gives 2.5 ppm (parts per million) frequency reference. Different USRPs begin to count individually after each power cycle such that they do not have an agreed time to support synchronized operation. After the GPSDO is used, the local oscillator of the USRP is disciplined by the GPS signal to achieve higher frequency accuracy. The frequency output of GPSDO is 10 MHz and the frequency reference accuracy is enhanced to 0.01 ppm, which is equivalent to +/- 0.1Hz frequency error. GPSDOs not only offer more accurate frequency output, but also provide an agreed time reference which is synchronized to the global GPS time among different USRPs. With this agreed time reference, synchronization based applications can be implemented using multiple SDRs. The 1 PPS time references of GPSDOs is synchronized to Coordinated Universal Time (UTC) and the achieved 1PPS accuracy is +/-50 nanoseconds.

To use the GPSDO to synchronize the SDRs, an appropriate external GPS antenna is required with a good view to the sky. SMA male straight black GPS antennas are used to compile with the connector of GPSDOs. It takes a few minutes for the GPSDO to lock on to the GPS signal. By checking the status of "gps locked" sensor on the USRP motherboard, the GPS receiver will declare "locked" or "unlocked". Once the GPSDO is locked to the GPS signal, the time of different USRPs is synchronized to the UTC time. By default, if a GPSDO is detected at startup, the USRP will be configured to use it as a frequency and time reference. The time output of GPSDO includes integer second and fractional second, e.g. "1333767848.21354165s".

3.3.3   TDOA measurement acquisition

After the synchronization among multiple spatially distributed SDRs is resolved, the TDOA measurements between pairs of SDRs can be obtained. In this passive source localisation, the SDRs overhear the signal source and they do not have any knowledge on the waveform or feature of the source signal, so the methods to obtain TDOA measurements which rely on the substraction of TOA measurements obtained by two individual SDRs do not work. Therefore, the cross correlation algorithm is

implemented to obtain TDOA measurements between multiple pairs of synchronized SDRs.

The signal transmitted from a remote source at two spatially separated sensors can be mathematically modeled as So et al. [2013]

$$x_1(m) = s(m) + \kappa_1(m)$$
$$x_2(m) = s(m - D) + \kappa_2(m)$$
$$m = 0, 1, ..., M - 1$$

(3.11)

where $s(m)$, $\kappa_1(m)$ and $\kappa_2(m)$ are independent zero-mean white Gaussian variables, M is the length of sampling. Digitalized signal $s(m)$ is assumed to be uncorrelated with noise $\kappa_1(m)$ and $\kappa_2(m)$. D is the delay of sampling points to be estimated, which is related to the TDOA measurements obtained by the two SDR-based receivers. $\hat{D}$ can be obtained by maximizing the cross-correlation between $x_1(m)$ and $x_2(m)$, that is

$$\hat{D} = arg \max_D J(D)$$
$$J(D) = \sum_{m=0}^{M-1} x_1(m - D)x_2(m)$$

(3.12)

In order to compute the cross correlation between the two signals in a more efficient way, both signals are first Fourier transformed. Their product is computed and then the inverse Fourier transform is applied. In the real-world applications though, there are many disturbing factors that will affect the position of the peak or mask it. These factors can be noise, reverberation and others. To address this disturbance, the Generalized Cross Correlation (GCC) was introduced Knapp and Carter [1976]. It implements a frequency domain weighting of the cross correlation according to different criteria in order to make it more robust to external disturbing factors. The general expression for the GCC is:

$$R^{GCC} = \mathcal{F}^{-1}(X_1(\omega_c)X_2^*(\omega_c)\psi(\omega_c))$$

(3.13)

where ψ is a weighting function. If $\psi = 1$ for all w, the standard cross correlation formula is formulated.

According to Knapp and Carter [1976], one weighting function is called ROTH correlation, which weights the cross correlation according to the Signal to Noise Ratio (SNR) value of the signal. Frequency bands with a low SNR obtain a poor estimate of the cross correlation and therefore are attenuated versus high SNR bands.

$$\psi_{ROTH}(w) = \frac{1}{X_1(w_c) \cdot X_1^*(w_c)}$$

(3.14)

A variation of the ROTH weight is the Smoothed Coherence Factor (SCOT) which acts upon the same SNR-based weighting concept, but allows both signals being

compared to have a different spectral noise density function.

$$\psi_{SCOT}(w) = \frac{1}{\sqrt{X_1(w_c) \cdot X_1^*(w_c) \cdot X_2(w_c) \cdot X_2^*(w_c)}} \tag{3.15}$$

In environments with high reverberation, the Phase Transform (PHAT) weighting function is the most appropriate as it normalizes the amplitude of the spectral density of the two signal and uses only the phase information to compute the cross correlation.

$$\psi_{PHAT}(w) = \frac{1}{|X_1(w_c) \cdot X_2^*(w_c)|} \tag{3.16}$$

Another weighting function of interest is the Hannan & Thomson, also known as Maximum Likelihood (ML) correlation, which also tries to maximize the SNR ratio of the signal.

$$\psi_{ML}(w_c) = \frac{|X_1(w_c)||X_2(w_c)|}{|N_1(w_c)|^2|X_2(w_c)|^2|N_2(w_c)|^2|X_1(w_c)|^2} \tag{3.17}$$

where $N_1(w_c)$ and $N_2(w_c)$ are the noise power spectra.

Finally, the Eckart filter maximizes the deflection criterion, i.e. the ratio of the changes in mean correlation output due to the signal present compared to the standard deviation of correlation output due to the noise alone. The weighting function achieving this is:

$$\psi_{eckart} = \frac{X_1(w_c)X_2^*(w_c)}{N_1(w_c)N_1^*(w_c) \cdot N_2(w_c)N_2^*(w_c)} \tag{3.18}$$

where $X_1(w_c)$ is the speech power spectra.

For this SDR-based TDOA source localisation system, different weights are evaluated, however, no large improvement on the TDOA measurements can be obtained. Therefore, for simplicity, the standard cross correlation is implemented on the digitalized signal received by pairs of SDRs. The TDOA is equal to $\frac{1}{f_s} * \hat{D}$ (f_s is the sampling rate of the SDR devices). The resolution of TDOA measurement is determined by the highest sampling rate that the SDR can achieve, 25M sps, which gives 40ns TDOA resolution, corresponding to 12m in distance.

3.3.4   The implementation of TDOA-based localisation using SDRs

3.3.4.1   Site investigation

To implement source localisation, the site investigation is an important step, which can make sure the SDRs can receive the signal source with reasonable SNR. It can be implemented by using one SDR to receive the signal of interest, followed by the time-frequency analysis of the received signal. Figure 3.21 shows the received signal in the time domain and the frequency domain. In the time domain, the waveform of the received signal can be observed. More importantly, from the signal spectrum in the frequency domain, the signal SNR can be obtained. If on a site where the SNR
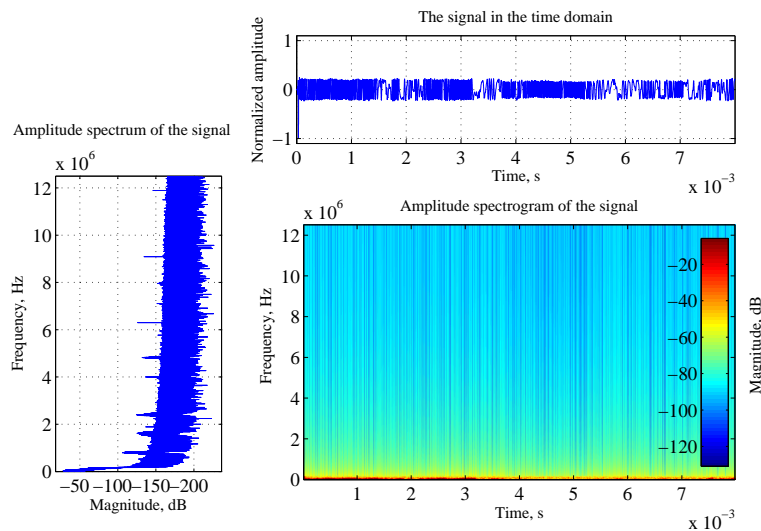
Figure 3.21: The time-frequency of the received signal

of the received signal is low or the source signal is submerged into the noise floor, it is very likely that the TDOA measurements will be very noisy or even wrong. In this situation, the site to take measurements needs to be changed. In addition, the bandwidth of the signal source can also be observed from the signal spectrum analysis so that we can check whether the parameters of the low pass filter are set properly.

Here are some examples to show why the site investigation is a must step before taking measurements and implementing source localisation. For the FM signal at 106.3 MHz, we found it can be received with reasonable SNR at all the investigated sites. However, when we want to receive the FM signal at 88 MHz from a different transmitter, we found that it can only be received in some regions that are relatively close to the signal emitter because the transmission power of that radio station is low. Even in the areas where the signal can be received properly, we found that the radio station of FM 88 MHz only works at certain hours during the day, while the radio station of 106.3 MHz works the whole day. For the reception of TV signal, at one site, signal from 5 TV stations can be received, their carrier frequency are 177.5 MHz, 184.5 MHz, 191.5 MHz, 219.5 MHz and 226.5 MHz. The first three TV signal have better signal reception quality than the latter two. However, at another site, only the last two TV signals at 219.5 MHz and 226.5 MHz can be detected. Therefore, we have to use the signal from one of the last two TV stations to implement the source localisation.

3.3.4.2 Signal acquisition and localisation

The signal processing diagram of one SDR-based receiver is shown in Figure 3.22, the UHD Source block manages the interaction between a USRP and its host PC. After
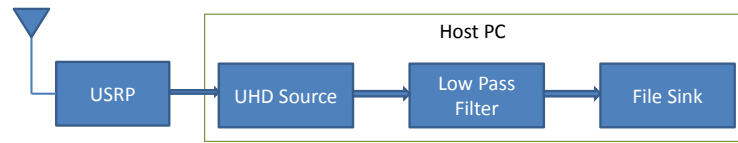
Figure 3.22: Processing diagram of SDR receiver
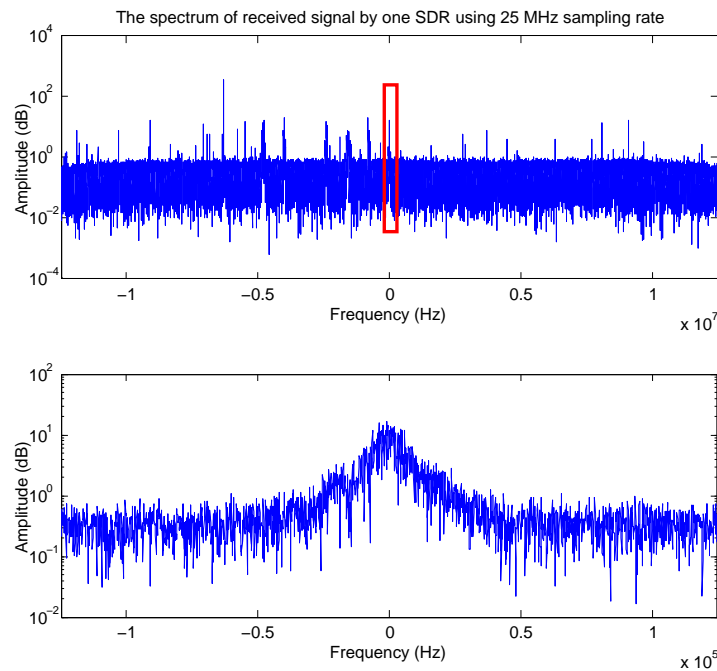
Figure 3.23: The use of LPF to extract signal of interest

being processed by the UHD Source block, the received baseband signal is passed to a Low Pass Filter (LPF), where the unwanted signal is attenuated. After the LPF, the received samples are passed to a File Sink block to be stored in the local host PC and uploaded to a central server.

The low pass filter plays an important role in obtaining accurate TDOA measurements. Since a high sampling rate is used to improve the time resolution of TDOA measurements, the unwanted interference signal can also be received under the sampling rate of 25M sps. The waveform of the received signal in the frequency domain is shown in Figure 3.23, where only the part included in the red box is the signal of interest. One can also see that the amplitude of some of the unwanted signals is even larger than the signal of interest. By zooming in the figure to the frequency of the signal of interest, the spectrum of the target signal can be observed. The aim of implementing a low pass filter is to remove all the unwanted signal and only keep the signal of interest.

Set up the system
- Identify the signal source of interest using frequency scan.
- Deploy SDRs spatially.
- Set up interest connection and communication between SDRs and their host PCs.

System monitoring and remote control
- Check whether multiple SDRs are synchronized.
- Set the trigger time of signal reception after they are synchronized.
- After signals are received by SDRs, they are uploaded automatically to a central server.

localisation
- At the central server, collect received signal and obtain TDOA measurements through cross correlation.
- Estimate the source location using localisation algorithms.

Figure 3.24: TDOA-based passive source localisation procedure

The work procedure of the passive source localisation system is shown in Figure 3.24. In practical source localisation, SDRs are deployed spatially in a large outdoor area to overhear the signal source of interest. The choice of the sites where the SDRs are deployed is determined by the previous site investigation based on the time-frequency analysis. A central server PC is used to monitor and control multiple SDRs remotely. After the synchronization is achieved through on-board GPSDOs, a specific time to trigger the event of SDR reception in the future is set for all SDRs. When the time arrives, SDRs begin to receive the signal, store the samples on the host computers and then upload to the central server PC automatically. At the central server, the TDOA measurements are calculated and then the location of the signal source is estimated. The whole procedure can be conducted many rounds to obtain multiple location estimates.

3.4 Joint TDOA and FDOA-based passive source localisation using two SDRs

In the previous section, multiple spatially distributed stationary SDRs have been used to implement a passive localisation of a stationary emitter. In general, by increasing the number of the SDRs, the localisation accuracy can be enhanced, but this will increase the system cost. To further reduce the system cost, and more importantly, to deal with the situation when the deployment of multiple SDRs is not feasible due to geographical restrictions, a mobile SDR platform is developed, and by having another stationary SDR, the passive localisation of the stationary emitter can still be achieved. In addition to the TDOA measurements, the FDOA measurements are also

used to capture the Doppler shift of the received signal. In the following parts, the design of the joint TDOA and FDOA-based localisation using only two SDRs will be provided.

3.4.1 Joint TDOA and FDOA-based source localisation

A localisation scenario with two mobile receivers and one stationary emitter is considered. Each receiver's position and velocity are assumed to be known at the moment when measurements are taken, and their clocks and frequency oscillators are assumed synchronized. The emitter is non-cooperative with the receivers, and the mobile receivers overhear the signal transmitted from the emitter at different time instants to obtain multiple pairs of TDOA and FDOA measurements which are used to implement the passive localisation of the emitter. Each TDOA measurement or FDOA measurement will determine a curve where the emitter lies on. By having multiple curves defined by multiple TDOA and FDOA pairs, the localisation of the emitter can be determined uniquely. In the absence of noise and interference, one can determine the position of the emitter by finding the intersection of those curves. In Figure 3.25, the source localisation using one stationary receiver and one mobile receiver in the noiseless case is described, where the black triangle denotes the stationary emitter, the black dot marked by $S1$ denotes the stationary sensor, the black dot marked by $S2$ denotes the position of the mobile sensor, the black arrow denotes the moving trajectory of the mobile sensor, the red curves are determined by the TDOA measurements and the green curves are determined by the FDOA measurements. However, in the presence of noise, these curves will no longer intersect exactly at the same point, as shown in Figure 3.25 in the noisy case. To obtain approximate source location estimates, the localisation problem can be converted to an optimization problem. Figure 3.25 shows that the measurements are taken at equal time interval and the mobile sensor moves on a straight line. Note that moving on a straight line is not necessary as long as the two sensors receiver the target signal synchronously. Increasing the way points where the measurements are taken will increase the number of TDOA and FDOA measurement pairs, which can improve the localisation accuracy.

The joint TDOA and FDOA-based localisation can be formalized as follows: in $\mathbb{R}^2$, suppose there is a stationary emitter whose initially unknown location is given by $\mathbf{p} = [x\ y]^T$. The known coordinates of the two sensors to receive signal from the emitter at the same time interval k can be denoted by $\mathbf{s}_k^1 = [x_k^1\ x_k^1]^T$ and $\mathbf{s}_k^2 = [x_k^2\ y_k^2]^T$. $k = 1, 2, 3..., K$ denotes time series when the signal is acquired by the two sensors. Likewise, their velocities at the kth time instant are denoted by $\mathbf{v}_k^1$ and $\mathbf{v}_k^2$. The distance vector between the emitter and the two sensors are thus denoted by $\mathbf{d}_k^1 = \mathbf{p} - \mathbf{s}_k^1$ and $\mathbf{d}_k^2 = \mathbf{p} - \mathbf{s}_k^2$, whereas the respective (scaler) distances are denoted by $r_k^1(\mathbf{p}) = \sqrt{(\mathbf{d}_k^1)^T \mathbf{d}_k^1}$ and $r_k^2(\mathbf{p}) = \sqrt{(\mathbf{d}_k^2)^T \mathbf{d}_k^2}$, so the true TDOA is given by

$$\tau_k(\mathbf{p}) = \frac{1}{c}(r_k^1(\mathbf{p}) - r_k^2(\mathbf{p})) \tag{3.19}$$
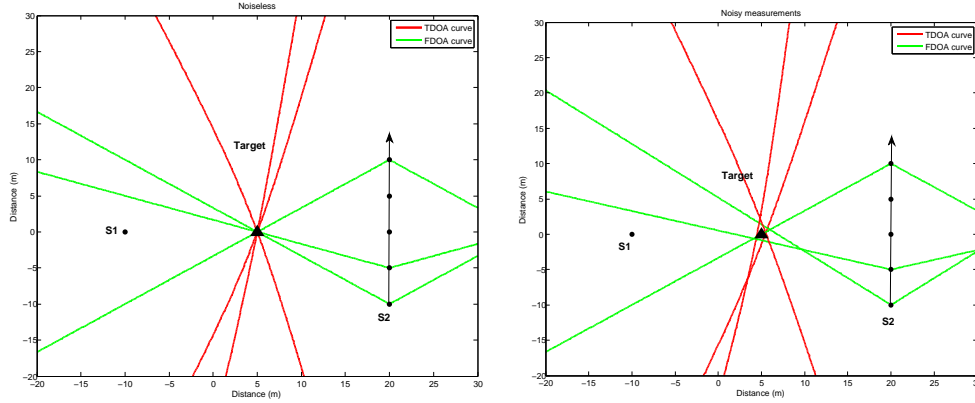
Figure 3.25: Joint TDOA and FDOA-based localisation in noiseless and noisy case

where c denotes the propagation speed of the electromagnetic signal and $c \approx 3 * 10^8$. Denote f_c as the carrier frequency of the target signal, the Doppler-induced FDOA is given by

$$\nu_k(\mathbf{p}) = \frac{f_c}{c}(\mathbf{v}_k^1)^T \mathbf{u}_k^1(\mathbf{p})) - (\mathbf{v}_k^2)^T \mathbf{u}_k^2(\mathbf{p})) \tag{3.20}$$

where

$$\mathbf{u}_k^1(\mathbf{p}) = \frac{\mathbf{d}_k^1}{r_k^1(\mathbf{p})}, \ \mathbf{u}_k^2(\mathbf{p}) = \frac{\mathbf{d}_k^2}{r_k^2(\mathbf{p})} \tag{3.21}$$

are the unit vectors in the direction pointing from the respective sensors to the source.

At the kth time instant, denote the TDOA and FDOA pair by $\hat{\mathbf{\Phi}}_k = [\hat{\tau}_k \ \hat{\nu}_k]$. $\hat{\tau}_k$ is the noisy TDOA measurement and given by

$$\hat{\tau}_k = \tau_k + \omega_k^t \tag{3.22}$$

where ω_k^t denotes the additive zero-mean white Gaussian noise with covariance σ_t^2. Similarly, $\hat{\nu}_k$ is the noisy FDOA measurement and given by

$$\hat{\nu}_k = \nu_k + \omega_k^f \tag{3.23}$$

where ω_k^f denotes the zero-mean white Gaussian noise with covariance σ_f^2. We also assume that ω_k^t and ω_k^f are mutually independent (uncorrelated) and their covariance matrix can be denoted by

$$\mathbf{Q}_k^{tf} = \begin{bmatrix} \mathbf{Q}_k^t & \mathbf{0} \\ \mathbf{0} & \mathbf{Q}_k^f \end{bmatrix} \tag{3.24}$$

where $\mathbf{0}$ is a $k-1 \times k-1$ matrix of zero.

3.4.2 TDOA and FDOA measurement acquisition

To compute the TDOA and FDOA pair at the kth time instant, the cross ambiguity function (CAF) is usually used. Assume the model for two complex baseband signal received by two sensors at one time interval is given by:

$$
\begin{aligned}
x_1[m] &= s[m - D_1]e^{j2\pi\frac{q_1}{M}m} \\
x_2[m] &= s[m - D_2]e^{j2\pi\frac{q_2}{M}m}
\end{aligned}
\tag{3.25}
$$

where $s[m]$ is the discrete-time version of the source signal, D_1 and D_2 are time delays of the source signal received at the two sensors in the units of samples, $\frac{q_1}{M}$ and $\frac{q_2}{M}$ are the Doppler shifts as a fraction of sampling frequency. The CAF between $x_1[m]$ and $x_2[m]$ is expressed by mathematically

$$
\begin{aligned}
\Lambda(\Delta D, \Delta q) &= \sum_{m=0}^{M-1} \hat{x}_1[m]\hat{x}_2^*[m + \Delta D]e^{-j2\pi\frac{\Delta q}{M}m} \\
&= s[m - D_1]s[m - D_2 + \Delta q] * e^{j2\pi\frac{D_1 - D_2 - \Delta q}{M}m}
\end{aligned}
\tag{3.26}
$$

In this case, $|\Lambda(\Delta D, \Delta q)|$ is maximized when $\Delta D = D_1 - D_2$ and $\Delta q = q_1 - q_2$. Using the sampling interval T_s and the sampling rate f_s, TDOA is calculated by $\Delta D * T_s$ in seconds and FDOA is calculated by $\frac{\Delta q}{M} * f_s$ in Hertz.

To obtain the TDOA and FDOA measurements that maximize the magnitude of the CAF, it is required to search over a wide range of ΔD and Δq. The searching space of TDOA measurements depends on the real deployment of the sensors and the signal source, which can be very large in large-area localisation. The searching space of FDOA measurements depends on the largest relative movement velocity between the sensors and the emitter and the carrier frequency of the signal source. For example, assume we have one stationary sensor and one mobile vehicle to take FDOA measurements from a stationary signal emitter. In a general situation, the highest speed of a vehicle (car) is up to 120 km/h in urban area. Since the signal sources we use are the FM signal and the TV signal with the carrier frequency range between 88 MHz and 300 MHz, the searching space for FDOA measurements can be obtained according to (3.27)

$$
\frac{\Delta v}{\Delta f} = \frac{c}{f_c}
\tag{3.27}
$$

where Δv and Δf denote the speed change in the direction which causes the largest Doppler shift and the frequency change respectively. $c \approx 3 * 10^8$ is the speed of light and f_c is the carrier frequency of the signal source. For the FM radio signal at the carrier frequency of 106.3 MHz, the maximum searching space of FDOA measurements is from -11.1 Hz to 11.1 Hz. For the TV signal at the carrier frequency of 226.5 MHz, the maximum searching space of FDOA measurements is from -25.2 Hz to 25.2 Hz.

Even the searching space can be restricted to reasonable range, the use of CAF is still computationally expensive even for modern computers. Instead of implementing

Figure 3.26: The mobile SDR

the CAF directly using the summation and iterating through each TDOA and FDOA value, the CAF can be computed more efficiently using a cross correlation and an FFT Johnson [2001]:

$$\Lambda(\Delta D, \Delta q) = FFT[\hat{x}_1[m]\tilde{x}_2^*[m + \Delta D]] \tag{3.28}$$

3.4.3 The implementation of joint TDOA and FDOA-based localisation using two SDRs

3.4.3.1 Mobile SDR development

The mobile SDR is developed by mounting the USRP N210 on a car, as shown in Figure 3.26. A shelf is made and fixed at the back of the car boot. The host PC and the USRP N210 are fixed at the top two tiers of the shelf. The GPS antenna and the signal antenna are attached outside the car on the top of the car roof to make sure good reception of the GPS signal and the source signal. The USRP is powered by a mobile power station and the host PC runs on its own battery. Another power supply solution is to use a power converter so that the car battery can be used to provide power supply to both the USRP and the host PC. The car can run at a speed up to 100 km/h to make sure the signal received by the mobile SDR has Doppler shift.

At the time when the thesis was written, a new version of USRP, USRP B200mini, is available from the Ettus Research Ettus [2008]. The attractive feature of this SDR is its small size which is 5.0 cm by 8.4 cm. With the small size and light weight, the SDR can be mounted on a UAV, which can extend the mobility the mobile SDR from 2D to 3D so that more applications can be possible. The development of UAV-based mobile SDR is not covered in this thesis.

GPS output	interpretation
65240.00	Taken at 18:52:40 UTC
A	Status A=active or V=Void
3516.1199,S	Latitude 35 deg 16.1199' S
14906.7520,E	Longitude 149 deg 06.7520' E
37.9	Speed over the ground in knots
151.6	Heading angle in degrees True
310515	Date - 31 May 2015
*1A	The checksum data, always begins with *

Table 3.6: GPRMC interpretation

3.4.3.2   Signal acquisition and localisation

The signal processing diagrams of the stationary SDR and the mobile SDR are the same as shown in Figure 3.22. The low pass filter is used to filter out the signal outside the frequency band of interest, and the received signal is stored in a data file for further processing. The position and the velocity of the two SDRs are obtained from on-board GPSDOs by decoding the GPSDO NMEA sentences. In this implementation, the GPSDO NEMA sentence in "GPRMC" format, which stands for "Recommended minimum specific GPS data", is used. At each time instant when the SDRs start to receive the signal from the emitter, a GPRMC formatted GPS data is recorded and then interpreted to extract useful information. Take one GPRMC output as an example:

$GPRMC, 105240.00, A, 3516.1199, S, 14906.7520, E, 37.9, 151.6, 310515, , *1A$

The decoding information can be found in Table 3.6, from which one can obtain the sensor's position and velocity to implement source localisation.

The localisation experiments are implemented in the outdoor environment, and during the localisation experiments, one SDR is stationary and it is used as the reference sensor. The other SDR is mobile and it takes measurements while it is moving. The two SDRs overhear the signal source of interest and take measurements after they are synchronized using GPSDOs. Since the two SDRs are distributed far from each other, to check whether they are synchronized, either an additional server PC or the host PC attached to the stationary SDR that runs "TeamViewer" software can be used. Script programs are designed on the two SDRs to allow synchronous sampling. The length of sampling time at each time instant is very short and we try to let the car move smoothly in order to avoid large variance of the Doppler shift during the sampling interval. After the signal is received and stored into a data file, the data file is uploaded automatically to a central PC through cellular network. When the data files contain signals received at the same time are received, the joint TDOA and FDOA measurements are calculated through the CAF, then the location of the signal source is estimated. The time delay in location estimation depends on the speed of signal transmission on cellular network, the speed of signal processing and location estimation on the central PC.

3.5 Summary

In this Chapter, the detailed design and implementation of the source localisation systems using SDRs are presented, including a RSSI-based localisation system, a TDOA-based localisation system and a joint TDOA and FDOA-based localisation system. Firstly, the devices for the source localisation implementation are introduced. The structure of the core device, USRP N210, and its reception and transmission principles are analysed. To cover the signals at different frequency bands and evaluate the quality of the received signals, the WBX daughterboard and three types of antennas, LP0410, VERT400 and telescopic antenna, are used in the system implementation. The working principle of the GPSDO unit is also discussed.

Secondly, the RSSI-based localisation system is developed using multiple SDRs. After reviewing the path loss model and the principle of RSSI-based localisation, the methods to obtain the RSSI measurements are proposed. However, the accuracy of the RSSI measurements is inevitably affected by the hardware precision and the signal propagation environment. To improve the RSSI measurement accuracy, efforts have been made to address the influence of the hardware and the environment. The RSSI-based localisation is demonstrated using multiple SDR-based transceivers in both an indoor and outdoor environment. Two localisation algorithms are implemented. One is the RSSI matching-based method, which determines the location of the emitter by finding the best matching RSSI pattern in the lookup table. The other is the commonly used distance estimation-based method, which transfers RSSI measurements into distance measurements and obtains the location estimate by using distance-based localisation algorithms. The localisation error is around 0.5m $\sim$ 2m in an average range of several metres for all the localisation implementations.

The drawback of the RSSI-based localisation system is the poor localisation accuracy. In contrast, time-based localisation can provide more accurate results, resulting in TDOA-based passive source localisation system that is demonstrated by using multiple spatially distributed SDRs. To design the localisation systems, the achievable performance of the USRP N210 is assessed. In the TDOA-based localisation system, the SDRs are developed as the receivers only, meaning the range of the system implementation can be large as long as the signal can be received with a reasonable level of SNR. An important issue of the TDOA-based localisation concerns the time synchronisation among multiple spatially distributed SDRs. Since each SDR unit runs on its own local oscillator with a different local time, the accurate synchronisation techniques must be developed. To solve the synchronisation problem, three synchronisation techniques are investigated in terms of their achievable time synchronisation accuracy. Finally, the GPSDO-based solution has been chosen. To obtain TDOA measurements between the SDR pairs, different cross-correlation-based methods are evaluated. After these two key problems in the TDOA-based localisation are solved, the SDR-based receivers are developed using USRP N210s and GNU Radio to implement signal sensing and localisation.

When it is not feasible to deploy multiple spatially distributed SDRs in the area of interest as a way of implementing source localisation, an alternative passive source

localisation solution is proposed; the joint TDOA and FDOA-based source localisation using only two SDRs. Another advantage of this solution is that it can reduce the system cost by using fewer SDRs. Similar to the TDOA-based localisation, a critical issue in the joint TDOA and FDOA-based localisation also concerns synchronisation. The TDOA measurements require the accurate time synchronisation across different SDRs and the FDOA measurements pose an additional requirement on the accurate frequency synchronisation. To solve the synchronisation problem, we found the GPSDO to be an effective solution. To obtain FDOA measurements, one stationary SDR-based receiver and one mobile SDR-based receiver are developed. The joint TDOA and FDOA measurements are obtained using the proposed computationally efficient CAF algorithm.

Measurement accuracy analysis

The implementation of source localisation is generally divided into two steps. The measurements need to be obtained first, and then they are used in the localisation algorithms to obtain the source location estimates. Therefore, the accuracy of measurements plays an important role in the accurate source localisation. In Section 4.1, the factors that influence the accuracy of the TDOA measurements and the joint TDOA and FDOA measurements are systematically analyzed from three aspects, including the hardware precision, the accuracy of signal processing methods and the environmental impact. Section 4.2 proposes the measurement error reduction approaches to address the error sources in order to improve the accuracy of measurements.

4.1 Measurement error source analysis

In the real-world localisation implementation, there are many factors that can cause measurement error and, thereby, influencing the localisation accuracy. During the implementation of the source localisation systems, we found that the measurement error is mainly from three types of error sources, including hardware precision, the accuracy of signal processing methods and, the environmental impact.

4.1.1 Hardware precision

The achievable precision of the hardware has a significant impact on the accuracy of measurements. Firstly, in the TDOA-based localisation, the time delay is estimated from the discrete signal received by a pair of SDRs through the cross correlation, therefore, the resolution of the sampling interval restricts the resolution of the TDOA measurements. For example, if the sampling rate of 1Msps is used in signal reception, the minimum time interval between two consecutive samples is 1 μs. Since the propagation speed of RF signal source is close to the speed of light, $3 * 10^8$ m/s, 1 μs time interval is equivalent to 300 m in distance. This distance error will cause a large localisation error. The SDR module we use, USRP N210, can achieve up to 25 Msps, which corresponds to 40 ns time interval between two consecutive samples and 12 m in distance. In other words, 40ns is the highest resolution of the TDOA measurements that is achievable by the SDR. Another factor that influences the accu-

racy of the TDOA measurement is the synchronisation accuracy. To realise the time synchronisation among multiple spatially distributed SDRs, the GPSDO is installed on each SDR unit. The 1 PPS time reference of the GPSDO is synchronised to the UTC and the achieved 1PPS accuracy is +/-50 nanoseconds, therefore, in the worst case, the error of TDOA measurements obtained by two synchronised SDRs is 100 ns, which is 30 m measurement error in distance. That is to say, up to 100 ns TDOA error can be expected in the TDOA measurements. If we also consider the measurement error caused by the resolution of sampling interval, in the worst case, the timing error caused by the hardware device is 140 ns, corresponding to 42 m in distance. In addition, during the location estimation process, the positions of multiple SDRs are also used such that the sensor position error caused by the GPSDOs will also influence the localisation accuracy.

In the joint TDOA and FDOA-based localisation, the time error caused by the precision of the hardware devices has a large impact on the localisation accuracy as well. Moreover, the frequency accuracy of the GPSDO influences the accuracy of the FDOA measurements. The frequency output of the GPSDO is 10 MHz and the frequency reference accuracy is 0.01 ppm, which is equivalent to +/- 0.1Hz frequency error, therefore, in the worst case, the GPSDO can give 0.2 Hz FDOA measurement error. In addition, the carrier frequency of the signal source influences the sensitivity of the FDOA measurements. According to (3.27), for the FM signal with the carrier frequency at 106.3 MHz, the change of 1 Hz FDOA measurements requires a speed change of 10.16 km/h in the direction which induces the Doppler shift. On the other hand, a speed change of 4.768 km/h in the direction that induces the Doppler shift will give 1 Hz FDOA change using the TV signal with the carrier frequency at 226.5 MHz.

4.1.2 The accuracy of signal processing methods

The methods to process the received signal using the SDRs plays an important role in obtaining high-quality signal which is beneficial for accurate measurements. In the TDOA-based localisation and the joint TDOA and FDOA-based localisation, a high sampling rate is used to improve the resolution of the TDOA measurements. However, the drawback of using a high sampling rate is that the received signal is a mixed version of the signal of interest and the signals at unwanted frequency bands. As shown in Figure 4.1, in a bandwidth of 10 MHz centered at the centred frequency of the signal of interest, there are other signals and most of them have higher SNR than the signal of interest, such as the baseband signal at the -3 MHz. The unwanted signals will definitely produce a large interference on the signal of interest and if the received signal is used without further processing, the TDOA measurements or the FDOA measurements could be wrong.

To solve this problem, applying a low-pass filter is an effective method to remove the unwanted interference signals within the sampling bandwidth Hua et al. [2012]. One key problem to implement an efficient low-pass filter is to choose the optimal parameters, such as the cut-off frequency and the width of transmission band. If
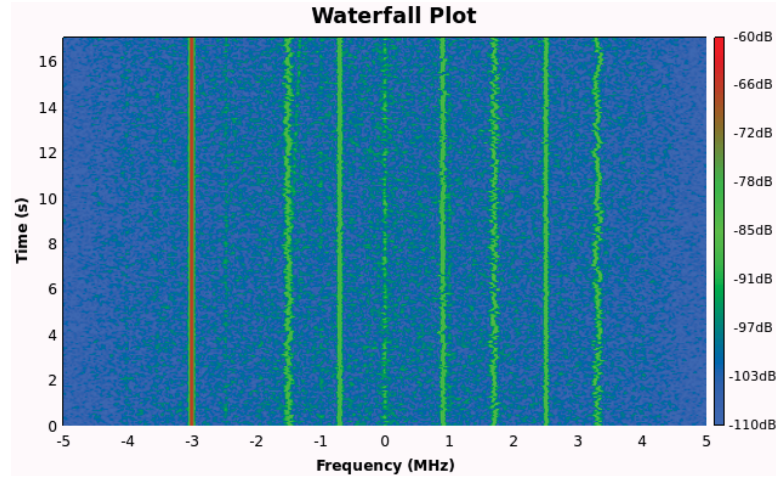
Figure 4.1: Three receivers and one target

those parameters are not chosen properly, the low pass filter will fail to remove or attenuate the interference signals, which will cause a large measurement error.

According to the Cramer Rao Lower Bound (CRLB) of the time difference estimate (4.1) introduced in Huang et al. [2015]:

$$\sigma_\tau^2 \sim \frac{1}{T_s * B^3 * SNR} \tag{4.1}$$

The variance of the TDOA measurements is related to the signal SNR, the length of sampling time T_s and the signal bandwidth B. The influence of the signal bandwidth on TDOA measurements can be explained as follows: the cross correlation of the narrow band signal has flat correlation peak which makes it difficult to find the true peak, so it is more likely to obtain wrong time delay estimates, as shown in Figure. 4.2. While the bandwidth of a particular signal B cannot be changed in the experiments, we use both the narrow-band and the wide-band signal to implement source localisation to demonstrate the influence of the bandwidth on the accuracy of TDOA measurements.

Similarly, according to the CRLB of FDOA estimate introduced in Stein [1981]:

$$\sigma_\nu^2 \sim \frac{1}{T_s^3 * B * SNR} \tag{4.2}$$

The variance of the FDOA measurements is also related to the signal SNR, the length of sampling time T_s and the signal bandwidth B. Therefore, we can see that large B improves TDOA measurement accuracy and large T_s improves FDOA measurement accuracy. Among the three variables, the signal SNR and the signal bandwidth depend on the features of the signal of interest. The length of sampling time is a relatively easily controlled variable during the reception of the signal. Decreasing T_s increases the variance of both TDOA measurements and FDOA measurements. To
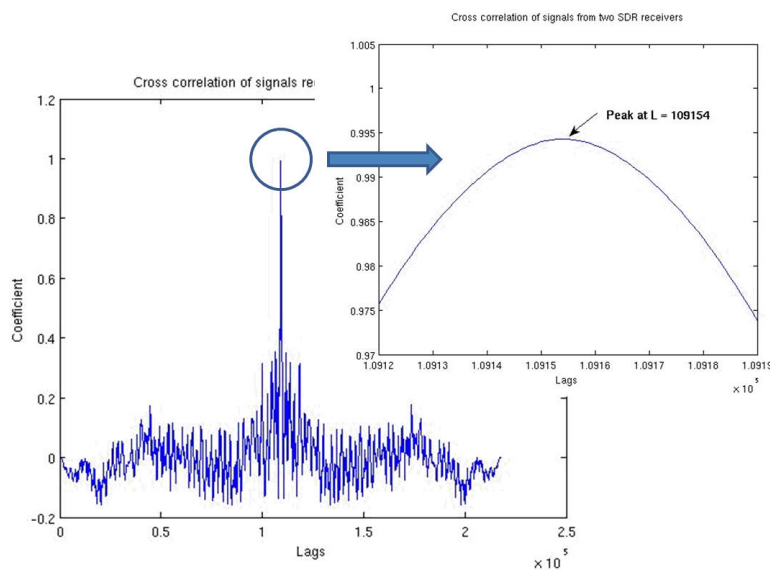
Figure 4.2: Flat cross correlation peak

increase the accuracy of TDOA and FDOA measurements, the accumulated sampling should be increased. However, for a practical localisation system, a long sampling time will produce a large number of samples, so it not only increases the computing burden of the sensors but also reduces the updating frequency of the system. Therefore, the length of sampling time T_s needs to be carefully chosen.

4.1.3 Environmental impact

In the real-world localisation, the environment also has a significant impact on the measurement accuracy. The complex electromagnetic environment affects the quality of the transmitted and received signals. Two types of environment related factors are almost inevitable, namely NLOS error and multipath effect.

Firstly, the availability of the power supply and wireless network for data exchange will facilitate the operation and signal acquisition of this SDR-based localisation system greatly, so the localisation experiments are all implemented in urban areas. During the experiments, we found that the accuracy of the TDOA and FDOA measurement are influenced by the none-line-of-sight (NLOS) error. The NLOS errors between two sensors can arise when the line-of-sight (LOS) propagation between them is obstructed by buildings or the impact of terrain. In urban areas, the influence of buildings and terrain is more serve than that in rural areas. When the NLOS error exists, the signal travels longer distance before being received because the direct signal propagation path is blocked. In the TDOA-based localisation and the joint TDOA and FDOA-based localisation, only the reference SDR is ensured to be under a LOS condition to the signal source. The other stationary SDRs are deployed without clear LOS condition to the signal source due to the availability of the power supply. The mobile SDR takes measurements under either LOS condition or NLOS condition dur-

ing its movement. Therefore, the accuracy of the TDOA and FDOA measurements is degraded by the NLOS error.

Another factor that widely influences the measurement accuracy of almost all practical localisation systems is the multipath effect. When the multipath effect exists, the received signal is actually the superposition of the signals travelling at the direct path and the reflected paths caused by terrestrial objects, e.g. buildings, walls, etc. This produces difficulties in distinguishing the signal on the direct path from other paths, which influences the measurement accuracy. The TDOA based-localisation system and the joint TDOA and FDOA-based localisation system are implemented in a large outdoor area. Even in a condition of LOS propagation, the reflected signals from buildings and trees will still exist. When a mobile SDR is used, the multipath can cause more severe and unpredictable influence on the measurement accuracy.

4.2   Measurement error reduction

After identifying the factors that influence the measurement accuracy, effective methods need to be implemented to reduce the measurement error. In this section, methods to improve the measurement accuracy are proposed and evaluated in the real-world experiments. The investigation of measurement error reduction methods will be discussed for the TDOA-based localisation system and the joint TDOA and FDOA-based localisation system.

4.2.1   Improvement of TDOA measurement accuracy

4.2.1.1   Hardware calibration

RF antennas play an important role in obtaining high SNR. We found that without using antennas the signal of interest is submerged into the noise floor, and it is impossible to distinguish the useful signal from the noise. In addition, different types of antennas have different effects on the signal amplification and noise attenuation. In the TDOA based-source localisation, three types of antenna are tested. At the beginning of the system development, we have ordered four directional PCB antennas "LP0410" together with the USRP N210s from the manufacturer, Ettus Research. This type of antenna covers the frequency band from 400 MHz to 1 GHz. However, no suitable signal source within these frequency bands can be found for the demonstration of the TDOA-based localisation system. At the end, we found an established signal tower is suitable for the large-area localisation demonstration because of its high transmission power and large coverage. The signal power provides the FM and TV service for the urban area. While the "LP0410" antenna is not specifically designed for the frequency bands of FM and TV signals, we can still use it to receive. We found that the signal can be received correctly and the TDOA measurements can be obtained with a reasonable accuracy. However, we suspected that the directional feature of the antenna may influence the quality of the signal and thus the measurement accuracy. Moreover, for the passive source localisation, the direction

of the signal sources is unknown, so omni-directional antennas are preferred. Then, the omni-directional antenna "VERT 400", which is designed for 144 MHz, 400 MHz and 1200 MHz Tri-band signal reception is used. This type of antenna is originally ordered for the RSSI-based localisation. However, for a preliminary investigation, even though the signals of interest do not fall in the range of the "VERT 400" antenna, they are still used in the experiments. The results actually show the similar measurement accuracy to the results obtained by using the "LP0410" antenna. In this situation, we can know that the "VERT 400" antenna will give better performance than the "LP0410" antenna in the passive source localisation. To further improve the quality of the received signal, the low-cost omni-directional telescopic antennas are ordered. The products cover the frequency band of the FM and TV signal. Another good thing is that the SMA male connector of the antenna suits the USRP N210s well, so this type of antenna does not require external connectors to work with the USRPs, which provides a good finishing to the localisation system. After some experiments were implemented, we found the measurement accuracy is also slightly enhanced. Therefore, the omni-directional telescopic antennas are used in the TDOA-based localisation system as well as the joint TDOA and FDOA-based localisation system.

On each WBX daughter board, there is only one signal receiving chain, but two antenna ports that can be selected. One antenna port is "Tx/Rx", which can be used for transmission and reception purpose, the other antenna port is "RX2", which can be used for receiving only. In experiments, we found that the two antenna ports for signal reception gave slightly different sensitivity. In passive source localisation, the antenna port with better signal sensing sensitivity is preferred. To determine which port is better, the two antenna ports are used to receive the signal respectively from a local FM radio station at the carrier frequency of 88 MHz. The radio transmission power of this FM signal is low. The antenna gain is set to 30 dB and the sampling rate is set to 1 MHz. Figure 4.3 shows the spectrum of the signal received using the "Tx/Rx" antenna port in the frequency domain, from which one cannot distinguish the signal of interest and the noise. In contrast, from Figure 4.4, which shows the spectrum of the signal received using the "RX2" antenna port in the frequency domain, one can easily distinguish the signal of interest from the noise floor, and one can see that the power of the signal of interest is 20 dB higher than the noise floor. After the investigation, we know that the noise floor of the antenna port "Tx/Rx" is -60 dB which is higher than the noise floor of the antenna port "Rx2" (-80 dB). Furthermore, other WBX daughter boards are investigated in the same way and we found that "Rx2" antenna ports do not always have higher sensitivity than "Tx/Rx" ports. For two daughter boards, the "Tx/Rx" ports have better sensitivity than the "Rx2" ports. In experiments, we always choose the ports with higher sensitivity to receive the signal of interest.

4.2.1.2   Parameter choosing for accurate measurements

In the process of signal reception and signal processing, proper parameter settings of the signal process components are important to obtain high-quality signal. As
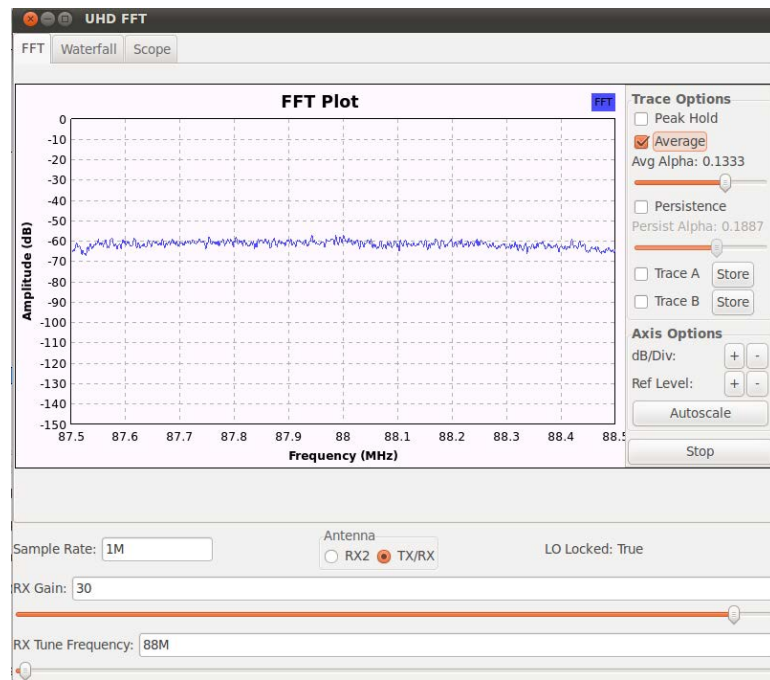
Figure 4.3: FM radio signal at 88 MHz received by the "Tx/Rx" port of one WBX
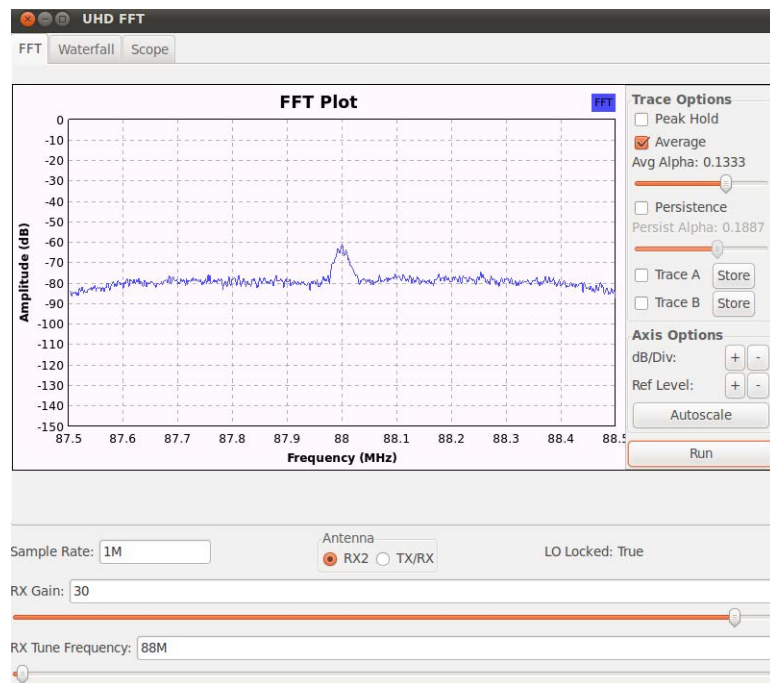
Figure 4.4: FM radio signal at 88 MHz received by the "RX2" port of one WBX

Figure 4.5: Experimental setup of two co-located SDRs

discussed, the parameters of the low pass filter and the length of sampling time in each signal acquisition cycle are important to reduce the variance of the TDOA measurements, so the optimal setting of them will be studied. To obtain the optimal parameter settings, two co-located synchronised SDRs are used to receive the signal of interest and investigate how these parameters influence the accuracy of the TDOA measurements. The experimental setup is shown in Figure 4.5. The two SDRs are synchronised by GPSDOs and the GPS antennas have good view to the satellites. Moreover, both of the SDRs' antennas have line-of-sight condition to the signal emitter to be localised. The reason why two co-located SDRs are used is that we can easily obtain a ground truth: $TDOA \approx 0$. In practice, every TDOA measurement includes the error caused by the synchronisation error, so the measurements will not be exactly zero. To obtain the optimal setting of signal processing parameters, we can take measurements by changing only one parameter and keep other parameters constant. By taking a lot of measurements under different values of one parameter, the optimal value of that parameter can be obtained empirically.

Cut-off frequency of the low pass filter   As can be seen from Figure 3.23, a lot of unwanted signals are also received by the SDRs. To keep the signal of interest only, an LPF is critical to attenuate the unwanted signal lying outside the bandwidth of interest. Two important parameters during the design of the low pass filter are the cut-off frequency and the width of the transmission band. Inappropriate cut-off frequency may filter out some frequency components of the signal of interest or cannot attenuate or remove the unwanted signal. Similarly, the wide transmission bandwidth may not be able to remove the unwanted signal and the very narrow transmission bandwidth may cause the high computational burden.

Since the FM radio signal usually occupies 200 kHz bandwidth, three cut-off frequencies, 50 kHz, 100 kHz and 200 kHz, are tested, and their influence on the accuracy of the TDOA measurements is compared. The transmission band is set to 50 kHz in the investigation. The results under the three cut-off frequencies are

Cut-off frequency of LPS	Standard deviation TDOA measurements	Standard deviation of distance error
50kHz	536.8ns	161.1m
100kHz	201.7ns	60.51m
200kHz	195.4ns	58.63m

Table 4.1: The influence of LPF cut-off frequency

shown in Table 4.1. The cut-off frequency of 50 kHz gives low accuracy with large standard deviations of measurement error, 536.8 ns in time and 161.1 m in distance. By increasing the width of the low pass filter, the standard deviations of the TDOA measurement error are reduced. The 100 kHz and 200 kHz bandwidth show similar accuracy of TDOA measurements, but 100 kHz bandwidth gives better signal reception quality. In addition, the accurate TDOA measurements always correspond to the high cross correlation coefficient using the low pass filter with 100 kHz cut-off frequency, which can help us to identify the erroneous TDOA measurements.

The empirical approach to obtain the optimal cut-off frequency of the low pass filter is time consuming. A more efficient approach is to obverse the spectrum of the received signal and to find the frequency points or range where the amplitude of its spectrum is attenuated close to the noise floor. Figure 4.6 shows the spectrum of the target FM radio signal. The amplitude of the signal spectrum is shown in the log and linear scale respectively. From Figure 4.6, we can see the amplitude of the signal of interest starts to drop at around 68 KHz, which is more visible in the log scale. The spectrum in the linear scale shows more clearly that the amplitude of the signal drops to zero at around 125 KHz. Based on the observation from the signal spectrum, the cut-off frequency of the LPF during the signal reception is set to 100 KHz, which is the same as the result obtained in the empirical study. While some frequency components between the frequency 100 KHz and 125 KHz are attenuated, the amplitude of their spectrum is very close to zero, so this will not influence the accurate reception of the signal of interest too much.

In addition to the cut-off frequency, the transmission bandwidth of the low pass filter also needs to be chosen. For an ideal LPF, the transmission bandwidth is zero, however, it is unrealistic in practice. A narrow transmission bandwidth requires a high order LPF, which can cause high computational burden on the processor. A wide transmission bandwidth may introduce some unwanted signal. In theory, as long as there is no interference signals in the transmission band, the transmission bandwidth can be set wider to obtain a low-order LPF. As for the received signal by the SDR, the spectrum in Figure 4.7 shows that the central frequency of the unwanted signals that have large amplitude are far from each other. The central frequency of the closest interference signal is 4.6 KHz, but the amplitude of the signal spectrum is very low. A strong interference signal is located at the frequency of 800 kHz. That is to say, if we set the transmission band that can exclude that strong interference signal, e,g, 700 kHz, the signal of interest will not be interrupted. In the experiments, the transmission bandwidth is set to 50 KHz to avoid closely distributed spectrum of
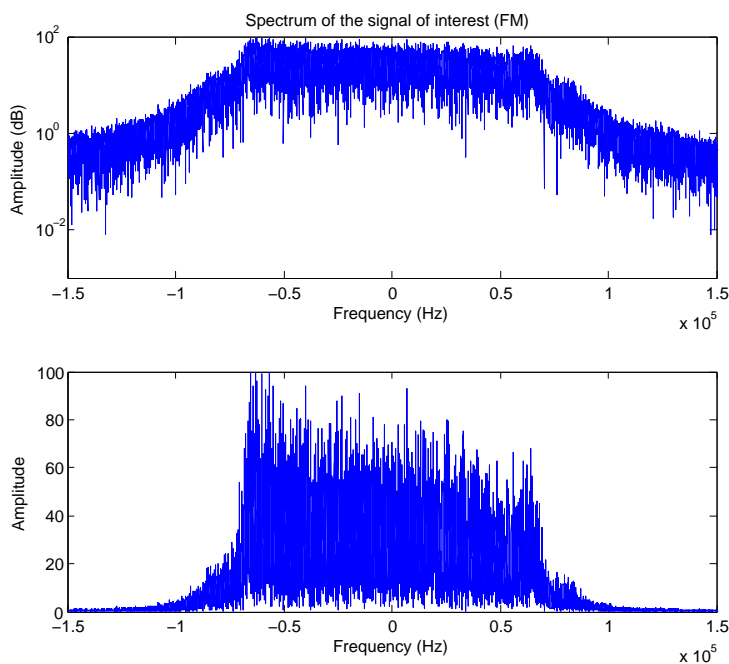
Figure 4.6: Spectrum of the signal of interest (FM)

the interference signal when other signal sources are received.

Figure 4.8 shows the output of the LPF using a Hann window. We can see that the unwanted signals are effectively removed. GNU Radio provides five window types for the implementation of the LPF: Hamming, Hann, Square, Blackman and KAISER. We have tried all the five windows in the experiments. The results show that they all give similar performance; therefore, the Hann window is used because it is simple and efficient. For the TV signal used in the localisation, the suitable parameter setting of the cut-off frequency and the transmission bandwidth of the low pass filter can be obtained in the same way.

Length of sampling time The length of sampling time in the signal reception not only influences the accuracy of the TDOA measurements, it is also related to the processing speed of the platform. From (4.1), we can see that the variance of the TDOA measurements obtained from the cross correlation is related to the SNR, the length of the sampling time T_s and the bandwidth of the target signal B. Among the three parameters, the signal SNR and the bandwidth are hard to control in the practical passive localisation. To reduce the variance of the TDOA measurements, the length of the sampling time needs to be increased.

However, long sampling time will cause a hardware-related problem. Since the high sampling rate of the SDRs is used to enhance the resolution of the TDOA measurements, a large amount of samples will be produced in a very short period of time, which leads to the "overflow" problem to the SDR. The "overflow" error hap-
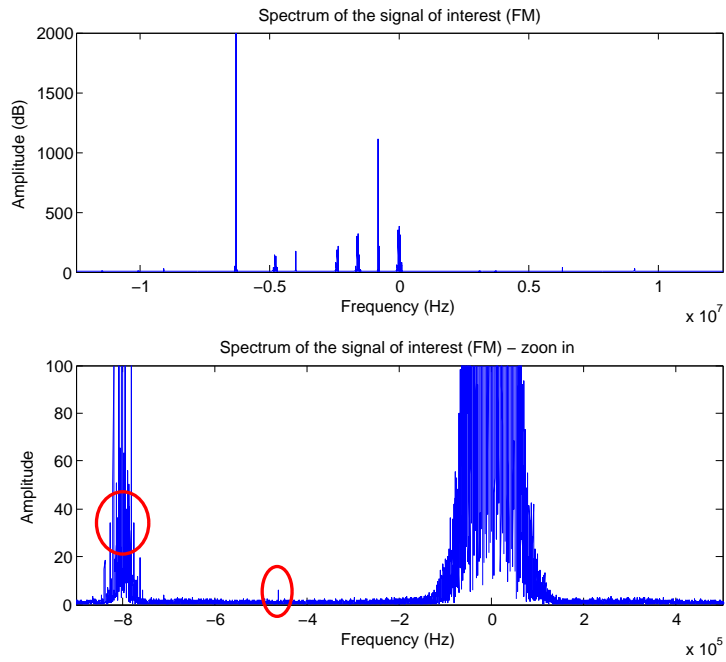
Figure 4.7: Signal spectrum in the sampling bandwidth
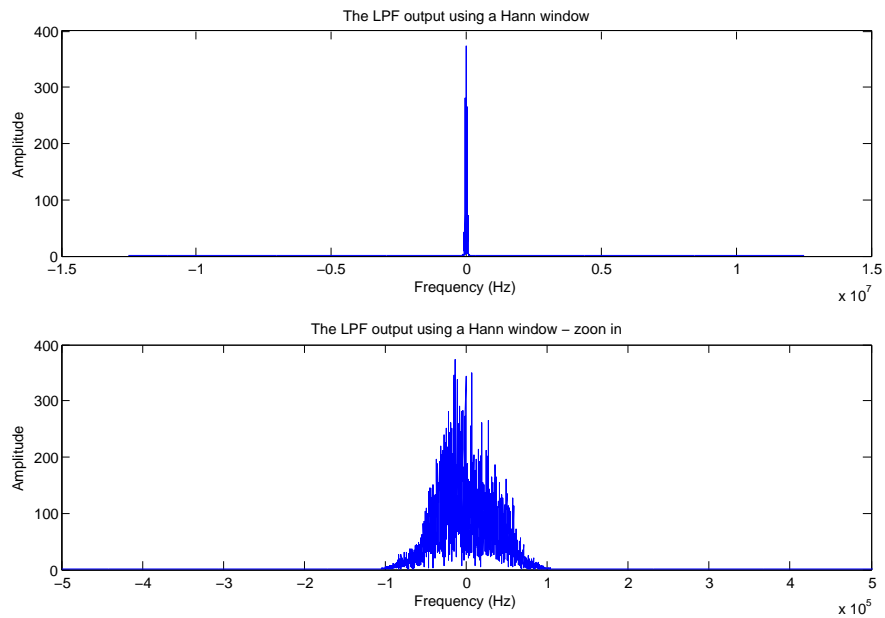
Figure 4.8: Signal spectrum in the sampling bandwidth after the LPF

Length of samples	Standard deviation TDOA measurements	Standard deviation distance error
$100\mu s$	170.4ns	51.1m
1ms	124.5ns	37.35m
10ms	203.9ns	61.2m

Table 4.2: The influence of length of sampling time

pens because the writing speed of the PC's hard driver cannot catch up with the speed of the incoming data from the USRP, and when it occurs, the samples will be dropped randomly. Moreover, a very long sampling time will degrade the real-time performance of the localisation system. Therefore, the length of the sampling time also needs to be restricted.

The influence of the length of sampling time on the accuracy of the TDOA measurements is investigated at the same sampling rate. As shown in Table 4.2, increasing the sampling time from $100\mu s$ to 1ms reduces the standard deviation of the TDOA measurements. However, increasing the sampling time further to 10ms makes the standard deviation of the TDOA measurements larger. Therefore, in the real-world localisation, 1ms under 25 Msps, which produces 25k samples in total, is taken as the optimal value of the sampling time T_s. This sampling time corresponds to 300 kilometers in distance, which is long enough for most of TDOA based-source localisation applications.

4.2.1.3 Approaches to achieve the time and frequency measurement accuracy of sub-sample level

Because the discrete signals are used in the cross correlation to obtain the TDOA measurements, the resolution of the TDOA measurements is limited by the reciprocal of the sampling rate used by the SDRs. Moreover, the actual cross-correlation peak may not exactly localise on the sampling points, it may be located at somewhere in the middle of the minimum sampling interval; therefore, the cross-correlation methods that can achieve the measurement accuracy of sub-sample level need to be implemented to enhance the resolution of the TDOA measurements.

One method to achieve the accuracy of sub-sample level is to implement a parabolic fit interpolation using the point at the cross-correlation peak and its left and right neighbouring points. This method is simple but it is known to have high bias Knapp and Carter [1976]. Another method is to implement the FFT pruning on the signals by appending zeros in the transform domain first, which is equivalent to increasing the sampling frequency in the time domain after the inverse Fourier transform and thus enhancing the resolution of the time delay estimation. Then, a Hilbert transform is implemented on the cross-correlation function. When the cross-correlation function passes through a maximum, its Hilbert transform cross zero. In practice, the received signal usually does not hit the multiple of the sampling instant during a sampling process by ADC, the zero crossing may occur at a point not explicitly
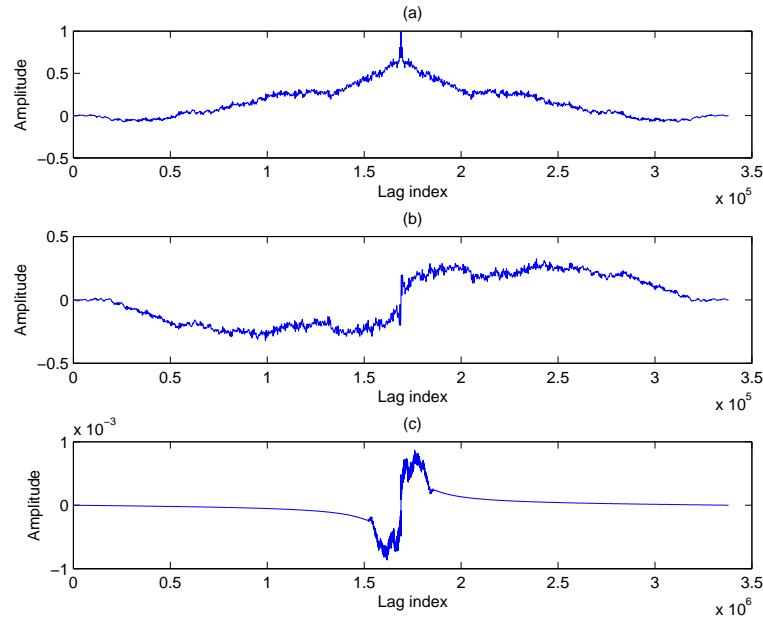
Figure 4.9: (a) Cross correlation (b) Hilbert Transformed Cross Correlation (c) Hilbert Transform of FFT Pruned Correlation correlation

defined by the data points; therefore, a simple linear interpolation using two points which are lying below and above zero respectively can be employed to locate the actual zero-crossing location. In Figure 4.9, (a) and (b) show that the peak of the cross correlation is transformed into zero-cross points. (c) shows how the cross correlation function looks like after the FFT pruning and the Hilbert transform is implemented.

To verify that the above two approaches can achieve the TDOA measurement accuracy of sub-sample level in experiments, firstly, two synchronised co-located SDRs are used to receive signals and obtain TDOA measurements. The system setup is the same as that in Figure 4.5. Table 4.3 gives the comparison on the estimation resolution of three time delay estimation algorithms using the experimental data obtained by two co-located SDRs. Under this setup, the ground truth of TDOA measurements should be zero. However, in the presence of noise, the TDOA estimation should be a value that is close to zero. As shown in the table, the standard cross correlation algorithm is not able to achieve sub-sample estimation accuracy, which means it only gives estimated value 0 sample or integer samples. In contrast, the cross correlation algorithm with the parabolic fit interpolation gives higher estimation resolution, which gives a delay of -0.50000592 samples. In addition, the cross correlation with the Hilbert transform of the FFT pruning algorithm also gives sub-sample level accuracy on the time delay estimation and it give an estimated value -0.15618373, which is more closer to the ground truth. Therefore, before the analysis above, we decided to use the third algorithm to obtain the estimation of time delay in practice which will provide more accurate TDOA measurements.

Methods	Results (samples)
Cross correlation	0
Parabolic fit interpolation	-0.50000592
Hilbert Transform of FFT Pruned Correlation	-0.15618373

Table 4.3: Comparison of time delay estimation methods using two co-located SDRs

	Interpolation	Hilbert
Accuracy TDOA1	2.485 samples	0.797 samples
Accuracy TDOA2	4.894 samples	3.631 samples
Accuracy TDOA3	3.419 samples	1.817 samples
Average computing time	80 ms	638 ms

Table 4.4: Comparison of time delay estimation methods using two spatially distributed SDRs

In addition, the experiments that use two spatially distributed SDRs are also implemented to verify the approaches that can achieve the TDOA measurement accuracy of sub-sample level. The experimental setup is similar to the practical localisation experiments. Table 4.4 gives a comparison of the two methods between the average TDOA measurement error after subtracting the ground truth and the computing time. Three groups of TDOA measurements are obtained, and the results show that the second algorithm provides higher accuracy but requires longer computing time.

4.2.1.4   Outlier identification

To achieve accurate source localisation, the outliers in the measurements must be identified and removed. Figure 4.10 shows an example of the TDOA measurements obtained by a pair of spatially distributed SDRs, in which two types of outliers are found. The unit of the delay in the figure is samples. The unit of amplitude in Figure 4.11 is the normalise coefficient in a range of 0 to 1. The TDOA measurements marked in red denote the outlier type 1, those marked in yellow denote the outlier type 2, and the remaining measurements are the effective measurements. Each TDOA measurement consists of two columns. The first column denotes the time delay estimates in units of "samples" and the second column denotes the normalised cross-correlation coefficient between the two signals.

The first type of outliers is caused by the failure of the synchronous sampling. To implement synchronous sampling automatically during the localisation process, a specific sampling time is defined in each signal acquisition cycle. When this time arrives, the SDRs begin to receive a certain number of samples. During the whole process, SDRs do not have any information about the time of the signal reception at other SDRs and only implement the sampling according to their local time, which is synchronised through the GPS signal. However, the difference in the processing speed of different host computers sometimes causes two SDRs to receive signals at

Delay	Cof	Delay	Cof	Delay	Cof	Delay	Cof
449.22	0.982764	-2096.78	0.883047	437.22	0.984151	-58654.8	0.092324
446.2	0.982228	441.2	0.983726	-2102.75	0.862757	-2460.76	0.909165
444.17	0.985973	-2461.78	0.926623	444.18	0.980403	443.2	0.983609
443.24	0.985189	-1734.83	0.9525	-2097.79	0.910593	442.17	0.984593
445.24	0.985411	444.22	0.985221	442.22	0.983371	-2459.85	0.904147
442.17	0.986283	447.16	0.983157	441.24	0.983643	444.21	0.977944
446.17	0.986765	443.18	0.982987	-14744.8	0.079803	-2457.77	0.910881
448.17	0.984194	-2098.81	0.884112	445.23	0.982096	-1367.83	0.896782
449.19	0.98561	439.2	0.984464	49902.19	0.097176	445.23	0.985474
445.21	0.984162	441.16	0.984751	447.21	0.985678	447.23	0.983123
446.22	0.985861	439.19	0.98414	1483.19	0.082103	-2455.82	0.904002
445.19	0.98426	437.21	0.98541	-2466.81	0.913348	24052.18	0.079435
440.24	0.980173	435.23	0.982926	440.16	0.983873	449.19	0.656281
-38868.8	0.114013	446.2	0.984144	441.23	0.98215	452.17	0.986139
443.24	0.986001	439.2	0.984358	440.21	0.982344	452.2	0.985363
442.18	0.984851	37421.15	0.10579	443.22	0.9843	452.18	0.984038
-2095.81	0.903863	438.23	0.985727	-1373.78	0.893461	458.22	0.562581
444.22	0.985763	437.17	0.986359	442.25	0.982605	446.24	0.983538
440.19	0.984899	435.24	0.985329	-89950.8	0.045959	449.23	0.984604
35841.17	0.085692	437.2	0.98665	-1379.83	0.862233	450.18	0.986064

Figure 4.10: TDOA measurement outlier identification example

different signal acquisition cycles, which can cause a large error in TDOA measurements. The second type of outlier is caused by the "overflow" error. (Recall that "overflow" occurs when the writing speed of the hard disk of the host PC cannot catch up with the speed of the incoming data from the SDR.) Since the SDRs use a high sampling rate, this error can happen more frequently than the situation of using a low sampling rate. When the "overflow" happens, SDRs will randomly drop some samples, and then the TDOA measurements will not be accurate.

The first type of outliers is easy to distinguish because they have very low cross-correlation coefficients. Figure 4.11 shows two cross-correlation results in obtaining two TDOA measurements using the signal received by two SDRs. The unit of amplitude in the figure is the normalise coefficient in a range of 0 to 1. When the two SDRs start to sample the signal at the same pre-defined time as expected, there is no synchronisation error, so the normalised cross correlation coefficient is high, which is close to 1. However, when two SDRs fail to implement synchronous sampling, the signal received by them has low correlation, so the normalised cross correlation coefficient is low, such as 0.3 or even lower. Therefore, setting a threshold of the cross correlation coefficient can effectively remove the first type of outliers. On the basis of the above observation, the threshold can be chosen to be 0.8 lower to identify whether the two SDRs are synchronised well. Actually, the value 0.8 is still a loss threshold. As long as the SDRs are synchronised, the cross correlation coefficient should be higher than 0.8, which has been verified in a number of experiments.

Identifying the second type of outliers needs to use other methods as they have the similar cross-correlation coefficients to the effective TDOA measurements, so it
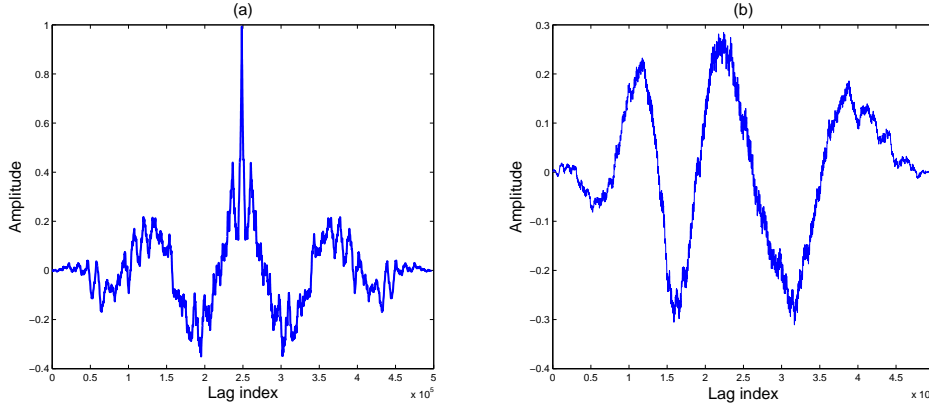
Figure 4.11: Cross correlation of received signal from two SDRs: (a) high correlation (≈ 1) (b) low correlation (≈ 0.3)

is hard to set a threshold to identify this type of outliers. To remove this type of outlier, one method is first to obtain the mean and the standard deviation of a group of TDOA measurements, denoted by μ_0 and σ_0, and only keep the TDOA measurements *tdoa* which meet the condition of $tdoa \in [\mu_0 - 2 * \sigma_0, \mu_0 + 2 * \sigma_0]$. This method has been proven to be effective using our experimental data. One may note that this method may cause large measurement error by removing all the effective measurements and keeping outliers in the situation when the majority of the measurements are outliers. We have been aware of this problem during the measurement selection, but we can confirm that outliers only constitute a small fraction of measurements in the experiments.

In addition, an approach is proposed to resolve the second type of outliers and transform them into effective measurements by reprocessing the signals that produce them. Remind that the second type of outliers is caused by the "overflow" error. While some samples are dropped in the middle and filled up with the following coming samples, the first segment of the received signal before the "overflow" happens can still produce effective TDOA measurements. To find them, instead of using the full-length signal in the cross correlation, the received signals are cut off from the beginning of the waveform (time duration) with different length $M_l = lM, l = 1, 2, ..., L$, and then M TDOAs are estimated. By using the first M samples, the effective TDOA measurement can be recovered. The value of L is obtained empirically. To make sure the first cut-off of the signal contains the correlation peak, $L = 10$ is used, so this segment contains 2500 samples and covers the range of our experiments because the time to obtain these samples is equivalent to 1ms in time and 30km in distance. To further enhance the accuracy of the recovered TDOA measurements, the value of L can be gradually decreased by taking longer observation times. While both methods work well in removing outliers after a large number of tests, the first method is used in practice for simplicity.

4.2.1.5   The analysis of the influence of NLOS and multipath effect

After the proposed measurement error reduction methods for the TDOA-based lo-
calisation are implemented, three sets of independent TDOA measurements are ob-
tained from four spatially distributed SDRs in one of the experiments. For simplicity,
2-dimensional space is considered in this localisation problem, which thus omits the
emitter's height in the calculation of the ground truth. Taking SDR1 as the reference,
three TDOA measurements t_{21}, t_{31} and t_{41} can be obtained from three SDR pairs:
SDR2 and SDR1, SDR3 and SDR1, SDR4 and SDR1. The TDOA measurement results
are compared with the ground truth obtained from the actual sensors' location and
the source location in Figure 4.11, where the black horizontal lines denote the ground
truth, the coloured dots denote multiple TDOA measurements from different SDR
pairs and the horizontal coloured lines denote the mean of TDOA measurements.

It is obvious that there is an offset between the mean of the TDOA measurements
and the ground truth, and most of the measurements stay on one side of the ground
truth. The dominant cause of the offsets is the non-line-of-sight (NLOS) error. In
the experiments, only the reference SDR is under a clear LOS condition; the other
three SDRs experience the NLOS error because the direct paths are fully or partially
blocked by terrestrial objects, as the localisation experiment is implemented in an ur-
ban environment. With the influence of the NLOS error, the signal received by these
three SDRs travels through longer paths than the direct paths, which produces the
offsets. In the practical situation, however, it is very common to have signals propa-
gating under a NLOS condition and this error is hard to remove in the measurements,
especially in the passive source localisation where the location of the target emitter
is unknown.

In addition, a further evaluation of the influence of NLOS error on the TDOA
measurement accuracy is conducted. Three experimental scenarios are implemented
using two closely deployed SDRs because this setting up gives the TDOA measure-
ment ground truth close to zero: 1) both of SDRs are under LOS condition; 2) one
SDR is under NLOS condition and the other SDR is under the LOS condition (in this
case, the distance difference from the emitter to the two SDRs is 6m, which gives
the TDOA ground truth of approximately 0.5 sample using 25 Msps); 3) both of the
SDRs are under the NLOS condition. Figure 4.12 shows the distribution of the TDOA
measurement error and we assume the measurement error has Gaussian distribution.

In Scenario 1, when both of the SDRs are under the LOS condition, the results
show smallest measurement error in distance has 6.13m mean error and 37.66m stan-
dard deviation. In Scenario 2, both the mean and the standard deviation of the TDOA
measurement error in distance increase to 39.96m and 55.80m respectively. When two
SDRs are both under the NLOS condition in Scenario 3, the mean and the standard
deviation of the TDOA measurement error in distance are 27.83m and 47.84m respec-
tively, which are larger than the measurement error in Scenario 1, but slight smaller
than the measurement error in Scenario 2. This is because in Scenario 3, the two
SDRs are co-located so that they suffer from similar influence of NLOS error, which
gives smaller influence on the cross correlation result than Scenario 2. Therefore,
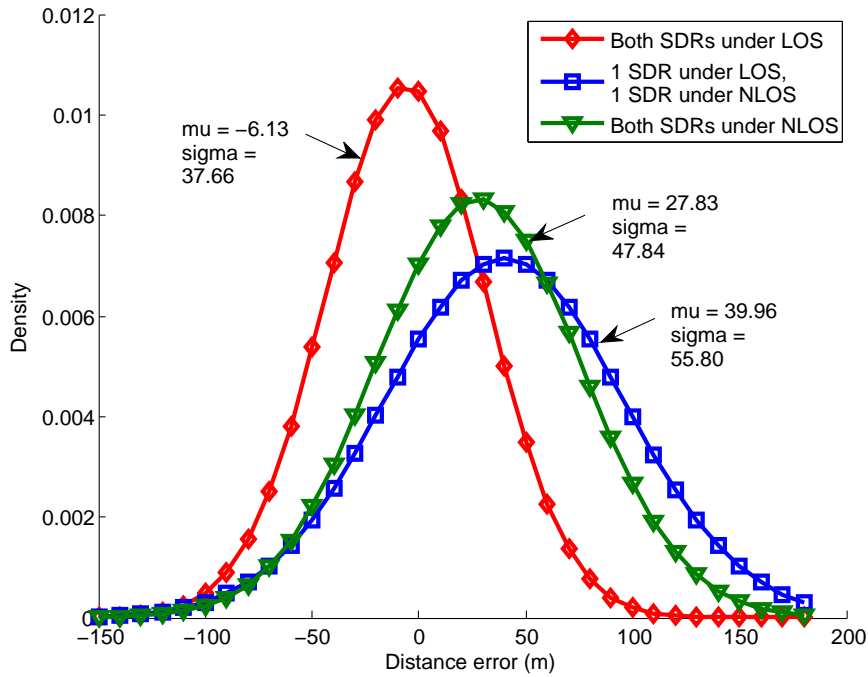
Figure 4.12: Influence of NLOS

we can see that when the NLOS error exists, the mean and the standard deviation of the TDOA measurement error obtained by a pair of SDRs are larger than those obtained under the LOS condition. In the real-world localisation, a certain standard deviation threshold of TDOA measurements can be set to identify the NLOS error if some information of the signal source is available.

It also can be seen from Figure 4.13 that there are variances in the TDOA measurements. Here we use range-difference-of-arrival to express the measurement error instead of TDOA measurements. $RDOA = c * TDOA$, where c denotes the constant signal propagation speed. The reason is that the unit of RDOA is meter, which is more visible and meaningful to the readers rather than the time unit (ns) in this localisation applications. If we consider the measurement offset caused by the NLOS error to be constant, which is reasonable because the emitter and the SDR-based receivers are stationary when the measurements are taken during the localisation, then the variances in Figure 4.13 are the results of the combined influence of the synchronisation error between pairs of SDRs and multipath effect. If there is no synchronisation error or multipath, the TDOA measurements at different time instants should remain the same. The multipath effect is very common in the urban environment when our experiments are implemented. Comparing to the synchronisation error, the multipath effect produces a more severe influence on the variance of TDOA measurement error because the synchronisation error only generates up to 30m distance error as discussed before.

NLOS error and multipath effect are two common error sources for almost all of
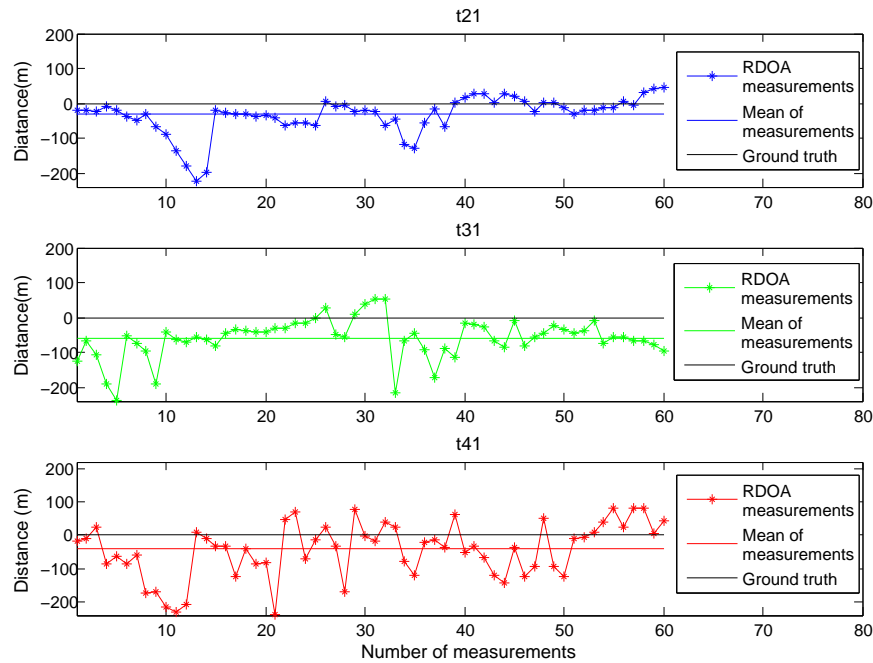
Figure 4.13: TDOA accuracy comparison with ground truth

practical localisation systems. If the features of the target are known, we can identify whether the signal received by the sensor is affected by analysing the change of the signal spectrum. If that sensor is identified, in the process of location estimation, the measurement obtained by that sensor can be removed. However, for the passive source localisation, it is very challenging to reduce the influences of these two error sources. Firstly, the signal source is not cooperative with the localisation system. We cannot know the features of the target signal, so it is difficult to even know whether the signal is affected by NLOS error and multipath effect. Secondly, in this practical localisation, we have to use the measurements obtained by almost all of the sensors to reduce the cost of the system, so we may not have enough sensors to keep the redundant measurements if we remove some. Therefore, in this situation, we have not resolved this problem completely in this thesis. Further studies are required.

4.2.2   Improvement of FDOA measurement accuracy

4.2.2.1   High-resolution FDOA measurements

Similar to how the TDOA measurements are obtained, the sampled signals are used to obtain the FDOA measurements through the Cross Ambiguity Function (CAF). Therefore, there is also a resolution problem in the FDOA measurements. Instead of being limited by the sampling rate, the resolution of the FDOA measurements is limited by the FFT length or the FFT resolution. In practice, the real frequency delay may not be located on the frequency bins of the cross correlation between the FFT of the signal received by a pair of SDRs. Therefore, the quadratic interpolation can also

be implemented to obtain the FDOA measurements with the resolution higher than the FFT resolution. To be specific, the quadratic interpolation is implemented using the peak of the CAF function on the frequency axis and its left and right neighboring points. In practice, the coarse measurements can be obtained first and then they can be refined using the interpolation algorithms continuously to reduce the computing cost.

4.2.2.2   Outlier removal for FDOA measurements

In the joint TDOA and FDOA based localisation, a pair of TDOA and FDOA measurements is usually obtained together to implement localisation, and therefore, a pair of TDOA and FDOA measurements is removed in the list of effective measurements when the TDOA measurement is an outlier for simplicity. Moreover, a direct method to identify FDOA measurement outliers is to check whether the FDOA measurements are reasonable value according to the highest relative speed to the emitter achieved by the mobile sensor and the carrier frequency of the signal source. In addition, the cross correlation coefficient of the FFT of the signal received by two SDRs can be used to identify the FDOA outliers, like what we did to identify the TDOA outliers.

4.3   Summary

In this Chapter, the accuracy of the measurements obtained using the SDRs is evaluated and systematically analysed. The measurement error mainly comes from three aspects. Firstly, the hardware precision sets restrictions on the measurement accuracy. For example, the highest sampling rate of the SDR, 25 Msps for 16-bit sample, limits the time resolution to 40 ns and the distance resolution to 12 m. In addition, the achievable time synchronisation error is +/- 50 ns, so the synchronisation error gives up to 30 m distance error. The frequency synchronisation error 0.2 Hz also influences the FDOA measurement accuracy. Secondly, during the process of the signal processing, apart from the features of the signal source, such as the bandwidth and the carrier frequency, the choice of the parameters in the signal processing, such as the length of sampling time, the cut-off frequency and the transmission bandwidth of the low pass filter will also influence the measurement accuracy. Thirdly, the signal propagation environment in the real world is complicated. The interference signal, multipath effect and NLOS error are inevitable, and they can significantly increase the measurement variance and even cause outliers.

   To fulfil the best performance of the hardware, the SNR of the signal received by the WBX daughterboard with different types of antennas are evaluated to make sure the high-quality signals are obtained. In addition, to break the hardware limitation on the resolution of TDOA measurements, two algorithms are investigated to obtain sub-sample level time delay estimation accuracy. While both the parabolic fit interpolation algorithm and the Hilbert transform of FFT pruned correlation algorithm can achieve desired resolution, the latter is more accurate, so it will be used in the

time delay estimation in practice. For the FDOA estimation, both the algorithms can give high-resolution estimation; however, the former algorithm has the feature of short computing time, so it is used in FDOA measurements. During the signal processing, the optimal parameters of the bandwidth of the low pass filter and the length of sampling time are obtained empirically to improve the measurement accuracy. The potential use of the proposed methods and results could be to design the desired signal sensing and localisation systems using other types of hardware. Furthermore, the effective methods are proposed to detect and remove the measurement outliers to avoid the collapse of the localisation estimation algorithms. To detect the outliers in the TDOA measurements, checking the value of the cross-correlation coefficient can thoroughly remove the outliers caused by asynchronous sampling. The rest of the outliers can be detected and removed by using a selection window defined by the mean and standard deviation of the remaining measurements or they can be transformed into the effective measurements by using the first segment of the received samples. Similar methods are described to detect and remove the FDOA measurement outliers. The influence of the multipath effect and NLOS error on the TDOA measurement accuracy is also discussed, but it is hard to resolve them in the real-world passive localisation.

In the next Chapter, the source localisation algorithms will be presented in order to determine the location of the signal source in the presence of noisy measurements.

RF source location estimation

The location estimation of the signal source involves solving the non-linear relationship between the noisy measurements and the source location. While many localisation algorithms have been proposed, we are more interested in the computationally efficient algorithms in order to achieve real-time source localisation. In Section 5.1, two types of computationally efficient localisation algorithms are studied. Firstly, the two-step weighted least-squares-based solution (2WLS) is introduced to obtain the location estimates of the TDOA-based localisation system. Then, by making the adjustment of the 2WLS, we propose the sequential weighted least-squares-based solution for the joint TDOA and FDOA-based localisation system. The other type of computationally efficient location estimation algorithms is the Bayesian filtering, so the Extended Kalman Filter-based localisation algorithm is introduced. It can be used to obtain the location estimates in the TDOA-based localisation and the joint TDOA and FDOA-based localisation. During the process of the location estimation, we found two generic factors that can influence the accuracy of most of localisation systems. The first factor is the geometry of sensor-target placement and the second factor is the location estimation bias. In Section 5.2 and 5.3, the methods to improve the localisation accuracy by exploring the optimal sensor-target geometry and implementing the location estimation bias reduction algorithm are discussed.

5.1 Computationally efficient location estimation algorithms

In terms of source location estimation, while the Maximum Likelihood Estimator (MLE) is well known to be able to achieve Cramer-Rao lower bound (CRLB), the non-linear relationship between the measurement and the source location requires a numerical grid search which is time-consuming. Even the grid search can be approximated using a gradient-based iterative technique through the linearization, such as Taylor-series methods, the iterative algorithms still require a good initial guess that is close to the true position and they may suffer from divergence problem. Therefore, in the real-world localisation applications, the closed-form solutions are preferred, especially in the practical passive localisation.

5.1.1   Two-step weighted least-squares-based solution for TDOA-based source localisation

In the absence of noise, d_{i1} in (3.8) becomes

$$d_{i1} = r_i - r_1 = \sqrt{(x - x_i)^2 + (y - y_i)^2} - \sqrt{(x - x_1)^2 + (y - y_1)^2}$$
$$\Rightarrow d_{i1} = \sqrt{(x - x_i)^2 + (y - y_i)^2} - \sqrt{(x - x_1)^2 + (y - y_1)^2}, i = 2, 3, ..., N \tag{5.1}$$

Squaring both sides of (5.1) and using an intermediate variable, r_1, which has the form

$$r_1 = \sqrt{(x - x_1)^2 + (y - y_1)^2} \tag{5.2}$$

The following linear equation can be obtained

$$(x - x_1)(x_i - x_1) + (y - y_1)(y_i - y_1) + d_{i1}r_1$$
$$= \frac{1}{2}[(x_i - x_1)^2 + (y_i - y_1)^2 - d_{i1}^2], i = 2, 3, ..., N \tag{5.3}$$

Writing (5.3) into matrix form gives

$$\mathbf{G}_t \boldsymbol{\vartheta}_t = \mathbf{h}_t \tag{5.4}$$

with

$$\mathbf{G}_t = \begin{bmatrix} x_2 - x_1 & y_2 - y_1 & d_{i2} \\ \vdots & \vdots & \vdots \\ x_N - x_1 & y_N - y_1 & d_{N2} \end{bmatrix}, \mathbf{h}_t = \frac{1}{2} \begin{bmatrix} (x_2 - x_1)^2 + (y_2 - y_1)^2 - d_{i2}^2 \\ \vdots \\ (x_N - x_1)^2 + (y_N - y_1)^2 - d_{N2}^2 \end{bmatrix} \tag{5.5}$$

and the parameter vector $\boldsymbol{\vartheta}_t = [x - x_1, y - y_1, r_1]^T$ consists of the source location as well as r_1.

Many algorithms has been proposed to solve the TDOA-based localisation problem. In the presence of measurement errors, the Spherical Interpolation (SI) technique determines the source position by simply solving (5.4) via standard least-squares, and the location estimate is found from Smith and Abel [1987]:

$$\hat{\boldsymbol{\vartheta}}_t = \arg\min_{\hat{\boldsymbol{\vartheta}}_t}(\mathbf{G}_t\hat{\boldsymbol{\vartheta}}_t - \mathbf{h}_t)(\mathbf{G}_t\hat{\boldsymbol{\vartheta}}_t - \mathbf{h}_t)^T = (\mathbf{G}_t\mathbf{G}_t^T)^{-1}\mathbf{G}_t^T\mathbf{h}_t \tag{5.6}$$

where $\hat{\boldsymbol{\vartheta}}_t = [\hat{x} - x_1, \hat{y} - y_1, \hat{r}_1]^T$ is an optimization variable vector and -1 represents the matrix inverse, without utilizing the known relationship between $\hat{x}$, $\hat{y}$ and $\hat{r}_1$.

Huang et al. [2001] proposes a linear-correction least-squares approach to improve the SI based approach, which solves the least-squares equation (5.6) subject to the constraint equation $(x - x_1)^2 + (y - y_1)^2 = r_1^2$, or equivalently

$$\hat{\boldsymbol{\vartheta}}_t^T \boldsymbol{\Sigma} \hat{\boldsymbol{\vartheta}}_t = \mathbf{0}, \tag{5.7}$$

where $\Sigma = diag(1, 1, -1)$.

On the other hand, Chan and Ho [1994] have improved the SI estimator through a two-step approach. In the first step, a coarse estimate is computed by minimizing a weighted least square equation

$$(\mathbf{G}_t \hat{\boldsymbol{\vartheta}}_t - \mathbf{h}_t) \mathbf{W}_t^{-1} (\mathbf{G}_t \hat{\boldsymbol{\vartheta}}_t - \mathbf{h}_t)^T \tag{5.8}$$

where $\mathbf{W}_t$ is a symmetric weighting matrix, which is a function of the estimate of r_1. A better estimate of $\boldsymbol{\vartheta}_t$ is then obtained in the second stage via minimizing $(x - x_1)^2 + (y - y_1)^2 - r_1^2$ according to another weighted least-squares procedure.

To evaluate the accuracy of the location estimates, it is well known that the Cramer-Rao lower bound (CRLB) is a lower bound on the covariance that is asymptotically achievable by any unbiased estimation algorithm based on the measurements. The CRLB can be calculated from the inverse of the Fisher Information Matrix (FIM) which is denoted by $\mathbf{J}_t$ in TDOA-based localisation. Let the estimated location be $\hat{\mathbf{p}}$, then the error covariance of the location estimate $\mathbf{E}[(\mathbf{p} - \hat{\mathbf{p}})(\mathbf{p} - \hat{\mathbf{p}})^T]$ is lower bounded by

$$\mathbf{E}[(\mathbf{p} - \hat{\mathbf{p}})(\mathbf{p} - \hat{\mathbf{p}})^T] \geq \mathbf{J}_t^{-1} \tag{5.9}$$

$$\mathbf{J}_t = \mathbf{E}[\nabla_{\mathbf{p}} \ln p(\mathbf{d}|\mathbf{p})(\nabla_{\mathbf{p}} \ln p(\mathbf{d}|\mathbf{p}))^T] \tag{5.10}$$

where $\mathbf{E}[\cdot]$ determines the expectation value and $\hat{\mathbf{d}} = (\hat{d}_{21}, \hat{d}_{31}, ..., \hat{d}_{N1})^T$ is a vector of noisy measurements which have joint conditional Gaussian distribution with covariance matrix

$$\mathbf{Q}_t = 2\sigma_t^2 \begin{pmatrix} 1 & 0.5 & \cdots & 0.5 \\ 0.5 & 1 & \cdots & 0.5 \\ \vdots & \vdots & \ddots & \vdots \\ 0.5 & 0.5 & \cdots & 1 \end{pmatrix} \tag{5.11}$$

Under the assumption of additive white Gaussian measurement noise and constant entries of the variance matrix $\mathbf{Q}_t$, the computation of the FIM can be expressed as Kaune et al. [2011]

$$\mathbf{J}_t = \mathbf{H}_t^T \mathbf{Q}_t^{-1} \mathbf{H}_t \tag{5.12}$$

where $\mathbf{H}_t$ can be expressed by the Jacobian matrix of the range difference measurement set $\mathbf{d}(\mathbf{p}) = (d_{21}, d_{31}, ..., d_{N1})$. The optimal attainable location estimation accuracy can be obtained from the square root of the trace of the inverse of the FIM, which can be used as criteria to evaluate root mean square error (RMSE) of the localisation results.

5.1.2   Sequential WLS for joint TDOA and FDOA-based source localisation using two SDRs

The TDOA measurements only allow the estimation of the source location and not the velocity. Moreover, the TDOA measurements may not be sufficient to provide

enough localisation accuracy, especially when there is relative motion between the sources and the sensors. FDOA measurements can catch the Doppler shift of the received signal caused by the relative motion between the signal source and the sensors. When the FDOA measurements are available, the location estimation accuracy of the source is able to be improved and, at the same time, the velocity of the signal source can be identified. The relationship between the range rate and the source location can be given by taking the time derivative of the range between the ith sensor $\mathbf{s}_i$ and the source $\mathbf{p}$ by $r_i = \|\mathbf{p} - \mathbf{s}_i\|$:

$$
\begin{aligned}
\dot{r}_i &= \frac{(\dot{\mathbf{p}} - \dot{\mathbf{s}}_i)^T(\mathbf{p} - \mathbf{p}_i)}{r_i} \\
&= \frac{(\dot{x} - \dot{x}_i)(x - x_i) + (\dot{y} - \dot{y}_i)(y - y_i)}{r_i}
\end{aligned}
\tag{5.13}
$$

To make use of the FDOA measurements in source location estimation, taking the derivative of (5.3) and using an intermediate variable r_1 as shown in (5.2) give:

$$
\dot{d}_{i1}d_{i1} + \dot{d}_{i1}r_1 + d_{i1}\dot{r}_1 =
$$
$$
\dot{x}_i x_i + \dot{y}_i y_i - \dot{x}_1 x_1 - \dot{y}_1 y_1 - (\dot{x}_i - \dot{x}_1)x - (\dot{y}_i - \dot{y}_1)y - (x_i - x_1)\dot{x} - (y_i - y_1)\dot{y} \tag{5.14}
$$
$$
i = 2, 3, ..., N
$$

where $\dot{d}_{i1}$ is the range rate differences.

Let $\mathbf{d} = [d_{21}, d_{31}, ...d_{N1}]^T$ and $\dot{\mathbf{d}} = [\dot{d}_{21}, \dot{d}_{31}, ..., \dot{d}_{N1}]^T$ be the vectors of range difference and range rate differences. Define an auxiliary vector $\boldsymbol{\vartheta}_{tf} = [\mathbf{p}^T, r_1, \dot{\mathbf{p}}^T, \dot{r}_1]$, which contains the unknown source location and two nuisance variables r_1 and $\dot{r}_1$. Writing (5.14) into matrix form gives:

$$
\mathbf{G}_{tf}\boldsymbol{\vartheta}_{tf} = \mathbf{h}_{tf} \tag{5.15}
$$

with

$$
\mathbf{h}_{tf} = \begin{bmatrix}
d_{21}^2 - x_2^2 - y_2^2 + x_1^2 + y_1^2 \\
\vdots \\
d_{N1}^2 - x_N^2 - y_N^2 + x_1^2 + y_1^2 \\
2(\dot{d}_{21}d_{21} - x_2\dot{x}_2 - y_2\dot{y}_2 + x_1\dot{x}_1 + y_1\dot{y}_1) \\
\vdots \\
2(\dot{d}_{N1}d_{N1} - x_N\dot{x}_N - y_N\dot{y}_N + x_1\dot{x}_1 + y_1\dot{y}_1)
\end{bmatrix} \tag{5.16}
$$

$$
\mathbf{G}_{tf} = -2 \begin{bmatrix}
(x_2 - x_1, y_2 - y_1) & d_{21} & \mathbf{0} & 0 \\
\vdots & \vdots & \vdots & \vdots \\
(x_N - x_1, y_N - y_1) & d_{N1} & \mathbf{0} & 0 \\
(\dot{x}_2 - \dot{x}_1, \dot{y}_2 - \dot{y}_1) & \dot{d}_{21} & (x_2 - x_1, y_2 - y_1) & d_{21} \\
\vdots & \vdots & \vdots & \vdots \\
(\dot{x}_N - \dot{x}_1, \dot{y}_N - \dot{y}_1) & \dot{d}_{N1} & (x_N - x_1, y_N - y_1) & d_{N1}
\end{bmatrix} \tag{5.17}
$$

and $\mathbf{0}$ is a 2×1 column vector of zero. In the presence of TDOA and FDOA noise, the error vector can be denoted by

$$\boldsymbol{\varepsilon}_{tf} = \begin{bmatrix} \varepsilon_t \\ \varepsilon_f \end{bmatrix} = \mathbf{h}_{tf} - \mathbf{G}_{tf}\boldsymbol{\vartheta}_{tf} \tag{5.18}$$

The source position can be estimated by simply solving (5.15) via standard least square:

$$\begin{aligned} \hat{\boldsymbol{\vartheta}}_{tf} &= \arg\min_{\hat{\boldsymbol{\vartheta}}_{tf}} (\mathbf{G}_{tf}\hat{\boldsymbol{\vartheta}}_{tf} - \mathbf{h}_{tf})(\mathbf{G}_{tf}\hat{\boldsymbol{\vartheta}}_{tf} - \mathbf{h}_{tf})^T \\ &= (\mathbf{G}_{tf}\mathbf{G}_{tf}^T)^{-1}\mathbf{G}_{tf}^T\mathbf{h}_{tf} \end{aligned} \tag{5.19}$$

where $\hat{\boldsymbol{\vartheta}}_{tf} = [(\hat{x}, \hat{y}), r_1, (\hat{x}, \hat{y}), \hat{r}_1]^T$ is an optimization variable vector without utilizing the known relationship between $\hat{x}$, $\hat{y}$ and $\hat{r}_1$ and the relationship between $\hat{x}$, $\hat{y}$ and $\hat{r}_1$.

According to Ho and Xu [2004], a weighted least-square solution of $\boldsymbol{\vartheta}_{tf}$ that minimizes $\boldsymbol{\varepsilon}_{tf}^T\mathbf{W}\boldsymbol{\varepsilon}_{tf}$ is given by

$$\boldsymbol{\vartheta}_{tf} = (\mathbf{G}_{tf}^T\mathbf{W}_{tf}\mathbf{G}_{tf})^{-1}\mathbf{G}_{tf}^T\mathbf{W}_{tf}\mathbf{h}_{tf} \tag{5.20}$$

where $\mathbf{W}_{tf}$ is a positive definite weighting matrix. There are many possible choices of $\mathbf{W}_{tf}$. The simplest one is identity. When the covariance of TDOA and FDOA measurements $\mathbf{Q}_{tf}$ is known, a better weighting matrix $\mathbf{W}_{tf}$ can be obtained Ho and Xu [2004].

The deviation above can solve the joint TDOA and FDOA-based passive source localisation problem obtained by multiple stationary sensors. For the localisation using only two sensors, one stationary sensor and one mobile sensor, the weighted least-squares algorithm can still be used after some modification. The idea of using the algorithm in two-SDR-based localisation is to process a time history of measurements and sensors' positions to determine the location of the signal source when the mobile sensor move to a new location and take new measurements. By using the measurements taken at new positions by the mobile sensor, it is similar to the situation where multiple stationary sensors are used. Once the number of sensors that can uniquely localise a signal source is achieved, the location of the source can be determined using the WLS algorithm. To be specific, at the kth time instant, $k = 1, 2, ..., K$, $k - 1$ pairs of TDOA and FDOA measurements can be obtained. By substituting $N = k + 1$ into (5.16) and (5.17), the location estimate at all K time instants can be obtained from (5.20). By having a number of measurements taken at a number of positions by the mobile sensor, the localisation accuracy can be enhanced gradually.

The CRLB of the location estimation changes over the time when new measurements are available. The CRLB at k^{th} time instant can still be calculated from the inverse of the Fisher Information Matrix (FIM) which is denoted by $\mathbf{J}_k^{tf}$ in the joint TDOA and FDOA based localisation using two SDRs. Define

$$\mathbf{h}_k(\mathbf{p}) = \begin{bmatrix} \tau(\mathbf{p}) \\ \nu(\mathbf{p}) \end{bmatrix} \tag{5.21}$$

where the definition of $\tau(\mathbf{p})$ and $\nu(\mathbf{p})$ can be found in (3.19) and (3.20). The 2×2 derivative matrix (Jacobian) of $\mathbf{h}_k(\mathbf{p})$ with respect to $\mathbf{p}$ can then be easily given by

$$\mathbf{H}_k(\mathbf{p}) = \frac{\partial \mathbf{h}_k(\mathbf{p})}{\partial \mathbf{p}} = \begin{bmatrix} \frac{1}{c}((\mathbf{u}_k^1(\mathbf{p}))^T - (\mathbf{u}_k^2(\mathbf{p}))^T) \\ \frac{f_c}{c}(\frac{1}{r_k^1}(\mathbf{v}_k^1)^T \mathbf{P}_k^1(\mathbf{p}) - \frac{1}{r_k^2}(\mathbf{v}_k^2)^T \mathbf{P}_k^2(\mathbf{p})) \end{bmatrix} \tag{5.22}$$

where

$$\mathbf{P}_k^1(\mathbf{p}) = \mathbf{I} - \mathbf{u}_k^1(\mathbf{p})(\mathbf{u}_k^1(\mathbf{p}))^T, \quad \mathbf{P}_k^2(\mathbf{p}) = \mathbf{I} - \mathbf{u}_k^2(\mathbf{p})(\mathbf{u}_k^2(\mathbf{p}))^T, \tag{5.23}$$

are projection matrices onto the directions perpendicular to $\mathbf{u}_k^1(\mathbf{p})$ and to $\mathbf{u}_k^2(\mathbf{p})$ respectively. $\mathbf{I}$ denotes the 2×2 identity matrix. By using the covariance matrix in (3.24), the CRLB of the joint TDOA and FDOA-based localisation using two SDRs at the kth time instant can be calculated by

$$\mathbf{CRLB}_k^{tf} = (\mathbf{J}_k^{tf})^{-1} = (\mathbf{H}_k(\mathbf{p})^T (\mathbf{Q}_k^{tf})^{-1} \mathbf{H}_k(\mathbf{p})) \tag{5.24}$$

5.1.3 Extended Kalman filter (EKF) for joint TDOA and FDOA-based source localisation

The EKF is the nonlinear version of the Kalman Filter which can be used to estimate the emitter location by linearizing the nonlinear components using a first-order Taylor series expansion. In our case, the nonlinear components are the measurement equations which are the mappings from the emitter location to TDOA measurements and FDOA measurements.

Assume that the EKF state estimate $\hat{\mathbf{p}}_{k-1|k-1}^E$ and the covariance $\mathbf{P}_{k-1|k-1}^E$ are available at time $k-1$, where E denotes the EKF. The state predication to time k is a linear process and follows Kalman filter

$$\hat{\mathbf{p}}_{k|k-1}^E = \mathbf{F}_{k-1} \hat{\mathbf{p}}_{k-1|k-1}^E \tag{5.25}$$

$$\mathbf{P}_{k|k-1}^E = \mathbf{F}_{k-1} \mathbf{P}_{k-1|k-1}^E \mathbf{F}_{k-1}^T + \mathbf{R}_{k-1} \tag{5.26}$$

where $\mathbf{F}_k$ is the state transition matrix and $\mathbf{R}_k$ is the process noise covariance. The measurement update proceeds as

$$\hat{\mathbf{p}}_{k|k}^E = \hat{\mathbf{p}}_{k|k-1}^E + \mathbf{K}_k^E V_k^E \tag{5.27}$$

$$\mathbf{P}_{k|k}^E = \mathbf{P}_{k|k-1}^E - \mathbf{K}_k^E S_k^E \mathbf{K}_k^{E^T} \tag{5.28}$$

where V_k^E is the innovation, S_k^E is the innovation covariance, and $\mathbf{K}_k^E$ is the gain defined by

$$V_k^E = z_k - h(\hat{\mathbf{p}}_{k|k-1}^E) \tag{5.29}$$

$$\mathbf{S}_k^E = \mathbf{H}_k \mathbf{P}_{k|k-1}^E \mathbf{H}^T + \mathbf{Q}_k \tag{5.30}$$

$$\mathbf{K}_k^E = \mathbf{P}_{k|k-1}^E \mathbf{H}_k S_k^{E^{-1}} \tag{5.31}$$

where $\mathbf{Q}_k$ denotes the measurement covariance. The measurement matrix $\mathbf{H}_k$ is the Jacobian of the nonlinear measurement function, $h_k(\hat{\mathbf{p}}_k^E)$, described in (2.3) and (2.4), evaluated at the predicted emitter state,

$$\begin{aligned}
\mathbf{H}_k &= \left. \frac{\partial h_k(\mathbf{p})}{\mathbf{p}} \right|_{\mathbf{p}=\hat{\mathbf{p}}_{k|k-1}} \\
&= \frac{(\hat{\mathbf{p}}_{k|k-1}^E - \mathbf{s}_k^1)^T}{\|\hat{\mathbf{p}}_{k|k-1}^E - \mathbf{s}_k^1\|} - \frac{\hat{\mathbf{p}}_{k|k-1}^E - \mathbf{s}_k^2)^T}{\|\hat{\mathbf{p}}_{k|k-1}^E - \mathbf{s}_k^2\|}
\end{aligned} \tag{5.32}$$

For an unbiased state estimate $\hat{\mathbf{p}}_{k|k}$ obtained from measurements $\mathbf{Z}^k = \{z_1, ..., z_k\}$, the Cramer-Rao lower bound (CRLB), defined as the inverse of the Fisher information matrix (FIM) $\mathbf{J}_k$ defines the theoretical minimum of the mean square error (MSE) of the state estimates:

$$\mathbf{E}[(\mathbf{p}_k - \hat{\mathbf{p}}_k)((\mathbf{p}_k - \hat{\mathbf{p}}_k)^T)] > \mathbf{J_k}^{-1} \tag{5.33}$$

In the absence of process noise, the CRLB may be obtained using the covariance of the EKF, where the Jacobian (5.32) is evaluated at the true emitter location rather than the predicted state. The CRLB at time $k-1$ is denoted by $\mathbf{P}_{k-1}^C$ and the recursion is defined by

$$\mathbf{P}_k^C = \mathbf{F}_{k-1} \mathbf{P}_{k-1}^C \mathbf{F}_{k-1}^T - \mathbf{K}_k^C \mathbf{S}_k^C \mathbf{K}_k^{C^T} \tag{5.34}$$

where

$$\mathbf{S}_k^C = \hat{\mathbf{H}}_k \mathbf{P}_{k|k-1}^C \hat{\mathbf{H}}_k^T + \mathbf{Q}_k \tag{5.35}$$

$$\mathbf{K}_k^C = \mathbf{F}_{k-1} \mathbf{P}_k^C \mathbf{F}_{k-1}^T \hat{\mathbf{H}}_k \mathbf{S}_k^{C^{-1}} \tag{5.36}$$

and

$$\begin{aligned}
\hat{\mathbf{H}}_k &= \left. \frac{\partial h_k(\mathbf{p})}{\mathbf{p}} \right|_{\mathbf{p}=\mathbf{p}_k} \\
&= \frac{(\mathbf{p} - \mathbf{s}_k^1)^T}{\|\mathbf{p}_k - \mathbf{s}_k^1\|} - \frac{(\mathbf{p}_k - \mathbf{s}_k^2)^T}{\|\mathbf{p}_k - \mathbf{s}_k^2\|}
\end{aligned} \tag{5.37}$$

5.2   Improved localisation accuracy with optimal sensor-target placement

For most of the cases, we only consider the source localisation problem with one stationary signal source and multiple stationary sensors. One special case is when the sensors are mobile. Instead of using the term "optimal sensor-target placement", the term "optimal mobile trajectory" is used in this thesis.

5.2.1 Generic metrics for optimal sensor placement

To determine the optimal sensor placement for source localisation, some metrics need to be defined Bishop et al. [2010]. For a general measurement vector $\hat{\mathbf{z}} = \mathbf{z}(\mathbf{p}) + \mathbf{e}$ and a general vector $\mathbf{p} \in \mathbb{R}^n$. Assume the vector of measurement noise $\mathbf{e} \in \mathbb{R}^n$ has Gaussian distribution with zero mean and a constant covariance matrix $\mathbf{\Sigma}$. The likelihood function of $\mathbf{p}$ given the measurement vector $\hat{\mathbf{z}} \sim \mathcal{N}(\mathbf{z}(\mathbf{p}), \mathbf{\Sigma})$ under the standard assumption of Gaussian measurement errors is given by

$$f_{\hat{\mathbf{z}}}(\hat{\mathbf{z}}; \mathbf{p}) = \frac{1}{(2\pi)^{\frac{N}{2}} |\mathbf{\Sigma}|^{\frac{1}{2}}} \times \exp\left(-\frac{1}{2}(\hat{\mathbf{z}} - \mathbf{z}(\mathbf{p}))^T \mathbf{\Sigma}^{-1}(\hat{\mathbf{z}} - \mathbf{z}(\mathbf{p}))\right) \tag{5.38}$$

where $|\mathbf{\Sigma}|$ is the determinant of $\mathbf{\Sigma}$ and $\mathbf{z}(\mathbf{p})$ is the mean of the measurement $\hat{\mathbf{z}}$. In general, the Cramer-Rao inequality lower bounds the covariance achievable by an unbiased estimator. For an unbiased estimate $\hat{\mathbf{p}}$ of $\mathbf{p}$, the Cramer-Rao bound states that

$$\mathbf{E}[(\hat{\mathbf{p}} - \mathbf{p})(\hat{\mathbf{p}} - \mathbf{p})^T] \geq \mathbf{J}^{-1} = \mathbf{CRB} \tag{5.39}$$

where $\mathbf{J}$ is called the Fisher information matrix, which quantifies the amount of information that the observable random measurement vector $\hat{\mathbf{z}}$ carries about the unobservable parameter $\mathbf{p}$.

Under the assumption of Gaussian measurement errors and when the error covariance is independent of the parameters, the entire Fisher Information Matrix (FIM) is given by

$$\mathbf{J} = \nabla_{\mathbf{p}} \mathbf{z}(\mathbf{p})^T \mathbf{\Sigma}^{-1} \nabla_{\mathbf{p}} \mathbf{z}(\mathbf{p}) \tag{5.40}$$

and the (i, j)th element of $\mathbf{J}$ is given by

$$\mathbf{J}_{(i,j)}(\mathbf{p}) = \mathbf{E}\left[\frac{\partial}{\partial p_i} \ln(f_{\hat{\mathbf{z}}(\hat{\mathbf{z}}; \mathbf{p})}) \frac{\partial}{\partial p_j} \ln(f_{\hat{\mathbf{z}}(\hat{\mathbf{z}}; \mathbf{p})})\right] \tag{5.41}$$

where $\mathbf{p}$ is the parameter to be estimated.

The FIM characterizes the nature of the likelihood function (5.38). If the likelihood function is sharply peaked then the true value $\mathbf{p}$ is easier to estimate from the measurement $\hat{\mathbf{z}}(\mathbf{p})$ than if the likelihood function is flatter. Independent measurements from additional sensors in general positions cannot decrease the total information.

Note that $\mathbf{CRB} = \mathbf{J}^{-1}$ is symmetric positive definite (so long as $\mathbf{J}$ is invertible) and defines a so-called uncertainty ellipsoid. Denote the eigenvalues of $\mathbf{CRB}$ by λ_i and note that $\sqrt{\lambda_i}$ for $i = 1, 2, ..., N$ is the length of the ith axis of the ellipsoid. Note also that axes lie along the corresponding eigenvectors of $\mathbf{CRB}$. A scalar functional measure of the 'size' of the uncertainty ellipse provides a useful characterization of the potential performance of an unbiased estimator. In this thesis, the volume of the uncertainty ellipsoid is used as an intuitively meaningful measure of the total uncertainty in an estimate $\hat{\mathbf{p}}$ of $\mathbf{p}$.

For computational simplicity, the determinant of the FIM $\det(\mathbf{J})$ is considered as a computable measure of the volume of the ellipse generated by $\mathbf{CRB}$ for range based localisation, which is known as D-criterion and for TDOA based localisation, we will

use the trace of **CRB**, which is known A-criterion Ucinski [2004].

5.2.2 Optimal sensor-target geometry for TDOA-based source localisation

In TDOA-based localisation, the time difference measured by pairs of sensors is involved to estimate the location of the signal source. The expression of the time difference measurement can be obtained from (5.1)

$$t_{i1} = \frac{d_{i1}}{c} = \frac{1}{c}(\sqrt{(x-x_1)^2+(y-y_1)^2} - \sqrt{(x-x_i)^2+(y-y_i)^2}), i = 2,3,...,N \quad (5.42)$$

where c denotes the constant propagation speed of the signal source. Take sensor 1 as the reference sensor, the Jacobian matrix of the TDOA measurement vector is given by

$$\frac{1}{c}\begin{bmatrix} \cos(\phi_2)-\cos(\phi_1) & \sin(\phi_2)-\sin(\phi_1) \\ \cos(\phi_3)-\cos(\phi_1) & \sin(\phi_3)-\sin(\phi_1) \\ \vdots & \vdots \\ \cos(\phi_N)-\cos(\phi_1) & \sin(\phi_N)-\sin(\phi_1) \end{bmatrix} \quad (5.43)$$

where ϕ_i is the angle of arrival of the ith sensor with respect to the signal source. Denote the covariance matrix of TDOA measurements by

$$\mathbf{Q}_t = \sigma_1\mathbf{1} + \begin{bmatrix} \sigma_2^2 & & & \mathbf{0} \\ & \sigma_2^2 & & \\ & & \ddots & \\ \mathbf{0} & & & \sigma_N^2 \end{bmatrix} \quad (5.44)$$

where $\mathbf{1}$ is the $(N-1) \times (N-1)$ matrix of ones.

According to (5.40), the FIM is given by Isaacs et al. [2009]

$$\mathbf{J} = \begin{bmatrix} J_{11} & J_{12} \\ J_{21} & J_{22} \end{bmatrix}$$

$$= \begin{bmatrix} \sum_{i=1}^{N}\frac{\cos(\phi_i)^2}{\sigma_i^2} - a(\sum_{i=1}^{N}\frac{\cos(\phi_i)^2}{\sigma_i^2})^2 & \frac{1}{2}\sum_{i=1}^{N}\frac{\sin(2\phi_i)}{\sigma_i^2} - a\sum_{i=1}^{N}\frac{\sin(\phi_i)}{\sigma_i^2}\sum_{i=1}^{N}\frac{\cos(\phi_i)}{\sigma_i^2} \\ \frac{1}{2}\sum_{i=1}^{N}\frac{\sin(2\phi_i)}{\sigma_i^2} - a\sum_{i=1}^{N}\frac{\sin(\phi_i)}{\sigma_i^2}\sum_{i=1}^{N}\frac{\cos(\phi_i)}{\sigma_i^2} & \sum_{i=1}^{N}\frac{\sin(\phi_i)^2}{\sigma_i^2} - a(\sum_{i=1}^{N}\frac{\sin(\phi_i)^2}{\sigma_i^2})^2 \end{bmatrix} \quad (5.45)$$

where $a = \frac{1}{\sum_{i=1}^{N}\frac{1}{\sigma_i^2}}$. Therefore, the determinant of the FIM denoted by $\det(\mathbf{J})$ is given by

$$\det(\mathbf{J}) = \frac{1}{4a^2} - \frac{1}{4}(\sum_{i=1}^{N}\frac{\sin(2\phi_i)}{\sigma_i^2})^2 - \frac{1}{4}(\sum_{i=1}^{N}\frac{\cos(2\phi_i)}{\sigma_i^2})^2$$

$$- a\sum_{i=1}^{N}\frac{1}{\sigma_i^2}(\sin\phi_i\sum_{i=1}^{N}\frac{\cos(\phi_j)}{\sigma_j^2} - \cos\phi_i\sum_{i=1}^{N}\frac{\sin(\phi_j)}{\sigma_j^2})^2 \quad (5.46)$$

Since the last three terms in the right-hand side of (5.46), for constant measurement noise $\sigma_i^2, i = 1, 2, ..., N$, to maximize the determinant of the Fisher information matrix **J**, the following minimization problem with respect to the angle of arrival vector $\boldsymbol{\phi} = [\phi_1, ..., \phi_N]^T$ needs to be solved:

$$\arg\min_{\boldsymbol{\phi}} \left(\frac{1}{4} \left(\sum_{i=1}^{N} \frac{\sin(2\phi_i)}{\sigma_i^2} \right)^2 + \frac{1}{4} \left(\sum_{i=1}^{N} \frac{\cos(2\phi_i)}{\sigma_i^2} \right)^2 \right.$$
$$\left. + a \sum_{i=1}^{N} \frac{1}{\sigma_i^2} \left(\sin\phi_i \sum_{i=1}^{N} \frac{\cos(\phi_j)}{\sigma_j^2} - \cos\phi_i \sum_{i=1}^{N} \frac{\sin(\phi_j)}{\sigma_j^2} \right)^2 \right) \tag{5.47}$$

Define

$$\mathbf{u}_i = \begin{bmatrix} \cos\phi_i \\ \sin\phi_i \end{bmatrix} \quad and \quad \mathbf{v}_i = \begin{bmatrix} \cos 2\phi_i \\ \sin 2\phi_i \end{bmatrix} \tag{5.48}$$

Then (5.47) can be rewritten as

$$\arg\min_{\boldsymbol{\phi}} \left\| \sum_{i=1}^{N} \frac{\mathbf{v}_i}{\sigma_j^2} \right\|^2 + 4a \sum_{i=1}^{N} \frac{1}{\sigma_j^2} \times \left(\left[\sin\phi_i - \cos\phi_i \right] \sum_{i=1}^{N} \frac{\mathbf{u}_j}{\sigma_j^2} \right)^2 \tag{5.49}$$

Under the same measurement noise variance $\sigma_1^2 = \sigma_2^2 = ... = \sigma_N^2 = \sigma_t^2$, the upper-bound of the determinant of the FIM, $\det(\mathbf{J})$, can be achieved when the angle of arrival of the sensors meets the conditions Meng et al. [2012]

$$\sum_{i=1}^{N} \sin 2\sigma_i = 0 \quad \sum_{i=1}^{N} \cos 2\sigma_i = 0$$
$$\sum_{i=1}^{N} \sin \sigma_i = 0 \quad \sum_{i=1}^{N} \cos \sigma_i = 0 \tag{5.50}$$

5.2.3   TDOA-based source localisation with geometric constraints

In source localisation, the determinant of the FIM provides a metric for optimal sensor placement. When the true emitter location is known, the optimal sensor-target placement can be obtained. However, in the practical passive localisation, the true emitter location is unknown, so the optimal sensor placement cannot be found. To improve the localisation accuracy, the geometric information of the sensor-target placement can still be used. In this subsection, the geometry of the sensor-target placement is used to formulate a constrained optimization problem to correct the measurement error and improve the localisation accuracy Bishop et al. [2008].

Consider the general localisation problem involving $N = n + 2$ or more sensors in n dimensional space where $n = 2$ or $n = 3$. Applying the law of cosines to the system of $n + 1$ triangles defined by the signal source, sensor 1, and sensor $i, \forall_i \in 2, ..., n + 2$, as shown in Figure 5.1, gives $n + 1$ equations of the form

$$\|\mathbf{r}_i\|^2 = \|\mathbf{r}_1\|^2 + \|\mathbf{r}_{1i}\|^2 - 2\mathbf{r}_{1i}^T\mathbf{r}_1 \tag{5.51}$$
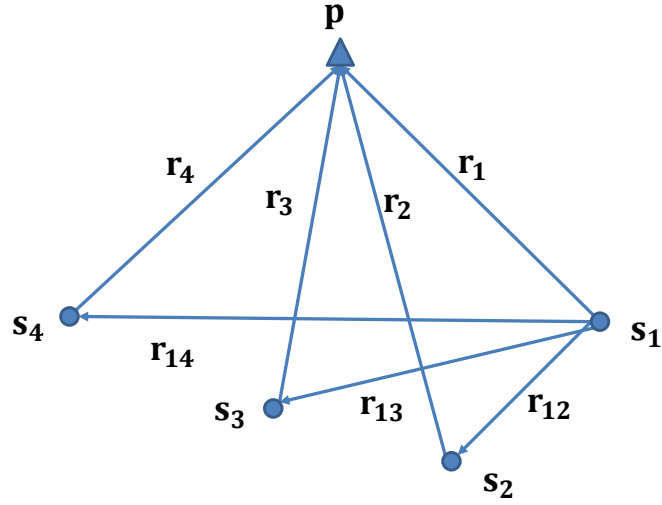
Figure 5.1: Example of TDOA-based localisation with 4 sensors

Squaring (5.1) gives

$$\|\mathbf{r}_i\|^2 = d_{i1}^2 + \|\mathbf{r}_1\|^2 + 2d_{i1}\|\mathbf{r}_i\| \tag{5.52}$$

and then substituting (5.52) into (5.51), we obtain $N-1$ equations of the form

$$\begin{bmatrix} \mathbf{r}_1^T & d_{i1} \end{bmatrix} \begin{bmatrix} \mathbf{r}_1 \\ \|\mathbf{r}_1\| \end{bmatrix} = (\|\mathbf{r}_{i1}\|^2 - d_{i1}^2) \tag{5.53}$$

Stacking the equations gives

$$2\mathbf{A} \begin{bmatrix} \mathbf{r}_1 \\ \|\mathbf{r}_1\| \end{bmatrix} = \mathbf{b} \tag{5.54}$$

where

$$\mathbf{A} = \begin{bmatrix} \mathbf{r}_{12}^T & d_{21} \\ \mathbf{r}_{13}^T & d_{31} \\ \vdots & \vdots \\ \mathbf{r}_{1N}^T & d_{N1} \end{bmatrix}, \quad \mathbf{b} = \begin{bmatrix} \|\mathbf{r}_{12}\|^2 - d_{21}^2 \\ \|\mathbf{r}_{13}\|^2 - d_{31}^2 \\ \vdots \\ \|\mathbf{r}_{1N}\|^2 - d_{N1}^2 \end{bmatrix} \tag{5.55}$$

Therefore, assuming $\mathbf{A}$ is nonsingular, we obtain

$$\begin{bmatrix} \mathbf{r}_1 \\ \|\mathbf{r}_1\| \end{bmatrix} = (2\mathbf{A})^{-1}\mathbf{b} \tag{5.56}$$

Letting $(2\mathbf{A})^{-1}\mathbf{b} = [\rho_1, \rho_2, \quad \ldots \quad , \rho_{N-1}]^T$, we have

$$\rho_1^2 + \rho_2^2 + \ldots + \rho_{N-2}^2 - \rho_{N-1}^2 = 0. \tag{5.57}$$

Defining $\mathbf{Y} = \mathbf{A}\mathbf{\Lambda}\mathbf{A}^T$ and simplifying (5.57) give

$$diag(\mathbf{Y})\mathbf{Y}^{-1}diag(\mathbf{Y}) = 0 \tag{5.58}$$

where $diag(\mathbf{Y}) = \mathbf{b}$. (5.58) can be used as a constraint on the unknown measurement errors e_{i1} with known parameters given by the sensor coordinates and the noisy measurement $\hat{d}_{i1}$.

For a localisation system with $N > n + 2$ sensors, $N - (n + 1)$ independent constraints can be obtained by considering the measurement and geometrical relationships between the sensors $\{1, 2, ..., n + 1\}$ and i for $i \in \{n + 2, ..., N\}$:

$$c_{i-(n+1)}(e_{21}, e_{31}, ..., e_{n1}, e_{(n+1)1}, e_{i1}) = 0, i \in \{n + 2, ..., N\} \tag{5.59}$$

and the column vector of constraint functions can be denoted by

$$\mathbf{c}(\mathbf{e}) = \begin{bmatrix} c_1(e_{21}, e_{31}, ..., e_{(i+1)1}, e_{(i+2)1}) \\ \vdots \\ c_{n-(i+1)}(e_{21}, e_{31}, ..., e_{(i+1)1}, e_{N1}) \end{bmatrix} \tag{5.60}$$

where $\mathbf{e}$ is the vector of measurement errors.

After the geometrical constraints are obtained, the localisation problem can be formulated into a constrained least-squares optimization problem. Under the assumption of zero-mean Gaussian errors, we have the objective function:

$$f(\mathbf{e}) = \mathbf{e}^T \mathbf{\Sigma}^{-1} \mathbf{e} \tag{5.61}$$

where $\mathbf{e}$ is a column vector of the errors $e_{21}, e_{31}, e_{41}, ..., e_{N1}$ and $\mathbf{\Sigma}$ is the error covariance matrix. We aim to minimize the cost function (5.61) subject to constraints (5.59) in $\mathbb{R}^n$.

Due to the nonlinearity of the constraints, the sequential quadratic programming (SQP) techniques Fletcher [2013]; Gill et al. [1981] can be employed to implement the optimization associated with (5.61). Consider the following general nonlinear programming problem:

$$\underset{\mathbf{e}}{\arg\min} \quad f(\mathbf{e}) \quad s.t. \quad \mathbf{c}(\mathbf{e}) = 0 \tag{5.62}$$

Since the vector of constraint functions $\mathbf{c}(\mathbf{e})$ is generally nonlinear and non-convex, the nonlinear programming methods that rely on iteration and initial estimates are required. One of the solutions can be found in Bishop et al. [2008].

5.2.4 Optimal sensor mobile trajectory for joint TDOA and FDOA-based source localisation using two sensors

When at least one mobile sensor is involved, the source location can be determined using only two sensors by taking TDOA and FDOA measurements. As discussed before, the geometry of the sensor placement with respect to the signal source influences the localisation accuracy. In this subsection, we investigate the optimal trajectory of the mobile sensors to minimize the location estimation error. The Cramer-Rao lower bound (CRLB) can be used as an optimization criteria to evaluate the perfor-

mance of the localisation for the optimal mobile sensor trajectory.

The CRLB at the time instant k can be calculated recursively from the previous time instant $k-1$ which can be obtained from (5.24). The recursive formula for calculating the FIM is

$$\mathbf{J}_k = \mathbf{J}_{k-1} + \mathbf{H}_k^T(\mathbf{p})(\mathbf{Q}_k^{tf})^{-1}\mathbf{H}_k(\mathbf{p}) \tag{5.63}$$

where $\mathbf{Q}_k^{tf}$ denotes the covariance matrix of the joint TDOA and FDOA measurements at the time instant k.

Different optimization criteria for mobile sensor trajectory can be derived from the CRLB. Three different performance measures are usually used, which are the square roots of the diagonal entries of the CRLB which represent the uncertainty in the x or y direction, the square root of the trace of the CRLB which gives the lower bound on the RMSE of any unbiased position estimate, and the determinant which is proportional to the lower bound on the volume of the uncertainty ellipse associated with any unbiased position estimate. As these optimization criteria were found to give almost identical performance, the determinant criteria, $\det(\mathbf{J}^{-1})$, is used for the optimization.

At each time instant k, denote $\mathbf{u}_{k+1}^1 \in U_{k+1}^1$ and $\mathbf{u}_{k+1}^2 \in U_{k+1}^1$ be the possible future sensor state of the next time instant for the two sensors. The state includes the location and the velocity. For simplicity we assume the speed of the sensor is constant and only the mobile direction varies. In addition, to reduce the computational cost, we assume the possible future way points has limited choice by discretizing the area into a number of grids. The future sensor state that forms optimal sensor trajectory can be evaluated by calculating the determinant of the approximated CRLB, $\det(\mathbf{J}^{-1})$.

For one stationary sensor $\mathbf{s}_k^1$ and one mobile sensor $\mathbf{s}_k^2$, the sensor state of $\mathbf{s}_k^2$ that meets the criteria of optimal trajectory is given by

$$\mathbf{s}_{k+1}^2 = \arg\min_{\mathbf{u}_{k+1}^2}(\det(\mathbf{J}_{k+1}^{-1}(\mathbf{p}, \mathbf{u}_{k+1}^2, \mathbf{s}_{k+1}^1))) \tag{5.64}$$

The complete mobile sensor trajectory is generated by iterating the process of finding the best way points for the next time instant. For two mobile sensors, the trajectory of both sensors needs to be optimized simultaneously. The sensor state of $\mathbf{s}_k^1$ and $\mathbf{s}_k^2$ that meets the criteria of optimal trajectory is given by

$$(\mathbf{s}_{k+1}^1, \mathbf{s}_{k+1}^2) = \arg\min_{\mathbf{u}_{k+1}^1, \mathbf{u}_{k+1}^2}(\det(\mathbf{J}_{k+1}^{-1}(\mathbf{p}, \mathbf{u}_{k+1}^1, \mathbf{u}_{k+1}^2))) \tag{5.65}$$

Following the optimization process, the mobile sensor trajectory that minimizes the location estimation error can be found.

5.3 Improve localisation accuracy with location estimation bias reduction

5.3.1 Estimation bias in localisation

Bias is a term in estimation theory which is defined as the difference between the expected value of a parameter estimate and the true value of the parameter Melsa et al. [1978]. For source localisation problem in n-dimensional (n=2 or 3) space, $N \geq n$ usable measurements obtained from N sensors whose locations are known can be used to determine the source location. Denote the coordinate vector of a signal source or an emitter by $\mathbf{p} = [x, y]^T$ in 2-dimensional space (n=2) and the localisation mapping from the noisy measurements to the source location estimates as $\mathbf{g} = (g_1, g_2)$. In the absence of noise, we have

$$\mathbf{p} = \mathbf{g}(\Theta) \tag{5.66}$$

where $\Theta = (\theta_1, \theta_2, ..., \theta_N)$ is the measurements from N sensors. θ_i, $i = 1, ..., N$, is the measurement obtained from sensor i.

In practical localisation, the noise in measurements is inevitable, so in the presence of noise, we have

$$\hat{\mathbf{p}} = \mathbf{p} + \delta\mathbf{p} = \mathbf{g}(\Theta + \delta\Theta) = \mathbf{g}(\hat{\Theta}) \tag{5.67}$$

where $\hat{\mathbf{p}}$ denotes the inaccurate source location estimate, $\delta\mathbf{p}$ is the source location estimation error, $\hat{\Theta} = (\hat{\theta}_1, \hat{\theta}_2, ..., \hat{\theta}_N)$ denotes the noisy measurements and $\delta\Theta = (\delta\Theta_1, \delta\Theta_2, ..., \delta\Theta_N)^T$ denotes the measurement noise which is generally assumed to be zero-mean Gaussian.

In practical localisation, the measurement process is usually repeated k times, and for each measurement process, an estimated source location can be obtained. The final source location estimate is usually obtained by averaging the k source location estimates. As $k \to \inf$, we would expect the estimate to go to:

$$\mathbf{E}[\hat{x}] = \mathbf{E}[g_1(\hat{\Theta})] \tag{5.68}$$

Now note that if g_1 and g_2 are nonlinear, we have

$$\begin{aligned} \mathbf{E}[\hat{x} &= \mathbf{E}[g_i(\hat{\Theta})] \neq g_i(\mathbf{E}(\hat{\Theta})) \\ &= g_i(\Theta) = x \end{aligned} \tag{5.69}$$

Therefore the bias appears in the source location estimation process and it can be given by

$$Bias_x = \mathbf{E}[\hat{x}] - x \tag{5.70}$$

and

$$Bias_y = \mathbf{E}[\hat{y}] - y \tag{5.71}$$

It is well known that once two conditions: 1) the measurements are noisy; and 2)

the localisation mapping is nonlinear are satisfied, the bias will almost always certainly appear in the localisation problem. In practical situations, the measurements are always noisy and the localisation mappings are normally nonlinear; therefore, the bias is almost inevitable. Since the bias is a systematic and possibly computable error, it is desirable to remove it.

5.3.2 Generic location estimation bias reduction algorithms

For simplicity, 2-dimensional space is considered. The extension of the proposed method to 3-dimensional space is straight-forward. To determine the bias on x-axis, consider $\hat{x} = g_1(\hat{\Theta})$. Because the localisation mapping **g** is well-defined, the function g_1 can be expanded by a Taylor series and truncated at second order:

$$
\begin{aligned}
x + \delta x &= g_{1,x}(\hat{\theta}_1, \hat{\theta}_2, ..., \hat{\theta}_N) \\
&= g_{1,x}(\theta_1 + \delta\theta_1, \theta_2 + \delta\theta_2, ..., \theta_N + \delta\theta_N) \\
&\approx g_{1,x}(\theta_1, \theta_2, ..., \theta_N) + \sum_{j=1}^{N} \frac{\partial g_{1,x}}{\partial \theta_j} \delta\theta_j \\
&\quad + \frac{1}{2!} \sum_{j=1}^{N} \sum_{l=1}^{N} \delta\theta_j \delta\theta_l \frac{\partial^2 g_{1,x}}{\partial \theta_j \partial \theta_l}.
\end{aligned}
\tag{5.72}
$$

Hence, the difference between the true value and the estimate is

$$
\mathbf{E}(\delta x) = \frac{1}{2!} \left[\sum_{j=1}^{N} 2\sigma^2 \frac{\partial^2 g_{1,x}}{\partial \theta_j^2} - \sum_{l=1}^{N} \sum_{l=1}^{N} 2\sigma^2 \frac{\partial^2 g_{1,x}}{\partial \theta_l \partial \theta_l} \right]
\tag{5.73}
$$

Note that (5.73) is the approximate bias expression for TDOA based localisation. For RSSI based localisation, the errors in measurements are independent of each other and have zero mean with covariance $\Sigma = diag(\sigma_{\theta_1}, \sigma_{\theta_2}, ..., \sigma_{\theta_N})$. Taking the expectation results in the approximate bias expression for RSSI based localisation:

$$
\mathbf{E}(\delta x) = \frac{1}{2!} \sum_{j=1}^{N} \sigma_{\theta_j}^2 \frac{\partial^2 g_{1,x}}{\partial \theta_j^2}
\tag{5.74}
$$

(5.73) and (5.74) give the analytical expression for the bias in TDOA-based localisation and RSSI-based localisation. However, in some situation, obtaining the analytical expression of the mapping **g** becomes very challenging if not impossible. If **g** cannot be obtained then the bias cannot be calculated, so it is highly desirable to find an alternative method to analytically express the derivatives of **g** to allow computation of the bias and its consequent reduction. The key to do this is to notice that **g** is the inverse of the mapping **f** for which often an analytic form is known, therefore the mapping **f** and its derivatives can be used to calculate the derivatives of **g** using the Jacobian identity, ultimately resulting in an estimate of the bias.

To obtain an analytical expression of the bias, the situation where the number of

measurements obtained from sensors N is equal to the dimension of source location n, $N = n = 2$, is discussed first. In addition, the mapping $\mathbf{f}$ is assumed as a known analytic function. Because $\mathbf{f}$ and $\mathbf{g}$ are inverse mappings, the Jacobian identity holds:

$$\begin{bmatrix} \frac{\partial f_1}{\partial x} & \frac{\partial f_2}{\partial x} \\ \frac{\partial f_1}{\partial y} & \frac{\partial f_2}{\partial y} \end{bmatrix} \begin{bmatrix} \frac{\partial g_1}{\partial \theta_1} & \frac{\partial g_2}{\partial \theta_1} \\ \frac{\partial g_1}{\partial \theta_2} & \frac{\partial g_2}{\partial \theta_2} \end{bmatrix} = \mathbf{I}_2 \tag{5.75}$$

Rearranging (5.75), we can obtain the analytical expression for $\partial g_i / \partial \theta_j (i = 1, 2; j = 1, 2)$ in terms of $\partial f_i / \partial x_j (i = 1, 2; j = 1, 2)$, and thus analytic functions of the x. Denote the expressions of $\frac{\partial g_i}{\partial \theta_i}$ as functions of x, y, e.g. $\frac{\partial g_1}{\partial \theta_1} = g_1^1$. If we differentiate $\partial g_i / \partial \theta_j (i = 1, 2; j = 1, 2)$ in respect to x and y respectively, we can obtain an equation set as follows:

$$\begin{bmatrix} \frac{\partial f_1}{\partial x} & \frac{\partial f_2}{\partial x} \\ \frac{\partial f_1}{\partial y} & \frac{\partial f_2}{\partial y} \end{bmatrix} \begin{bmatrix} \frac{\partial^2 g_1}{\partial \theta_1^2} \\ \frac{\partial^2 g_1}{\partial \theta_1 \partial \theta_2} \end{bmatrix} = \begin{bmatrix} \frac{\partial^2 g_1}{\partial \theta_1 x} \\ \frac{\partial^2 g_1}{\partial \theta_1 y} \end{bmatrix} \tag{5.76}$$

Hence, by solving the equation set (5.76), a formula for $\frac{\partial^2 g_1}{\partial \theta_1^2}$ that contains derivatives of only f_i is obtained. The formulas for $\frac{\partial^2 g_i}{\partial \theta_j^2}$ for all i,j can be obtained in the same way. Substituting the formulas into (5.73) and (5.74), the easily-calculated expressions for the bias for TDOA based localisation and RSSI based localisation can be finally obtained.

In practice the inaccurate estimated position of the signal source by using existing localisation algorithms can be obtained first. Then, the inaccurate source location can be input into the obtained analytical expression of the bias. Finally, the accuracy of the localisation can be improved by subtracting the obtained bias, viz., $\hat{x} - bias_x$ and $\hat{y} - bias_y$.

If the number of measurements N is greater than the dimension of source location n, (5.75) and (5.76) cannot be obtained. In other words, because $N \neq n$ the Jacobian identity between $\mathbf{f}$ and $\mathbf{g}$ does not hold, and so the bias cannot be expressed using the derivatives of $\mathbf{f}$. To start with, $N = n + 1$ is considered. In the noisy case generally, the equation $\mathbf{f}(\hat{x}) = \hat{\Theta}$ is overdetermined and has no solution. To determine the bias, a least-squares approach can be used.

Consider n-dimensional space, with axes corresponding to the N measurements. Assume that a surface consists of points which correspond to all sets of noiseless measurements $(\theta_1, \theta_2, ..., \theta_N)$, i.e., $\theta_i = f(x, y)$ for $i = 1, 2, ..., N$ when $n = 2$. According to the least-squares method, the cost function has the following form:

$$F_{cost-function}(\mathbf{p}, \hat{\Theta}) = \sum_{i=1}^{N} (f_i - \hat{\theta}_i)^2 = \sum_{i=1}^{N} \delta \theta_i^2 \tag{5.77}$$

In fact the least-squares method attempts to find a point $(\theta_1, \theta_2, ..., \theta_N)$ on the surface corresponds to an obtained set of noisy measurements $(\hat{\theta}_1, \hat{\theta}_2, ..., \hat{\theta}_N)$ to minimize the distance between the two points. Therefore, the distance between the two points can

be formulated as

$$D_{min} = \sqrt{\sum_{i=1}^{N} \delta\theta_i^2} = \varepsilon_1 \|\mathbf{u}\| \tag{5.78}$$

where $\mathbf{u}$ denotes the normal vector from the noiseless point to the obtained noisy point and ε_1 is a coefficient to set the distance. Therefore, for the noisy measurements, a new analytical mapping $\mathbf{F} = (F_1, F_2, ..., F_N)^T$ can be obtained by moving from $\mathbf{f}$ along the normal vector for a distance $\varepsilon_1\|\mathbf{u}\|$. The new mapping $\mathbf{F}$ is no longer overdetermined because an extra variable ε_1 has been introduced into the mapping.

Now, we have a new mapping $\mathbf{F} : R^N \to R^N$ as follows.

$$\hat{\mathbf{\Theta}} = \mathbf{F}(\hat{\mathbf{p}}, \varepsilon_1) = \mathbf{f}(\hat{\mathbf{p}}) + \varepsilon_1\mathbf{u} \tag{5.79}$$

After introducing the extra variable ε_1, $\mathbf{F}$ is invertible. Therefore, we can consider the localisation mapping (call it $\mathbf{G}$) as the inverse mapping of $\mathbf{F}$. We can then proceed along the same lines as previously.

When the number of input measurements N exceeds $n + 1$, the situation is similar to the case $N = n + 1$. We need to introduce more than one extra variable in order to solve the overdetermined problem. The number of coefficients that vary the normal vector $\mathbf{u}$ and the dimension of $\mathbf{u}$ are equal to $N - n$.

5.3.3 Localisation bias reduction in sensor network localisation

The bias reduction algorithm can not only be used in source localisation of a single emitter, it can also be used to correct the location estimation bias in sensor network localisation by utilizing network information. Consider a sensor network in n-dimensional space (where n=2 or 3) consisting of N nodes. The nodes can be divided into two types: 1. unlocalised sensors which are labelled from 1 to h and 2. anchor nodes whose locations are already known indexed from $h + 1$ to N. There will be a link between two nodes (one at least of which is a sensor) only if they are within some specified range (in which case it is assumed they can measure the distance between them). Each link provides one independent range measurement d_i ($i = 1, 2, ..., N$).

Under these assumptions, a network can be modeled by an undirected graph. Let $G = (V, E)$ be an undirected graph with a set of nodes $V = \{v_1, v_2, ..., v_N\}$ and edges of the unordered pairs $e = (v_i, v_j) \in E(E \subseteq V \times V)$ (here E includes the subset of edges linking all pairs of anchors, denoted as E_A). We also assume that the graph is connected and simple (no self-loops or multiple edges). To guarantee a network can be localisable, the underlying graph of the network must be globally rigid Jackson and Jordán [2005] and the network must have at least three non-collinear anchors at known positions in 2-dimensional space (at least four non-coplanar anchors at known positions in 3-dimensional space), with all the sensors generically positioned Aspnes et al. [2006].

Now in the noiseless case, which means all N independent measurements are

exact, the sensor network localisation problem can be formulated as one of solving the following equation for **p**:

$$\mathbf{d} = \mathbf{f}(\mathbf{p}_s) \qquad (5.80)$$

Here $\mathbf{r} = (r_1, r_2, ..., r_N)$ represents the set of noiseless independent range measurements associated with existing edges which includes at least one unknown sensor, $\mathbf{P}_s = (\mathbf{p}_1, \mathbf{p}_2, ..., \mathbf{p}_h)$ denotes the true positions of the unknown sensors, and **f** is a vector function with entries such as $||\mathbf{p}_i - \mathbf{p}_j||$.

In the practical situations, noise in the measurements is inevitable. Therefore the measurements we can obtain are **r** corrupted by additive noise δr, which is normally assumed to be zero-mean Gaussian noise with known diagonal covariance matrix Σ. Further in this thesis we assume δr_i is independent of δr_j ($i \neq j$). Though **f** is defined for the noiseless case, it seems logical still to try to use **f** when noise is present. Now we have:

$$\hat{\mathbf{r}} = \mathbf{r} + \delta \mathbf{r} = \mathbf{f}(\mathbf{P}_s + \delta \mathbf{P}_s) = \mathbf{f}(\hat{\mathbf{P}}_s) \qquad (5.81)$$

where $\hat{\mathbf{r}}$ denotes the set of noisy measurements and $\hat{\mathbf{P}}_s$ represents inaccurate estimated targets positions perturbed by estimation errors $\delta \mathbf{P}_s$.

There is however a difficulty: when the number of independent measurements is greater than the number of unknown variables ($N > hn$), the above equation (5.81) becomes overdetermined, which means the estimated sensor positions cannot be obtained directly by exactly solving the equation since generically it will have no solution. In such a case, the localisation problem is normally converted to an optimization problem via maximum likelihood or least squares:

$$\hat{\mathbf{P}}_s = \arg \min_{\mathbf{P}_s} C(\mathbf{P}_s, \hat{\mathbf{r}}) \qquad (5.82)$$

where the cost function C is related to **f** and can be formulated as follows:

$$C = \sum_{l=1}^{N} [||\mathbf{p}_i - \mathbf{p}_j||^2 - \mathbf{r}_l^2]^2 \qquad (5.83)$$

where $\hat{r}_l$ denotes the noisy distance measurement between unknown sensors i and j. By solving the minimization problem, one can obtain estimated positions of the unlocalised sensors.

After defining the sensor network localisation problem, the use of localisation bias reduction algorithms in sensor network localisation can be presented Ji et al. [2015]. For ease of exposition, a minor notational adjustment is made here, in which r_{ij} instead of r_i is used to denote the range measurement provided by an edge $e(i,j)$ linking sensors i and j.

In 2-dimensional space, let the location $\mathbf{p}_i$ of vertex v_i be $[x_i, y_i]^T$; we use the rigidity matrix Anderson et al. [2010] which indicates the geometry of a network with an arbitrary ordering of the vertices and edges and has $2|V|$ columns and $|E|$
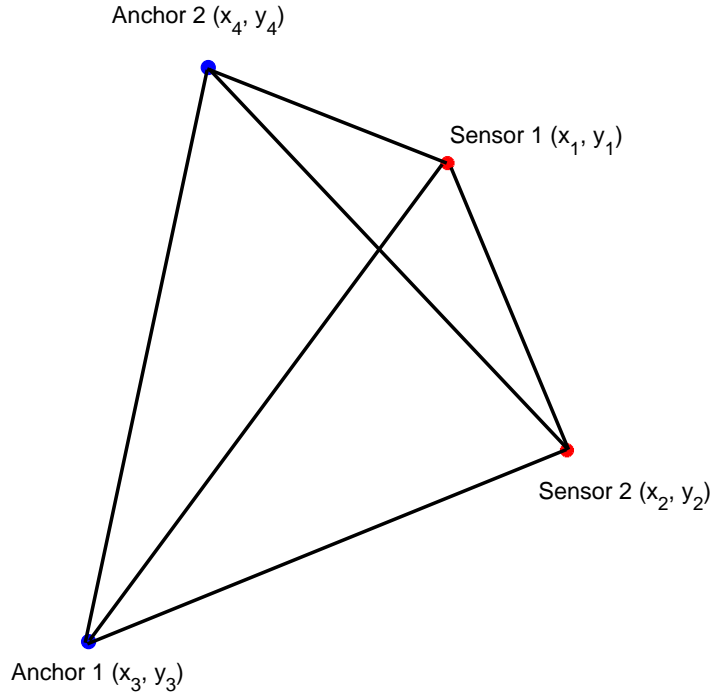
Figure 5.2: A network with two anchors and two unknown sensors

rows. Each edge gives rise to a row, and if the edge links vertices i and j, the nonzero entries of the row of the matrix are in columns $2i - 1$, $2i$, $2j - 1$ and $2j$ and are, respectively, $x_i - x_j$, $y_i - y_j$, $x_j - x_i$ and $y_j - y_i$. For example, for the graphs shown in Figure 5.2, the matrix can be written as (5.84).

$$R = \begin{bmatrix} x_1 - x_2 & y_1 - y_2 & x_2 - x_1 & y_2 - y_1 & 0 & 0 & 0 & 0 \\ 0 & 0 & x_2 - x_3 & y_2 - y_3 & x_3 - x_2 & y_3 - y_2 & 0 & 0 \\ x_1 - x_3 & y_1 - y_3 & 0 & 0 & x_3 - x_1 & y_3 - y_1 & 0 & 0 \\ 0 & 0 & x_2 - x_4 & y_2 - y_4 & 0 & 0 & x_4 - x_2 & y_4 - y_2 \\ 0 & 0 & 0 & 0 & x_3 - x_4 & y_3 - y_4 & x_4 - x_3 & y_4 - y_3 \\ x_1 - x_4 & y_1 - y_4 & 0 & 0 & 0 & 0 & x_4 - x_1 & y_4 - y_1 \end{bmatrix}$$
$$(5.84)$$

Now provided that the number of measurements is equal or greater than the number of unknown variables, as is often the case in practical situations, the localisation problem is in fact equivalent to minimizing a cost function such as the following:

$$\hat{\mathbf{P}}_s[\mathbf{p}_1, \mathbf{p}_2, ..., \mathbf{p}_i] = \arg\min_{\mathbf{P}_s} C(\mathbf{P}_s, \hat{\mathbf{r}}) \tag{5.85}$$

where

$$C = \sum_{ij \in E \setminus E_A} [||\mathbf{p}_i - \mathbf{p}_j||^2 - (r_{ij} + \delta r_{ij})^2]^2 \tag{5.86}$$

where E_A denotes the set of edges in which the edge links two anchors, $r_{ij} + \delta r_{ij}$ denotes the noisy measurement information provided by edge $e(i, j)$ and δr_{ij} represents the noise which is assumed to be Gaussian with zero mean and a known variance σ_{ij}^2. Equation (5.86) is the same as equation (5.83), and the only difference being that we use $r_{ij} + \delta r_{ij}$ to replace $\hat{r}_l$ in equation (5.83).

Recall that the bias derived in subsection 5.3.2 is analytically expressed in terms of derivatives of the cost function. Therefore, in order to apply the bias reduction algorithm in sensor network, we should relate the derivatives of the cost function to the rigidity matrix. We first require some adjustments of the rigidity matrix. In the above cost function we observe that the edges linking two anchors are not included, which means they do not contribute to the localisation process. Therefore here we use a reduced matrix R_r to denote the submatrix of R containing those columns corresponding to vertices $1, 2, ..., i$ (all the unlocalised sensors) and those edges joining vertex pairs of which at least one is a sensor. For example, the reduced matrix R_r of Figure 5.2 can be expressed as follows:

$$R_r = \begin{bmatrix} x_1 - x_2 & y_1 - y_2 & x_2 - x_1 & y_2 - y_1 \\ 0 & 0 & x_2 - x_3 & y_2 - y_3 \\ x_1 - x_3 & y_1 - y_3 & 0 & 0 \\ 0 & 0 & x_2 - x_4 & y_2 - y_4 \\ x_1 - x_4 & y_1 - y_4 & 0 & 0 \end{bmatrix} \tag{5.87}$$

Now using a straightforward calculation, the following formulation can be obtained:

$$\mathbf{w} = \nabla C = 4R_r^T \mathbf{c} \tag{5.88}$$

where $\mathbf{c}$ denotes a vector of quantities $c_{ij} = ||\mathbf{p}_i - \mathbf{p}_j||^2 - (r_{ij} + \delta r_{ij})^2$ when $e(i, j) \in E \setminus E_A$ and with the same ordering as the rows of R_r. Take the sensor network in Figure 5.2 for example, $\mathbf{w} = [\frac{\partial C}{\partial x_1}, \frac{\partial C}{\partial y_1}, \frac{\partial C}{\partial x_2}, \frac{\partial C}{\partial y_2}]^T$.

Further the Hessian matrix $\nabla^2 C$ is given by

$$\nabla \mathbf{w} = \nabla^2 C = 4[\nabla R_r^T \mathbf{c} + 2R_r^T R_r] \tag{5.89}$$

where $\nabla R_r^T = [\frac{\partial R_r}{\partial x_1}, \frac{\partial R_r}{\partial y_1}, \frac{\partial R_r}{\partial x_2}, \frac{\partial R_r}{\partial y_2}, ..., \frac{\partial R_r}{\partial x_h}, \frac{\partial R_r}{\partial y_h}]^T$ and $\frac{\partial R_r}{\partial x_i}$ and $\frac{\partial R_r}{\partial y_i}$ ($i = 1, 2, ..., h$) are defined as follows:

- Each $\frac{\partial R_r}{\partial x_i}$ is a matrix in which each row is derived from an edge joining vertex pairs of which at least one is a sensor. If the edge links vertices i and j, the nonzero entries of the row of the matrix are in columns $2i - 1$ and $2j - 1$ and are 1 and -1 respectively.

- Each $\frac{\partial R_r}{\partial y_i}$ has a the similar definition, save that the nonzero entries of the row of the matrix corresponding to $e(i, j)$ are in columns $2i$ and $2j$ and are 1 and -1 respectively.

Because the underlying graph $G = (V, E)$ is assumed to be globally rigid, according to Anderson et al. [2010] (Lemma 3.4), one can conclude that the reduced matrix R_r has generically full column rank. Thus the matrix $R_r^T R_r$ is positive definite and certainly nonsingular. Further $\nabla R_r = [\frac{\partial R_r}{\partial x_1}, \frac{\partial R_r}{\partial y_1}, \frac{\partial R_r}{\partial x_2}, \frac{\partial R_r}{\partial y_2}, ..., \frac{\partial R_r}{\partial x_h}, \frac{\partial R_r}{\partial y_h}]$ and $\frac{\partial R_r}{\partial x_i}$ and $\frac{\partial R_r}{\partial y_i}$ ($i = 1, 2, ..., h$) are matrices whose entries are either 1 (-1) or 0. Therefore if $\mathbf{c}$ is sufficiently small, $\nabla \mathbf{w}$ will be positive definite and in particular, nonsingular. From the definition of $\mathbf{c}$ it is evident that if the measurement noise is small, $\mathbf{c}$ is small.

Again, take Figure 5.2 for instance, we have

$$\nabla \mathbf{w} = \begin{bmatrix} \frac{\partial^2 C}{\partial x_1^2} & \frac{\partial^2 C}{\partial x_1 \partial y_1} & \frac{\partial^2 C}{\partial x_1 \partial x_2} & \frac{\partial^2 C}{\partial x_1 \partial y_2} \\ \frac{\partial^2 C}{\partial y_1 \partial x_1} & \frac{\partial^2 C}{\partial y_1^2} & \frac{\partial^2 C}{\partial y_1 \partial x_2} & \frac{\partial^2 C}{\partial y_1 \partial y_2} \\ \frac{\partial^2 C}{\partial x_2 \partial x_1} & \frac{\partial^2 C}{\partial x_2 \partial y_1} & \frac{\partial^2 C}{\partial x_2^2} & \frac{\partial^2 C}{\partial x_2 \partial y_2} \\ \frac{\partial^2 C}{\partial y_2 \partial x_1} & \frac{\partial^2 C}{\partial y_2 \partial y_1} & \frac{\partial^2 C}{\partial y_2 \partial x_2} & \frac{\partial^2 C}{\partial y_2^2} \end{bmatrix} \tag{5.90}$$

and

$$\nabla R_r^T \mathbf{c} = [\frac{\partial R_r}{\partial x_1}^T \mathbf{c}, \frac{\partial R_r}{\partial y_1}^T \mathbf{c}, \frac{\partial R_r}{\partial x_2}^T \mathbf{c}, \frac{\partial R_r}{\partial y_2}^T \mathbf{c}]^T \tag{5.91}$$

where

$$\frac{\partial R_r}{\partial x_1} = \begin{bmatrix} 1 & 0 & -1 & 0 \\ 0 & 0 & 0 & 0 \\ 1 & 0 & 0 & 0 \\ 0 & 0 & 0 & 0 \\ 1 & 0 & 0 & 0 \end{bmatrix} \quad \frac{\partial R_r}{\partial y_1} = \begin{bmatrix} 0 & 1 & 0 & -1 \\ 0 & 0 & 0 & 0 \\ 0 & 1 & 0 & 0 \\ 0 & 0 & 0 & 0 \\ 0 & 1 & 0 & 0 \end{bmatrix} \tag{5.92}$$

and

$$\frac{\partial R_r}{\partial x_2} = \begin{bmatrix} -1 & 0 & 1 & 0 \\ 0 & 0 & 1 & 0 \\ 0 & 0 & 0 & 0 \\ 0 & 0 & 1 & 0 \\ 0 & 0 & 0 & 0 \end{bmatrix} \quad \frac{\partial R_r}{\partial y_2} = \begin{bmatrix} 0 & -1 & 0 & 1 \\ 0 & 0 & 0 & 1 \\ 0 & 0 & 0 & 0 \\ 0 & 0 & 0 & 1 \\ 0 & 0 & 0 & 0 \end{bmatrix} \tag{5.93}$$

From equation (5.14), it is known that the second derivatives of $\mathbf{w}$ are also used in calculating the bias. Therefore we need further computations. Here the second derivative with respect to x_i is taken for example:

$$\frac{\partial \nabla \mathbf{w}}{\partial x_i} = 8[\nabla R_r^T R_r(x_i) + \frac{\partial R_r}{\partial x_i} R_r + R_r^T \frac{\partial R_r}{\partial x_i}] \tag{5.94}$$

where $R_r(x_i)$ denotes a column vector which is the column of R_r corresponding to x_i.

In order to explain the above (5.94) clearly, here the sensor network in Figure 5.2

is taken again. For example, assuming $x_i = x_1$ we have:

$$\frac{\partial \nabla \mathbf{w}}{\partial x_1} = \begin{bmatrix} \frac{\partial^3 C}{\partial x_1^3} & \frac{\partial^3 C}{\partial x_1 \partial y_1 \partial x_1} & \frac{\partial^3 C}{\partial x_1 \partial x_2 \partial x_1} & \frac{\partial^3 C}{\partial x_1 \partial y_2 \partial x_1} \\ \frac{\partial^3 C}{\partial y_1 \partial x_1 \partial x_1} & \frac{\partial^3 C}{\partial y_1^2 \partial x_1} & \frac{\partial^3 C}{\partial y_1 \partial x_2 \partial x_1} & \frac{\partial^3 C}{\partial y_1 \partial y_2 \partial x_1} \\ \frac{\partial^3 C}{\partial x_2 \partial x_1 \partial x_1} & \frac{\partial^3 C}{\partial x_2 \partial y_1 \partial x_1} & \frac{\partial^3 C}{\partial x_2^2 \partial x_1} & \frac{\partial^3 C}{\partial x_2 \partial y_2 \partial x_1} \\ \frac{\partial^3 C}{\partial y_2 \partial x_1 \partial x_1} & \frac{\partial^3 C}{\partial y_2 \partial y_1 \partial x_1} & \frac{\partial^3 C}{\partial y_2 \partial x_2 \partial x_1} & \frac{\partial^3 C}{\partial y_2^2 \partial x_1} \end{bmatrix} \tag{5.95}$$

and

$$\nabla R_r^T R_r(x_1) =$$
$$[\frac{\partial R_r}{\partial x_1}^T R_r(x_1), \frac{\partial R_r}{\partial y_1}^T R_r(x_1), \frac{\partial R_r}{\partial x_2}^T R_r(x_1), \frac{\partial R_r}{\partial y_2}^T R_r(x_1)]^T \tag{5.96}$$

$$R_r(x_1) = [x_1 - x_2, 0, x_1 - x_3, 0, x_1 - x_4]^T \tag{5.97}$$

The other second derivatives of $\mathbf{w}$ with respect to the coordinates (x_i and y_i) can be obtained in the same way and we do not show the details here. One point to notice is that only the partial derivatives $\frac{\partial \mathbf{w}}{\partial x_i}$ ($\frac{\partial \mathbf{w}}{\partial y_i}$) and $\frac{\partial^2 \mathbf{w}}{\partial x_i \partial y_j}$ ($\frac{\partial^2 \mathbf{w}}{\partial x_i^2}$ and $\frac{\partial^2 \mathbf{w}}{\partial y_j^2}$) have been expressed in terms of the reduced matrix.

Now how to obtain the expressions for $\frac{\partial \mathbf{w}}{\partial d_{ij}}$ and $\frac{\partial^2 \mathbf{w}}{\partial d_{ij}^2}$ is shown. First by differentiating equation (5.88) with respect to d_{ij} one can obtain:

$$\frac{\partial \mathbf{w}}{\partial d_{ij}} = -8R_r^T \frac{\partial \mathbf{c}}{\partial d_{ij}} \tag{5.98}$$

where $\frac{\partial \mathbf{c}}{\partial d_{ij}}$ denotes the first derivative of $\mathbf{c}$ with respect to d_{ij} and $\frac{\partial \mathbf{c}}{\partial d_{12}} = [d_{12}, 0, 0, 0, 0]^T$. Further differentiating the above equation in respect to r_{ij}, one can have:

$$\frac{\partial^2 \mathbf{w}}{\partial r_{ij}^2} = -8R_r^T \frac{\partial^2 \mathbf{c}}{\partial r_{ij}^2} \tag{5.99}$$

where $\frac{\partial^2 \mathbf{c}}{\partial r_{ij}^2}$ is the second derivatives of $\mathbf{v}$ and $\frac{\partial^2 \mathbf{c}}{\partial r_{12}^2} = [1, 0, 0, 0, 0]^T$.

The derivatives of the form $\frac{\partial^2 \mathbf{w}}{\partial x_i \partial r_{ij}}$ ($\frac{\partial^2 \mathbf{w}}{\partial y_i \partial r_{ij}}$) can be obtained by differentiating (5.89), which shows the first derivative of $\mathbf{w}$ respect to the coordinates (x_i and y_i in two dimensional space), with respect to r_{ij}. We notice only $\mathbf{c}$ is dependent on r_{ij}. Therefore the following formulation can be obtained:

$$\frac{\partial \nabla \mathbf{w}}{\partial r_{ij}} = -8 \nabla R_r^T \nabla \mathbf{c}_{r_{ij}} \tag{5.100}$$

Therefore, an analytically expression of bias in sensor network can be obtained by relating all the necessary first and second derivatives of the cost function. In practical situations, we can obtain the inaccurate estimated position of the sensor by using existing localisation algorithms. Then the inaccurate sensor location can

be input into the obtained analytical expression of bias. Finally the accuracy of the localisation can be improved by subtracting the obtained bias, viz. $\hat{\mathbf{P}}_s - bias_{\hat{\mathbf{P}}_s}$.

5.4 Summary

Our contribution in this chapter is to identify the proper localisation estimation algorithms that fit the SDR-based localisation system. When existing localisation algorithms can meet our demand, we need to find the optimal one for the practical situation. Otherwise, the algorithms need to be adjusted to suit the localisation system.

In the practical source localisation, the noise in the measurements is actually inevitable. In the presence of noisy measurements, effective localisation estimation algorithms must be used to find the localisation solutions. For a practical localisation system, the localisation algorithms with a good trade-off between the localisation accuracy and the computational complexity are desired. In this Chapter, the computationally efficient closed-form localisation solutions are first discussed and they are adjusted to fit our localisation systems. For the TDOA-based localisation, the two-step weighted least-squares-based solution is presented, which can give accurate localisation results using only the coordinates of spatially distributed sensors and noisy TDOA measurements without requiring an initial guess of the source location. This algorithm is not new, but we found it is suitable for our system after an exclusive investigation of existing localisation algorithms.

In the joint TDOA and FDOA-based localisation, existing works typically consider using multiple sensors to take measurements and implement location estimation. In this thesis, we implement a passive source localisation system using only two sensors developed using SDRs, one stationary SDR and one mobile SDR, by taking joint TDOA and FDOA measurements. The two-step weighted least-squares-based solution is extended for joint TDOA and FDOA based localisation. The novelty of this adjustment is that the solution requires multiple sensors to obtain the results and we expand the application domain of the algorithm to fit two-sensor based localisation. By using mobile sensors, we can estimate the source location sequentially using the algorithm. Extended Kalman filter (EKF) is a widely used algorithm. In this thesis, we derive the EKF expression using both TDOA and FDOA measurement functions, which is different from the EKF using only one type of measurement function. This study successful solves the problem of how to use EKF to obtain the source location estimation using joint TDOA and FDOA measurements.

Apart from being influenced by the noise level of the measurements, the accuracy of the localisation algorithms is also influenced by other factors. Among them, the sensor-target geometry and the location estimation bias are two generic factors that influence the accuracy of almost all localisation systems. On the basis of the existing work on generic metrics for optimal sensor placement, we derive the rules for TDOA-based localisation and joint TDOA and FDOA based localisation. Since the generic metric only considers the equal noise level in the measurements, we obtained the

results on the optimal sensor-target placement for the measurements with a different level of noise, which is more useful in practice. In addition, the result is verified using real-world data.

Location estimation bias is another generic factor that influences the accuracy of most of localisation systems. In this thesis, we review the algorithm to calculate bias and reduce the bias in the localisation results. In addition, instead of solving bias reduction problem for a signal emitter, we utilize network information of multiple sensors and multiple emitters to obtain the bias reduction algorithm for the localisation problems in the sensor network. Furthermore, the result is verified using real-world data obtained by SDRs.

In the next Chapter, the localisation results of the localisation systems will be shown and systematically analyzed.

Experimental results

This Chapter gives the real-world localisation experiments using multiple SDRs and evaluates the performance of the localisation systems. Section 6.1 gives the improved results of the RSSI-based localisation system after the bias reduction algorithms are applied, including the results obtained in the indoor experiments and the outdoor experiments described in subsection 3.2.3. In Section 6.2 and Section 6.3, after the experimental setups are presented, the localisation results of two TDOA-based localisation implementations are analyzed. The localisation performance using a different number of SDRs and different types of source signals is also compared. Section 6.4 gives the results of the practical joint TDOA and FDOA-based localisation system developed using two SDRs.

6.1 RSSI-based localisation with location estimation bias reduction

According to the discussion in subsection 3.2.3, even though the methods to deal with RSSI measurement error caused by the hardware and the environment have been implemented, the RSSI-based localisation system still shows around 0.5m ∼ 2m localisation error in a range of several metres. This obtained accuracy cannot meet the requirement of accurate positioning. To improve the localisation accuracy, another strategy is to implement localisation optimization algorithms to reduce the influence of the noisy measurements. Figure 6.1 shows the distribution of the RSSI measurements at some training points in the indoor environment, from which one can see that the RSSI measurements obey Gaussian distribution approximately. Therefore, the location estimation bias reduction algorithm is implemented to enhance the localisation accuracy. According to the implementation of the RSSI-based localisation system in the subsection 3.2.3, where three indoor localisation scenarios and one outdoor localisation scenario are implemented, the bias reduction algorithms are used to correct the location estimation bias of the existing localisation results in order to enhance the localisation accuracy.

Firstly, the generic bias reduction algorithm introduced in subsection 5.3.2 is applied to the three indoor RSSI-based localisation implementations. After the generic
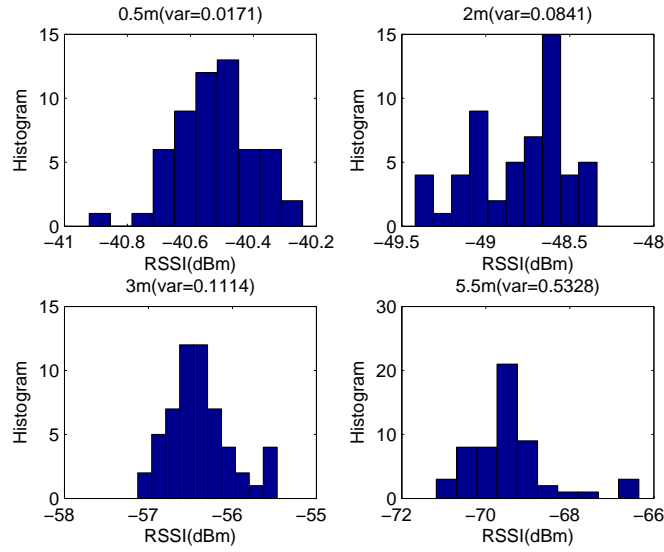
Figure 6.1: Distribution of RSSI measurements (indoor)

bias reduction algorithms are implemented, the RMSE of the location estimates of the first indoor localisation implementation is reduced by 77.3% from 0.3521m to 0.08m, as shown in Figure 6.2. For the second indoor localisation implementation, the RMSE of the location estimates is reduced by 79.7% from 0.4193m to 0.0853m for *Emitter*1 and by 67.2% from 0.2011m to 0.066m for *Emitter*2 after the generic bias reduction algorithm is implemented, as shown in Figure 6.3. For the third indoor localisation implementation, the RMSE of the location estimates of *Emitter*1, *Emitter*2, *Emitter*3 and *Emitter*4 is reduced by 55.4% from 1.35m to 0.602m, by 46.5% from 0.9434m to 0.5047m, by 77.8% from 2.2245m to 0.4929m and by 66.3% from 1.6055m to 0.5406m respectively after the bias reduction algorithm is used, as shown in Figure 6.4.

Secondly, for the outdoor RSSI-based localisation implementation in subsection 3.2.3, we view it as a sensor network localisation problem, so the bias reduction algorithm discussed in Subsection 5.3.3 is implemented. By combining the generic bias reduction algorithm with the underlying graph topological information of the sensor network, the localisation accuracy is enhanced, as shown in Figure 6.5. For *Emitter*1, the RMSE of the location estimates is enhanced by 64.24% from 1.65m to 0.59m. For *Emitter*2, the RMSE of the location estimates is enhanced by 72.14% from 1.40m to 0.39m.

Overall, the RMSE of the location estimates of the RSS-based localisation system is reduced to around 0.5m in both the indoor and the outdoor implementation, which has verified the effectiveness of the bias reduction algorithms in practice.
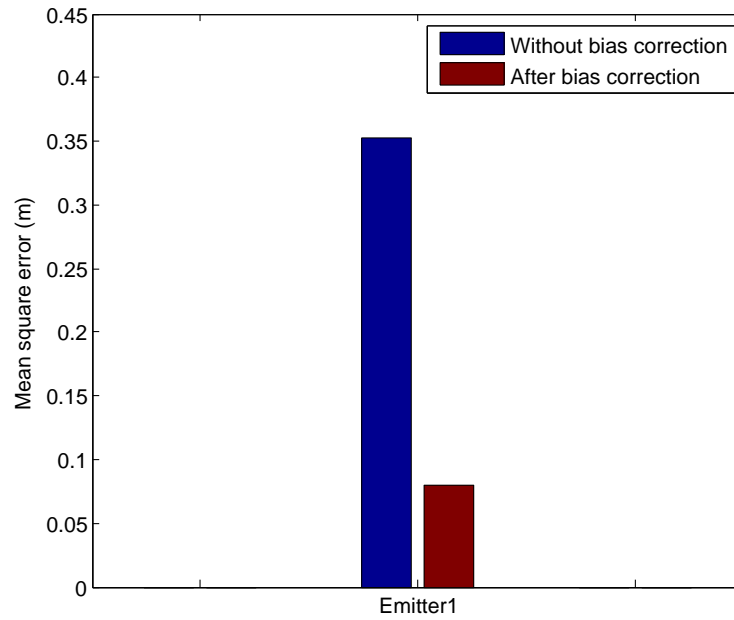
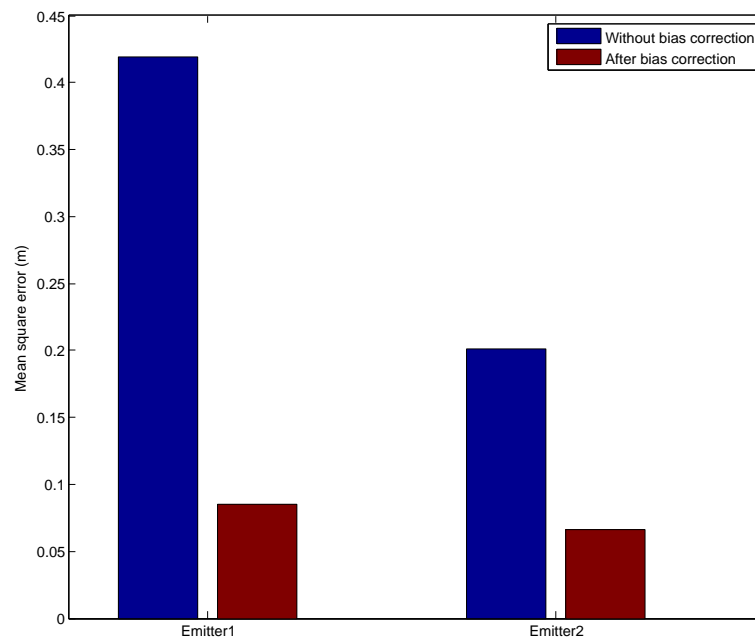Figure 6.2: Improved localisation accuracy (scenario 1)

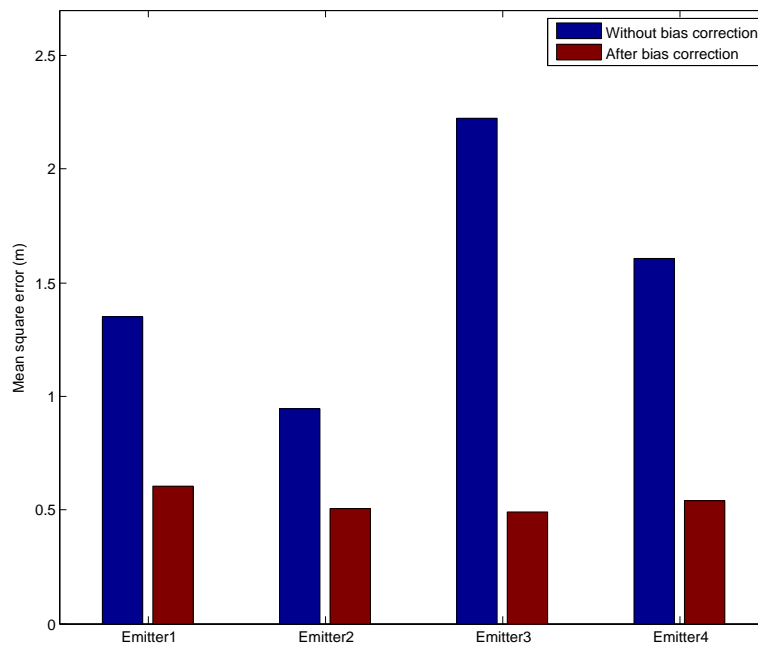Figure 6.3: Improved localisation accuracy (scenario 2)

Figure 6.4: Improved localisation accuracy (scenario 3)
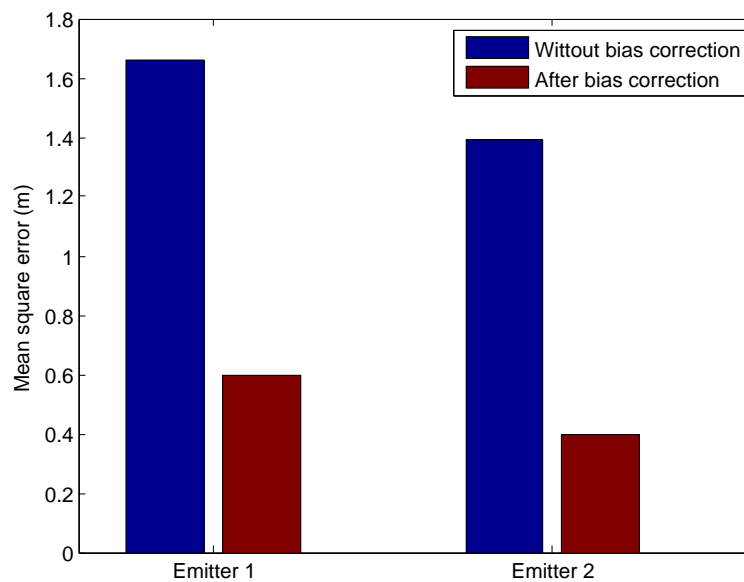

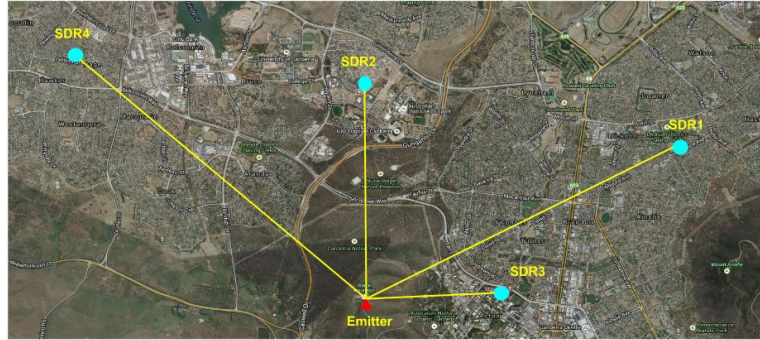Figure 6.5: RSSI-based localisation results in outdoor environment

Figure 6.6: Deployment of the emitter and 4 SDRs

6.2 TDOA-based localisation results (preliminary investigation experiments)

6.2.1 System setup

In the TDOA-based source localisation experiments, the public broadcast signal from a stationary signal transmitting tower is chosen as the signal source to demonstrate the TDOA-based localisation system using multiple spatially distributed SDRs. Firstly, the signal emitter has high transmission power (20kw) and it provides FM radio and TV service for the whole urban area, so the localisation can be implemented with a sensor-target range of several kilometres and with different types of signals. Secondly, the signal tower is an established infrastructure and the waveform of the signal transmitter is ever-changing and unknown to the localisation system, so it is a good candidate to demonstrate the passive source localisation systems. Two types of signals from the signal tower are used in different experiments. One is the narrow band FM signal at the nominal carrier frequency of 106.3 MHz. The other one is the TV signal at the nominal carrier frequency of 226.5 MHz, which has a higher bandwidth than the FM signal.

Multiple SDRs, equipped with omnidirectional antennas, are deployed spatially at different locations around the emitter to receive the target signal. The GPSDO module is installed on each SDR for time synchronisation. In the experiments of the preliminary investigation, four SDRs are used to receive the FM radio signal only to implement source localisation as shown in Figure 6.6. The four SDRs are located approximately at the same plane and the emitter is approximately 200m above the plane formed by the four SDRs. To give an idea of the coverage of the implementation, the distances between the emitter and SDRs are obtained, which are around 5.4km, 3.6km, 2.0km and 6.1km respectively. For simplicity, we consider the localisation as a 2-dimensional problem that omits the emitter's height. Take SDR1 as the reference, three TDOA measurements t_{21}, t_{31} and t_{41} can be obtained from three pairs of SDRs: SDR2 and SDR1, SDR3 and SDR1, SDR4 and SDR1, which are used to estimate the emitter location.

6.2.2   Localisation results

In this subsection, the results of the TDOA-based localisation using multiple station-ary SDRs under the setup shown in Figure 6.6 are presented. Different localisation algorithms are evaluated in the experiments, including the closed-form solution, the localisation optimization with the optimal sensor-target placement and the geometric constraints, and the localisation optimization with bias reduction.

6.2.2.1   Closed-form solution

In the practical passive source localisation, the initial location estimate of the source is unknown, so the closed-formed localisation algorithms are preferred. Closed-formed solutions do not involve iteration and they obtain the location estimates through sim-ple operations such as matrix inversion. To obtain the localisation results, the two-step weighted least-squares (2WLS) Chan and Ho [1994] algorithm is implemented. The first step of the 2WLS is to transform the nonlinear measurement equation to a pseudo-linear one by introducing nuisance parameters. After solving the pseudo-linear equations, the nuisance parameter estimates are utilised to refine the source location estimate in the second stage. The average localisation error by averaging the location estimates from multiple experimental trials, which contains the error intro-duced by omitting the emitter's height, shows 47.12m localisation error in Figure 6.7, where the blue circles are the four SDRs, the red point denotes the true emitter lo-cation, the green marks denote the location estimates at different trials, and the blue point is the average estimate of the emitter location.

6.2.2.2   Localisation optimization with optimal sensor-target geometry

The geometry of the sensor placement is important in the source localisation because bad localisation geometry is adversely suited to accurate localisation. For exam-ple, in far-field localisation, the target's range to the sensor's baseline ratios is very large, which means that the target is likely to appear (in a noisy environment) al-most collinear with the sensors. The optimal target-sensor localisation geometries are studies in Bishop et al. [2008]; Dogancay and Hmam [2009]; Meng et al. [2012]. According to the lower bound of error variance of an unbiased and efficient estimate of target location, one particular optimal sensor-position configuration under equal TDOA noise variances occurs when

$$\alpha_i = \frac{2\pi}{N}(i-1) + \phi, i = 1, 2, ..., N, \tag{6.1}$$

where α_i denotes the angle between the target-sensor line of ith sensor and the pos-itive direction of x-axis and $\phi \in (0 \ 2\pi]$ is any constant. Moreover, the optimal lo-calisation geometry is independent of the individual sensor-target range. For $N = 4$ sensors, an optimal geometry is achieved when the target is located at the centre of the unit square in 2-dimensional space. The bad geometry and the optimal geometry of sensor placement can be seen in Figure 6.8.
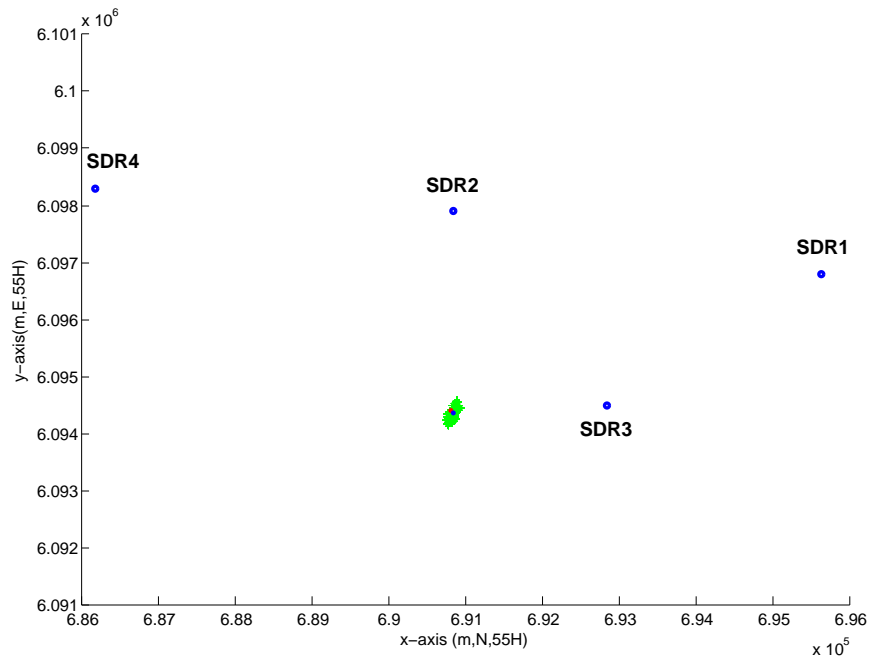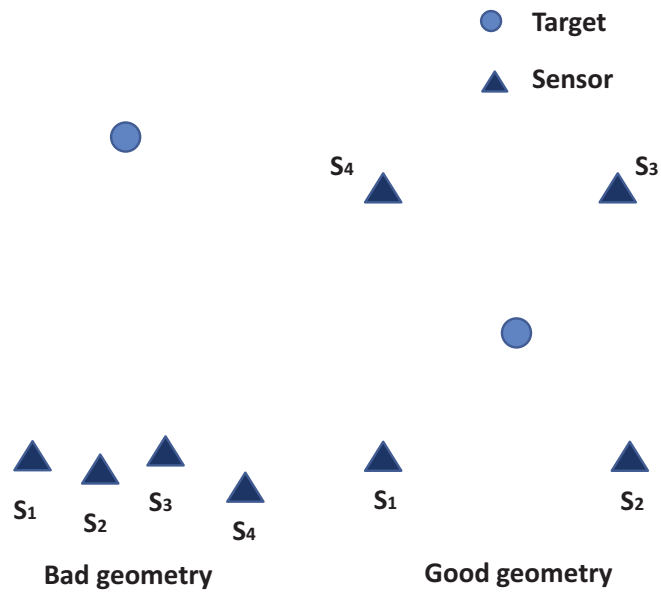
Figure 6.7: Localisation results of the 2WLS

Figure 6.8: Localisation geometry (N=4 sensors)
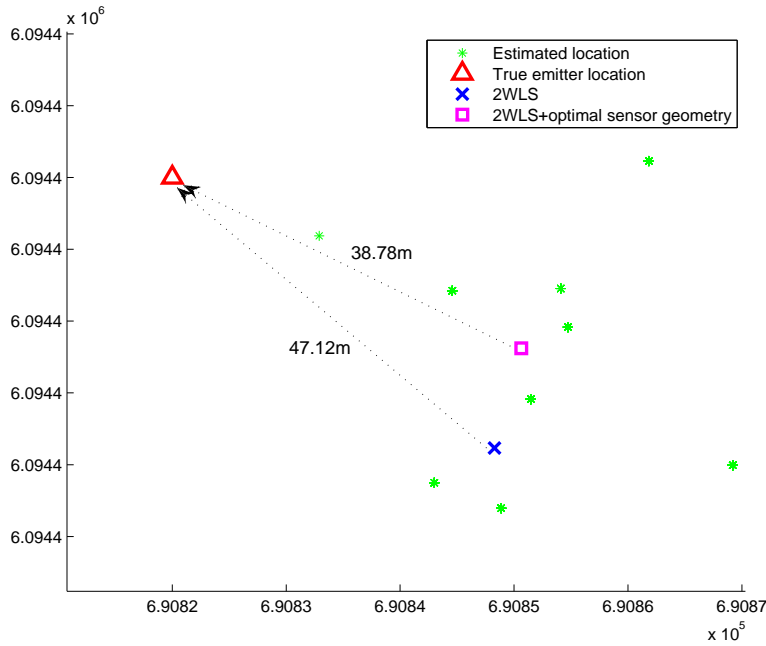
Figure 6.9: Localisation result with optimal sensor-target geometry

Accordingly, since the optimal localisation geometry is independent from the sensor-target range, we keep the range from each sensor to the emitter unchanged and rearrange the placement of the four SDRs to make the differences of angles of arrival between adjacent SDRs α_i equal to 90 $^\circ$. After the sensor-target geometry is re-arranged, the average location estimation error using the 2WLS algorithm, is reduced to 38.78m (see Figure 6.9). Therefore, the principle of the optimal sensor placement is verified to be able to enhance the accuracy of this source localisation system in practice.

6.2.2.3 Localisation optimization with bias reduction

The localisation algorithm normally includes a nonlinear transformation of the measurements. Once the errors are present in the measurements, it is then virtually guaranteed that, from the nonlinear processing of measurements to achieve localisation, the biased estimates of the source location will be obtained. Therefore, to improve the localisation accuracy, the influence of the bias in the location estimates is considered and a systematic bias correction algorithm Ji et al. [2015] based on computing an approximation of the bias is applied. After the bias in the location estimates is approximately removed, close to unbiased estimates of the target location can be obtained.

The algorithm first expands the localisation mapping **g** (which maps from the measurements to produce target location estimates) by a Taylor series and truncates to the second order in the measurement noise. It then considers the expected values
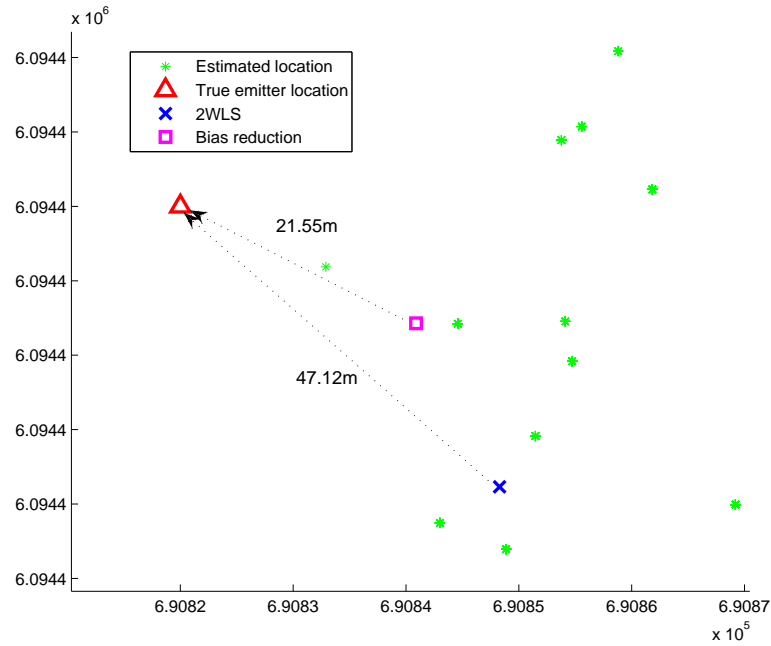
Figure 6.10: Localisation optimisation with bias reduction

of the second-order term, expressible using the derivatives of **g**, as bias. While it is very hard to calculate the derivatives of **g** analytically, it is much easier to obtain the inverse mapping of **g** (denoted by **f**) that maps the source location to a set of measurements and its derivatives. Therefore, the Jacobian matrix of **f** can be used to compute the derivatives of the localisation map **g** in terms of **f**, which results in a simple expression of bias Ji et al. [2013]. In the implementation of bias reduction, the computable bias can be used to systematically correct any single location estimate from a set of TDOA measurements and, thus, enhancing the localisation accuracy in a statistical sense. After the bias reduction algorithm is applied, the localisation result shows that the average localisation error is reduced by 54.3% to 21.55m, as compared to the localisation results obtained from the 2WLS algorithm, as shown in Figure 6.10, where the red triangle is the true emitter location, the blue cross is the average estimate of the emitter location before the bias reduction algorithm is used and the pink square denotes the localisation result improved by the bias reduction algorithm.

6.2.2.4   Localisation results analysis

To further evaluate the three localisation algorithms, the mean square error of the location estimates are comparing with the CRLB. In Figure 6.11, one can see that the RMSE of the localisation algorithms are close to the square root of the trace of the CRLB matrix which is 102.973 m. The RMSE of location estimates using the 2WLS algorithm is 116.687m. By using the optimal sensor placement, the RMSE is
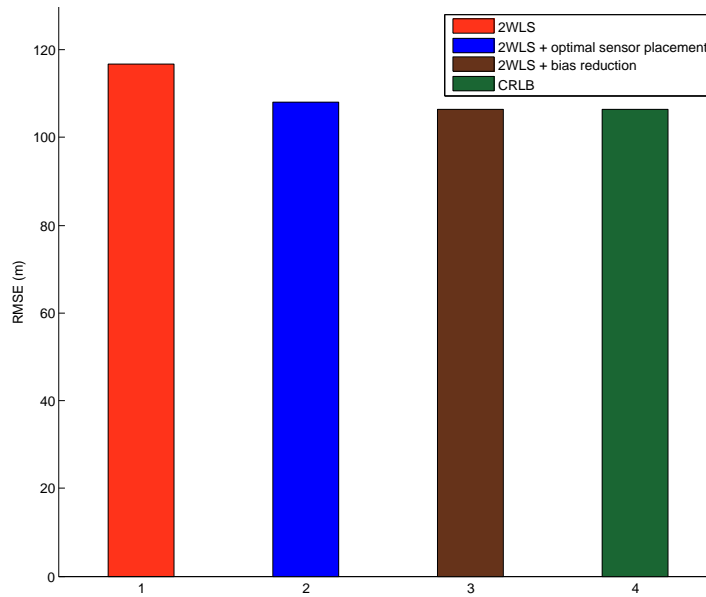
Figure 6.11: Localisation RMSE of different algorithms (preliminary experiments)

reduced to 107.975m, and then further reduced to 105.362m by effectively correcting the location estimation bias.

6.3 TDOA-based localisation results (further verification experiments)

6.3.1 System setup

The experiments for further verification are implemented with the same stationary signal tower as the signal source, in which we consider the influence of the number of SDRs on the localisation accuracy by gradually increasing the number of SDRs from four to eight. Moreover, the influence of the signal bandwidth is also considered. Apart from the FM signal, the TV signal with higher bandwidth is also used to demonstrate the source localisation using SDRs. Figure 6.12 shows the deployment of the emitter and the eight SDRs, where "E" in red denotes the target emitter. "1" in blue is the reference SDR which is 9.1 kilometres from the emitter. The other SDRs marked by "2" to "8" in blue are around 4.0km, 2.0km, 4.3km, 3.6km, 8.2km, 8.5km and 2.3km far from the emitter, respectively. We start by using the SDR1 $\sim$ SDR4 to receive the FM signal and the TV signal, respectively, to localise the emitter. Then, we increase the number of the SDRs up to eight to localise the signal emitter. The eight deployment locations of the stationary SDRs are all different from those in Figure 6.6.
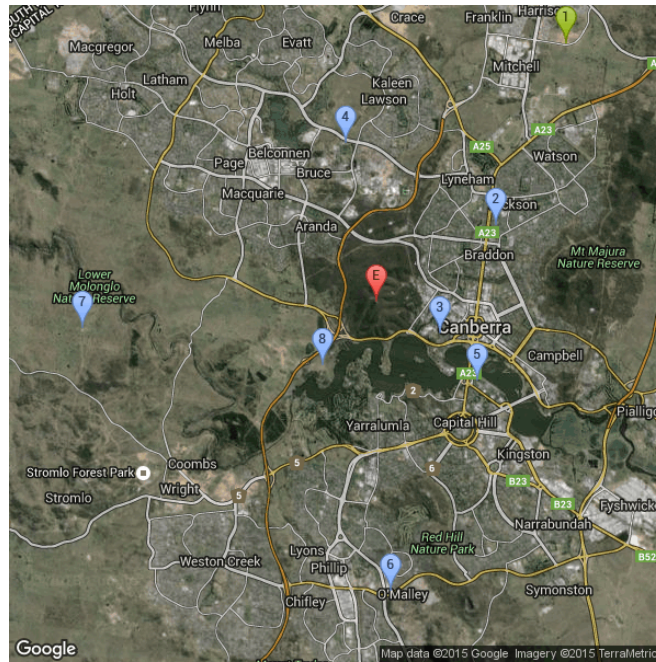
Figure 6.12: Deployment of the emitter and 8 SDRs

6.3.2   Results of TDOA-based localisation with four sensors

In this subsection, the localisation results using four spatially distributed SDRs are shown to compare with the localisation results in the preliminary investigation experiments. Here, only the FM signal is acquired to implement source localisation. Similar to what we did in the preliminary investigation experiments, the measurement error reduction approaches are implemented to enhance the measurement accuracy in these further verification experiments of the TDOA-based localisation, and then different localisation algorithms are implemented respectively and their performances are evaluated.

The localisation results obtained using the 2WLS algorithm is shown in Figure 6.13, where the size of the area that contains all location estimates is 500m by 500m; the green dots denote the location estimates in different time slots using the TDOA measurements; the blue ellipse denotes the 95% confidence region of the estimates; the red triangle denotes the true emitter location; and the blue cross denotes the average location estimate of multiple estimates. The root mean square error (RMSE) of the location estimates is 83m.

To investigate the influence of the sensor-target geometry, different from theoretical studies in which equal measurement noise is usually used in the simulation, here an optimal sensor-target placement for four sensors under the experimental (unequal) TDOA measurement noise variance is found by maximising the determinant of the Fisher Information Matrix (FIM). Figure 6.14 shows an example of the optimal sensor-target placements for four sensors under the equal and the experimental TDOA measurement noise. To implement the optimal sensor-target placement, since
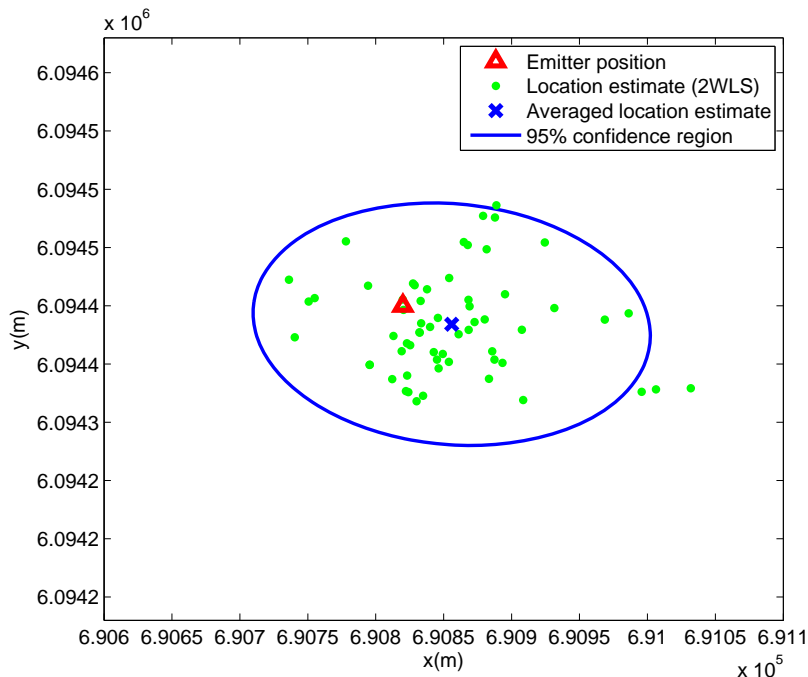
Figure 6.13: Localisation results of 2WLS with 4 SDRs

the optimal localisation geometry is independent from the sensor-target range, the range from each SDR sensor to the emitter is kept unchanged and the placement of the four SDR receivers is rearranged to meet the optimal sensor-target placement under experimental measurement noise. After the sensor-target geometry is re-arranged, the RMSE of the location estimates obtained using the 2WLS is reduced to 59.8m. While the good sensor-target geometry cannot be guaranteed in practice, the result has verified the effectiveness of the optimal sensor-target placement in the real-world source localisation experiments.

In the practical passive source localisation, the information on the source location is not available. In order to use the underlying geometry to enhance the accuracy of the location estimates, the geometrical constraints on the measurement errors can be formulated in terms of the known sensor coordinates and the noisy measurements Bishop et al. [2008], then an optimal solution to the localisation problem can be obtained by formulating the localisation problem as a constrained optimization problem. After the optimization problem is solved, the estimates of the measurement error are obtained. By subtracting these errors from the actual noisy TDOA measurements, the adjusted TDOA values are obtained. The adjusted values have the property that the over-determined system of equations linking the source location and measurements has a solution. Once the measurement errors are corrected, the 2WLS algorithm gives more accurate location estimates. Under the particular sensor-target geometry in our implementation as shown in Figure 6.12, the localisation optimization algorithm with geometrical constrains, the GWLS Bishop et al.
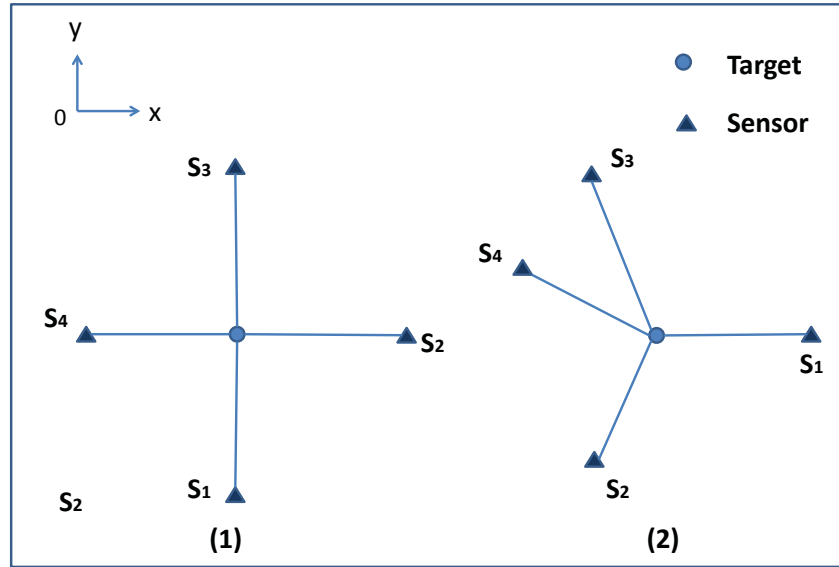
Figure 6.14: Optimal sensor placement: (1) Equal measurement noise ($\alpha_1 = \alpha_2 = \alpha_3 = \alpha_4 = 90°$), (2) Experimental measurement noise ($\alpha_1 = 0°, \alpha_2 = 248°, \alpha_3 = 99°, \alpha_4 = 152°$)

[2008], is implemented. The algorithm is initialized with measurement error $\mathbf{e} = \mathbf{0}$. After the estimates of measurement error are subtracted from the noisy measurements, the localisation results using the 2WLS are obtained and the RMSE of the location estimates is 82m.

The influence of the location estimation bias is also investigated. According to Ji et al. [2015], when there are more measurements than unknowns (we have three TDOA measurements but two unknowns), the bias cannot be straightforwardly expressed by using the derivatives of the mapping **f**. To express the bias, an extra variable needs to be introduced to form a new mapping with equal number of measurements and unknowns. The estimates of the emitter location and the extra variable are first obtained by solving non-linear equations iteratively. The location estimates are initialised with the estimates obtained using the 2WLS and the variable is initialized with zero. Then the approximate bias in the localisation estimates is calculated and subtracted from the original location estimates. The localisation results after the bias reduction algorithm is implemented shows that the RMSE of the location estimates is further reduced to 80m.

In the practical source localisation, the final localisation result is usually obtained recursively as each location estimate using a localisation algorithm comes in. To take advantage of multiple sequential location estimates obtained in each experimental run, a Kalman Filter (KF) is used Faragher et al. [2012] to obtain the final localisation estimate because it is well known to have good noise control capability and small

computational requirement. A general system model can be expressed as

$$\mathbf{x}_t = \mathbf{F}_t \mathbf{x}_{t-1} + \mathbf{B}_t \mathbf{u}_t + \mathbf{w}_t \qquad (6.2)$$

$$\mathbf{z}_t = \mathbf{H}\mathbf{x}_t + \mathbf{v}_t \qquad (6.3)$$

where $\mathbf{x}_t$ is the state vector at time t and it denotes the location of the emitter. $\mathbf{u}_t$ is the control inputs, $\mathbf{B}$ is the control input matrix, $\mathbf{w}_t$ is the process noise term, $\mathbf{z}_t$ is the vector of measurements, $\mathbf{H}$ is the transformation matrix and $\mathbf{v}_t$ is the measurement noise term.

Because the signal emitter to be localised is stationary, $\mathbf{F}_t = \mathbf{I}$, $\mathbf{u}_t = \mathbf{0}$ and there is no processing noise. The measurements are the location estimates, which are the same scale as the state estimates, so $\mathbf{H} = \mathbf{I}$. According to the standard deviations of the location estimates in the x and y direction, which range from 40m to 70m for all the three localisation algorithms, the standard deviation of the measurement noise is set to 100m in the x and y direction. The initial location estimate of the Kalman filter is randomly generated from a Gaussian distribution centred at the first location estimate for all the three localisation algorithms with the standard deviation 1000m in the x and y direction. By using multiple location estimates recursively through the Kalman Filter, the filtering process of the location estimates obtained using the 2WLS algorithm is shown in Figure 6.15 and the final localisation error is 39m. Similarly, the Kalman filter output of the location estimates obtained using the GCLS algorithm gives 38m localisation error. Among the three localisation algorithms, the bias reduction algorithm gives the best localisation accuracy with 34m error. In addition, the average location error of the algorithms obtained by calculating the mean of the localisation error in both x-axis and y-axis shows similar localisation accuracy to that using the EKF.

To evaluate the performance of the three localisation algorithms, the 2WLS, the GCLS and the localisation bias reduction, the RMSE of location estimates obtained from the three algorithms are compared with the square root of the trace of the CRLB matrix. As shown in Figure 6.16, the value of the square root of the trace of the CRLB matrix evaluated at the true emitter location is 74m. One can see that the accuracy of the three localisation algorithms is close to the CRLB. Moreover, the localisation results also show that the localisation optimization using the optimal sensor-target placement and the location estimation bias reduction can effectively enhance the localisation accuracy. By taking advantage of multiple location estimates from multiple experiments, the average localisation error and the localisation error obtained from the KF are reduced largely.

Overall, the feasibility and localisation accuracy of the practical TDOA-based passive source localisation are verified in experiments by using multiple spatially distributed SDRs. With the experience of the preliminary investigation experiments, the RMSE of the location estimates is reduced in the further verification experiments by approximately 25% from more than 100m error to less than 100m error. The final localisation accuracy can be enhanced by averaging multiple location estimates or
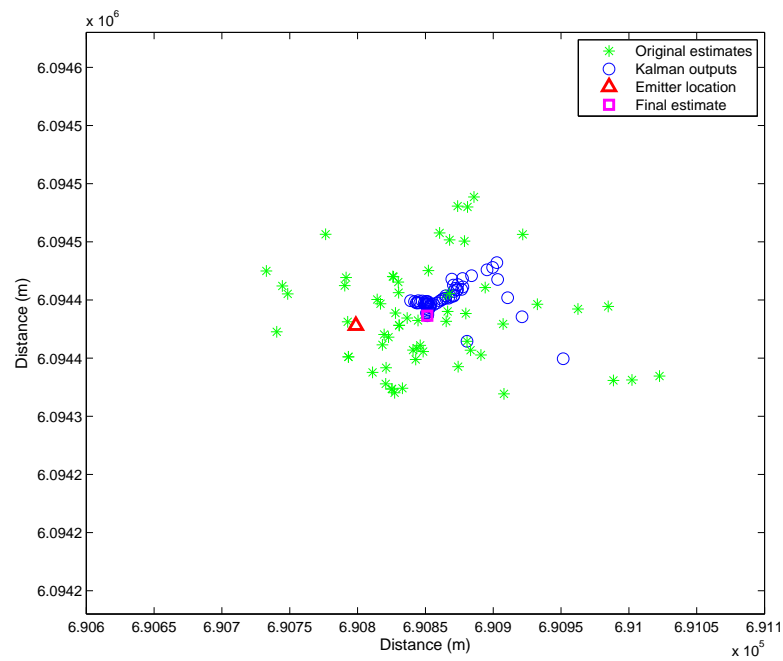
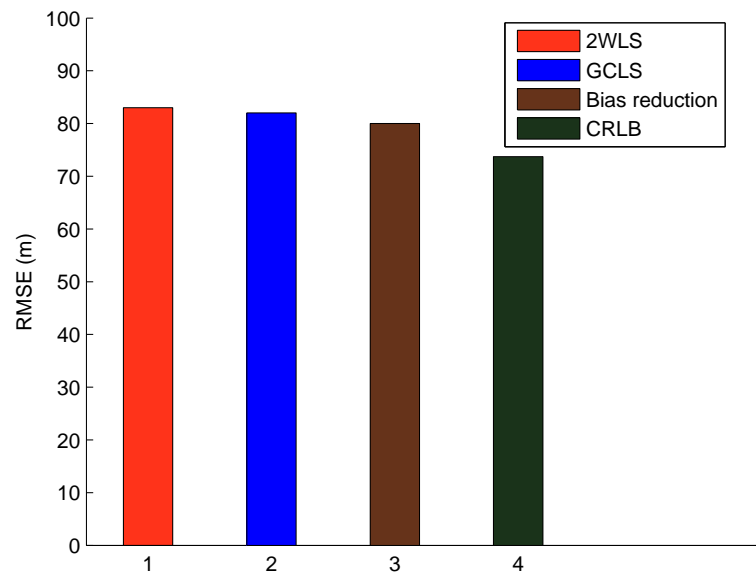Figure 6.15: Iteration results with Kalman Filter

Figure 6.16: Localisation RMSE of different algorithms

using the KF to update the location estimates when new measurements are available.

6.3.3   Results of TDOA-based localisation with more than four sensors using different signal sources

To further evaluate the performance of the TDOA-based localisation system, the increasing number of SDR-based receivers is used to receive the target signal and implement source localisation. Moreover, the localisation results using the FM signal and the TV signal are compared to investigate whether the use of the signal with wider bandwidth can enhance the localisation accuracy in practice. To obtain the localisation results, the 2WLS algorithm is implemented. In addition, the optimal sensor target placement with true measurement error is obtained for all the localisation scenarios. Both the RMSE and the error ellipse are obtained to evaluate the localisation accuracy.

6.3.3.1   Localisation results using the FM signal and TV signal (4 $\sim$ 7 sensors)

Firstly, the increasing number of SDRs is used to receive the target signal and implement passive source localisation. The localisation results with different numbers of SDRs using the FM signal and the TV signal are obtained, respectively, to verify the influence of both the number of sensors and the signal bandwidth on the localisation accuracy.

Firstly, the localisation results using the FM signal are illustrated. As shown in Figure 6.12, an additional SDR, the SDR5, is used together with SDR1 $\sim$ SDR4 to implement the passive source localisation. Take the SDR1 as the reference SDR, TDOA measurements from the SDR5 and the SDR1 can be obtained. The distance from the SDR5 to the emitter is similar to the distance from the SDR2 to the emitter, and the SDR5 has a clear LOS condition to the emitter. The RMSE of location estimates using SDR1 $\sim$ SDR5 is 75m, which is smaller than the localisation error using the SDR1 $\sim$ SDR4. Furthermore, the TDOA measurements obtained from the SDR6 and the SDR1 are obtained to implement the passive source location using SDR1 $\sim$ SDR6. The distance from the location of the SDR6 to the emitter is 3.6 km which is similar to the distance between the location of the SDR2 and the location of the emitter, but the SDR6 is under a NLOS condition to the emitter. The RMSE of the location estimates using SDR1 $\sim$ SDR6 is further reduced to 74m. Comparing to the localisation error obtained by SDR1 $\sim$ SDR6, the quantity of the localisation error reduction is only 1 m. The reason why the localisation accuracy is not improved a lot is because the TDOA measurements obtained from the SDR1 and the SDR6 suffer from NLOS error. By adding the SDR7 into the system, a new pair of TDOA measurements can be obtained from the SDR7 and the SDR1. The distance between the SDR7 and the emitter is more than twice the distance between the SDR2 and the emitter. The SDR7 has the LOS condition to the emitter. The RMSE of the location estimates is further reduced to 69 m.

In Figure 6.17, the value denoted by the square symbol on the solid blue line is
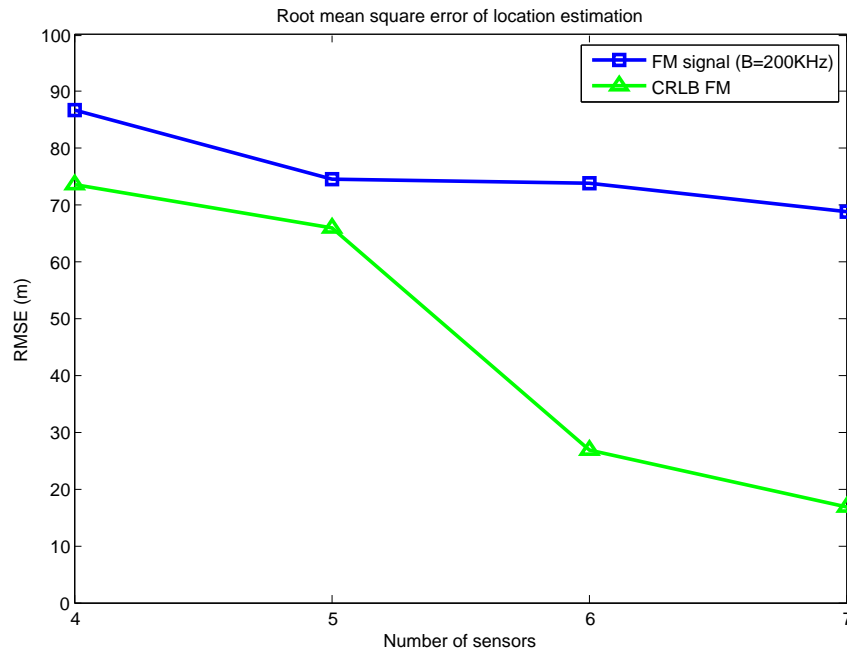
Figure 6.17: Localisation error of different number of SDRs using FM signal

the localisation RMSE using different number of SDRs by receiving the FM signal. One can see that the RMSE is reduced gradually when the number of the SDRs is increased. The value denoted by the triangle symbol on the solid green line denotes the value of the square root of the trace of the CRLB, which also shows an obvious downward trend when the number of the SDRs is increased. The CRLB matrix also defines a so-called uncertainty ellipsoid. A scalar functional measure of the "size" of the uncertainty ellipse provides a useful characterization of the potential performance of an unbiased estimator. Figure 6.18 shows the uncertainty ellipse of the FM signal localisation results using multiple SDRs spatially distributed at the seven locations, where the green dots denote the location estimates in different time slots using the TDOA measurements, the blue ellipse denotes the 95% confidence region of the estimates, the red triangle denotes the true emitter location, and the blue cross denotes the average result of multiple location estimates. The size of the window is 500m by 500m, which is the same as the size of the window with four SDRs in Figure 6.13. One can see that the size of the uncertainty ellipse obtained from SDR1 $\sim$ SDR7 is apparently smaller than that obtained from SDR1 $\sim$ SDR4.

Apart from the FM signal, the performance of source localisation of the TV signal with the increasing number of SDRs is also evaluated. The locations of multiple spatially distributed SDRs do not change (see Figure 6.12). The RMSE of the source location estimates using SDR1 $\sim$ SDR4 is 56.8m which is smaller than the RMSE of the location estimates using the FM signal. By adding the SDR5 into the system, the RMSE of the source location estimates obtained from SDR1 $\sim$ SDR5 is jumped to 73m. Remember that the TDOA measurements calculated from the SDR5 and the
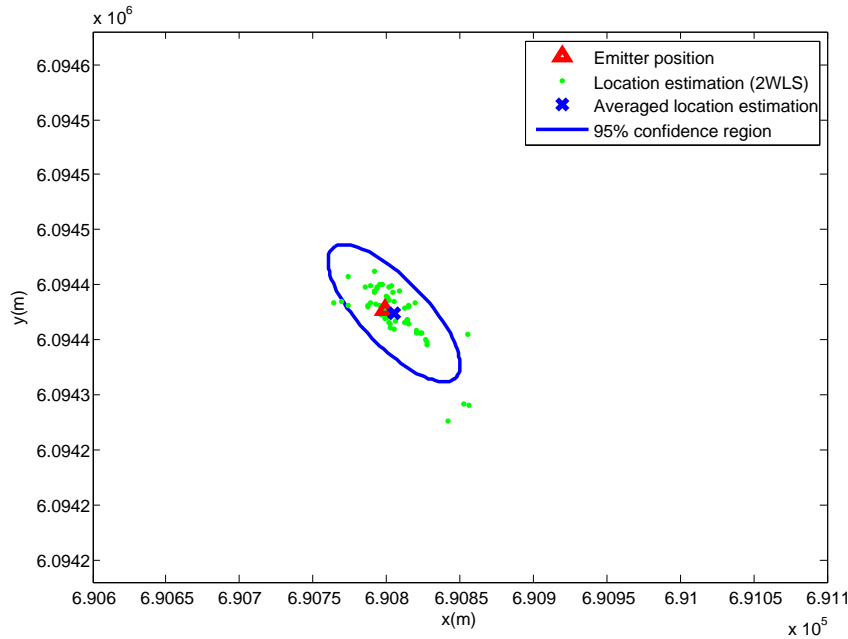
Figure 6.18: Localisation uncertainty ellipse of the FM signal with 7 SDRs

SDR1 suffer from the NLOS error; that is why the RMSE is increased. Since the additional SDR, the SDR6, has the LOS condition to the emitter, the RMSE of the source location estimates using SDR1 $\sim$ SDR6 is reduced to 60.5 m, which reduces the influence of the NLOS error of the SDR5 to some extent. By using the SDR7 which is under a LOS condition to the emitter, the localisation RMSE using SDR1 $\sim$ SDR7 is further reduced to 32m.

The localisation results are also shown in Figure 6.19, where the blue solid line is the RMSE of the source location estimates using the TV signal, the blue dash line is the localisation RMSE using the FM signal for the purpose of accuracy comparison, the green solid line denotes the value of the square root of the trace of the CRLB of the localisation using the TV signal, and the green dash line is the value of the square root of the trace of the CRLB of the localisation using the FM signal for comparison. One can see that, while the RMSE obtained using the increasing number of SDRs does not show an obvious downtrend, the CRLB of the location estimates shows obvious reduction of the localisation error by increasing the number of the SDRs in the localisation of the TV signal. Comparing the localisation results using the FM signal with those obtained using the TV signal, the use of the TV signal that has higher bandwidth can always obtain smaller localisation error than the use of the FM signal. This is reflected from both the RMSE of the location estimates and the value of the square root of the trace of the CRLB.

In addition, the uncertainty ellipse for the TV signal localisation using the four SDRs and the sevev SDRs are shown in Figure 6.20, where one can see that the size of uncertainty ellipse is apparently reduced after the number of SDRs that is used in
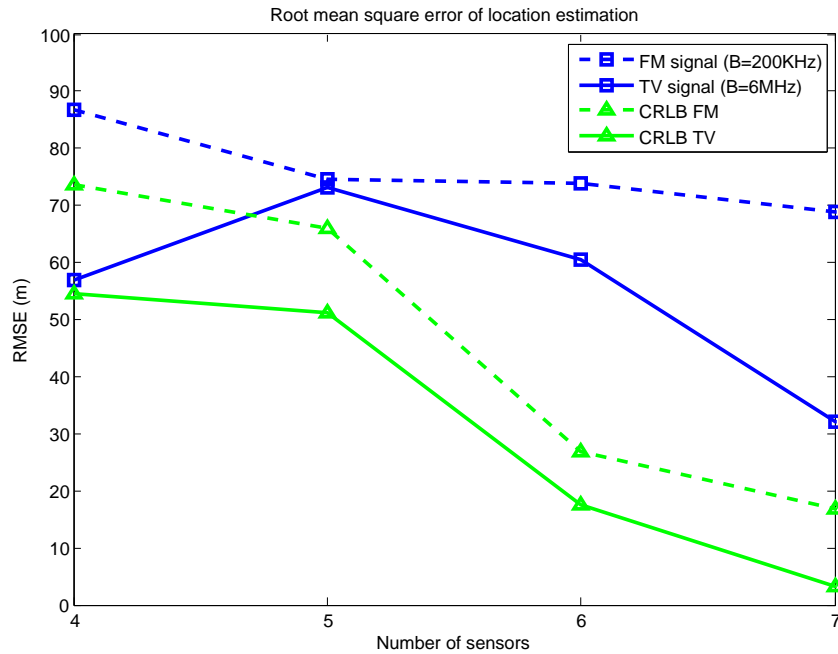
Figure 6.19: Localisation error of different number of SDRs using FM signal
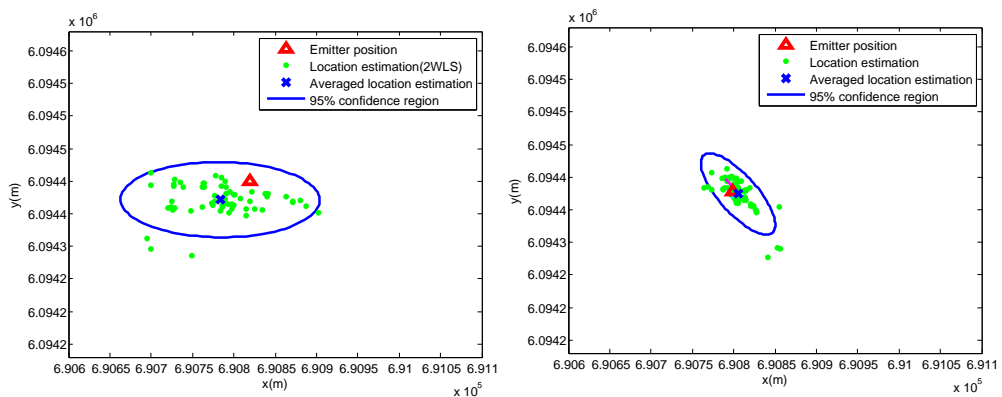
Figure 6.20: Localisation uncertainty ellipse of TV signal with 4 SDRs and 7 SDRs

the source localisation is increased.

6.3.3.2 Optimal sensor-target placement with real measurement error ($4 \sim 7$ sensors)

The geometry of the sensor-target placement can influence the localisation accuracy significantly. Here, the performance of the localisation system under the optimal sensor-target placement is evaluated. During the evaluation, the number of the SDRs used in the localisation is increased, and the FM signal and the TV signal are used respectively. When the noise in the TDOA measurements is equal, (6.1) can be used
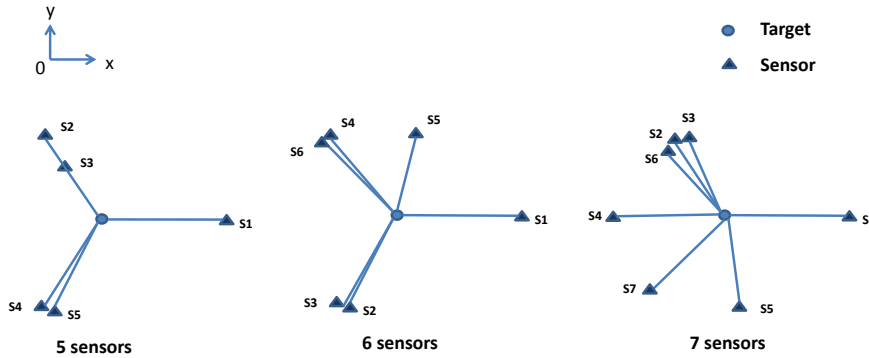
Figure 6.21: Optimal sensor-target placement for the FM signal source localisation using 5, 6 and 7 sensors under unequal measurement error

to obtain the optimal sensor-target placement by just knowing the number of the SDRs without requiring further computation. However, in the practical source localisation, the noise of the TDOA measurements from different pairs of SDRs is almost impossible to be equal. The simple use of (6.1) does not give an optimal sensor-target placement for the TDOA-based localisation.

To obtain optimal sensor target placement for the source localisation under real TDOA measurement noise, instead of assuming $\sigma_1^2 = \sigma_2^2 = ... = \sigma_N^2 = \sigma^2$, the real variance of the measurement error needs to be used when one tries to maximize the determinant of the Fisher Information Matrix (5.47). By employing a grid search-based algorithm, the optimal sensor placement can be obtained. Note that the optimal placement is not unique. When the number of SDRs is increased, the dimension for the grid search is increased, which increases the computational cost. In this case, a coarse resolution of the angle for the grid search can be implemented as the first step, then, the refinement can be implemented.

Denote $\alpha_i, i = 1, 2, 3, 4, 5, 6$ ($\alpha_i \in 360°$) as the angles between the sensor-target lines and the positive direction of x axis. The optimal sensor-target placements of the practical TDOA-based localisation of the FM signal using SDR1 $\sim$ SDR5, SDR1 $\sim$ SDR6 and SDR1 $\sim$ SDR7 the under experimental noise are given in Figure 6.21. For the source localisation using SDR1 $\sim$ SDR5, the optimal sensor-target placement can be achieved when $\alpha_1 = 120°$, $\alpha_2 = 120°$, $\alpha_3 = 241°$ and $\alpha_4 = 239.5°$. After the positions of the SDRs are re-arranged accordingly, the RMSE of the location estimates is reduced from 75m to 66m. For the localisation using SDR1 $\sim$ SDR6, the optimal sensor placement can be achieved when $\alpha_1 = 120°$, $\alpha_2 = 120°$, $\alpha_3 = 241°$, $\alpha_4 = 239.5°$ and $\alpha_5 = 239.5°$. After the SDRs' position is re-arranged accordingly, the RMSE of the location estimates is reduced from 74m to 70m. For the localisation using SDR1 $\sim$ SDR7, the optimal sensor placement can be achieved when $\alpha_1 = 120°$, $\alpha_2 = 120°$, $\alpha_3 = 241°$, $\alpha_4 = 239.5°$, $\alpha_5 = 239.5°$ and $\alpha_6 = 239.5°$. After the sensor position is rearranged accordingly, the RMSE of the location estimates is reduced from 69m to 51m.

Figure 6.22: The RMSE of the FM signal source localisation using different number of SDRs

Figure 6.22 shows the comparison of the localisation RMSE using the FM signal without the sensor-target geometry optimization, with the sensor-target geometry optimization under equal measurement noise, and with the sensor-target geometry optimization under unequal measurement noise. One can see that the localisation error by assuming the equal measurement noise in the sensor-target geometry optimization is sometimes even larger than the original sensor-target placement, such as in the localisation using five SDRs, six SDRs and seven SDRs. By contrast, deploying the SDRs according to the angles calculated from the principle of optimal sensor-target placement under the unequal measurement noise always provides improved localisation accuracy.

The optimal sensor-target placement for the localisation of the TV signal can be obtained in the same way from (5.47). Figure 6.23 shows the optimal placement of the source localisation using SDR1 ∼ SDR4, SDR1 ∼ SDR5, SDR1 ∼ SDR6 and SDR1 ∼ SDR7 in practice with the optimal sensor-target placement under the experimental noise. For the localisation of the TV signal using SDR1 ∼ SDR4, the optimal sensor placement can be achieved when $\alpha_1 = 254°$, $\alpha_2 = 237°$ and $\alpha_3 = 109°$. After the sensor position is rearranged accordingly, the RMSE of the location estimates is increased from 59m to 202m. For the localisation using SDR1 ∼ SDR5, the optimal sensor placement can be achieved when $\alpha_1 = 254°$, $\alpha_2 = 237°$, $\alpha_3 = 138.5°$ and $\alpha_4 = 109°$. After the sensor position is rearranged accordingly, the RMSE of the location estimates is reduced from 73m to 54m. For the localisation using SDR1 ∼ SDR6,
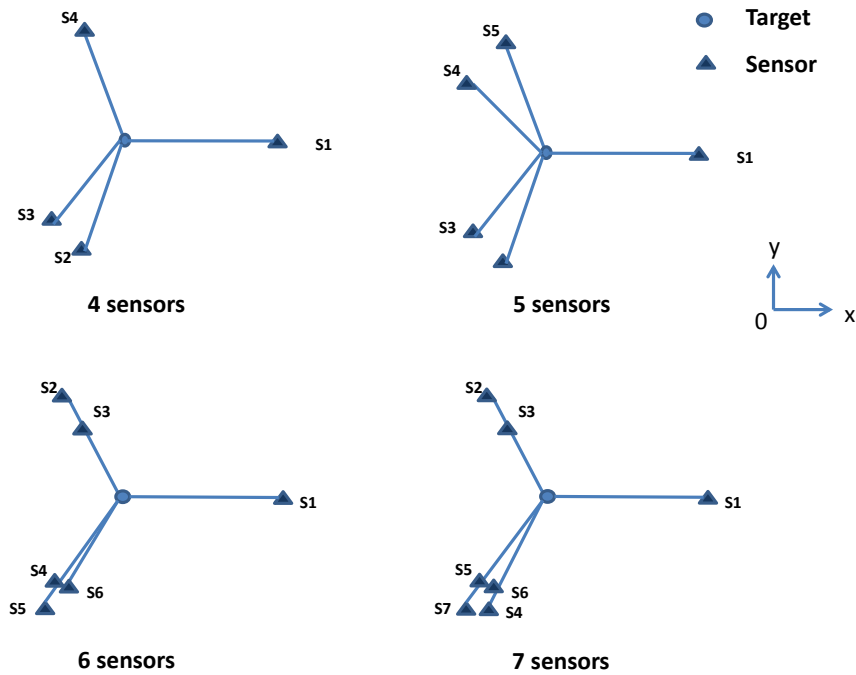
Figure 6.23: Optimal sensor-target placement for the TV signal source localisation using 4, 5, 6 and 7 sensors under unequal measurement error

the optimal sensor placement can be achieved when $\alpha_1 = 120°$, $\alpha_2 = 120°$, $\alpha_3 = 241°$, $\alpha_4 = 239.5°$ and $\alpha_5 = 239.5°$. After the sensor position is rearranged accordingly, the RMSE of the location estimates is reduced from 60m to 49m. For the localisation using SDR1 $\sim$ SDR7, the optimal sensor placement can be achieved when $\alpha_1 = 120°$, $\alpha_2 = 120°$, $\alpha_3 = 241°$, $\alpha_4 = 239.5°$, $\alpha_5 = 241°$ and $\alpha_6 = 239.5°$. After the sensor position is rearranged accordingly, the RMSE of the location estimates is increased from 32m to 38m.
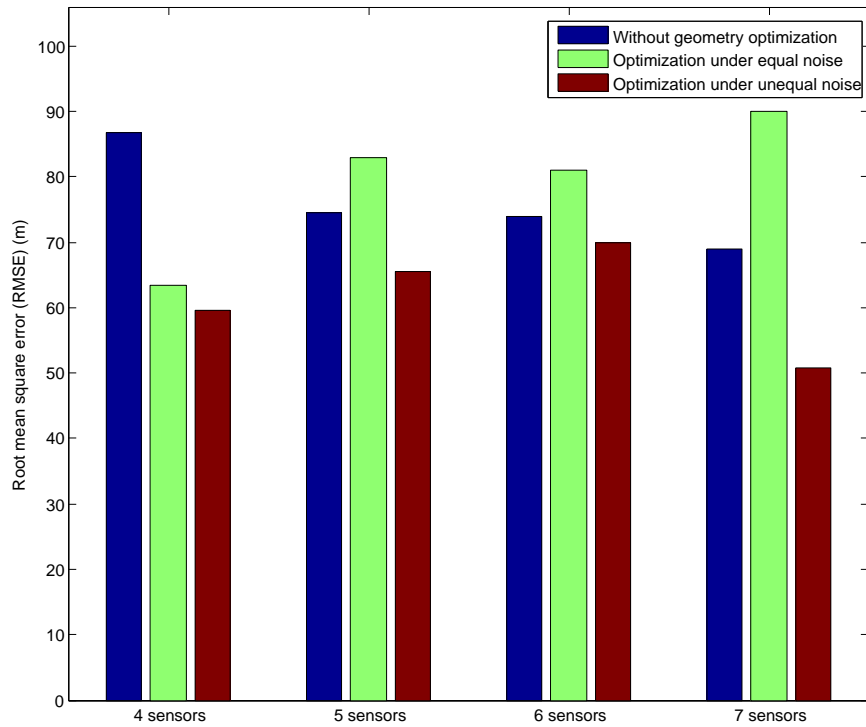
Figure 6.24 shows the comparison of the localisation RMSE without the geometry optimization, with the geometry optimization under equal measurement noise and with the geometry optimization under the unequal measurement noise. One can see that the deployment of SDRs according to the angles calculated from the optimal sensor-target placement under the real measurement noise provides better localisation accuracy in five-SDR and six-SDR cases. However, it is also shown that in the results four-SDR and seven-SDR cases, higher localisation error than the original sensor-target placement is observed. For the four-SDR case, the development of SDRs according to the angles calculated from equal measurement noise gives the best accuracy; while for the seven-SDR case, the original development of the SDRs gives the best localisation accuracy. This can be explained by the fact that the localisation accuracy is actually influenced by a combination of many factors. Only correcting the influence of one factor, such as the sensor-target placement, will not always guarantee the enhancement of the localisation accuracy.
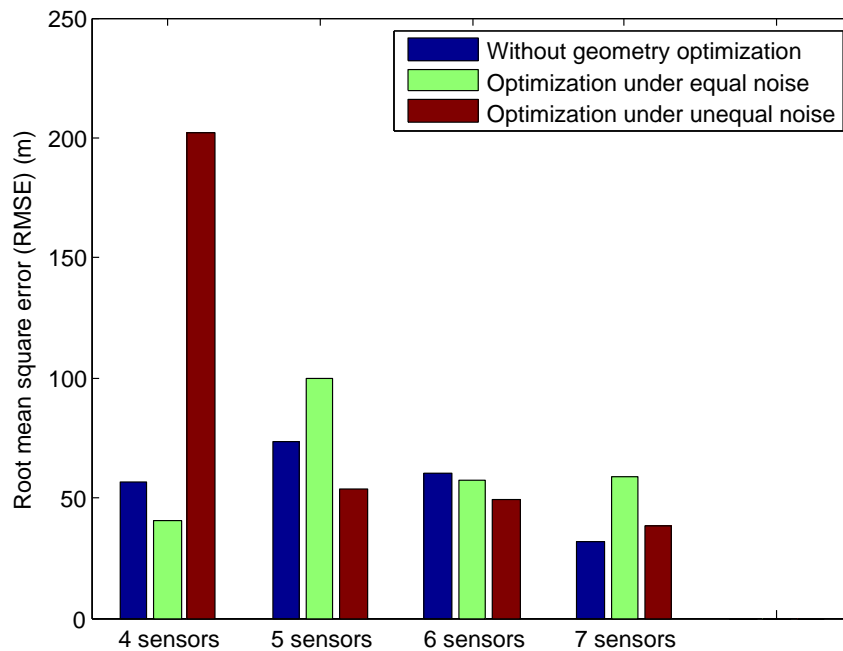
Figure 6.24: The RMSE of the TV signal source localisation using different number of SDRs

6.4 Joint TDOA and FDOA-based localisation using only two SDRs

6.4.1 System setup

After verifying the TDOA-based passive source localisation using multiple spatially distributed SDRs, we will show the results of practical passive source localisation using only two spatially distributed SDRs. In the joint TDOA and FDOA-based localisation using two SDRs, the same stationary signal tower used in TDOA-based localisation is used. To capture the Doppler shift of the target signal and obtain FDOA measurements, at least one SDR needs to move at a fast speed. To achieve a fast moving, we mount one SDR on a car and drive the car on an urban highway. For simplicity, the other SDR is stationary. By taking the advantage of the large transmission power of the emitter, the mobile SDR can travel in a large area. The development of SDRs is similar to that in TDOA-based localisation. Both SDRs are equipped with omni-directional antennas and GPSDOs are used for both time and frequency synchronisation.

The stationary SDR is 9.1km from the emitter and has lone of sight (LOS) condition to the emitter. The distance from the mobile SDR to the emitter varies from 2 $\sim$ 10km, but it does not always has LOS condition to the emitter due to its movement in urban areas. Figure 6.25 and Figure 6.26 show the long and short moving trajectories of the mobile SDR and the deployment of the emitter and the stationary SDR,
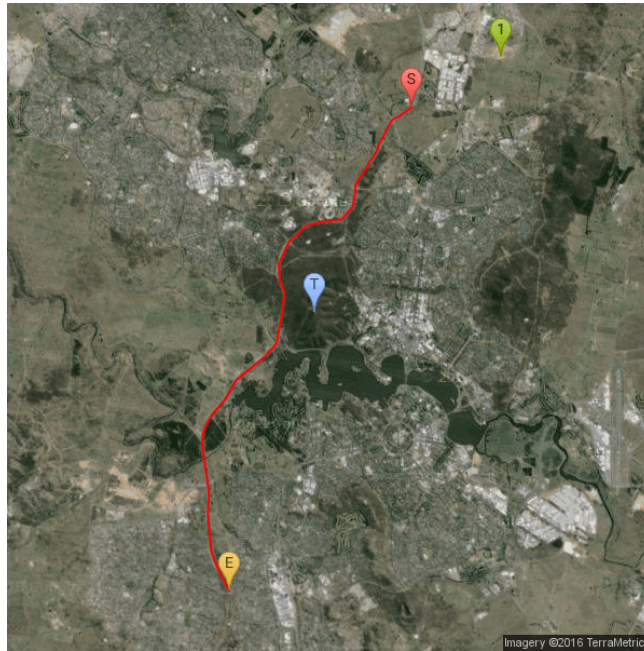
Figure 6.25: The trajectory of the mobile SDR on the short path

respectively, where the red line denotes the trajectory of the mobile SDR, "1" denotes the position of the stationary SDR, "S" in red denotes the starting point of the mobile path, "E" in green denotes the end point of the mobile path, and "T" in blue denotes the emitter to be localised.

6.4.2 Localisation results using two SDRs

To obtain the location estimates, two computationally efficient algorithms are implemented to evaluate the accuracy of the joint TDOA and FDOA-based localisation system. As a metric, the CRLB is used to evaluate the localisation performance. The deviation and expression of the CRLB can be found in Okello et al. [2011] and Ho and Xu [2004].

Firstly, the Extended Kalman Filter (EKF) is a viable technique to track the location of a signal source. By using a recursive estimation procedure, the location estimate can be updated when a new pair of TDOA and FDOA measurements is obtained. A similar solution is discussed in Okello et al. [2011], but we have extended the algorithm from using TDOA measurements only to using joint TDOA and FDOA measurements. To implement the EKF, the initial estimate of the emitter location was randomly generated from a Gaussian distribution centered at the true emitter location with the standard deviation 1000m in both x and y directions. The true values of the standard deviation of the TDOA measurement error and the FDOA measurement error are used in the measurement model and the processing noise of the EKF is set to zero. The root mean square error of the location estimates is ob-
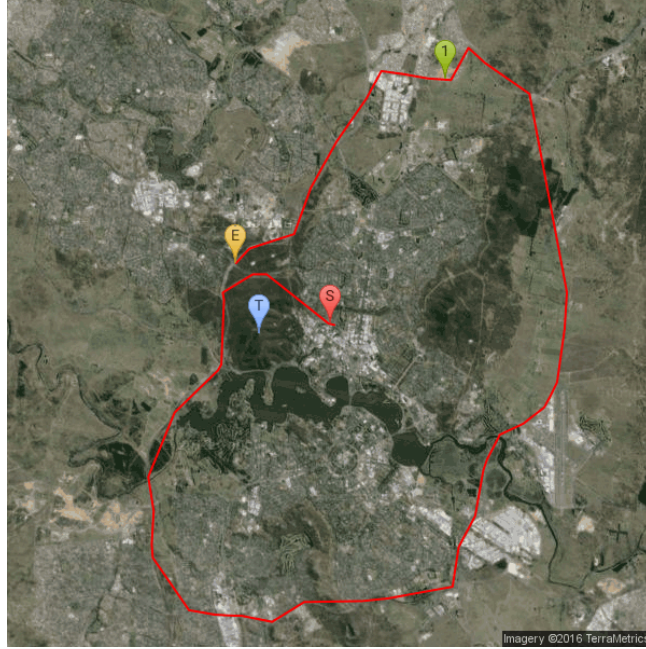
Figure 6.26: The trajectory of the mobile SDR on the long path

tained after 1000 runs of the EKF. In this thesis, we only focus on the demonstration of passive localisation of a stationary emitter because the suitable mobile emitters are not available.

Another type of computationally attractive algorithms is closed-form solutions which involve weighted least-squares minimization only and do not require initial guess of the source location. Inspired by the work Ho and Xu [2004], we modify the algorithm to fit the localisation scenario with a stationary source and only two sensors. The idea of the algorithm is to process a time history of measurements and sensors' positions to determine the location of the source when the mobile sensors move to new locations and take new measurements. By using new sensor position, it is similar to the situation where additional stationary sensors are used to improve the localisation accuracy. The algorithm involves a two-step processing by using two weighting matrix $\mathbf{W}_k^{tf1}$ and $\mathbf{W}_k^{tf2}$ at the kth time instant. We start with $\mathbf{Wtf}_k^1 = (\mathbf{Q}_k^{tf})^{-1}$ and repeat the location estimation twice to obtain the final location estimates.

Figure 6.27 presents the source location estimation process using the FM signal when the mobile SDR moves along the short path (see Fig. 6.25) and takes measurements at each time instant. The x-axis stands for the number of TDOA and FDOA pairs used to localise the source and it starts from four pairs of TDOA and FDOA measurements. The y-axis stands for the RMSE of the location estimates. For the FM signal, the localisation error using the sequential weighted least-squares solution is very large at the first few time instants. This error is caused by the large TDOA and FDOA measurement error. When the measurements obtained from more time instants are obtained, while the accuracy of TDOA and FDOA measurements keeps
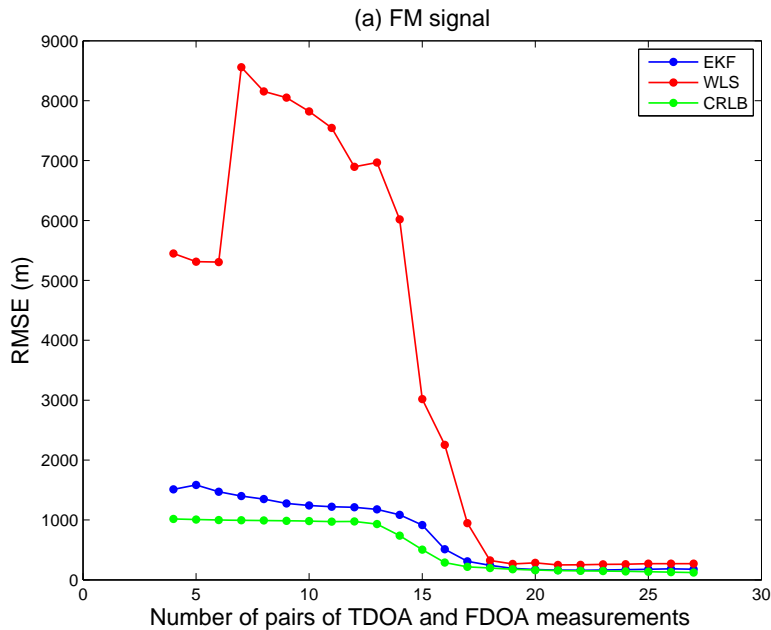
Figure 6.27: The use of FM signal on the short path

similar, the localisation error starts to reduce. After the 18th time instant, the local-isation error keeps almost constant. By contrast, the localisation process using the EFK is smoother and shows smaller RMSE at the first few time instants. The final localisation results of both the sequential WLS and the EKF asymptotically closing to the CRLB at the end of the localisation experiments.

Figure 6.28 shows the localisation process using the TV signal on the same short path. Since both the TDOA measurements and the FDOA measurements have a higher accuracy than those obtained using the FM signal, both the WLS and the EKF give smoother localisation process and higher localisation accuracy.

To further evaluate the accuracy of the source localisation using two SDRs, an-other group of experiments are conducted by moving the mobile SDR along a longer path, as shown in Figure 6.26. The localisation processes of the FM signal source using the sequential WLS and the EKF are demonstrated in Figure 6.29. While both algorithms give large localisation error at the first few time instants, by taking more measurements at multiple time instants, the localisation error is reduced and almost stable at a constant value. One can also see that the localisation process shows some fluctuation. The sudden increase of the RMSE showing on the red curve in Fig-ure 6.29 is caused by the larger noise level of the measurements obtained at those time instants than the noise level of previous measurements. As more measurements are obtained, the influence of larger measurement noise at some time instants are cancelled out, so the RMSE starts to reduce. Figure 6.30 illustrates the localisation processes of the TV signal source using the sequential WLS and the EKF. One can see the similar process to the localisation using the FM signal.
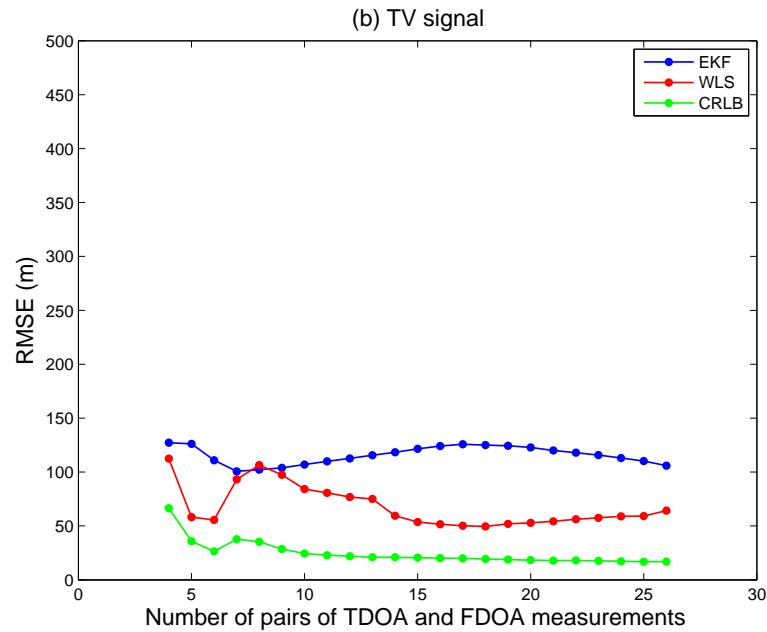
Figure 6.28: The use of TV signal on the short path

Table 6.1 presents the value of the final location estimates using the sequential WLS and the EKF by comparing with the square root of the trace of the CRLB for all above four localisation scenarios. As can be seen from the value of the square of the trace of the CRLB, with the similar number of TDOA and FDOA measurement pairs, the higher bandwidth TV signal provides better localisation accuracy, especially when the number of measurements is small. For the localisation of the same signal source, the increasing measurements help to improve the localisation accuracy. The RMSE of the localisation of the FM signal using the sequential 2WLS on the short path is 269 m, but from the same number of the joint TDOA and FDOA measurements obtained from the TV signal, the localisation error is reduced significantly to 64m. On the long path, the use of the sequential WLS gives 84 m error for the FM signal and 80 m for the TV signal. Notice that for the column "FM long", one needs to see the value in the brackets as more measurements are taken on the long path using the FM signal than the TV signal. For the localisation using the EKF, similar conclusions can be made. The TV signal gives better localisation accuracy. The localisation using the same signal, such as the FM signal or the TV signal, can provide improved localisation by taking more measurements.

Overall, one can see from the localisation results that the practical joint TDOA and FDOA-based passive source localisation can be achieved using only two SDRs. The final localisation solution can be obtained using two computationally efficient algorithms: the sequential WLS and the EKF. The final localisation error is around 100m, which is reasonable if one considers the sensor-target ranges in our demonstration are several kilometres. In general, by taking more measurements, the localisation
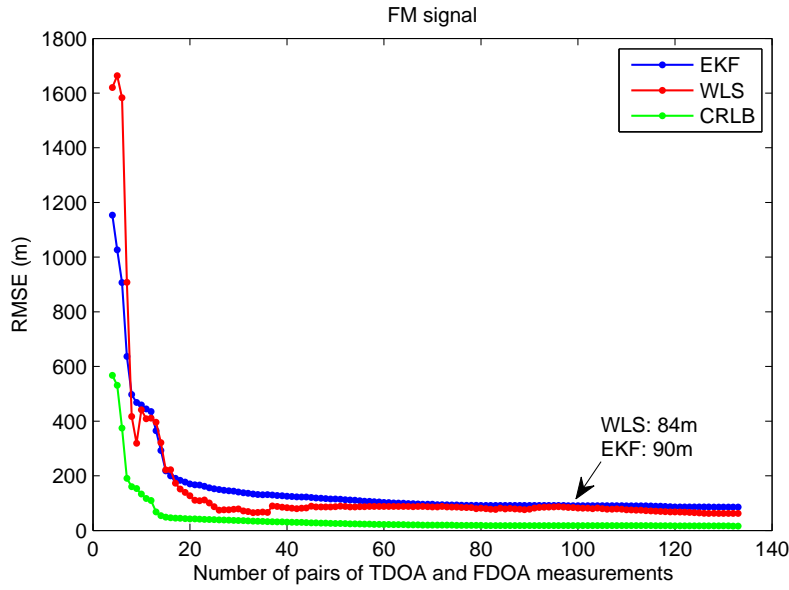
Figure 6.29: The use of FM signal on the long path

	FM short	TV short	FM long	TV long
RMSE WLS	269m	64m	62m (84m)	80m
RMSE EKF	161m	128m	85m (90m)	82m
CRLB	120m	17m	16m	11m

Table 6.1: Location estimates using joint TDOA and FDOA measurements

accuracy can be enhanced. We are also considering implementing some effective data selection strategies to throw out some noisy measurements apart from outliers to make the localisation system obtain the final location estimate faster to save the system processing time. In addition, by using the measurements with relatively less error, the accuracy of the location estimate may be improved. The specific strategies are still under investigation.

6.5 Summary

In this Chapter, the location estimation results using the measurements obtained from the real-world experiments are presented.

In the RSSI-based localisation, as discussed in section 3.2, the inconsistency and unpredicted variance of the RSSI measurements can cause large localisation error, so the localisation optimization algorithm needs to be used:

- The bias reduction algorithm is applied in the RSSI-based localisation system. The experimental results of localising a single emitter and multiple emitters simultaneously in the sensor network are shown. By effectively reducing the
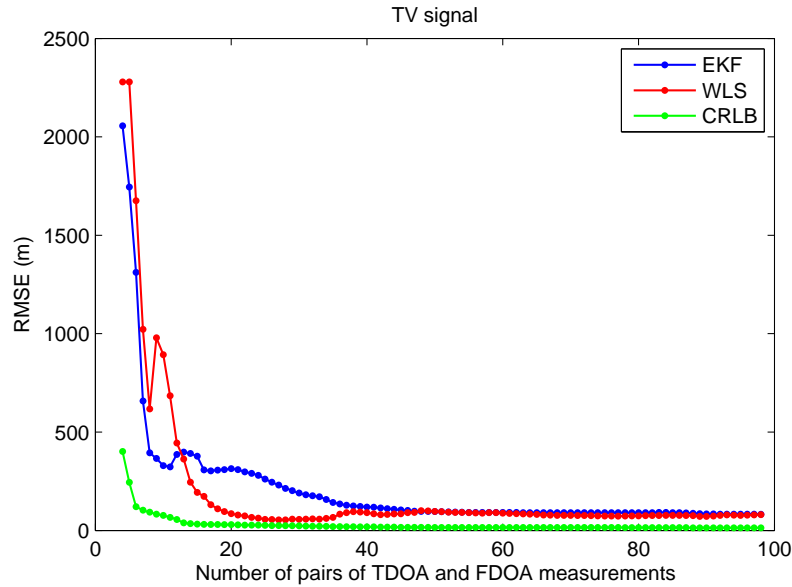
Figure 6.30: The use of TV signal on the long path

bias in the source location estimation, the localisation accuracy of the RSSI-based localisation system is significantly enhanced.

For the TDOA-based localisation, the localisation results of two implementations are shown. In the first implementation, four SDRs are spatially distributed to receive the FM signal. In the second implementation, the SDRs are deployed at four locations which are different from the previous implementation and more than four locations. Both the FM signal and the TV signal are used as the signal source respectively. The localisation accuracy is evaluated by comparing the RMSE of the localisation results against the square root of the trace of the CRLB matrix. The localisation results using the 2WLS algorithm, the optimal sensor-target placement, the localisation optimization with geometric constraints and the bias reduction algorithm are calculated and evaluated. The following results are obtained:

- The 2WLS algorithm can give reliable localisation accuracy. To further improve the localisation accuracy, the localisation optimization with the geometric constraints and the bias reduction can effectively reduce the localisation error.

- While the optimal sensor-target placement cannot be guaranteed in the passive location as the initial guess of the source location is unknown, the metric to determine the optimal sensor-target placement can be used to evaluate the accuracy of the localisation systems. Another way to use the optimal sensor-target placement rule is to re-arrange the deployment of the sensors after the location estimates from the closed-form solution is obtained. In practice, the noise of the TDOA measurements obtained from different pairs of SDRs is different, so

the optimal sensor-target placement needs to be found by maximizing the FIM under the experimental noise instead of under the equal pre-defined noise.

- In general, the use of the TV signal gives higher localisation accuracy than the FM signal because the bandwidth of the TV signal is much higher than the FM signal.

- Increasing the number of sensors and the number of TDOA measurements can effectively enhance the localisation accuracy as long as the new measurements have similar or better accuracy compared with the previous measurements.

- The localisation error obtained from different experiments using multiple low-cost SDRs is around 50 m in a sensor-target range between 2 km and 10 km. The localisation accuracy is expected to be higher if high-quality SDRs are used at the expense of the system cost.

In the joint TDOA and FDOA-based localisation, the localisation results using two SDRs are evaluated using two computationally efficient algorithms, our findings are:

- The Extended Kalman Filter gives smoother localisation process and converges faster than the sequential weighted least-squares solution. As for the final localisation error, two algorithms give similar accuracy.

- Increasing the length of the trajectory of the mobile SDR can increase the number of TDOA and FDOA measurement pairs, which can improve the localisation accuracy.

- The TV signal source generally gives more accurate localisation results than the FM signal.

- The localisation error is around 100 m in average with a sensor-target range of several kilometers. The increasing localisation error is mainly caused by the noisy FDOA measurements.

Conclusion and Future Work

7.1 Conclusion

Location-based service has become increasingly important in our daily life. A fundamental problem in location-based service is the location awareness or how to determine the location of a signal source. Many theoretical works, including measurement acquisition methods and location estimation algorithms, have been proposed, and they have established the foundation for the source localisation research. However, the practical implementation of accurate localisation systems still needs considerable attention because it is very challenging to determine the source location accurately in the complex real-world electromagnetic environment. This motivates us to implement further research on practical source localisation solutions in the real-world environment.

In this thesis, our focus is to seek to fill the gap between localisation theories and practical implementation of localisation systems by demonstrating the source localisation systems using three types of measurement techniques, including RSSI measurements, TDOA measurements, and joint TDOA and FDOA measurements. The signal sensing and location estimation platform developed in this thesis is based on the flexible software-defined-radio devices. The specific SDR model we use is the USRP N210. Compared to conventional systems, the signal processing components of the USRP N210 are software-defined and programmable, which offers large flexibility and adaptation in the system design and development. The system design, the measurement acquisition approaches, and the location estimation algorithms are presented, and finally, the results of the source localisation experiments are shown.

Firstly, an RSSI-based source localisation system is demonstrated using multiple stationary SDRs. It is a non-passive localisation because both the signal transmitters and the receivers are developed using SDRs. Since the RSSI measurements are not reliable in a long-distance propagation, the RSSI-based localisation is implemented in small indoor and outdoor areas with a sensor-target range of several metres. The error sources RSSI-based localisation are investigated, including the hardware precision, the change of transmission power, multipath effect, etc., and effective solutions are proposed. To determine the source location, the RSSI matching-based localisation algorithm and the distance estimation-based localisation algorithm is applied in the indoor localisation. For the outdoor localisation, only the distance estimation-based

localisation algorithm is applied. The localisation results show limited accuracy with 0.5m âĹij 2m localisation error. To improve the localisation accuracy, the localisation bias reduction algorithm is applied. The experimental results show that the use of the bias reduction algorithm can significantly enhance the accuracy of the RSSI-based localisation system in both the single source localisation and the simultaneous localisation of multiple sources in a sensor network.

RSSI-based localisation is simple to implement, but it has low localisation accuracy and small positioning range. By contrast, time-based measurement techniques generally offer higher localisation accuracy and they can be used to implement large-area source localisation. In addition, people from the defence area in Australia are interested in developing low-cost localisation systems using SDRs. Therefore, a TDOA-based localisation system is demonstrated to localise an established signal tower using multiple spatially distributed SDRs with a sensor-target range of several kilometres in the outdoor environment. The system is implemented in a fully passive way, so it is able to localise non-cooperative sources. This demonstration is one of the first works on SDR-based localisation research all over the world when the study was started. To achieve accurate time synchronisation among multiple spatially distributed SDRs, the GPS signal-based synchronisation solution is proposed. While the GPSDO still could not offer perfect synchronisation, it is the most optimal solution for this implementation. After the signal is received, TDOA measurements between synchronised SDR pairs are obtained through the generalised cross-correlation. To improve the localisation accuracy, the accuracy of TDOA measurements is systematically analysed. The measurement error is mainly from three aspects. Firstly, the hardware precision of USRP N210s sets a limit on the TDOA measurement accuracy. The highest achievable sampling rate restraints the resolution of the time measurements to 40 ns. The synchronisation accuracy provided by the GPSDOs gives around 100 ns time synchronisation error. Therefore, at the worst case, the TDOA measurement error caused by the hardware only is 140 ns, which corresponds to 42m distance error. When the signal is received and processed, the measurement accuracy is influenced by the cut-off frequency of the low-pass filter, the length of sampling time, the signal bandwidth and the signal carrier frequency. To improve measurement accuracy, the effective signal processing approaches are implemented to not only enhance the signal processing accuracy but also compensate hardware precision. An empirical study is implemented to obtain the optimal cut-off frequency of the low-pass filter and the optimal length of sampling time. Then, the parabolic fit interpolation algorithm and the Hilbert transform of FFT pruning algorithm are implemented to achieve the time accuracy of the sub-sample level and, thus, improving the resolution of TDOA measurements. In addition, the measurement outliers are identified and removed using the cross correlation coefficient-based approach, the dynamically defined window and measurement recovery approach. In the process of source location estimation, the computationally efficient two-step weighted least-square (2WLS) algorithm is applied and the localisation error is around 50m. Moreover, we have also verified in experiments that the localisation accuracy can be enhanced when localising a signal with a higher bandwidth, such as the TV signal rather than the

FM signal, or using the increasing number of spatially distributed SDRs. To further improve the localisation accuracy, the optimal sensor-target placement is discussed. In addition, the effectiveness of the use of the geometric constraints based on the underlying sensor-target placement and the use of localisation bias reduction algorithm are verified in the practical TDOA-based passive source localisation.

To take a step further, instead of using multiple spatially distributed SDRs, the passive RF source localisation solution using two SDRs is proposed, which is able to deal with the case when the use of multiple SDRs is not feasible and further reduce the system cost. One mobile SDR-based receiver is developed using one SDR device and a car. By having one mobile SDR and one stationary SDR receiving the signal from the same established signal tower, the joint TDOA and FDOA measurements are obtained through the computationally efficient cross ambiguity function to localise the signal source. The system is also a fully passive localisation implementation in a large outdoor area with the sensor-target range between 2km and 10km. The source of the FDOA measurement error can also be analysed from three aspects: the hardware precision, the accuracy of signal processing methods and the environmental impact. In addition, the methods to deal with these error sources are proposed and verified. To determine the source location using the joint TDOA and FDOA measurements taken by two SDRs, the sequential weighted least-square localisation algorithm is proposed by modifying the 2WLS algorithm. In addition, the EKF-based location estimation algorithm is also implemented. After extensive experiments, the passive source localisation is successfully demonstrated using two SDRs and the localisation error is around 100m. The obtained localisation accuracy is reasonable by taking account of the limitation of hardware precision, the system coverage and complex real-world environment. This work is a timely report on the practical implementation of the joint TDOA and FDOA-based localisation using two SDRs.

7.2   Future work

Since the real-world signal propagation environment is highly complicated, environmental factors, especially the multipath effect and NLOS error, degrade the localisation accuracy of almost all practical localisation systems. In practice, the path of signal propagation is highly unpredictable. Even in the LOS condition, the reflected signals from terrain factors, buildings and indoor objects, etc. always exist and produce interference to the signal of interest. NLOS error is hard to avoid when either signal emitters or signal receivers are moving. Many works have been proposed to model the signal propagation through the environment parameter estimation; however, the solutions to addressing multipath effect and NLOS error are still not fully achieved. Our aim is to propose a generic approach to identify, qualify, estimate and mitigate this environmental impact.

There is no single practical localisation system widely applicable when it comes to the real-world environment. Specific design and implementation approaches are

usually required for the localisation systems using different measurement technologies in different environments. In this work, effort has been made to develop localisation systems using flexible SDR devices. After the investigations, we found the new software defined radio technology offers the potential for the development of localisation systems using different measurement techniques. For the localisation using a single measurement technique, a TDOA-based localisation system and an RSSI-based localisation system are developed using multiple SDRs. For the localisation using hybrid measurement techniques, a joint TDOA and FDOA-based localisation system is demonstrated. The related work on AOA-based localisation systems developed using SDRs can also be found Chen et al. [2012]; Zhang et al. [2014]. Therefore, the capabilities of using SDRs to develop localisation systems that can simultaneously use the widely-used measurement techniques are fully verified. Starting from here, we could develop a universal localisation framework for localisation systems using multiple SDRs. This framework should be able to dynamically choose the appropriate measurement technique that should be used to achieve the best localisation performance according to the desirable localisation accuracy, the environment, and the system coverage. This integrated localisation system can be used for location-based services (LBS) in a variety of contexts, such as health, indoor object search, entertainment, work, personal life, etc., in both indoor and outdoor environment. Furthermore, after the performance of the universal platform is verified, a dedicated positioning system with smaller size and even lower cost can be developed and manufactured. The localisation system with compact size and lower cost can be put on UAVs to increase the sensing capability of the system and widely applied in both civil and military areas. In this thesis, we have covered parts of the work, but due to the limitation of application demands, funding and research priority, this work has not been fully implemented.

Another research topic for future work, and a bit remote from the focus of this thesis will be the integration of Software Defined Radio (SDR) and Software Defined Network (SDN) for 5G. The 5G network is a revolutionary technology, which is faster, with better quality, and is more secure. However, with the increasing demand of 5G service, the use of bandwidth and frequency spectrum resources is beyond expectations. The SDR can scan wide frequency bands by just changing the software without modifying any hardware and integrate different connection technologies in a single device. For example, one SDR device can receive signals of WiMAX, Wi-Fi, GSM, or LTE interface. The cognitive radio solution using SDRs can dynamically obtain spectrum information and implement a user-oriented mechanism to allocate spectrum resource. The major contribution of SDN is that the network can be reconstructed. In the seven layers of OSI, the SDN can step over the MAC layer to the application layer. The administrators can use the controller to easily assign the policy to any router and switch to achieve monitoring functions. A cross-layer architecture combining SDR and SDN characteristics can be designed to improve spectrum utilization and channel flow interactions. Another application of SDN could be to adjust network traffic flow on the fly to meet changing needs of the bandwidth to put profitable services in place rapidly and reduce the operational risk.

Bibliography

ABEL, J. AND SMITHT, J., 1987. The spherical interpolation method for closed-form passing source localization using range difference measurements. In *Proc. International Conference on Acoustics, Speech, Signal Processing*. IEEE. (cited on page 18)

AFTANAS, M.; ROVŇÁKOVÁ, J.; DRUTAROVSKỲ, M.; AND KOCUR, D., 2008. Efficient method of TOA estimation for through wall imaging by UWB radar. In *Proc. International Conference on Ultra-Wideband*, vol. 2, 101–104. IEEE. (cited on page 11)

ALSINDI, N.; CHALOUPKA, Z.; ALKHANBASHI, N.; AND AWEYA, J., 2014. An empirical evaluation of a probabilistic rf signature for WLAN location fingerprinting. *IEEE Transactions on Wireless Communications*, 13, 6 (2014), 3257–3268. (cited on page 14)

ALSINDI, N. A.; ALAVI, B.; AND PAHLAVAN, K., 2009. Measurement and modeling of ultrawideband TOA-based ranging in indoor multipath environments. *IEEE Transactions on Vehicular Technology*, 58, 3 (2009), 1046–1058. (cited on page 11)

ALYAFAWI, I.; DIMITROVA, D. C.; AND BRAUN, T., 2014. SDR-based passive indoor localization system for GSM. In *Proc. 2014 ACM workshop on Software radio implementation forum*, 7–14. ACM. (cited on pages 27 and 31)

AMAR, A.; LEUS, G.; AND FRIEDLANDER, B., 2012. Emitter localization given time delay and frequency shift measurements. *IEEE Transactions on Aerospace and Electronic Systems*, 48, 2 (2012), 1826–1837. (cited on page 15)

AMAR, A. AND WEISS, A. J., 2008. Localization of narrowband radio emitters based on Doppler frequency shifts. *IEEE Transactions on Signal Processing*, 56, 11 (2008), 5500–5508. (cited on pages 14 and 15)

ANDERSON, B. D.; SHAMES, I.; MAO, G.; AND FIDAN, B., 2010. Formal theory of noisy sensor network localization. *SIAM Journal on Discrete Mathematics*, 24, 2 (2010), 684–698. (cited on pages 108 and 111)

ARYA, A.; GODLEWSKI, P.; AND MELLÉ, P., 2009. Performance analysis of outdoor localization systems based on RSS fingerprinting. In *Proc. 6th International Symposium on Wireless Communication Systems*, 378–382. IEEE. (cited on page 14)

ASPNES, J.; EREN, T.; GOLDENBERG, D. K.; MORSE, A. S.; WHITELEY, W.; YANG, Y. R.; ANDERSON, B.; AND BELHUMEUR, P. N., 2006. A theory of network localization. *IEEE Transactions on Mobile Computing*, 5, 12 (2006), 1663–1678. (cited on page 107)

BARNES, J.; RIZOS, C.; WANG, J.; SMALL, D.; VOIGT, G.; AND GAMBALE, N., 2003. Locata: a new positioning technology for high precision indoor and outdoor positioning. In *Proc. International Symposium on GPS\GNSS*, 9–18. (cited on page 13)

BHATTI, J.; HUMPHREYS, T.; AND LEDVINA, B., 2012. Development and demonstration of a TDOA-based GNSS interference signal localization system. In *Proc. IEEE/ION Position Location and Navigation Symposium*, 455–469. IEEE. (cited on page 29)

BISHOP, A. N., 2011. Transmitter power estimation for uncooperative emitters with the Cayley-Menger determinant. In *Proc. 19th Mediterranean Conference on Control & Automation*. (cited on page 14)

BISHOP, A. N.; ANDERSON, B. D.; FIDAN, B.; PATHIRANA, P. N.; AND MAO, G., 2009. Bearing-only localization using geometrically constrained optimization. *IEEE Transactions on Aerospace and Electronic Systems*, 45, 1 (2009), 308–320. (cited on page 20)

BISHOP, A. N.; FIDAN, B.; ANDERSON, B.; DOGANÇAY, K.; AND PATHIRANA, P. N., 2008. Optimal range-difference-based localization considering geometrical constraints. *IEEE Journal of Oceanic Engineering*, 33, 3 (2008), 289–301. (cited on pages 20, 100, 102, 120, and 126)

BISHOP, A. N.; FIDAN, B.; ANDERSON, B.; DOĞANÇAY, K.; AND PATHIRANA, P. N., 2010. Optimality analysis of sensor-target localization geometries. *Automatica*, 46, 3 (2010), 479–492. (cited on pages 19, 52, and 98)

BISHOP, A. N. AND PATHIRANA, P. N., 2008. Optimal trajectories for homing navigation with bearing measurements. In *Proc. International Federation of Automatic Control Congress*. (cited on page 20)

BISWAS, P.; LIAN, T.-C.; WANG, T.-C.; AND YE, Y., 2006. Semidefinite programming based algorithms for sensor network localization. *ACM Transactions on Sensor Networks*, 2, 2 (2006), 188–220. (cited on page 18)

BSHARA, M.; ORGUNER, U.; GUSTAFSSON, F.; AND VAN BIESEN, L., 2010. Fingerprinting localization in wireless networks based on received-signal-strength measurements: a case study on WiMAX networks. *IEEE Transactions on Vehicular Technology*, 59, 1 (2010), 283–294. (cited on page 14)

CAFFERY, J. J. AND STUBER, G. L., 1998. Overview of radiolocation in cdma cellular systems. *IEEE Communications Magazine*, 36, 4 (1998), 38–45. (cited on page 22)

CAFFERY JR, J. J., 2006. *Wireless location in CDMA cellular radio systems*, vol. 535. Springer Science & Business Media. (cited on page 1)

CARTER, G. C., 1993. *Coherence and time delay estimation: an applied tutorial for research, development, test, and evaluation engineers*. IEEE. (cited on page 1)

CHAN, Y. AND HO, K., 1994. A simple and efficient estimator for hyperbolic location. *IEEE Transactions on Signal Processing*, 42, 8 (1994), 1905–1915. (cited on pages 18, 93, and 120)

CHEN, C.-L. AND FENG, K.-T., 2005. An efficient geometry-constrained location estimation algorithm for nlos environments. In *Proc. International Conference on Wireless Networks, Communications and Mobile Computing*, vol. 1, 244–249. IEEE. (cited on page 22)

CHEN, H.-C.; LIN, T.-H.; KUNG, H.; LIN, C.-K.; AND GWON, Y., 2012. Determining RF angle of arrival using COTS antenna arrays: a field evaluation. In *Proc. IEEE Military Communications Conference*, 1–6. IEEE. (cited on pages 28 and 148)

CHEN, J. C.; YAO, K.; AND HUDSON, R. E., 2002. Source localization and beamforming. *IEEE Signal Processing Magazine*, 19, 2 (2002), 30–39. (cited on page 8)

CHESTNUT, P. C., 1982. Emitter location accuracy using TDOA and differential Doppler. *IEEE Transactions on Aerospace Electronic Systems*, 18 (1982), 214–218. (cited on page 15)

CHEUNG, K. W.; SO, H.-C.; MA, W.-K.; AND CHAN, Y.-T., 2006. A constrained least squares approach to mobile positioning: algorithms and optimality. *EURASIP Journal on Advances in Signal Processing*, 2006, 1 (2006), 1–23. (cited on page 18)

COMMISSION, F. C. ET AL., 1996. Revision of the commissionâĂŹs rules to ensure compatibility with enhanced 911 emergency calling systems. *Report and Order and Further Notice of Proposed Rulemaking, Tech. Rep. CC Docket*, 94, 102 (1996). (cited on page 1)

COULSON, A. J.; WILLIAMSON, A. G.; AND VAUGHAN, R. G., 1998. A statistical basis for lognormal shadowing effects in multipath fading channels. *IEEE Transactions on Communications*, 46, 4 (1998), 494–502. (cited on page 13)

COX, D. C.; MURRAY, R. R.; AND NORRIS, A., 1984. 800-MHz attenuation measured in and around suburban houses. *AT&T Bell Laboratories technical journal*, 63, 6 (1984), 921–954. (cited on page 13)

DE DONNO, D.; RICCIATO, F.; AND TARRICONE, L., 2013. Listening to tags: Uplink RFID measurements with an open-source software-defined radio tool. *IEEE Transactions on Instrumentation and Measurement*, 62, 1 (2013), 109–118. (cited on page 27)

DERPANIS, K. G., 2010. Overview of the RANSAC Algorithm. *Image Rochester NY*, 4 (2010), 2–3. (cited on page 16)

DI, R.; PENG, S.; TAYLOR, S.; AND MORTON, Y., 2012. A usrp-based gnss and interference signal generator and playback system. In *Position Location and Navigation Symposium (PLANS), 2012 IEEE/ION*, 470–478. IEEE. (cited on page 26)

DOGANÇAY, K., 2007. Optimized path planning for UAVs with AOA/scan based sensors. In *Proc. 15th Europian Signal Processing Conference*, vol. 37. (cited on page 20)

DOGANCAY, K. AND HMAM, H., 2009. On optimal sensor placement for time-difference-of-arrival localization utilizing uncertainty minimization. In *Proc. 17th European Signal Processing Conference*, 1136–1140. IEEE. (cited on page 120)

DURGIN, G. D., 2003. *Space-time wireless channels*. Prentice Hall Professional. (cited on page 13)

EKANAYAKE, S. W.; PATHIRANA, P. N.; AND CAELLI, T., 2012. Multiple emitter localization using range only measurements considering geometrical constraints. In *Proc. IEEE International Conference on Robotics and Biomimetics*, 1991–1995. (cited on page 20)

EL GEMAYEL, N.; KOSLOWSKI, S.; JONDRAL, F. K.; AND TSCHAN, J., 2013. A low cost TDOA localization system: setup, challenges and results. In *Proc. 10th Workshop on Positioning Navigation and Communication*, 1–4. IEEE. (cited on page 29)

ENGELBRECHT, R. S., 1983. Passive source localization from spatially correlated angle-of-arrival data. *IEEE Transactions on Acoustics, Speech and Signal Processing*, 31, 4 (1983), 842–846. (cited on page 8)

ETTUS, M., 2008. Ettus research, LLC. *Online information on USRP board). http://www. ettus. com*, (2008). (cited on pages 23 and 64)

ETTUSRESEARCH, 2014. SDR software. https://www.ettus.com/sdr-software. [Online; accessed 19-June-2014]. (cited on page 25)

ETTUSRESEARCH, 2015. Application Note: Selecting an RF Daughterboard Ettus Research. http://www.ettus.com/content/files/kb/Selecting_an_RF_Daughterboard. pdf. [Online; accessed 19-July-2015]. (cited on page 32)

FARAGHER, R. ET AL., 2012. Understanding the basis of the kalman filter via a simple and intuitive derivation. *IEEE Signal processing magazine*, 29, 5 (2012), 128–132. (cited on page 127)

FIROOZ, M. H.; CHEN, Z.; ROY, S.; AND LIU, H., 2013. Wireless network coding via modified 802.11 MAC/PHY: design and implementation on SDR. *IEEE Journal on Selected Areas in Communications*, 31, 8 (2013), 1618–1628. (cited on page 26)

FISCHLER, M. A. AND BOLLES, R. C., 1981. Random sample consensus: a paradigm for model fitting with applications to image analysis and automated cartography. *Communications of the ACM*, 24, 6 (1981), 381–395. (cited on page 16)

FLETCHER, R., 2013. *Practical methods of optimization*. John Wiley & Sons. (cited on page 102)

Fox, D.; Hightower, J.; Kauz, H.; Liao, L.; and Patterson, D., 2003. Bayesian techniques for location estimation. In *Proc. workshop on location-aware computing*, 16–18. Citeseer. (cited on page 19)

Foy, W., 1976. Position-location solutions by Taylor-series estimation. *IEEE Transactions on Aerospace and Electronic Systems*, AES-12, 2 (1976), 187–194. (cited on pages 18 and 37)

Gardner, W. A. and Chen, C.-K., 1992. Signal-selective time-difference-of-arrival estimation for passive location of man-made signal sources in highly corruptive environments. I. theory and method. *IEEE Transactions on Signal Processing*, 40, 5 (1992), 1168–1184. (cited on page 12)

Gavish, M. and Weiss, A. J., 1992. Performance analysis of bearing-only target location algorithms. *IEEE Transactions on Aerospace and Electronic Systems*, 28, 3 (1992), 817–828. (cited on page 21)

Gholami, M. R.; Gezici, S.; and Strom, E. G., 2013. TDOA based positioning in the presence of unknown clock skew. *Communications, IEEE Transactions on*, 61, 6 (2013), 2522–2534. (cited on page 52)

Gill, P. E.; Murray, W.; and Wright, M. H., 1981. *Practical optimization*. Academic press. (cited on page 102)

GNURadio, 2012. GNU Radio wiki. http://gnuradio.org/redmine/projects/gnuradio/wiki/WikiStart. [Online; accessed 2-December-2011]. (cited on page 25)

Gorji, A. and Anderson, B., 2013. Emitter localization using received-strength-signal data. *Signal Processing*, 93, 5 (2013), 996–1012. (cited on page 14)

Gustafsson, F. and Gunnarsson, F., 2005. Mobile positioning using wireless networks: possibilities and fundamental limitations based on available wireless network measurements. *IEEE Signal Processing Magazine*, 22, 4 (2005), 41–53. (cited on page 19)

Guvenc, I. and Chong, C.-C., 2009. A survey on toa based wireless localization and nlos mitigation techniques. *IEEE Communications Surveys & Tutorials*, 11, 3 (2009), 107–124. (cited on page 21)

Güvenç, I.; Chong, C.-C.; Watanabe, F.; and Inamura, H., 2007. Nlos identification and weighted least-squares localization for uwb systems using multipath channel statistics. *EURASIP Journal on Advances in Signal Processing*, 2008, 1 (2007), 1–14. (cited on page 22)

Hashemi, H., 1993. The indoor radio propagation channel. *Proceedings of the IEEE*, 81, 7 (1993), 943–968. (cited on page 13)

Ho, K., 2012. Bias reduction for an explicit solution of source localization using TDOA. *IEEE Transactions on Signal Processing*, 60, 5 (2012), 2101–2114. (cited on page 21)

Ho, K. and Chan, Y., 1997. Geolocation of a known altitude object from TDOA and FDOA measurements. *IEEE Transactions on Aerospace and Electronic Systems*, 33, 3 (1997), 770–783. (cited on page 15)

Ho, K. and Xu, W., 2004. An accurate algebraic solution for moving source location using TDOA and FDOA measurements. *Signal Processing, IEEE Transactions on*, 52, 9 (2004), 2453–2463. (cited on pages 95, 138, and 139)

Hodge, V. J. and Austin, J., 2004. A survey of outlier detection methodologies. *Artificial Intelligence Review*, 22, 2 (2004), 85–126. (cited on page 15)

Hua, J.; Ruan, C.; Zheng, Z.; Wu, Y.; and Meng, L., 2012. Comparative study of applications of square root raised cosine filter and low pass filter in digital down converter. In *Proc. International Conference on Automatic Control and Artificial Intelligence*, 654–658. IET. (cited on page 70)

Huang, B.; Xie, L.; and Yang, Z., 2015. TDOA-based source localization with distance-dependent noises. *IEEE Transactions on Wireless Communications*, 14, 1 (2015), 468–480. (cited on page 71)

Huang, Y.; Benesty, J.; Elko, G. W.; and Mersereati, R. M., 2001. Real-time passive source localization: a practical linear-correction least-squares approach. *IEEE Transactions on Speech and Audio Processing*, 9, 8 (2001), 943–956. (cited on pages 17 and 92)

Huang, Y. A. and Benesty, J., 2007. *Audio signal processing for next-generation multimedia communication systems*. Springer Science & Business Media. (cited on page 1)

Huang, Y.-D. and Barkat, M., 1991. Near-field multiple source localization by passive sensor array. *IEEE Transactions on Antennas and Propagation*, 39, 7 (1991), 968–975. (cited on page 8)

Huber, P. J., 2011. *Robust statistics*. Springer. (cited on page 16)

Hyndman, R. J. and Fan, Y., 1996. Sample quantiles in statistical packages. *The American Statistician*, 50, 4 (1996), 361–365. (cited on page 37)

Isaacs, J. T.; Klein, D. J.; and Hespanha, J. P., 2009. Optimal sensor placement for time difference of arrival localization. In *Proc. 48th IEEE Decision and Control Conference and 28th Chinese Control Conference*, 7878–7884. IEEE. (cited on page 99)

Jackson, B. and Jordán, T., 2005. Connected rigidity matroids and unique realizations of graphs. *Journal of Combinatorial Theory, Series B*, 94, 1 (2005), 1–29. (cited on page 107)

JAGOE, A., 2003. *Mobile location services: The definitive guide*, vol. 1. Prentice Hall Professional. (cited on page 1)

JI, Y.; YU, C.; AND ANDERSON, B., 2013. Systematic bias correction in source localization. *IEEE Transactions on Aerospace and Electronic Systems*, 49, 3 (2013), 1692–1709. (cited on pages 21, 27, and 123)

JI, Y.; YU, C.; WEI, J.; AND ANDERSON, B., 2015. Localization bias reduction in wireless sensor networks. *IEEE Transactions on Industrial Electronics*, 62, 5 (2015), 3004–3016. (cited on pages 27, 108, 122, and 127)

JOHNSON, J. J., 2001. Implementing the cross ambiguity function and generating geometry-specific signals. Technical report, DTIC Document. (cited on page 64)

JONES, N. A. AND HUM, S. V., 2013. An ultra-wideband spatial filter for Time-of-Arrival localization in tunnels. *IEEE Transactions on Antennas and Propagation*, 61, 10 (2013), 5237–5248. (cited on page 11)

JUANG, P.; OKI, H.; WANG, Y.; MARTONOSI, M.; PEH, L. S.; AND RUBENSTEIN, D., 2002. Energy-efficient computing for wildlife tracking: Design tradeoffs and early experiences with zebranet. *ACM Sigplan Notices*, 37, 10 (2002), 96–107. (cited on page 7)

KAUNE, R. AND CHARLISH, A., 2013. Online optimization of sensor trajectories for localization using TDOA measurements. In *Proc. 16th International Conference on Information Fusion*, 484–491. IEEE. (cited on page 20)

KAUNE, R.; HÖRST, J.; AND KOCH, W., 2011. Accuracy analysis for TDOA localization in sensor networks. In *Proc. 14th International Conference on Information Fusion*, 1–8. IEEE. (cited on page 93)

KAY, S. M., 1993. *Fundamentals of statistical signal processing, volume I: estimation theory*. Prentice Hall. (cited on page 16)

KELLY, D., October, 2012. The Universal Hardware Driver. http://people.bu.edu/mrahaim/NEWSDR/Presentations/NEWSDR_Kelly.pdf. [Online; accessed 19-July-2015]. (cited on page 25)

KIM, W.; LEE, J. G.; AND JEE, G.-I., 2006. The interior-point method for an optimal treatment of bias in trilateration location. *IEEE Transactions on Vehicular Technology*, 55, 4 (2006), 1291–1301. (cited on page 22)

KNAPP, C. AND CARTER, G., 1976. The generalized correlation method for estimation of time delay. *IEEE Transactions on Acoustics, Speech and Signal Processing*, 24, 4 (1976), 320–327. (cited on pages 11, 56, and 80)

LEONARD, J. J. AND DURRANT-WHYTE, H. F., 1991. Mobile robot localization by tracking geometric beacons. *IEEE Transactions on Robotics and Automation*, 7, 3 (1991), 376–382. (cited on page 19)

LEVY, A.; GANNOT, S.; AND HABETS, E. A., 2011. Multiple-hypothesis extended particle filter for acoustic source localization in reverberant environments. *IEEE Transactions on Audio, Speech, and Language Processing*, 19, 6 (2011), 1540–1555. (cited on page 18)

LI, Z.; BRAUN, T.; AND DIMITROVA, D. C., 2015. A time-based passive source localization system for narrow-band signal. In *Proc. IEEE International Conference on Communications*. (cited on page 29)

LI, Z.; DIMITROVA, D. C.; RALUY, D. H.; AND BRAUN, T., 2014. Tdoa for narrow-band signal with low sampling rate and imperfect synchronization. In *Proc. 7th Wireless and Mobile Networking Conference*, 1–8. IEEE. (cited on page 29)

LIU, B.; CHEN, H.; ZHONG, Z.; AND POOR, H. V., 2010. Asymmetrical round trip based synchronization-free localization in large-scale underwater sensor networks. *IEEE Transactions on Wireless Communications*, 9, 11 (2010), 3532–3542. (cited on page 12)

LOHRASBIPEYDEH, H.; GULLIVER, T. A.; AND AMINDAVAR, H., 2014a. A minimax sdp method for energy based source localization with unknown transmit power. *IEEE Wireless Communications Letters*, 3, 4 (2014), 433–436. (cited on page 14)

LOHRASBIPEYDEH, H.; GULLIVER, T. A.; AMINDAVAR, H.; AND DAKIN, T., 2014b. Efficient RSSD-based source positioning with system parameter uncertainties. In *Proc. 80th Vehicular Technology Conference (VTC Fall)*, 1–4. IEEE. (cited on page 14)

LUO, J.-A.; ZHANG, X.-P.; AND WANG, Z., 2013. A new passive source localization method using AOA-GROA-TDOA in wireless sensor array networks and its Cramér-rao bound analysis. In *Proc. International Conference on Acoustics, Speech and Signal*, 4031–4035. IEEE. (cited on page 15)

MAO, G.; ANDERSON, B.; AND FIDAN, B., 2007a. Path loss exponent estimation for wireless sensor network localization. *Computer Networks*, 51, 10 (2007), 2467–2483. (cited on pages 14 and 35)

MAO, G.; FIDAN, B.; AND ANDERSON, B., 2007b. Wireless sensor network localization techniques. *Computer networks*, 51, 10 (2007), 2529–2553. (cited on page 9)

MARTÍNEZ, S. AND BULLO, F., 2006. Optimal sensor placement and motion coordination for target tracking. *Automatica*, 42, 4 (2006), 661–668. (cited on page 20)

MELSA, J. L.; COHN, D. L.; ET AL., 1978. *Decision and estimation theory*. McGraw-Hill. (cited on page 104)

MENG, W.; XIAO, W.; AND XIE, L., 2011. Optimal sensor pairing for TDOA based source localization in sensor networks. In *Proc. 8th International Conference on Information, Communications and Signal Processing*, 1–5. IEEE. (cited on page 20)

Meng, W.; Xie, L.; and Xiao, W., 2012. Optimal sensor pairing for TDOA based source localization and tracking in sensor networks. In *Proc. 15th International Conference on Information Fusion*, 1897–1902. IEEE. (cited on pages 20, 100, and 120)

Moeglein, M. and Krasner, N., 1998. An introduction to SnapTrack server-aided GPS technology. In *Proc. 11th International Technical Meeting of the Satellite Division of The Institute of Navigation*, 333–342. (cited on page 13)

Nash, J. C. and Walker-Smith, M., 1987. Nonlinear parameter estimation. *New York: Marcel Decker*, (1987). (cited on page 18)

Nguyen, N. H. and Dogangay, K., 2015. Optimal sensor-target geometries for Doppler-shift target localization. In *Proc. 23rd European Signal Processing Conference*, 180–184. IEEE. (cited on pages 14 and 15)

Okello, N.; Fletcher, F.; Mušicki, D.; and Ristic, B., 2011. Comparison of recursive algorithms for emitter localisation using TDOA measurements from a pair of UAVs. *IEEE Transactions on Aerospace and Electronic Systems*, 47, 3 (2011), 1723–1732. (cited on page 138)

Oshman, Y. and Davidson, P., 1999. Optimization of observer trajectories for bearings-only target localization. *IEEE Transactions on Aerospace and Electronic Systems*, 35, 3 (1999), 892–902. (cited on page 20)

Pahlavan, K. and Levesque, A. H., 2005. *Wireless information networks*, vol. 93. Wiley. com. (cited on page 36)

Papakonstantinou, K. and Slock, D., 2009. Hybrid TOA/AOD/Doppler-shift localization algorithm for NLOS environments. In *Proc. 20th International Symposium on Personal, Indoor and Mobile Radio Communications*, 1948–1952. IEEE. (cited on page 15)

Patwari, N.; Ash, J. N.; Kyperountas, S.; Hero III, A. O.; Moses, R. L.; and Correal, N. S., 2005. Locating the nodes: cooperative localization in wireless sensor networks. *IEEE Signal Processing Magazine*, 22, 4 (2005), 54–69. (cited on pages 9 and 13)

Picard, J. S. and Weiss, A. J., 2010. Bounds on the number of identifiable outliers in source localization by linear programming. *IEEE Transactions on Signal Processing*, 58, 5 (2010), 2884–2895. (cited on page 17)

Priyantha, N. B.; Chakraborty, A.; and Balakrishnan, H., 2000. The cricket location-support system. In *Proc. 6th annual international conference on Mobile computing and networking*, 32–43. ACM. (cited on page 11)

Quitin, F.; Rahman, M. M. U.; Mudumbai, R.; and Madhow, U., 2013. A scalable architecture for distributed transmit beamforming with commodity radios: design and proof of concept. *IEEE Transactions on Wireless Communications*, 12, 3 (2013), 1418–1428. (cited on page 27)

RAPPAPORT, T. S.; REED, J. H.; AND WOERNER, B. D., 1996a. Position location using wireless communications on highways of the future. *Communications Magazine*, 34, 10 (1996), 33–41. (cited on pages 9, 10, and 12)

RAPPAPORT, T. S. ET AL., 1996b. *Wireless communications: principles and practice*, vol. 2. Prentice Hall PTR New Jersey. (cited on page 13)

RIBA, J. AND URRUELA, A., 2004. A non-line-of-sight mitigation technique based on ml-detection. In *Proc. IEEE International Conference on Acoustics, Speech, and Signal Processing*, vol. 2, ii–153. IEEE. (cited on page 22)

RISTIC, B. AND FARINA, A., 2013. Target tracking via multi-static doppler shifts. *IET Radar, Sonar & Navigation*, 7, 5 (2013), 508–516. (cited on pages 14 and 15)

ROBINSON, E. R. AND QUAZI, A. H., 1985. Effect of sound-speed profile on differential time-delay estimation. *The Journal of the Acoustical Society of America*, 77, 3 (1985), 1086–1090. (cited on page 12)

ROLSHOFEN, W.; DIETZ, P.; AND SCHAFER, G., 2005. TAI-CHI: Tangible acoustic interfaces for computer-human interaction. *FORTSCHRITTE DER AKUSTIK*, 31, 2 (2005), 773. (cited on page 1)

ROY, R. AND KAILATH, T., 1989. ESPRIT-estimation of signal parameters via rotational invariance techniques. *IEEE Transactions on Acoustics, Speech and Signal Processing*, 37, 7 (1989), 984–995. (cited on page 10)

SATHYAN, T.; HUMPHREY, D.; AND HEDLEY, M., 2011. WASP: a system and algorithms for accurate radio localization using low-cost hardware. *IEEE Transactions on Systems, Man, and Cybernetics, Part C: Applications and Reviews*, 41, 2 (2011), 211–222. (cited on page 11)

SCHAU, H. AND ROBINSON, A., 1987. Passive source localization employing intersecting spherical surfaces from time-of-arrival differences. *IEEE Transactions on Acoustics, Speech and Signal Processing*, 35, 8 (1987), 1223–1225. (cited on page 18)

SCHMIDT, R. O., 1986. Multiple emitter location and signal parameter estimation. *IEEE Transactions on Antennas and Propagation*, 34, 3 (1986), 276–280. (cited on page 10)

SHAMES, I.; BISHOP, A. N.; SMITH, M.; AND ANDERSON, B. D., 2013. Doppler shift target localization. *IEEE Transactions on Aerospace and Electronic Systems*, 49, 1 (2013), 266–276. (cited on pages 14 and 15)

SHIRAHAMA, J. AND OHTSUKI, T., 2008. Rss-based localization in environments with different path loss exponent for each link. In *Proc. Vehicular technology conference (VTC spring)*, 1509–1513. IEEE. (cited on page 13)

SMITH, J. O. AND ABEL, J. S., 1987. Closed-form least-squares source location estimation from range-difference measurements. *IEEE Transactions on Acoustics, Speech and Signal Processing*, 35, 12 (1987), 1661–1669. (cited on page 92)

SO, H.; CHAN, Y.; HO, K.; AND CHEN, Y., 2013. Simple formulae for bias and mean square error computation. *IEEE Signal Processing Magazine*, 30, 4 (2013), 162 – 165. (cited on page 56)

SO, H. C., 2011. Source localization: algorithms and analysis. *Handbook of Position Location: Theory, Practice, and Advances*, (2011), 25–66. (cited on pages 1 and 7)

SPILKER, J. J., 1978. GPS signal structure and performance characteristics. *Navigation*, 25, 2 (1978), 121–146. (cited on page 1)

SPRANG, J. S., 2015. Non-linear optimization applied to angle-of-arrival satellite-based geolocation with correlated measurements. Technical report, DTIC Document. (cited on page 15)

STEGGLES, P. AND GSCHWIND, S., 2005. The ubisense smart space platform. In *Proc. International Conference on Pervasive Computing*, vol. 191, 73–76. (cited on page 11)

STEIN, S., 1981. Algorithms for ambiguity function processing. *IEEE Transactions on Acoustics, Speech and Signal Processing*, 29, 3 (1981), 588–599. (cited on page 71)

STEIN, S., 1993. Differential delay/Doppler ML estimation with unknown signals. *IEEE Transactions on Signal Processing*, 41, 8 (1993), 2717–2719. (cited on page 15)

STOJMENOVIC, I., 2005. *Handbook of sensor networks: Algorithms and architectures*, vol. 49. John Wiley & Sons. (cited on page 1)

TORRIERI, D., 1984. Statistical theory of passive location systems. *IEEE Transactions on Aerospace and Electronic Systems*, AES-20, 2 (1984), 183–198. (cited on page 37)

TSENG, P., 2007. Second-order cone programming relaxation of sensor network localization. *SIAM Journal on Optimization*, 18, 1 (2007), 156–185. (cited on page 18)

UCINSKI, D., 2004. *Optimal measurement methods for distributed parameter system identification*. CRC Press. (cited on pages 19 and 99)

VAN DER WALLE, D.; FIDAN, B.; SUTTON, A.; YU, C.; AND ANDERSON, B., 2008. Non-hierarchical uav formation control for surveillance tasks. In *Proc. American Control Conference*, 777–782. IEEE. (cited on page 7)

VENKATESH, S. AND BUEHRER, R. M., 2007. Nlos mitigation using linear programming in ultrawideband location-aware networks. *IEEE transactions on Vehicular Technology*, 56, 5 (2007), 3182–3198. (cited on page 22)

WANG, G.; CHEN, H.; LI, Y.; AND ANSARI, N., 2014. Nlos error mitigation for toa-based localization via convex relaxation. *IEEE Transactions on Wireless Communications*, 13, 8 (2014), 4119–4131. (cited on page 22)

WANG, G.; SO, A. M.-C.; AND LI, Y., 2016. Robust convex approximation methods for tdoa-based localization under nlos conditions. *IEEE Transactions on Signal Processing*, 64, 13 (2016), 3281–3296. (cited on page 22)

WANG, H. AND CHU, P., 1997. Voice source localization for automatic camera pointing system in videoconferencing. In *Proc. IEEE International Conference on Acoustics, Speech, and Signal Processing*, vol. 1, 187–190. IEEE. (cited on page 18)

WANG, J.; CHEN, J.; AND CABRIC, D., 2013. Stansfield localization algorithm: Theoretical analysis and distributed implementation. *IEEE Wireless Communications Letters*, 2, 3 (2013), 327–330. (cited on page 21)

WANG, X.; WANG, Z.; O DEA, B.; ET AL., 2003. A toa-based location algorithm reducing the errors due to non-line-of-sight (nlos) propagation. *IEEE Transactions on Vehicular Technology*, 52, 1 (2003), 112–116. (cited on page 22)

WANG, Y. AND HO, K., 2013. TDOA source localization in the presence of synchronization clock bias and sensor position errors. *IEEE Transactions on Signal Processing*, 61, 18 (2013), 4532–4544. (cited on page 52)

WEI, J.; JI, Y.; AND YU, C., 2014. Improvement of Software Defined Radio based RSSI localization with bias reductionâŃȨ. In *Proc. 19th World Congress of the International Federation of Automatic Control*. (cited on page 27)

WEN, Y.; TIAN, X.; WANG, X.; AND LU, S., 2015. Fundamental limits of RSS fingerprinting based indoor localization. In *Proc. IEEE Conference on Computer Communications*, 2479–2487. IEEE. (cited on page 14)

WERB, J. AND LANZL, C., 1998. Designing a positioning system for finding things and people indoors. *Spectrum, IEEE*, 35, 9 (1998), 71–78. (cited on page 12)

XIAO, Y.-C.; WEI, P.; AND YUAN, T., 2010. Observability and performance analysis of bi/multi-static Doppler-only radar. *IEEE Transactions on Aerospace and Electronic Systems*, 46, 4 (2010), 1654–1667. (cited on pages 14 and 15)

XU, C.; FIRNER, B.; ZHANG, Y.; HOWARD, R.; AND LI, J., 2011. Poster: statistical learning strategies for RF-based indoor device-free passive localization. In *Proc. 9th ACM Conference on Embedded Networked Sensor Systems*, 365–366. ACM. (cited on page 8)

YANG, K.; WANG, G.; AND LUO, Z.-Q., 2009. Efficient convex relaxation methods for robust target localization by a sensor network using time differences of arrivals. *IEEE Transactions on Signal Processing*, 57, 7 (2009), 2775–2784. (cited on page 18)

Yang, Z.; Jian, L.; Wu, C.; and Liu, Y., 2013a. Beyond triangle inequality: sifting noisy and outlier distance measurements for localization. *ACM Transactions on Sensor Networks*, 9, 2 (2013), 26. (cited on page 15)

Yang, Z.; Wu, C.; Chen, T.; Zhao, Y.; Gong, W.; and Liu, Y., 2013b. Detecting outlier measurements based on graph rigidity for wireless sensor network localization. *IEEE Transactions on Vehicular Technology*, 62, 1 (2013), 374–383. (cited on page 16)

Yeredor, A. and Angel, E., 2011. Joint TDOA and FDOA estimation: A conditional bound and its use for optimally weighted localization. *IEEE Transactions on Signal Processing*, 59, 4 (2011), 1612–1623. (cited on page 15)

Youssef, M.; Mah, M.; and Agrawala, A., 2007. Challenges: device-free passive localization for wireless environments. In *Proc. 13th annual ACM international conference on Mobile computing and networking*, 222–229. ACM. (cited on page 8)

Zhang, C.; Li, F.; Luo, J.; and He, Y., 2014. iLocScan: harnessing multipath for simultaneous indoor source localization and space scanning. In *Proc. 12th ACM Conference on Embedded Network Sensor Systems*, 91–104. ACM. (cited on pages 28 and 148)

Zhang, J.; Jia, J.; Zhang, Q.; and Lo, E. M. K., 2010. Implementation and evaluation of cooperative communication schemes in Software-Defined Radio testbed. In *Proceedings of IEEE*, 5618–5621. (cited on page 26)

Zheng, J. and Jamalipour, A., 2009. *Wireless sensor networks: a networking perspective*. John Wiley & Sons. (cited on page 2)

Zhou, Y.; Law, C. L.; Guan, Y. L.; and Chin, F., 2011. Indoor elliptical localization based on asynchronous UWB range measurement. *IEEE Transactions on Instrumentation and Measurement*, 60, 1 (2011), 248–257. (cited on page 11)